Low complexity wireless sensors for power-efficient communiation and energy harvesting

Bo, Han

Publication date:
2013

Document Version
Accepted author manuscript, peer reviewed version

LOW COMPLEXITY WIRELESS SENSORS FOR POWER-EFFICIENT COMMUNICATION AND ENERGY HARVESTING

BY
BO HAN

DISSERTATION SUBMITTED 2017

AALBORG UNIVERSITY
DENMARK

Low complexity wireless sensors for power-efficient communication and energy harvesting

Ph.D. Dissertation

Bo Han

Aalborg University
Department of Electronic Systems
DK-9220 Aalborg

Preface and Acknowledgments

This thesis is submitted as partial fulfillment of the requirements

for the degree of *Doctor of Philosophy* at Aalborg University, Denmark.

The main part of the thesis is a collection of papers published in or submitted to peer-reviewed conferences or journals.

It is the results of 3 years of research at the *Department of Electronic Systems*, Aalborg University, in the period *September 2010 - September 2013*.

I would like to express my sincere gratitude to my advisor Prof. Constantinos B Papadias for his encouragement and kind assistance during my PhD study. His positive energy encouraged me to overcome all kinds of difficulties during the most harsh period; such kind of positive energy is the most valuable treasurer that raises my sprit and morale. His enthusiasm and involvement have been immense, which has created a sense of being part of a team rather than alone in the work. His expertise, has been a great source of knowledge for me to draw upon. It has been a privilege.

I would also like to express my gratitude to my advisor Prof. Ramjee Prasad, For his kindness and encourage all the three years. His global view on the scientific research and education create immersible positive influence on the spreading of scientific knowledge in a global domain, which is important for the PhD study with a global view.

Also I would say many thanks for co-advisor Prof. Antonis Kalis, who guided me during my first one and half years PhD period, and for his efforts in the project, the European Commission founded Marie Curie program - Initial Training Network, which built both scientific connection and friendship among the researchers from outstanding institutes in Europe. My thanks also goes to co-advisor Dr. Rasmus H. Nielsen who helped and assisted on all kinds of PhD issues during the PhD study. Also many tanks for Dr. Richard Orme, who helped me a lot in England and provided significant

assistance on this thesis write up.

During these three years, I appreciate to have all those international friendships with multi culture background in the B-WiSE Lab, also the home culture friendship in Electronic System Department at Aalborg University. Thanks for all of you to give me all kinds of helps and encourages during these three years.

Bo Han
Aalborg University, September 30, 2013

Abstract

As modern communication goes towards the direction of a *green* and environment friendly solution, many issues have been raised and analyzed, i.e. better usage of spectrum, lower system complexity, or lower energy consumption (especially for the battery powered devices). Among all these aspects, energy efficiency has drawn special attention, which moves as a trend of considering better usage of energy in wireless communications. Such concern influences heavily on the life time of the wireless sensor network, as most of the sensor nodes get power from energy limited sources, i.e., the batteries.

At the same time, a reliable communication link is euqally necessary and the spectral efficiency has also to be considered. Towards this direction, a number of solutions have been made, such as: spatial multiplexing, or Multiple Input Multiple Output(MIMO). This technology enhances the communication link leading to a larger system capacity, higher data rate and better spectrum usage efficiency. However, these techniques require more radio chains, thus more power is consumed. In order to maintain the low cost and low power consumption constrains, and keep the advantage of the MIMO techniques, the so called single RF MIMO technique is introduced. With the help of adjacent parasitic antenna arrays, the single RF MIMO uses only one RF chain while the data streams are mapped into radiation patterns altered by the parasitic loads. In this way, the performance of the communication link is kept at almost as good as conventional MIMO, but the power consumption is reduced greatly.

In considering about the energy efficiency in the wireless communication, the commonly used energy per bit (J/bit) is adopted in this dissertation; meanwhile, both the transmission energy radiated by the communication link and the circuit energy dissipated by the corresponding components on the RF chain are considered jointly for the total energy cost. At short distance, due to the higher power consumption of the circuit component , the energy efficiency is sensitive to different modulation schemes; while at the long distance, the transmission loss dominates. As been evaluated that, within a limited bandwidth/data rate the conventional MIMO technique will get worse than the single RF MIMO after certain distance.

The goal of the energy efficient design is to prolong the lifetime of the mobile termi-

nals and wireless sensor networks. Although there are so many kinds of low cost, low power designs, the batteries of a mobile terminal ultimately need to be recharged. The backup design is for the sensor node to harvest energy from the environment. In order to have such energy harvesting capability, considerable investigation has been made into self-powered sensor nodes. Although the energy source conversion may differ, e.g., the solar converter, piezoelectric and magnetic conversion techniques for vibration based kinetic energy, the resonate antennas for radiation energy, etc. most techniques could not provide a high output voltage. so a rectifying circuit is needed to boot the voltage for the succeeding circuit stages.

With the low cost techniques for the power efficient communications, together with self-powered/self-rechargeable techniques, we can anticipate that the life time of the wireless sensor network can be increased dramatically.

In this dissertation, the energy and low cost analysis is addressed in the introduction chapter; the low cost sensor node communication with reduced complexity MIMO transmission technique is introduced in chapter 2, and the energy analysis as well as the quantized energy efficiency on different network models are given chapter 3, while for the applications of the low cost sensor network, such as Structural Health Monitoring where the structural has rich vibrations, the energy harvesting technique for sensor node is introduced in chapter 4. The conclusion is given in chapter 5.

Abstrakt

Som moderne kommunikation går i den retning af en textit grøn og miljøvenlig løsning, har mange spørgsmål blevet rejst, og analyseret, dvs bedre udnyttelse af frekvenser, lavere systemets kompleksitet, eller lavere energiforbrug (især for de batteridrevne enheder). Blandt alle disse aspekter er energi effektiviteten trukket særlig opmærksomhed, som bevæger sig som en trend for at overveje en bedre udnyttelse af energien inden for trådløs kommunikation. En sådan bekymring påvirker tungt på levetiden for den trådløse sensor netværk, da de fleste af sensor noder få strøm fra energikilder begrænsede kilder, dvs batterier.

På samme tid, er en pålidelig kommunikations forbindelse euqally nødvendig og den spektrale effektivitet har også tages i betragtning. Mod denne retning, har en række løsninger er foretaget, såsom: rumlige multiplexing eller Multiple Input Multiple Output (MIMO). Denne teknologi forbedrer kommunikationen link, der fører til et større system kapacitet, højere datahastighed og bedre frekvensanvendelse effektivitet. Men disse teknikker kræver flere radio kæder, dermed mere strøm. For at opretholde de lave omkostninger og lavt strømforbrug begrænser og holder den fordel af de MIMO teknikker, er den såkaldte enkelt RF MIMO teknik indført. Med hjælp fra tilstødende parasitiske antennegitre bruger enkelt RF MIMO kun en RF kæde, mens datastrømme mappet ind stråling mønstre ændres af parasitiske belastninger. På denne måde bliver udførelsen af kommunikations forbindelsen holdes på næsten så godt som konventionelle MIMO, men strømforbruget reduceres betydeligt.

I forbindelse med overvejelserne om energi effektivitet i den trådløse kommunikation, er almindeligt anvendt energi pr bit (J/b), vedtaget i denne afhandling, i mellemtiden, både transmissions energi udstrålede ved kommunikationsforbindelse og kredsløbet energi, der spredes af de tilsvarende komponenter på RF kæden er behandles i fællesskab for den samlede energi- omkostninger. På kort afstand, på grund af den højere strømforbrug af kredsløbet komponent energieffektiviteten er følsom over for forskellige modulationsordninger, mens den lange afstand, transmissionstabet dominerer. Som det er blevet vurderet, at der inden for en begrænset båndbredde/data rate den konventionelle MIMO teknikken vil blive værre end den enkelt RF MIMO efter en bestemt distance.

Målet med energieffektive design er at forlænge levetiden af de mobile terminaler

og trådløse sensor netværk. Selv om der er så mange slags lave omkostninger, lavt strømforbrug design, batterierne i en mobil terminal i sidste ende skal genoplades. Den backup design er for sensoren node at høste energi fra omgivelserne. For at få en sådan energi høst kapacitet, har store undersøgelse foretaget i selv -drevne sensor noder. Selvom energikilde konvertering kan variere, fx sol konverter, piezoelektriske og magnetiske konvertering teknikker til vibrationer baseret kinetisk energi, kunne genlyd antenner til stråling energi osv. fleste teknikker ikke giver en høj udgangsspænding. så en berigtigelse kredsløb er nødvendig for at starte spændingen for de efterfølgende kredsløb etaper.

Med de lave omkostninger teknikker til den magt effektiv kommunikation, sammen med self-powered/self-rechargeable teknikker, kan vi forudse, at levetiden for den trådløse sensor netværk kan øges dramatisk.

I denne afhandling er den energi og lave omkostninger analyse behandles i det indledende kapitel, de lave omkostninger sensor node kommunikation med reduceret kompleksitet MIMO transmission teknik introduceres i kapitel 2, og energien analyse samt den kvantiserede energieffektivitet på forskellige netværksmodeller er givet kapitel 3, mens der for de anvendelser af de lave omkostninger sensor netværk, såsom strukturel Health Overvågning hvor den strukturelle har rige vibrationer, er energi høst teknik til sensor node introduceret i kapitel 4. Konklusionen er givet i kapitel 5.

Contents

List of Papers

The main body of this thesis consists of the following papers.

[A] B. Han, V.I. Barousis, A. Kalis, A.G. Kanatas, "Active Parasitic Arrays for Low Cost Compact MIMO Transmitters," *Proceeding of 5th European Conference on Antenna and Propagation, IEEE*, pp. 3663–3667, 2011.

[B] B. Han, A. Kalis, R. Prasad "Matching Parasitic Antenna for Single RF MIMO," *International Conference on Microwave and Millimeter Wave Technology (ICMMT), IEEE*, pp. 1–4, 2012.

[C] B. Han, A. Kalis, P. Tragas, R.H. Nielsen, R. Prasad "Low Cost Wireless Sensor Network for Continuous Bridge monitoring," *Proceedings of the Sixth International IABMAS Conference on Bridge Maintenance, Safety, Management, Resilience and Sustainability* , pp. 96–98, 2012.

[D] B. Han, A. Kalis, C.B. Papadias, R.H. Nielsen, R. Prasad "Explore the Capability of ESPAR Antennas for Low Cost Communication," *The 28th Conference on Technologies and Visions for a Sustainable Wireless Internet*, 2012.

[E] B. Han, A. Kalis, C.B. Papadias, P. Tragas, R.H. Nielsen, R. Prasad, "Low Cost Localization Techniques in Structural Damage Detection," *The IABSE Conference on Assessment Upgrading and Refurbishment of Infrastructures*, pp.826-831, 2013.

[F] B. Han, A. Kalis, C.B. Papadias, R. Soman, M.A. Kyriakides, T. Onoufriou, R.H. Nielsen, R. Prasad, "Energy Harvesting for Sensors in Infrastructure Monitoring and Maintenance," *The IABSE Conference on Assessment Upgrading and Refurbishment of Infrastructures*, pp.404-410, 2013.

[G] B. Han, S. Vassilaras, C.B. Papadias, R.Soman, M.A. Kyriakides, T. Onoufriou, R.H. Nielsen, R. Prasad "Harvesting Energy from Vibration of the Structure," *Journal of Vibration and Control*, Published, 2013, DOI: 10.1177/1077546313501537

[H] B. Han, R.H. Nielsen, C.B. Papadias, R. Prasad, "Radio Frequency Energy Harvesting for Long Lifetime Wireless Sensor Networks," *International Symposium on Wireless Personal Multimedia Communications (WPMC)*, pp. IME-T3, 2013.

[I] B. Han, R.H. Nielsen, C.B. Papadias, R. Prasad, "Directional Transmission by 3-D Beam-forming using Smart Antenna Arrays," *International Conference on Wireless Communications, Vehicular Technology, Information Theory and Aerospace Electronic Systems Technology(Wireless ViATE)*, pp 26-28, 2013.

[J] B. Han, A. Kalis, C.B. Papadias, R. Prasad, "Energy Efficient MIMO Transmission with High Order Modulation for Wireless Sensor Network," *European Signal Processing Conference(EUSIPCO)*, to appear, 2013.

[K] B. Han, V.I. Barousis, C.B. Papadias, A. Kalis, R. Prasad, "MIMO over ESPAR with 16-QAM Modulation," *Wireless Communication Letters, IEEE*, DOI 10.1109/WCL.2013.13.130433, 2013.

[L] B. Han, V.I. Barousis, A. Kalis, C.B. Papadias, A.G. Kanatas, R. Prasad, "A single RF MIMO Loading Network for High Order Modulation Schemes," *International Journal of Antenna and Propagation*, submitted, 2013.

In addition to the main papers, the following publications have also been made.

[M] R. Soman, T. Onoufriou, R.A. Votsis, C.Z. Chrysostomou, M.A. Kyriakides, B. Han, "Wireless Sensor Placement based on SHM Requirements and net Energy Consumption," *The 2nd International Conference on Civil Engineering and Building Materials*, pp. 271–275, 2012.

[N] Ma. Rajashekara, B. Han, S. Vassilaras, A. Kalis, "Energy efficiency of cooperative beamforming in wireless sensor networks," *International Journal of Antenna and Propagation*, submitted, 2013.

Part I

Thesis Introduction

Chapter 1

Introduction

1 A Short Story

In 1844, Samuel Finley Breese Morse sent the first telegraph with *Morse code* over several kilometers. In 1897, Marconi sent the first wireless telegraph. The Bell Labs tested the first mobile communication in 1946, with equipment that weighed 36kg and had to be carried by car. It was not until 1973 that the first portable mobile communication was shown to the media by Motorola. After that, people started to realize the convenience of using mobile phones in their daily life and since then wireless communication has exploded dramatically. During this evolutionary period, the electronic devices also changed from vacuum tubes to bipolar transistors, even to today's *nanometer* CMOS transistors. The scaling down and integration of electronic components has enabled communication terminals to become even smaller. Nowadays the functions of cellular network, WiFi, bluetooth and GPS can be integrated all together into a hand sized device to accommodate high definition video/voice and high speed data instead of sending "." and "-" as Morse did 170 years ago.

The development of modern communications requires a reliable, high data rate and large capacity communication system [13]. With the help of advanced digital signal processing as well as the scaling down of electronic components dimensions, such requirement can be satisfied. Meanwhile, the spectrum becomes congested as the number of wireless communication systems increase. It is necessary for the contemporary communications to use the spectrum efficiently, since most of the communications are limited to a specific band in the spectrum.

In order to increase the data rate and use the spectrum efficiently, higher order modulation schemes were proposed, which can encode (map) more complex signals in one symbol period. For example, with modulation order of 2, the QPSK signaling carries twice the information of BPSK (binary) signaling. It has been proved that the data rate

of M-ary signaling is $\log_2 M$ times its symbol rate.

However, the higher order modulation itself is not an ultimate solution to solve all the problems. Thus the MIMO approach was proposed in order to increase the link's spectrum efficiency. A MIMO system with M_t transmission antennas and N_r receiving antennas, can transmit/receive $min(M_t, N_r)$ multiple streams simultaneously. Diversity gain in MIMO systems can overcome the channel fading and improve error performance. Spatial multiplexing can increase the system capacity and spectrum efficiency. In spatial multiplexing, different data streams are transmitted through different antennas at the same frequency. With the assumption that the spatial sub channels between the transmission and receiving antenna arrays are different from each other, the spatial degrees of freedom can enable the transmitted signals to be distinguishable at the receiver [15]. Thus multiple data streams are transmitted together by spatial multiplexing without an extra bandwidth (frequency) burden. MIMO techniques can also increase the signal coverage range, extending the communication link range with even higher order modulations.

However, the performance gains of MIMO systems are obtained at the cost of using more antennas, that require more radio frequency chains leading to more circuit complexity and more power consumption. Multiple antennas also constrain the device dimension, because the separation of radio frequency chains from each other requires certain spacing between antennas. Moreover, the power consumption of the multiple antenna system restricts its application on mobile devices.

2 Energy Concerns

Energy constraints are one of the biggest obstacles for the MIMO techniques to be used on mobile devices. Indeed, the power consumption problems on mobile communications can be traced back to when the first mobile communication equipment was invented at Bell Labs. At that time, the circuit component dimensions were large and the power consumption was high, so heavy batteries were used and an automobile was used for the *mobile* communication test. Although there have been great advances in down scaling and integration of electronic components, the power consumption of the mobile device remains a problem because the applications on mobile terminals become more and more demanding. As *cloud* computing and storage become popular, more and more mobile devices are linked to the internet, such as smart phones. However, the high speed radio links in today's mobile networks are power hungry, meaning that the batteries in mobile devices are exhausted so quickly that they cannot support long working time. One of the solutions for this problem is to use larger capacity batteries. After smart phones have become more widely used, the capacity of a mobile battery has increased from several hundred mAh to several thousand mAh. However, this has meant that extra weight has been added to the mobile devices in the form of larger batteries. Moreover, larger battery capacity is a potential safety concern, so not an ideal solution for portable device.

In short, energy is a big concern in mobile communications. It is of great importance for a mobile terminal to use the power efficiently. Instead of going the direction of creating large capacity batteries, this thesis focuses on using the energy more efficiently. It addresses the following areas:

- low cost MIMO transmission
- energy efficient sensor networks
- energy harvesting

3 Low Cost MIMO Transmission

The MIMO system can increase the reliability of the channel and reduce the error probability of the link by the diversity gain, which can overcome the fading effects on the channel. Assuming a MIMO system with $M_t \times N_r$ configuration, where the Rayleigh fading coefficients among M_t transmitters and N_r receivers are independent and uniformly distributed, then a maximum of diversity gain can be achieved. The MIMO system can also increase the system capacity by the spatial multiplexing gain. Assuming the fadings among the Tx/Rx antenna pairs are independent, the aerial degree of freedom can be exploited to attain a large system capacity.

However, multiple antennas are typically used in MIMO systems, in a way that each antenna is linked to an individual radio frequency chain. A simple radio chain contains a power amplifier (PA) and low noise amplifier (LNA), which are the most power hungry components in a communication link. Thus an $M_t \times N_r$ MIMO system needs M_t PAs and N_r LNAs. Those additional electronic components make the power consumption of MIMO system approximately $M_t \times N_r$ bigger than a SISO system.

As mentioned in Section 2 of this chapter, power consumption on mobile terminals is a major concern in today's communication systems. Thus a low cost MIMO transmission technique is needed [6] to maintain the performance of the MIMO system with low power consumption. The single RF MIMO transmission [20] was proposed as a low cost solution. Instead of having multiple active antennas to transmit MIMO data streams, this technique uses only one RF chain while it maps MIMO symbols on to the radiation patterns [23]. Through proper reception, an equivalent MIMO system performance can be achieved with low complexity hardware.

Mapping MIMO symbols on to the radiation pattern can be achieved with the help of Electronically Steerable Parasitic Array Radiators (ESPAR) This is an antenna array made of one active element surrounded by controlled passive elements [19]. Due to the mutual coupling among the antenna elements, the current on the active elements can be changed by changing the load of the passive elements [19]. Changing the current distribution on the antennas in turn alters the radiation pattern, and different patterns can be used to represent different MIMO symbol combinations. Fig. 1.1 provides a

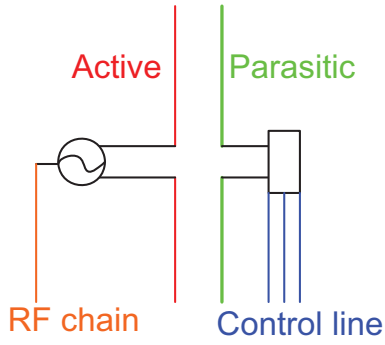

Fig. 1.1: The brief diagram on concept of single RF over ESPAR antenna

basic depiction of the single RF MIMO ESPAR array, where the sole RF chain goes to the active antenna element. MIMO symbols are mapped on to the radiation patterns by changing the parasitic load. As it shown in previous work [19], this kind of single RF MIMO transmission can achieve a similar performance to the traditional MIMO techniques [12]. In [19] a single RF MIMO transmission was proposed and measured under a BPSK modulation scheme [19]. Following this direction further, higher order modulation with a single RF MIMO transmitter was investigated. The QPSK signaling was first tried in [10] and followed by a 16-QAM signaling trial in [12]. The performance of a single RF channel was simulated and found to be similar to conventional RF, while the energy consumption was reduced due to the fact that only one RF chain is used. Detailed information on the analysis can be found in papers [3] [11] [12], whereas an overview of the recent field of parasitic arrays for MIMO communication can be found in [1].

4 Energy Efficiency of Sensor Networks

Low cost MIMO transmission is a promising technology for mobile networks [16]. Apart from mobile networks, wireless communication has another significant application, that is: wireless sensor networks. The wireless sensor network is composed by a number of sensor nodes that can sense and capture the target information, and send the data wirelessly to the "observation center" (fusion center). It can be a self-organized network that can change its topology (routing) dynamically according to the configuration of its new nodes typically without central control. Today wireless sensor networks are used in a wide range of application such as logistics systems and monitoring systems (weather monitoring, climate monitoring, structural health monitoring), etc. Despite its wide acceptance in daily life, the service life of the wireless sensor network has raised

significant concerns. Since most of the sensor nodes are powered by batteries, how to use the energy efficiently is the subject of considerable attention. The energy used in a wireless sensor network can be categorized into two parts: the sensor nodes power consumption and the radio link (for sensor nodes communications) power consumption. The sensor node power consumption includes the power used for sensing and data processing and any other circuit power consumption. The radio link consumption contains the hopping/routing power consumption in the wireless link.

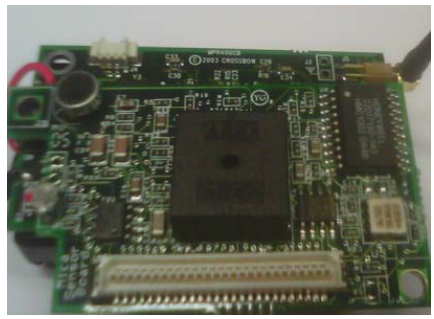

Fig. 1.2: A wireless sensor node

Fig.1.2 shows a picture of a wireless sensor node. As seen in the picture, the node contains several sensing units (microphone, light sensor, accelerometer) and one radio unit (900MHz). The power management unit is on the back along with the battery. To increase the energy efficiency of the wireless sensor network, both the sensor nodes power consumption and the radio link power consumption have to be considered together. Low cost, low complexity sensor node architectures were proposed in [5]; several novel wireless sensor network topologies were proposed in [5] to reduce the unnecessary relay/routing radio link power consumption. The quantization of energy efficiency in wireless sensor networks was analyzed in [12] and [21], which considered both sensor node consumption and radio link consumption together. Based on the bit error rate requirement in a bandwidth limited system, the evaluation was made in [22] for different communication protocols. In addition an energy efficiency analysis of the communication link was given in [14]. In practice, there is more than one factor that influences the radio link performance, which in turn affects the energy efficiency of the radio link [7]. More details of the energy analysis of wireless sensor network can be found in papers [2], [5], [7].

5 Energy Harvesting

Although there are several methods for improving the energy efficiency of the wireless sensor network, as well as a plethora of designs for low complexity low cost radio link

architectures, the battery-powered mobile terminals [4] will run out of power sooner or later. Moreover, in certain applications such as structural health monitoring, the wireless sensor nodes are embedded inside the structures. The battery replacement in such system is not an easy task [17], either because of the extra labor involved in the task or because of potential damage to the structure. It is attractive for such systems to have a backup power supply. Thus, harvesting energy [18] from the environment was proposed [4]. Energy harvesting converts the energy from one physical (thermal, radiation, kinetic, etc.) domain [9] into another physical (electrical) domain. More specifically, the conversion can be from energy sources such as solar energy, radio frequency electromagnetic radiation energy [8], kinetic (wind, tide, vibration) energy [4], thermal energy, etc. Energy is converted in the physical domain instead of the chemical domain which avoids the pollution offering an environmental friendly energy solution. Moreover, the sources for energy harvesting usually contain abundant energy providing a long term solution that extends system lifetime.

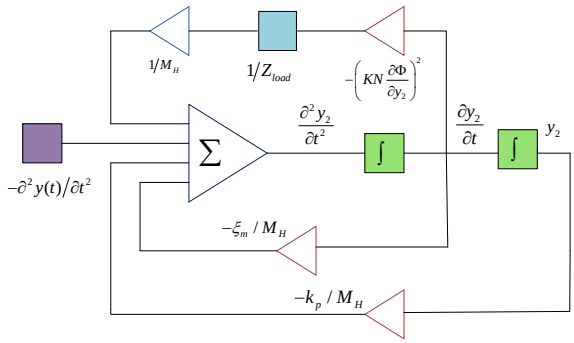

Fig. 1.3: The vibration model of an energy harvester

In this thesis, two main energy harvesting techniques are analyzed: radio frequency energy harvesting and vibration energy harvesting. Taking the vibration energy harvesting as an example, as shown in Fig. 1.3, the mathematical model of the vibration energy harvester links the mechanical domain with electrical domain. Where M_H is the mass of the energy harvester, $-\partial^2 y(t)/\partial t^2$ stands for the vibration source, ξ_m is the mechanical damping factor, k_p is the damping of the spring connected to the harvester. $N\partial\Phi/\partial z$ is the electrical parameter representing the magnetic flux changing ratio of the harvester, $\partial^2 y_2/\partial t^2$,$\partial y_2/\partial t$,$y_2$ are the acceleration, the velocity and the displacement

of the harvester respectively. More detailed information can be found in [9] One of the key techniques in energy harvesting is the voltage boosting, which converts the low voltage at harvester to high voltage on the electrical load [9]. The voltage regulator with voltage boosting technique is needed especially for the harvester to provide a high enough output voltage. Several voltage boosting techniques are also discussed in the manuscript. More details on this can be found in papers [7], [8], [9].

6 Thesis outline

The thesis contains an introduction part and appendix with published or to be appeared papers. Thin traduction part contains 5 small chapters and each of them are summary of the published papers. Apart from the introduction part The main body of the thesis contains 12 papers which are listed from A-L appended after the introduction part. Two additional papers are also in that list ranged from M to N.

Table 1.1: Composition of the Chapters with relevant papers

Chapter	Name	Relevant Papers
Chapter 1	Introduction	
Chapter 2	Low complexity MIMO	[A] [B] [D] [K] [L]
Chapter 3	Energy efficient sensor networks	[C] [E] [J] [M] [N]
Chapter 4	Harvesting Energy from the Environment	[F] [G] [H] [I]
Chapter 5	Conclusions and Future work	

Under the frame work of the European Commission founded Marie Curie Project, (namely " Smart Management for Sustainable Human Environment "-in short, SmartEN) the research is applied and validated from the experts in Civil Engineering inside the project. Based on the practical parameters from Civil Engineering, the energy harvesting part gives an insight of the application of energy efficient wireless senor network in the real world.

7 Scientific Contributions

In this thesis, the following main contributions have been made.

- A novel single RF MIMO transmission architecture was proposed which supports two data streams with 16-QAM modulation.
- Extensions of the above techniques that work with higher order modulation schemes.

- The modelling of the energy efficiency of sensor nodes that are quipped with single RF antenna arrays, considering both the circuit dissipation and transmission power of the sensor nodes.
- The analysis of the energy efficiency of single hop cooperative beamforming sensor networks, using the above model.
- A low cost architecture for sensor nodes in single hop cooperative beamforming sensor networks.
- A quantification of the harvestable energy by use of micro-generator equipped sensors in structural health monitoring.
- A dynamic adjustable voltage rectifier circuit topology that can optimize the power delivery in the above applications.
- A "floating gate" voltage rectifier architecture that can boost up the voltage and with reduced threshold voltage.

References

[1] A. Kalis, A.G. Kanatas, C.B. Papadias, Ed., *Parasitic Antenna Arrays for Wireless MIMO Systems*. Springer, 2013.

[2] B. Han, A. Kalis, C.B. Papadias, P. Tragas, R.H. Nielsen, R. Prasad, "Low cost localization techniques in structural damage detection," *The IABSE Conference on Assessment Upgrading and Refurbishment of Infrastructures*, vol. 1, pp. 826–831, 2013.

[3] B. Han, A. Kalis, C.B. Papadias, R. Prasad, "Energy efficient MIMO transmission with high order modulation for wireless sensor network," *European Signal Processing Conference (EUSIPCO)*, vol. 1, pp. 1–5, 2013.

[4] B. Han, A. Kalis, C.B. Papadias, R. Soman, M.A. Kyriakides, T. Onoufriou, R.H. Nielsen, R. Prasad, "Energy harvesting for sensors in infrastructure monitoring and maintenance," *The IABSE Conference on Assessment Upgrading and Refurbishment of Infrastructures*, vol. 1, pp. 404–410, 2013.

[5] B. Han, A. Kalis, P. Tragas, R.H. Nielsen, R. Prasad, "Low cost wireless sensor network for continuous bridge monitoring," *The 6th International IABMAS Conference on Bridge Maintenance, Safety, Management, Resilience and Stainability*, vol. 1, pp. 96–97, 2012.

[6] B. Han, A. Kalis, R. Prasad, "Matching parasitic antenna for single RF MIMO," *IEEE International Conference on Microwave and Millimeter Wave Technology (ICMMT)*, vol. 1, pp. 1–4, 2012.

[7] B. Han, R.H. Nielsen, C.B. Papadias, R. Prasad, "Directional transmission by 3-D beamforming using smart antenna arrays," *International Conference on Wireless Communications, Vehicular Technology, Information Theory and Aerospace Electronic Systems Technology (Wireless ViATE)*, vol. 1, pp. 26–28, 2013.

[8] ——, "Radio frequency energy harvesting for long lifetime wireless sensor networks," *International Symposium on Wireless Personal Multimedia Communications (WPMC)*, vol. 1, pp. 1–5, 2013.

[9] B. Han, S. Vassilaras, C.B. Papadias, R. Soman, M.A. Kyriakides, T. Onoufriou, R.H. Nielsen, R. Prasad, "Harvesting energy from vibration of the structure," *Journal of Vibration and Control*, vol. DOI: 10.1177/1077546313501537, pp. 1–10, 2013.

[10] B. Han, V.I. Barousis, A. Kalis, A.G. Kanatas, "Active parasitic arrays for low cost compact MIMO transmitters," *IEEE 5th European Conference on Antennas and Propagation (EUCAP)*, vol. 1, pp. 3663–3667, 2011.

[11] B. Han, V.I. Barousis, A. Kalis, C.B. Papadias, A.G. Kanatas, R. Prasad, "A single RF MIMO loading network for high order modulation schemes," *International Journal of Antennas and Propagation*, vol. to appear, pp. 1–10, 2013.

[12] B. Han, V.I. Barousis, C.B. Papadias, A. Kalis, R. Prasad, "MIMO over ESPAR with 16-QAM modulation," *IEEE Wireless Communication Letters*, vol. DOI: 10.1109/WCL.2013.13.130433, 2013.

[13] M. Dohler, R. Heath, A. Lozano, C. Papadias, and R. Valenzuela, "Is the phy layer dead?" *Communications Magazine, IEEE*, vol. 49, no. 4, pp. 159–165, 2011.

[14] E.P. Tsakalaki, O.N. Alrabadi, A. Kalis, C.B. Papadias, R. Prasad, "Non cooperative space-time communication for energy efficiency in sensor networks," *IEEE Transactions on Communications*, vol. 60, pp. 48–54, 2012.

[15] H. Bolcskei, D. Gesbert, C.B. Papadias, A.J. V. Veen, Ed., *Space-Time Wireless Systems*. Cambridge, 2006.

[16] H. Huang, C. B. Papadias, S. Venkatesan, *MIMO Communication for Cellular Networks*. Springer, 2012.

[17] M. Bhardwaj, A.P. Chandrakasan, "Bounding the life time of sensor networks via optimal role assignments," *IEEE Proceedings of INFOCOM*, vol. 3, pp. 1587–1596, 2002.

[18] N.G. Elvin, N. Lajnef, A. ElviN, "Feasibility of structural monitoring with vibration powered sensors," *Smart Materials and Structures*, vol. 15, pp. 976–986, 2006.

[19] O.N. Alrabadi, C.B. Papadias, A. Kalis, R. Prasad, "A universal encoding scheme for MIMO transmission using a single active element for PSK modulation schemes," *IEEE Transactions on Wireless Communications*, vol. 8, pp. 5133–5142, 2009.

[20] O.N. Alrabadi, J. Perruisseau-Carrier, A. Kalis, "MIMO transmission using a single RF source: theory and antenna design," *IEEE Transactions on Antennas and Propagation*, vol. 60, pp. 654–664, 2012.

[21] S. Cui, A.J. Goldsmith, A. Bahai, "Energy efficiency of MIMO and cooperative MIMO techniques in sensor networks," *IEEE Journal on Selected Areas in Communications*, vol. 22, pp. 1089–1098, 2004.

[22] S.K. Jayaweera, "Virtual MIMO based cooperative communication for energy-constrained wireless sensor networks," *IEEE Transactions on Wireless Communications*, vol. 5, pp. 984–989, 2006.

[23] V.I. Barousis, A.G. Kanatas, A. Kalis, "Beamspace domain analysis of single RF front-end MIMO systems," *IEEE Transactions on Vehicular Technology*, vol. 60, pp. 1195–1199, 2011.

Chapter 2

Low complexity MIMO Transmitters

1 Low Complexity Communications

Low cost low complexity communication has attracted a lot of attention, and great amount of work has been conducted towards that goal. e.g., the low cost routing techniques, the low cost adaptive modulation methods/coding techniques, as well as low cost delay and power control algorithms. These methods all consider the communication cost on the air link [3], but it is actually the power consumption on the RF/IF circuit also need to be addressed.

For wireless sensor networks, most of the power is consumed in the communication link [4]. In order for the sensor network to achieve a long lifetime, it needs to have a power efficient design [5], suggesting that all the blocks/sensor nodes need to have as low complexity as possible. Moreover, the communication protocol should be as simple as possible so that only basic components on the commination link are used. In some approaches, the signals are processed in the analog domain in order to avoid signal processing cost.

The network topology also influences the energy efficiency; it is obvious that in multi-hop techniques, often the sensor nodes are just forwarding packets instead of sending their own useful data. Such redundancy reduces the overall system energy efficiency. A critical attribute for multi hop topology is a good routing algorithm, so that the information is passing through a minimal number of relay nodes.

Paper [5] gives an insight about how low-cost wireless sensor networks can be designed by considering some new topologies, e.g. the low-complexity communication link by the active reflection, where the sensor node just modulates the incoming wave with

the information bit and reflects it back. This results in simple sensor node architecture with very low power consumption [1]. The so called Frequency Modulated Continuous Wave communication (FMCW) can reduce the senor node to an extremely low complexity which is a good solution for asymmetric network topologies.

In some network topologies, the MIMO technique is used, where the communication link enjoys the benefits of spatial multiplexing, such as better spectrum efficiency, lower error probability, etc [17]. But the MIMO technique itself is not a low-complexity/low-cost solution. Recent research has attained to emulate MIMO mass mission while avoiding disadvantages such as the large power consumption. This is particularly useful when large number of antennas are used in MIMO techniques to support large capacity and high data rate, drive the circuit power consumption to unacceptably high levels.

The device size of the wireless sensor node is another constraint. In the application of environmental sensing, the sensor nodes are usually very small with dimensions of a few centimeters and compact components. Usually the sensor antennas are printed directly on the circuit board making it difficult to have enough space for the MIMO antennas to be mounted. This has to be considered very carefully and demands a different approach to enable MIMO techniques to be implemented in wireless sensor nodes.

To use the MIMO techniques without the extra power burden as well as within compact size constraints, an alternate way is to exploit the multi path as controlling the radiation beam angle from the transmit antenna. "Angular degrees of freedom" can replace aerial degrees of freedom if the transmitter can alter its radiation pattern with different symbols. So if a special antenna or radio frequency front end circuit can be designed to do the job, then the problem is well on its way to being solved. However, according to the MIMO requirement, to have independent fading/multi paths, the antenna spacing should be larger than 2λ, (where λ is the wavelength) []. It does not seem easy to apply such requirement on a sensor node with compact design.

So, in summary, the required solution for a wireless sensor network is a communication system with low complexity and low power consumption which, at the same time, is of a compact size compatible with the sensor node dimensions.

2 The ESPAR Antenna

It seems that a MIMO-based solution that can ensure the functionality of the spatial multiplexing and still be of compact size is needed to support low-cost, low-complexity requirements.

From the point of compact size, the recently investigated electronic steerable parasitic array radiator (ESPAR) [11]is a possibility. It is a kind of compact antenna array where one of the elements is connected with an active radio frequency source, while the remaining antenna elements are parasitic. They are located close to the active element within λ/N, where N is an integer. Because of such short inter-element distance, the mutual coupling among the antenna elements comes into effect. In the conventional

MIMO transmission case, this mutual coupling is considered a drawback and should be avoided so that the symbols are faded independently through the channel. However, the mutual coupling can be used as an advantage in the case when the electronic steerable parasitic array radiator is considered.

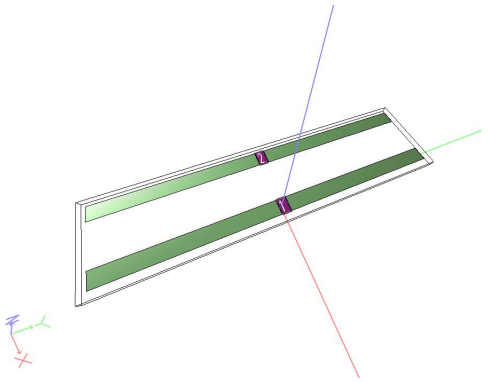

Fig. 2.1: A 3D view of an ESPAR antenna with two elements

Fig. 2.1 gives a space view of a printed ESPAR antenna with two dipole elements spaced at $\lambda/16$. The two ports "1" and "2" are the active port, and the parasitic port respectively. The active port is connected to the conventional radio frequency chain which ideally should be matched to 50 Ω to reduce the return loss; while the parasitic port is connected to the load which has complex values. The parasitic port does not need to be matched to 50 Ω, it is connected to tunable antenna load with variable value.

According to the antenna theory, changing the current distribution on the antenna elements can influence the far field pattern. It holds true for all antennas, because the current distribution changes the initial electromagnetic field. For ESPAR antennas, due to mutual coupling among the elements, changing the current distribution on one element will influence the other elements as well. Hence, the radiation patterns of the ESPAR antenna can be altered by changing the current distribution on the parasitic element.

To change the current distribution, there are several approaches: change the self-characteristic of the parasitic element (such as change the length/width); change the inter-element distance among the parasitic and active element; or change the antenna load connected to the parasitic element. In modern communications, antennas are designed and fabricated on a fixed layout so it seems impractical to change the inter-element distance as well as the length or width of antenna element. So the most convenient way of changing the current distribution is to change the antenna load connected to the parasitic elements, because changing of load does not require dynamically changing the antenna layout.

So the parasitic antenna array can be considered as a compact solution for the low cost communication, since the antenna elements are placed within λ/N which is considerably more compact than the $N\lambda$ requirement in some protocols. By changing the load of the parasitic elements, the radiation pattern can also be changed. An extreme case of the antenna load is ground, where the parasitic elements are considered to be switched on/off to the antenna array.

It is noted that the active element on the parasitic array antenna is connected to a conventional radio frequency chain, which means that the information data stream still goes through this active port to be radiated. At the same time, it is different from the conventional radiation which is omnidirectional; the ESPAR radiation pattern can be altered by changing the load on the parasitic element. Different radiation patterns have different maximum gain direction, which means the symbols undergo different fading. The different radiation patterns achieve an angular degrees of freedom, so even with one active element, it is still possible to support several data streams through independent fading.

So the parasitic antenna array can be considered the capable of MIMO transmissions. Although just one active element is used, it still has the ability to encode the extra space (angle) information. Moreover, such extra encoding does not require power hungry radio frequency circuits. The changing of load values on the parasitic element can be even done by normal digital signals at the frequency of the symbol rate.

3 Single RF MIMO over ESPAR

As mentioned in the last section, the electronic steerable parasitic array radiator can be used to encode with angular degrees of freedom. This capability can be used for MIMO transmission, especially for 2×2 MIMO systems. From the previous section we know that the ESPAR antenna is able to *modulate* different radiation patterns by changing the load connected to the parasitic element [2]. Such kind of pattern *modulation* can be used to transmit information. Thus if the data streams can have certain kind of mapping to such radiation patterns, and let the other data stream go through the active port, then single RF MIMO transmission is feasible.

Thus a new concept namely as Single RF MIMO transmission was proposed, which only uses one RF chain in the communication link, while still keeping the capability of MIMO transmission by changing the different radiation patterns. This technique is inseparable from the parasitic antenna arrays, for the reason that it is implemented by changing the radiation patterns using different parasitic loads. It has the inherent compact size advantage since the parasitic elements on such arrays are usually placed close to one another. Without loss of generality, considering propagation over the azimuth plane, i.e. $\theta = \pi/2$, the radiation pattern of an ESPAR antenna with M elements, including the active one, is expressed as a linear combination of M basis patterns as:

$$P(\varphi) = \sum_{n=0}^{M-1} w_n \Phi_n(\varphi) \tag{2.1}$$

It has been shown that the shape of all basis patterns depends on the inter-element distance, while the coefficients w_n depend on the inter-element distance and the currents.

The MIMO data streams are expected to go through independent fading so that the receiver can have the diversity gain due to the multi-path of the information traveling through the air. It is critical for the radiation patterns of the EAPAR antenna to be as different as possible from each other, so that the performance of the MIMO transmission can be as close as that in conventional MIMO transmission. Here "different" means that the correlation should be as small as possible (One of the independent cases is orthogonal). It is widely accepted that the two orthogonal variables are independent to each other.

The orthogonally of the radiation pattern has been used for single RF MIMO transmission, based on the construction of basis patterns. It has been mathematically proven that, for single RF MIMO transmission with two data streams of BPSK signals, the orthogonal basis patterns combined with certain re-formulated data streams will have orthogonal combined far field patterns at the receiver [13]. One data stream goes through the active port and the other goes to a *XOR* gate to generate a *mapping* data stream to change the radiation patterns. For an ESPAR antenna with 2 elements the basis patterns are given by [18]:

$$\begin{aligned} \Phi_0(\varphi) &= 1/k_0 \\ \Phi_1(\varphi) &= \left(e^{jb\cos\varphi} - 2\pi I_0(jb)/k_0^2\right)/k_1 \end{aligned} \tag{2.2}$$

where

$$\begin{aligned} k_0 &= \sqrt{2\pi} \\ k_1 &= \sqrt{2\pi + \left(\pi/k_0^2 - 1\right) 8\pi^2 I_0^2(jb)/k_0^2} \end{aligned} \tag{2.3}$$

and the coefficients in (2.1) are given by

$$\begin{aligned} w_0 &= i_0 k_0 + 2\pi i_1 I_0(jb)/k_0 \\ w_1 &= i_1 k_1 \end{aligned} \tag{2.4}$$

where $b = 2\pi d$, d is the inter-element distance normalized to wavelength and $I_0(x)$ is the zero-th order modified Bessel function of the first kind. Equation (2.1) reveals the functionality of the single RF MIMO transmitter: Indeed, letting the coefficients w_n be the complex symbols for transmission of any signal constellation, (2.1) shows that two symbols have been attached, i.e. mapped, to different basis patterns.

Previous work towards this goal has successfully shown that the single RF MIMO transmission is theoretically feasible and practically implementable under BPSK modulation schemes [15]. It was verified by using an ESPAR antenna with three elements, one

active with two surrounding parasitic elements, that the BPSK signal goes through the *XOR* gate to generate combined mapping symbols [13]. Such mapping symbols control the parasitic antenna loads which are built with varactors. The radiation pattern is modified by changing the capacitance of the varactor (which is actually changing the load value of the parasitic element.) by mapping the symbols, where the mapping symbols only have two status, "0" and "1". It has been verified, by having two conventional MIMO receiving antennas, that the single RF MIMO transmission is successful for two data streams with BPSK signaling over the air [14].

The BPSK constellation is not particularly bandwidth efficient in modern communications. Although the single RF transmission was proven feasible under BPSK constellation, the trend for today's communication is to have more complex signaling (such as 16-QAM, 64-QAM, OFDM, etc.) that can support high data rates with better bandwidth efficiency. A solution for any PSK modulation has been proposed by [12], thus it is necessary to direct research towards adopting higher order modulation schemes under the framework of single RF MIMO transmission.

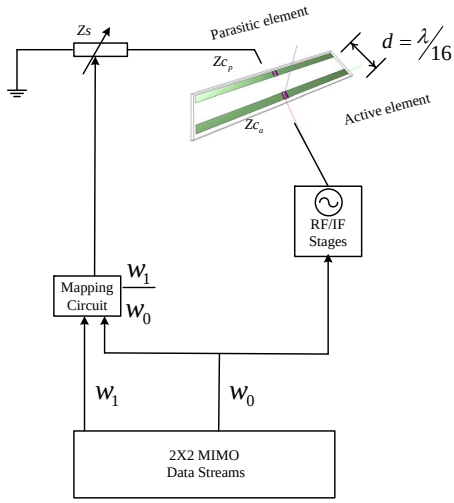

Fig. 2.2: Topology of the proposed single RF MIMO Transmission system.

In search of a solution for higher order non constant-modules modulation on Single RF MIMO transmission over ESPAR antenna, the 16-QAM signaling was researched in this thesis. The M-ary signals are quite different from BPSK signals in the mapping symbols generation. Due to the fact that M-ary signaling has both phase and amplitude differences, it is difficult to have an orthogonal combination of the mapping symbols as it was in the case of BPSK signaling.

So the high order modulation of single RF MIMO over ESPAR antenna actually requires a different approach for non-PSK signaling. Where the single RF MIMO with 16-QAM is used, the symbols are combined as simply as possible while the basis patterns are orthogonal. For two data streams w_0 and w_1, One easy method of combination is w_0/w_1 , which means the mapping symbols for the parasitic elements are actually from the combination of two MIMO data streams with a simple "division" circuit block in contrast to BPSK where it was an *XOR* gate. Such method of combination has some advantages and disadvantages. Firstly, it is simple and does not require a very complex circuit, which is important for high speed transmission. The less complex the circuit is, the higher is the potential for high speed operation. The disadvantage of combining in this way is that the mapped symbols become complex signals. According to the parasitic load calculation, this combination can cause negative load values.

For 2×2 MIMO data streams w_0, w_1, with 16-QAM modulation, recalling (2.1), the pattern becomes:

$$P(\varphi) = w_0 \left(\Phi_0(\varphi) + \sum_{n=1}^{M-1} \frac{w_n}{w_0} \Phi_n(\varphi) \right) \tag{2.5}$$

Equation (2.5) describes the triggering operation of the transmit ESPAR antenna. The first symbol w_0 is driven to the sole RF port, while the ratio w_n/w_0 $(n = 1, ...M-1)$ determines the shape of the pattern.

The impedance of the parasitic antenna shown in Fig.2.1 is considered as Z_{11}, Z_{22} for the self impedance of the active port and parasitic port respectively, and Z_{12}, Z_{21} are the mutual impedances due to the mutual coupling on the ESPAR antenna.

The current distribution $[i_0 \ , i_1]^T$and the parasitic load jx_1 are considered in the following equation:

$$\left(\begin{bmatrix} Z_{11} & Z_{12} \\ Z_{21} & Z_{22} \end{bmatrix} + \begin{bmatrix} 50 & 0 \\ 0 & jx_1 \end{bmatrix} \right) \begin{bmatrix} i_0 & i_1 \end{bmatrix}^T = \begin{bmatrix} u_s & 0 \end{bmatrix}^T \tag{2.6}$$

As mutual coupling impedances are identical $(Z_{21} = Z_{12})$, so the parasitic load value x_1 can be derived from (2.6) by:

$$x_1 = -\left(\frac{i_0}{i_1} Z_{21} + Z_{22} \right) \tag{2.7}$$

According to (2.4), the above value can be rewritten as:

$$x_1 = -\left(\left[\frac{w_0}{w_1} - \frac{2\pi I_0(jb)}{k_0 k_1} \right] \frac{k_1}{k_0} Z_{21} + Z_{22} \right) \tag{2.8}$$

where Z_{21} is the mutual coupling of the two antenna elements shown in Fig. 2.1.

As shown in equation (2.8), the required parasitic load x_1 becomes negative in order to satisfy the mathematical calculation. However, it is not often to have negative resistance values, because negative resistance means extra power is required to *looks like* negative. Moreover, no passive components can have such function.

To solve the negative load value problem, the active circuit is used to generate the required value at the cost of extra power. If the negative load consumes even more power than an active RF chain, then the approach of single RF MIMO transmission is ruled out. Hence, the CMOS circuit for the negative load value generation is considered.

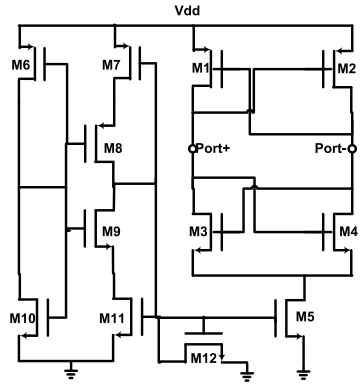

Fig. 2.3: Active circuit for negative resistance generation.

By using the cross coupling technique, the negative resistance for a crossing coupling core is given by [7]:

$$R_{neg} = -1/g_m \tag{2.9}$$

where g_m is the trans-conductance of the CMOS transistor given by:

$$g_m = \mu C_{ox}\frac{W}{L}(V_{gs} - V_{th}) = 2\frac{\mu C_{ox}}{2n}\frac{W}{L}I_{ds} = \frac{2I_{ds}}{V_{GS} - V_T} \tag{2.10}$$

where g_{mn} and g_{mp} are the trans-conductances of NMOS transistor and PMOS transistor respectively, (2.10) expressed as:

$$g_{m(n,p)} = u_{(n,p)}C_{ox}\frac{W}{L}(V_{gs} - V_{th}) = 2\frac{I_{ds}}{V_{gs} - V_{th}} \tag{2.11}$$

Moreover, $\mu_{(n,p)}C_{ox}$ is a process-related coefficient, W/L is the ratio of channel width and channel length of the transistor, I_{ds} is the current flowing through the transistor, V_{gs} is the voltage between gate and source and V_{th} is the threshold voltage of the transistor. The smaller the current I_{ds}, the smaller negative resistance we get. In sub micro-meter processes, the effect of the channel length should be taken into consideration [16]:

Under UMC0.18 μm CMOS process, the simulated power consumption of the negative circuit is of the order of several hundred μW [8]. This sounds promising for the

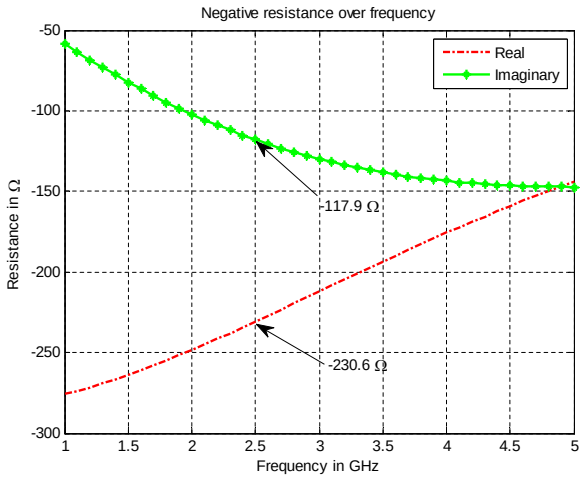

Fig. 2.4: Simulated negative resistance values.

single RF MIMO transmission, because the power consumption of a typical RF chain ranges from several mW to several hundred mW. Moreover, when the distance of the communication link increases, the power consumption in the RF chain also increases, but the power consumption for the active load remains the same since it is just used for changing the load value instead of transmitting the signal into the air.

A further challenge of higher order modulation for single RF MIMO is the load switching. For two data streams of 16-QAM modulation MIMO symbols, theoretically, there should be 256 combinations. However, due to the symmetry of w_0/w_1, only 64 different values are required. Even though the required number of loads is reduced to 64, a certain number of stages are still needed to select the loads to be connected to the parasitic antenna element.

To select the right value for a desired radiation pattern, many different approaches have been tried. Direct control of the CMOS circuit generates unwanted and uncontrollable side effects. Since the load value for a radiation pattern must control the real and imaginary parts simultaneously, a special control unit was investigated. The analog control method [6] needs a very fast analog signal that can be changed rapidly and precisely in a symbol period. In contrast, digital control, using a 8×8 array with predefined values inside each unit [9], seems more convenient.

The system performance of the single RF MIMO over ESPAR antenna with 16-QAM modulation was simulated and compared that with conventional MIMO transmitter [10]. Due to the process variation and the error tolerance of the load values (which are actually frequency sensitive), it appears that the system performance remains quite similar to

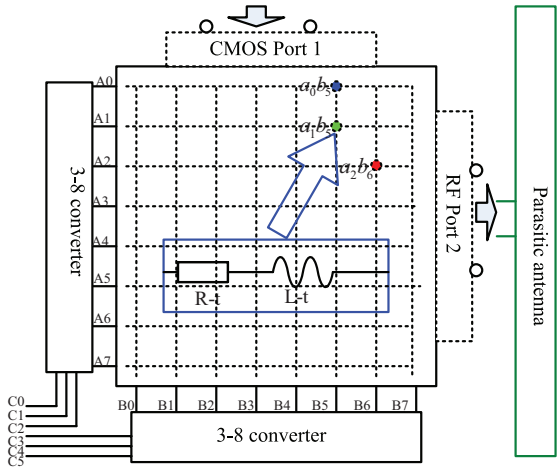

Fig. 2.5: The digital controllable impedance switching circuit block.

conventional MIMO techniques.

4 Conclusion of Compact RF Designs for MIMO Transmission

The desired low cost, low-complexity MIMO technique can be realized by the single RF MIMO transmission which maps the MIMO symbols on to the radiation patterns. By using the Electronic Steerable Parasitic Array Radiators, one data stream of the MIMO symbols is re-directed to a mapping circuit that converts the symbol in to a control signal for the antenna load, whereas the other data stream goes through the normal active port to be radiated into the air as the conventional radio frequency chain.

The use of ESPAR antennas also gives an advantage of compact system size, which is an inherent characteristic of the parasitic antenna array as the antenna elements must be close to each other (less than one wavelength). It is beneficial for the application of the wireless sensors network since most of the sensor nodes are required to be of limited physical size.

For higher order modulation to be adopted for single RF MIMO transmission techniques, a new mapping mechanism was used; that is, to use the ratio of two data streams with M-ary signaling from the MIMO baseband. This mapping leads to a requirement for negative load values, which can be generated from the low cost CMOS circuit. For

16-QAM modulation, the combination of symbols w_0/w_1 has 64 different values, which can be switched through an impedance array. This thesis has proposed the development ideas on single RF MIMO transmission over ESPAR antenna with 16-QAM modulation, which gives a promising possibility for higher order modulations MIMO transmission over ESPAR antenna.

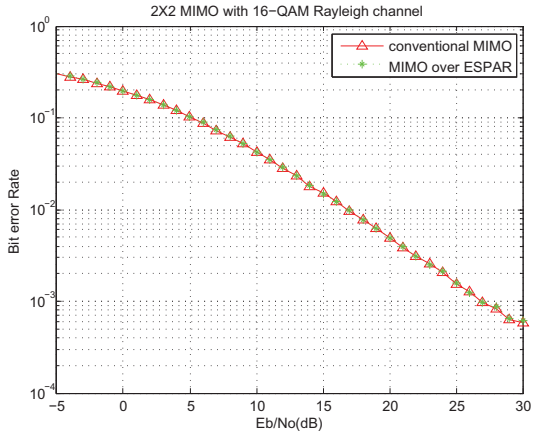

Fig. 2.6: Simulated bit error rate performance.

Compared with the conventional MIMO transmission techniques that use two independent radio frequency circuit chains, the proposed single RF MIMO modulation has similar system performance, while keeping low power consumption, since only one active radio frequency chain is used.

Thus single RF MIMO techniques provide an energy efficiency method of communication since they achieve similar system performance while requiring less power. Moreover, the single RF MIMO transmission is a low complexity and compact solution for wireless sensor network applications, since the sensor node only needs one radio frequency circuit and an extra controlling circuit to change the parasitic antenna load.

References

[1] A. Kalis, A.G. Kanatas, "Cooperative beamforming in smart dust- getting rid of multi-hop communications," *IEEE Pervasive Computing*, vol. 9, pp. 47–53, 2010.

[2] A. Kalis, A.G. Kanatas, C.B. Papadias, "A Novel approach to MIMO transmission using single RF front end," *IEEE Journal on Selected Areas in Communications*, vol. 26, pp. 972–980, 2008.

[3] A. Mohammadi, F.M. Ghannouchi, "Single RF front End MIMO transceivers," *IEEE Communications Magazine*, vol. 49, pp. 104–109, 2011.

[4] B. Han, A. Kalis, C.B. Papadias, R. Prasad, "Energy efficient MIMO transmission with high order modulation for wireless sensor network," *European Signal Processing Conference (EUSIPCO)*, vol. 1, pp. 1–5, 2013.

[5] B. Han, A. Kalis, P. Tragas, R.H. Nielsen, R. Prasad, "Low cost wireless sensor network for continuous bridge monitoring," *The 6th International IABMAS Conference on Bridge Maintenance, Safety, Management, Resilience and Stainability*, vol. 1, pp. 96–97, 2012.

[6] B. Han, A. Kalis, R. Prasad, "Matching parasitic antenna for single RF MIMO," *IEEE International Conference on Microwave and Millimeter Wave Technology (ICMMT)*, vol. 1, pp. 1–4, 2012.

[7] B. Han, V.I. Barousis, A. Kalis, A.G. Kanatas, "Active parasitic arrays for low cost compact MIMO transmitters," *IEEE 5th European Conference on Antennas and Propagation (EUCAP)*, vol. 1, pp. 3663–3667, 2011.

[8] ——, "Active parasitic arrays for low cost compact MIMO transmitters," *IEEE 5th European Conference on Antennas and Propagation (EUCAP)*, vol. 1, pp. 3663–3667, 2011.

[9] B. Han, V.I. Barousis, A. Kalis, C.B. Papadias, A.G. Kanatas, R. Prasad, "A single RF MIMO loading network for high order modulation schemes," *International Journal of Antennas and Propagation*, vol. to appear, pp. 1–10, 2013.

[10] B. Han, V.I. Barousis, C.B. Papadias, A. Kalis, R. Prasad, "MIMO over ESPAR with 16-QAM modulation," *IEEE Wireless Communication Letters*, vol. DOI: 10.1109/WCL.2013.13.130433, 2013.

[11] H. Ochiai, "Collaborative beamforming for distributed wireless Ad Hoc sensor networks," *IEEE Transactions on Signal Processing*, vol. 53, pp. 4110–4124, 2005.

[12] O.N. Alrabadi, A. Kalis, C.B. Papadias, A.G. Kanatas, "Spatial multiplexing by decomposing the far-field of a compact ESPAR antenna," *IEEE PIMRC*, vol. 1, pp. 1–4, 2008.

[13] O.N. Alrabadi, C.B. Papadias, A. Kalis, R. Prasad, "A universal encoding scheme for MIMO transmission using a single active element for PSK modulation schemes," *IEEE Transactions on Wireless Communications*, vol. 8, pp. 5133–5142, 2009.

[14] O.N. Alrabadi, C.Divarathne, P. Tragas, A. Kalis, N.Marchetti, C.B. Papadias, R. Prasad, "Spatial multiplexing with a single radio: proof -of- concept experiments in and Indoor enviroment with a 2.6GHz prototype," *IEEE Communications Letters*, vol. 15, pp. 178–180, 2011.

[15] O.N. Alrabadi, J. Perruisseau-Carrier, A. Kalis, "MIMO transmission using a single RF source: theory and antenna design," *IEEE Transactions on Antennas and Propagation*, vol. 60, pp. 654–664, 2012.

[16] B. Razavi, *RF Microelectronics*. Prentice Hall, 1998.

[17] C. D. T. Thai, P. Popovski, E. de Carvalho, and F. Sun, "Diversity-multiplexing trade-off for coordinated direct and relay schemes," *Wireless Communications, IEEE Transactions on*, vol. 12, no. 7, pp. 3289–3299, 2013.

[18] V.I. Barousis, A.G. Kanatas, A. Kalis, "Single RF MIMO systems: exploiting the capabilities of parasitic antennas," *IEEE 74th Vechicular Technology Conference*, vol. Sep, pp. 5–8, 2011.

Chapter 3

Energy Efficient Sensor Networks

1 Low Cost Wireless Sensor Network

Wireless sensor networks are by now widespread. They are generally composed of a number of sensor nodes locally distributed with their sensed information transmitted wirelessly to the data center. Without the constraints of wired connections, the wireless sensor can be installed almost everywhere when it is necessary. Such easy and convenient installation greatly extends its sensing and information collecting capabilities. Wireless sensors can be found almost everywhere around, e.g. in the distribution centre, the airport, the hospital, even on the street and the highway. They can be used for production process monitoring, for smart transportation, for low cost localization [2] or structural health monitoring and environment sensing [4]. All these applications of wireless sensor networks have made the human life more easy, convenient and safe [7].

Although there are so many advantages to the wireless sensor, it has a basic flaw compared to the wired sensors, that is, the life time. The convenience of going wireless without the need for cable is at the expense of internal power sources: the batteries. Due to the fact that most batteries rely on chemical reactions, when the materials are used up, the batteries cannot supply electrical power. This means the wireless sensors cannot guarantee a very long lifetime [10] which in turn means the sensor network will have a limited lifetime. In the worst case it is not possible to replace the batteries of the sensor nodes. In order to have a long service life it is very important for the wireless sensors to be low power (and low cost).

Traditional sensor networks [18], adopting standard wireless schemes to organize the network topology (e.g. Zigbee), are not optimal in terms of energy efficiency [19]. Prop-

agation of information is achieved through multiple hops, suffering from collisions and retransmissions thereby incurring high energy consumption. To overcome these drawbacks, the network topology needs to be reconsidered to take into account the number of sensor nodes and the energy of the radio link jointly, i.e. make an optimal sensor node placement according to the energy consumption [12]; or have another network topology with a minimal number of hops in place of the mesh network, such as the single hop network based on cooperative beam forming [8] [1].

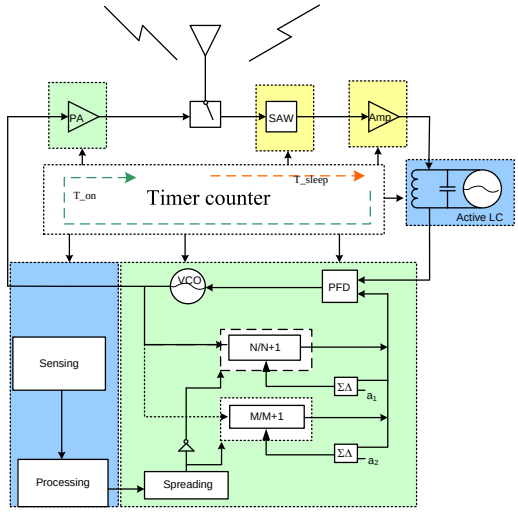

Fig. 3.1: Block diagram of sensor node with active reflector.

Fig.3.1 gives an overview of a low complexity sensor node structure. In this architecture, the node itself doesn't require a very complicated and power-hungry circuit for communication.

Several low cost, energy efficient wireless sensor network techniques are discussed in [4]. An energy efficient RF front end circuit on the sensor node, which is composed of an adaptive antenna scheme and an active reflector node architecture [15] [16] is also proposed as a possible low cost solution, which shifts the main tasks of information fusion and signal processing to the base station. The base station transmits a modulated frequency through its antenna, which serves as a synchronizing and clocking signal for the nodes. When the sensor node receives this signal, it modulates it with sensed data by means of a voltage controlled amplifier and frequency selection circuit, in order to send information back to the base station.

To take full advantage of the improved sensor node design, a single hop method [1] was also considered for increasing the energy efficiency of the whole sensor network. It

assumes that all the nodes are randomly placed within an area and can be configured to act as a random antenna array to produce a directional beam toward the desired direction [9]. In this way, the sensor node can be configured with a very simple circuit, since the required transmission power for each node is reduced significantly and there's no need for a sensor node to be multiplexed: i.e., a work as a transponder or relay.

Moreover, an energy efficient communication structure is also very important for the wireless sensor network combined with an energy efficient communication link. These will be addressed in more detail in the next section.

2 Energy Analysis

As mentioned in the previous section, the proper use of energy in a wireless sensor network is vitally important in supporting a long service life. This must be approached both from system level and node level. From the system level, it is obvious that the less complex the topology the better, resulting in a fewer number of sensor nodes optimally placed in the network [12]. At the sensor node level, as indicated in Fig.3.1, a low cost, low complexity circuit can reduce the unnecessary and redundant power consumption.

In order to quantify the energy efficiency, a commonly defined ratio is used to represent the proportion of the total energy that is used effectively for the desired functionality. It is noted that the functionality has to be ensured; otherwise the so called energy efficiency becomes meaningless. This means the energy efficiency must be considered with the basic requirement being satisfied, i.e., the communication link must be kept at certain stable status, or in other words, the error probability must be below the specified level for the system.

At the same time, the working status of the sensor nodes can be idle, transient(part of the circuit is working) or fully working (all the circuit components are switched on). The energy efficiency in this thesis mainly focus on the sensors status when the radio link is active.

However, even when the basic requirement of a radio link is satisfied, there are still many other factors to be considered in order to assess the energy efficiency. Such parameters are:

- the modulation depth (constellation size) of the radio link
- the symbol (data) rate
- the bandwidth of the link
- the number of users (whether multiple accesses should be considered), etc. [3].

For a bandwidth limited system:

- the higher order modulation,

- the worse error probability performance;

Higher order modulation transfers more information (bits) per symbol period than the binary constellation. The energy efficiency should be considered with minimal required energy to transmit one bit over a stable communication link, which is called joule per bit (J/b). From the definition, it is not related to the data rate in a straightforward fashion, but the data rate will influence the circuit consumption and so contribute for the total energy efficiency. Depending on the network topology, when the multiple access is considered (such as code division multiple access) [11], the effective information bits instead of chip (for the code) bits [11] should be considered for the energy efficiency comparison.

There are two main types of energy cost in a wireless sensor network: the circuit power consumption and the transmission power consumption [13]. The circuit power consumption generally includes:

- the circuit on the sensing interface,
- the analog to digital converter,
- the basic signal processing unit, and
- the radio frequency transceiver circuit.

For the sensor network, the total power consumption is dependent on the number of sensors used in the topology and the energy consumed by the sensor nodes.

Assuming the data rate of such a link is given by R_b, thus the energy efficiency (required energy for one bit) is defined as [13]:

$$E_{bt} = (P_T + P_C)/R_b \tag{3.1}$$

The energy efficiency is quantified in Joules per bit (J/bit). (3.1) Indicates that, the data rate also influences the energy efficiency. Although in most conditions (except multiple access protocols where the information bits are separated into chip R_c bit), P_T/R_b is a constant. The data rate can influence the circuit power consumption and thus influences the total system energy efficiency.

A typical circuit power consumption of a radio link includes mixers (P_{mix}), frequency synthesizers (P_{syn}), power amplifier (P_A) (transmission), low noise amplifier (P_{LNA}) (receiving), as well as analog to digital converter (P_{ADC}) and digital to analog converter (P_{DAC}).

The power amplifier is the last stage on the transmission chain, and its efficiency and linearity influence the output power, which is considered in the transmission power. The modulation depth (constellation size) influences the energy efficiency for two reasons. Firstly, the modulation depth changes the power amplifier efficiency, since the linearity of a higher order modulation is worse than a low order one; this will cause the peak to

average power ratio higher and will therefore reduce the amplifier efficiency. Secondly, the higher order modulation means higher data rate, implying the data are transmitted in a shorter time. The circuit will switch on for a shorter period, leading to reduced circuit power consumption.

We assume that P_T relates to the actual power amplifier consumption P_A as $P_T = (1+\alpha)P_A$, where α is given by $\alpha = \xi/\eta - 1$, and ξ, η are linearity factor and drain efficiency respectively. For a M-arry signaling, ξ is related to the Peak to Average Power Ratio (PAPR) given by $\xi = 3(M - 2\sqrt{M} + 1)/(M-1)$.

The circuit power consumption P_C is modeled with minimal circuit blocks required in sensor communication, as shown in(3.2), where for a SISO link, M_t, M_r is assumed to be 1.

$$P_C = M_t(P_{adc} + P_{mix} + P_{sys}) + M_r(P_{mix} + P_{sys} + P_{lna} + P_{dac}) \tag{3.2}$$

The required transmission power from the power amplifier P_A can be calculated through the radio link budget. The channel $\mathbf{H}$ among the transmitters and receivers is modeled as follows: the distance d_{ij} among the i^{th} transmitter and j^{th} receiver is assumed to be d; the attenuation coefficient κ is assumed to represent the fading (with κ ranging from 2 to 4 according to the fading condition). According to [13], the energy budget is shown as:

$$P_A = \overline{E}_b \times R_b \times \left(\frac{4\pi}{\lambda}\right)^2 \times \frac{U_{link} N_F}{G_t G_r} \times d^{\kappa} \tag{3.3}$$

where $\bar{E}_b$ is the required energy per bit for a given error probability $\bar{P}_b$, and R_b is the data rate noted by bit/s, U_{link} is the link compensation due to the hardware variation and system interferences is $G_t G_r$ the transmitting and receiving antenna gain. N_F is the noise figure given by $N_F = N_r/N_o$.

Thus the energy required for a single radio link with data rate R_b is given by [6]:

$$P_T = (1+\alpha) \times \overline{E}_b \times R_b \times \left(\frac{4\pi}{\lambda}\right)^2 \times \frac{U_{link} N_F}{G_t G_r} \times d^{\kappa} \tag{3.4}$$

One of the main reasons the signal gets attenuated is the wireless channel; a better channel will exhibit a better error probability performance. In a sensor network, the channel is usually assumed to be time-invariant over a symbol period. With the help of spatial multiplexing, i.e., the MIMO techniques, the error performance is improved as a result of the wireless channel being scattered with maximum diversity gain of $M_t \times N_r$ where M_t is the number of transmission antennas, N_r is the number of receiving antennas. It doesn't seems reasonable to employ MIMO on a wireless sensor node, since the such techniques require large inter-element antenna spacing not possible on a small

sensor node. It also requires more power than the conventional communications since it needs more than one RF chain.

The theoretical error probability for BPSK signaling is given by:

$$\overline{P}_b = Q(\sqrt{2\gamma_b}) \tag{3.5}$$

where γ_b is given by $\gamma_b = \overline{E}_b/N_o$ in a SISO link, for MIMO systems, $\gamma_b = (|\mathrm{H}|_F^2 \cdot \overline{E}_b)/(M_t \cdot N_o)$, and $|\mathrm{H}|$ is the channel matrix [13]. According to the Chernoff bound, the error probability is upper bounded as:

$$\overline{P}_b = \varepsilon_{\mathrm{H}}(Q(\sqrt{2\gamma_b})) \leq (\frac{|\mathrm{H}|_F^2 \cdot \overline{E}_b}{M_t \cdot N_o})^{-M_t} \tag{3.6}$$

where M_t is the number of transmission antennas. The required energy per bit $\overline{E}_b$ (J/bit) can be derived as:

$$\overline{E}_b \geq \frac{M_t \cdot N_o}{|\mathrm{H}|_F^2 \, \overline{P}_b^{\frac{1}{M_t}}} \tag{3.7}$$

For higher order signaling, e.g., M-ary signaling (i.e., 16-QAM), the error probability [17] is given by:

$$\overline{P}_b \approx \varepsilon_H \left(\frac{4}{b}(1 - 1/2^{b/2}) Q(\sqrt{\frac{3b}{M-1}\gamma_b}) \right) \tag{3.8}$$

where $M = 2^b$ and b is the constellation size. M-ary signaling has better data rate than BPSK within the same bandwidth. Error probability (3.8) can be approximated as following under the Chernoff bound.

$$\overline{P}_b \leq \frac{4}{b}(1 - 1/2^{b/2}) \left(\frac{3\overline{E}_b b \, |\mathrm{H}|_F^2}{2M_t \cdot N_o(2^b - 1)} \right)^{-M_t} \tag{3.9}$$

The required energy per bit for M-ary signaling with constellation size b is given by:

$$\overline{E}_b \geq \frac{2}{3} \left(\frac{4\left(1 - 1/2^{b/2}\right)}{b\overline{P}_b} \right)^{1/M_t} \frac{M_t \cdot N_o}{|\mathrm{H}|_F^2} \frac{(2^b - 1)}{b} \tag{3.10}$$

Recalling the definition (1), the energy efficiency of the single user system (or a single full communication link) can be analyzed. However, in practice, the network topology also influences the energy efficiency as shown in the next section. Fig.3.2 gives an comparison of the energy efficiency of different configurations, it can be seen that, with distance less than 20 meters, the single RF MIMO with 16-QAM modulation gives better energy efficiency than others.

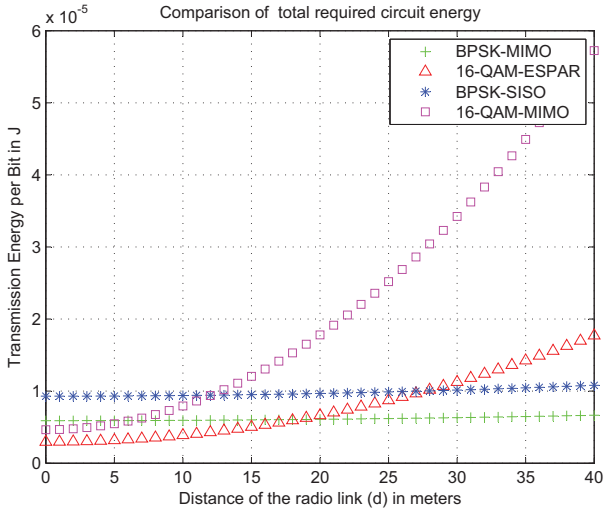

Fig. 3.2: Comparison of minimal required energy.

3 Energy Efficiency of the Sensor Network

As previously mentioned, the energy consumption of a complete wireless radio link includes two parts, the transmission power consumption and the circuit power consumption. When the energy efficiency is addressed, both parts have to be considered together. For a wireless sensor network, the total power consumption is not based solely on the wireless radio link. The network topology influences the number of radio links and the number of relay nodes. Thus energy consumption on the system level has to be considered.

Many methods have been proposed to achieve low power consumption of the sensor system. Virtual MIMO techniques assume the sensor nodes cooperate, and the number of receiving nodes are also working cooperatively [14]. The antennas in the network are considered as M_t number of transmission antennas in a "Virtual" MIMO system, while the data gathering nodes are considered as N_r number of receiving antennas. In this way, the information sent by one sensor node reaches all the receiving antennas. "Virtual" MIMO techniques seem an interesting direction for energy efficient transmission in wireless sensor networks.

Sensor communication can be divided into short range links and long range links. With Virtual MIMO, the network can be partitioned such that short range communication is used to link the sensors within one cluster and the long range communication used between the clusters. Based on the configuration, different modulation schemes

can influence the energy efficiency. It is advantageous to use a lower modulation scheme for the long range communication link and higher order modulating scheme for the short range. When these methods are combined with spatial multiplexing, i.e., MIMO techniques, the trade off is complex, especially when a single RF MIMO technique is considered. It is possible that there might be a trade off of circuit power consumption and constellation size as well as link distance.

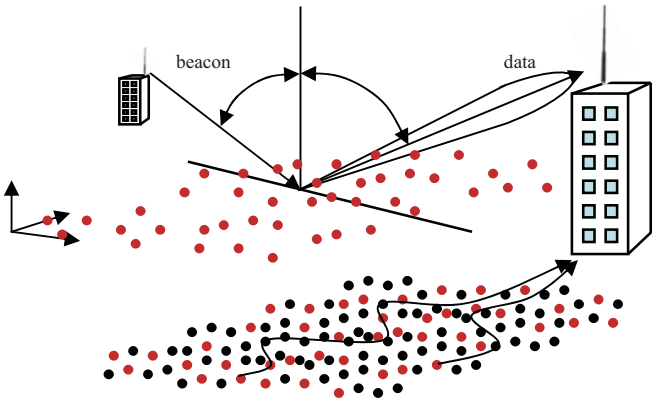

Fig. 3.3: The cooperative beamforming network topology.

An alternative system configuration having better efficiency of the wireless sensor network is to use beam forming techniques to control the energy flow in the analog domain, i.e., cooperative beamforming [8] which considers that the entire sensor network acts as a phased array. Directional transmission seeks to reduce the interference among the sensor signals. The advantage of cooperative beamforming is that the array gain is so large that each sensor does not need to use as much energy to transmit the signal, facilitating longer range transmission [4]. Instead of using multi-hop as in conventional wireless sensor networks, this topology can make relay and routing nodes redundant. By using a one hop technique, significant energy can be saved even from analog domain. Directional transmission is another approach for energy saving sensor networks. It is assumed that each sensor has its own directional antennas that can control the transmission direction. This would avoid the interference with the neighboring nodes while maintaining increased directive gain towards the desired direction [5]. Fig. 3.5gives the beamforming gains of an random distributed sensor array.

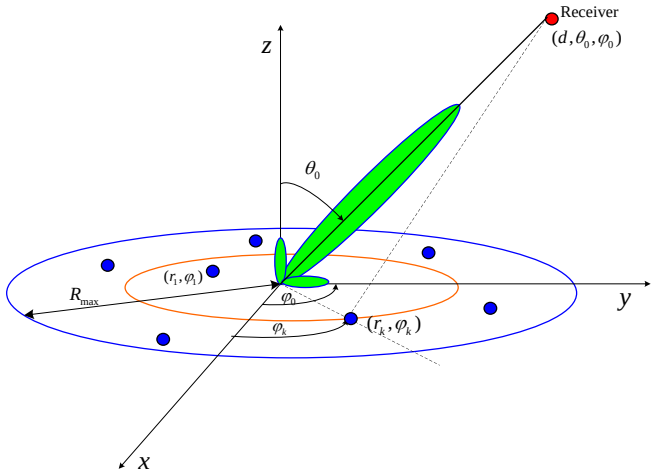

Fig. 3.4: The random senors array beamforming.

4 Conclusion of Energy Efficiency WSN

Wireless sensor networks have become an indispensable part of everyday life. They are characterized by convenient installation and easy network construction. The use of wireless sensor networks extends the scope of monitoring to a large geographical area. Sensor nodes have the ability to sense, store, and transmit information wirelessly.

As increasing numbers of wireless sensors are used, the total power consumption in a large network is no longer negligible so a low cost and low complexity implementation is essential and its energy efficiency was discussed. Section 1 in this chapter discusses the low complexity wireless sensor networks, and the application of the low cost sensors for structural health monitoring [4] and low cost localization [2].

The energy efficiency analysis, section 2 in this chapter presents the widely used quantization Joule per bit(J/bit) to represent the energy efficiency. Various parameters of interest that can influence the performance are listed. Multiple access is considered and it is pointed out that the effective information instead of actual signal bit should be considered for a fair comparison. The linearity of the power amplifier influences its power drain efficiency. The MIMO channel influences the error probability which in turn influence the required minimal energy.

Wireless sensors are configured with different topologies. In some topologies the sensor node can function both as a sensing node and relaying node. Smart sensor nodes can also form a self-organized network. All these forward the data with additional

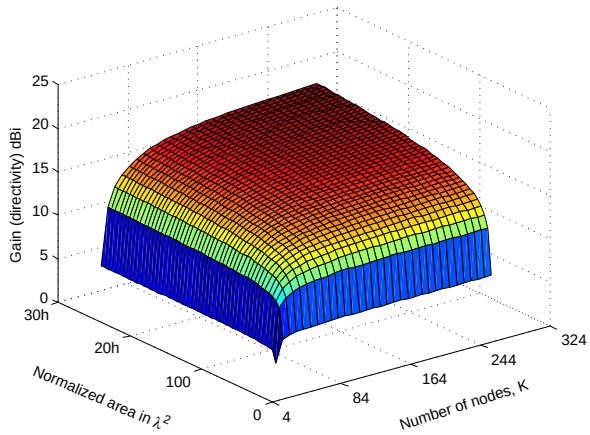

Fig. 3.5: The beamforming gain of the random sensor array.

routing information, which actually adds redundancy and reduces the energy efficiency.

Instead of a mesh network, some other kinds of network topology like the virtual MIMO that supports clustering sensors into small groups and combines these to reduce the number of long distance relay nodes have been considered. In addition, cooperative beam forming synchronizing multiple nodes to form a highly directive beam from a phased array was also investigated as a means to improve the energy efficiency.

References

[1] A. Kalis, A.G. Kanatas, "Cooperative beamforming in smart dust- getting rid of multi-hop communications," *IEEE Pervasive Computing*, vol. 9, pp. 47–53, 2010.

[2] B. Han, A. Kalis, C.B. Papadias, P. Tragas, R.H. Nielsen, R. Prasad, "Low cost localization techniques in structural damage detection," *The IABSE Conference on Assessment Upgrading and Refurbishment of Infrastructures*, vol. 1, pp. 826–831, 2013.

[3] B. Han, A. Kalis, C.B. Papadias, R. Prasad, "Energy efficient MIMO transmission with high order modulation for wireless sensor network," *European Signal Processing Conference (EUSIPCO)*, vol. 1, pp. 1–5, 2013.

[4] B. Han, A. Kalis, P. Tragas, R.H. Nielsen, R. Prasad, "Low cost wireless sensor network for continuous bridge monitoring," *The 6th International IABMAS Conference on Bridge Maintenance, Safety, Management, Resilience and Stainability*, vol. 1, pp. 96–97, 2012.

[5] B. Han, R.H. Nielsen, C.B. Papadias, R. Prasad, "Directional transmission by 3-D beamforming using smart antenna arrays," *International Conference on Wireless Communications, Vehicular Technology, Information Theory and Aerospace Electronic Systems Technology (Wireless ViATE)*, vol. 1, pp. 26–28, 2013.

[6] E.P. Tsakalaki, O.N. Alrabadi, A. Kalis, C.B. Papadias, R. Prasad, "Non cooperative space-time communication for energy efficiency in sensor networks," *IEEE Transactions on Communications*, vol. 60, pp. 48–54, 2012.

[7] F.X. Li, A. Islam, G.C. Perera, P.K. Kolli, "Real time urban bridge health monitoring using a fixed wireless mesh network," *IEEE Radio and Wireless Symposium (RWS)*, vol. 1, pp. 384–387, 2010.

[8] H. Ochiai, "Collaborative beamforming for distributed wireless Ad Hoc sensor networks," *IEEE Transactions on Signal Processing*, vol. 53, pp. 4110–4124, 2005.

[9] L. Dong, A.P. Petropulu, H.V. Poor, "A cross-layer approach to collaborative beamforming for wireless Ad Hoc networks," *IEEE Transactions on Signal Processing*, vol. 56, pp. 2981–2993, 2008.

[10] M. Bhardwaj, A.P. Chandrakasan, "Bounding the life time of sensor networks via optimal role assignments," *Proceedings of INFOCOM*, vol. 3, pp. 1587–1596, 2010.

[11] Manoj BR, B. Han, S. Vassilaras, A. Kalis, "Energy efficiency of cooperative beamforming in wireless sensor networks," *International Journal of Antennas and Propagation*, vol. 1, p. submitted, 2013.

[12] R. Soman, T. Onoufriou, R.A. Votsis, C.Z. Chrysostomou, M.A. Kyriakides, B. Han, "Wireless sensor placement based on SHM requirements and net energy consumption," *The 2nd International Conference on Civil Engineering and Building Materials*, vol. 1, pp. 271–275, 2012.

[13] S. Cui, A.J. Goldsmith, A. Bahai, "Energy efficiency of MIMO and cooperative MIMO techniques in sensor networks," *IEEE Journal on Selected Areas in Communications*, vol. 22, pp. 1089–1098, 2004.

[14] ——, "Energy efficiency of mimo and cooperative mimo techniques in sensor networks," *IEEE Journal on Selected areas in Commun*, vol. 22, pp. 1089–1098, 2004.

[15] S. Krishnan, V.P. Kumar, W. Wang, "UWB-IR active reflector for high precision ranging and positioning applications," *IEEE International Conference on Com-munication Systems (ICCS)*, vol. 1, pp. 14–18, 2010.

[16] S. Wehrli, D. Barras, F. Ellinger, H. Jackel, "Inte-grated active pulsed reflector for FMCW radar localization," *IEEE MTT-S International Microwave Symposium Digest*, vol. 1, pp. 81–84, 2009.

[17] S.K. Jayaweera, "Virtual MIMO based cooperative communication for energy-constrained wireless sensor networks," *IEEE Transactions on Wireless Communications*, vol. 5, pp. 984–989, 2006.

[18] T. Harms, S. Sedigh, F. Bastianini, "Structural health monitoring of bridges using wireless sensor networks," *Instrumentation and Measurement Magazine*, vol. 13, pp. 14–18, 2010.

[19] Z. Liu, B. Wang, W. Yang, "Design and deployment of bridge structural health monitoring system based on wireless sensor network," *6th International Conference on Wireless Communications, Networking and Mobile Computing (WiCOM)*, vol. 1, pp. 1–4, 2010.

Chapter 4

Harvesting Energy from the Environment

1 Why Energy Harvesting

Energy storage is of great concern in mobile communications; most mobile terminals in a communication system are powered by batteries which cannot supply power indefinitely. The same holds for wireless sensor networks, where almost all the sensor nodes are battery powered. As mentioned in the previous chapters, the lifetime of the system depends heavily on power efficiency. Motivated to improve efficiency, efforts have been made to introduce energy efficient, single radio frequency, transmission techniques and low cost, low complexity, communication terminals. As well as the radio link energy efficiency, quantization and new network architecture for wireless sensor networks have been considered. These techniques/methods are based on the common assumption that the system is operating from batteries, and seek to reduce the power consumption to extend the life time.

But, self-evidently, no matter how low the complexity, low cost devices or energy efficient circuit/algorithms are employed the lifetime of the battery and hence the system is finite. Moreover, in the recent application of the sensors/electronics, such as devices implanted into human body, it is desirable to have a perpetual power source to avoid having additional painful surgery to replace the batteries. Thus, an alternative way or a back-up plan to extend the lifetime of the electronic devices to increase the life time of the whole network is sought. A solution is to harvest energy from the surroundings/environment.

Moreover, in the content of the recent calls for a sustainable environment, chemical batteries contain several kinds of poisonous materials (like Hg) that cannot be

decomposed by nature, and cause indefinite pollution to the environment. In some applications, like structural health monitoring, expended wireless sensor nodes will be left when the batteries are used up, because of their working conditions does not allow battery replacement.

"Energy Harvesting" is highlighted as a possible solution to the aforementioned problems. Generally, it is an energy conversion technique that exists in many different forms; it converts energy from one physical domain (e.g., solar, thermal, kinetic or radiation) to another physical domain (e.g., electrical). In this chapter, we mainly focus on the energy conversion to the electrical domain.

Although potential harvestable energy sources were actually quite common, energy harvesting was not a hot topic over the last decade; there was not enough attention to consider using or reusing it for communication devices. That was because the available amount of harvested energy was too little compared to the contemporary systems/circuits. However, with the development of microelectronics in the recent years, a transceiver can be scaled down to one silicon chip and the power requirement is no longer that big compared to the harvested energy. This makes it possible for the electronic devices, especially for the low cost sensors, to have at least a backup energy supply resourced from the energy harvesting rather than solely from batteries.

Energy harvesting seems to be a promising technique in low cost, long life wireless sensor networks. Having energy harvesting techniques as a backup plan for the power supply, e.g., through a super capacitor to store the harvested energy, or with power management techniques to charge the rechargeable batteries on the sensor nodes, the wireless sensor nodes are expected to work much longer than when purely battery powered. The lifetime of the sensor network is predicted to be significantly extended due to the longer lasting sensor nodes.

How to harvest the energy and convert it into electricity depends on the form of the available energy resources and differs from one to another. Most of the time, the application environment of the devices (sensor nodes) will determine the approach to be used.

2 Ways of Energy Conversion

There are rich potential energy sources available in nature, and some of them exist widely, i.e., solar (contains radiation and thermal energy), wind (kinetic energy), vibration (kinetic energy), etc. Among these energy harvesting techniques, several of them are listed for a brief review.

The solar panel converts the solar radiation energy by the emission of photoelectrons from the material inside the solar panel, where the voltage on the solar panel is caused by the electrons to jump among different energy levels with absorption of photons at certain wavelength.

The micro windmill converts the wind (kinetic) energy into electricity through the gears to the built-in electromagnetic generator, which converts kinetic energy to electromagnetic energy to electrical energy.

Vibration contains kinetic energy, which it is possible to convert to electrical energy by using piezoelectric materials. Bending forces on the material generate voltage differences between the two surfaces. Alternatively, the vibration energy can be harvested by a micro-generator based harvester, which is actually a scaled-down generator that uses magnetic flux change to generate electricity. The thermal energy harvester can generate a voltage difference as long as there is enough thermal difference (usually 9 degrees) between two electrical probes. This can be used in some structural health monitoring applications where, for example, there may be a stream pipeline.

The wireless radio wave contains electromagnetic energy [6], which is mainly radiation energy in the far field, and electromagnetic energy at the near field. Far field energy harvesting is more challenging since the radio frequency radiation is usually weak at the receiver; while the near field energy harvesting is much easier, since the harvester can extract energy through magnetic coupling (the near field electromagnetic field contains more energy). Typical of electromagnetic energy harvesting in the near field is RFID devices and the recently introduced wireless charging []devices. e.g, NOKIA Lumia phones.

There are other possible sources for harvesting power and this is by no means an exhaustive list. As mentioned before, applicable techniques depend on the wireless sensors environment. In practice, there are some parameters that limit the application of other techniques. A power density based on the harvestable power per square centimeter (W/cm^2) is considered as reference for the design, as shown in Table. 4.1.

Table 4.1: Comparison of Energy Harvesting Techniques

Type	Power Density(W/cm^2)	Limitations
$Solar$	20μ-200m	Light intensity
$Thermal$	30μ-30m	Thermal diffeence
$RFwave$	200p-1m	Distance and RF harmonic
$Vibration/PZT$	4μ-200μ	Vibration frequency
$Vibration/EM$	25μ-10m	AC/DC conversion

Table.4.1 gives a comparison of the most commonly used energy harvesting techniques in wireless sensor networks, where their power density and application limitations are listed above.

Two of the most common energy harvesting techniques are analyzed in this thesis. They are the radio frequency energy harvesting (Fig. 4.1) and vibration energy harvesting (Fig. 4.2). One is purely in the electromagnetic (radiation at far field)-electrical domain; the other is in the mechanical-electrical domain.

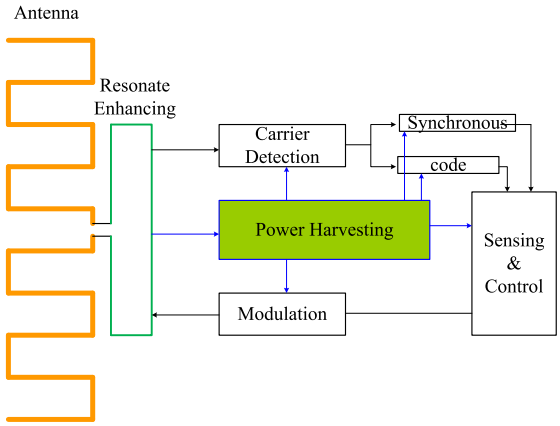

Fig. 4.1: Sensor node with Radio Frequency energy harvesting.

Fig.4.1 gives a general view of a sensor node with a radio frequency energy harvesting technique. When the antenna receives the signal with radio energy, the resonance enhancing stage will enhance the output voltage, then the power harvesting/management circuit will supply power supply to the rest of the circuit blocks.

A similar technique has been widely used in the near field electromagnetic energy harvesting, in the short range electromagnetic field with low frequency (usually 13MHz). A typical example of near field EMF harvesting is the passive RFID tags, where the energy is transferred through magnetic coupling [9]. The recent research trend is toward high frequency (i.e., 900MHz, 2.4GHz, etc.) far field energy harvesting. To increase the available harvested power, several techniques are proposed, i.e. super directional antenna [5] can be used for radio energy transmission by knowing the exact location of the sensor node [2], or the resonance enhancement [3]. Kinetic energy is also widely available in the environment where the wireless sensors are located, and in some situations, it is the only reliable energy source to be harvested, e.g., the wireless sensors used for structural health monitoring, where there is often no sunlight but a rich vibrational energy [10]. Instead of converting from the electromagnetic domain to the electrical domain, this type of harvester converts energy from the mechanical domain to the electrical domain.

Piezoelectric materials can convert the energy from mechanical domain into the electrical domain [1]. A piezoelectric transducer will generate a voltage difference from the deformation of the surface. In an environment where vibration can be used to deform the piezoelectric material, it is a good way to harvest energy, especially when the vibration frequency is similar to the self- resonance frequency. Unfortunately, for structural

health monitoring, i.e., bridges or buildings, where the self-resonance frequency is much lower than in the piezoelectric material, it is not a good solution to harvest energy, so an alternative method has to be investigated.

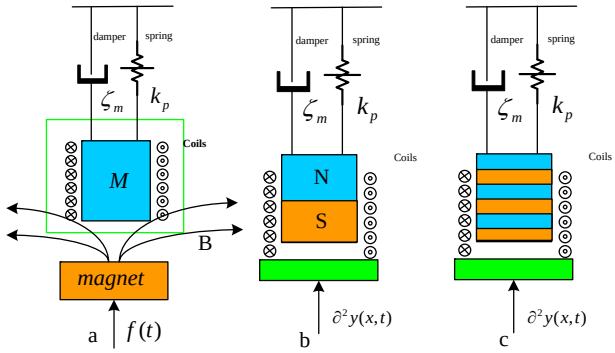

Fig. 4.2: Electromagnetic based vibration energy harvester.

Fig. 4.2 gives a brief view of micro-generator-based vibration energy harvester, where a moving mass (magnetic,or magnetic stack) is connected to the vibration base with a spring, the damper represents the mechanical damping of the mass movement. The vibration function can be represented by:

$$M_H \frac{\partial^2 y_2}{\partial t^2} + \xi_m \frac{\partial y_2}{\partial t} + \xi_e \frac{\partial y_2}{\partial t} + k_p y_2 = -M_H \frac{\partial^2 y(x,t)}{\partial t^2} \tag{4.1}$$

where M_H is the mass of the harvester, ξ_m is the mechanical damping factor, ξ_e is the equivalent electrical damping factor by the virtual force $f(t)$ given by the electrical load, k_p is the stiffness of the spring, $\partial^2 y(x,t)/\partial t^2$ is the acceleration of the vibration base (external excitation), and y_2 is the movement of the mass inside the harvester.

This equation is a general equation for all kinds of vibration based energy harvesters; it can be either a piezoelectric energy harvester or an electromagnetic energy harvester. The total energy that is harvested from the energy harvester is given by:.

$$E = \int_0^t \xi_e \left(\frac{\partial y_2}{\partial t} \right)^2 dt \tag{4.2}$$

In the configuration of Fig.4.2(c), each displacement will cause K times the magnetic flux change obtained in Fig. 4.2 (a). Assuming Φ is the magnetic flux inside each coil turn of the harvester, the output voltage of such an EM energy harvesting system is given by

$$V_i = KN \frac{\partial \Phi}{\partial t} = KN \frac{\partial \Phi}{\partial y_2} \frac{\partial y_2}{\partial t} = KN \frac{\partial \Phi}{\partial y_2} y_2{}' \tag{4.3}$$

where K is the number of magnetic stacks, and y_2 is the displacement of the vibrating magnet. Assuming a load with impedance $Z_{Load} = R + jX_{c,l}(\omega)$ is connected to the energy harvester, the current is given by $i = V_i/Z_{Load}$. The total energy harvested in a time interval [0, t] can be expressed as

$$E_{em} = \int_0^t V_i \cdot i \, dt = \int_0^t \left(\frac{KN}{Z_{load}} \frac{\partial \Phi}{\partial y_2} \frac{\partial y_2}{\partial t} \right)^2 Z_{load} \, dt = \int_0^t \left(\frac{KN}{Z_{load}} \frac{\partial \Phi}{\partial y_2} \right)^2 Z_{load} \left(\frac{\partial y_2}{\partial t} \right)^2 dt \tag{4.4}$$

The micro generator energy harvester is made of a coil with relative movement of the magnetic field [8]. When the magnetic flux changes in the coil, it induces a current flow throughout the circuit and produces a voltage difference on the output. Theoretically, by having a large amount of flux changes, i.e., increased number of coil turns, or a larger magnetic flux around the coil, the output can be increased. However, this will lead to greater electrical damping force impeding the coil movement. In practice, the coil is designed according to the working environment. The advantage of a micro generator based energy harvester is that the working frequency can be very low and can cover the range of most bridge/building self-resonance frequencies. As a powering solution for wireless sensor nodes the micro generator based energy harvester can be a good solution. Fig. 4.3 gives the maximum harvestable energy from the bridge vibration according to different vehicle speed, more detailed information can be found in [7].

3 Voltage Boosting Techniques

Unlike the common battery power sources which provide a relatively high output voltage, the energy harvester normally has a limited output voltage (the energy harvester is not usually directly connected to the rest of the circuit). In practice, a voltage boosting stage is used (often called a voltage regulator) or if is integrated into the power management unit.

To boost the voltage, different types of energy harvesters employ different approaches, i.e., the micro-generator based vibration energy harvester can increase the number of coils or the magnetic stack to increase the maximum output voltage. However, such changes will affect the equivalent electrical damping factor and consequently the vibration function. When the vibration function alters, the frequency response of the micro-generator also changes accordingly. This might not be a viable solution, since the vibration source has its own vibration frequency, the energy harvester should correspond to that frequency accordingly to have the maximum resonance response.

Moreover, for vibration energy harvesters, the different electrical (circuit) load will also influence the effective electrical damping factors on the vibration function. In order to minimize this effect, the maximum power tracking technique is used [7] for the voltage

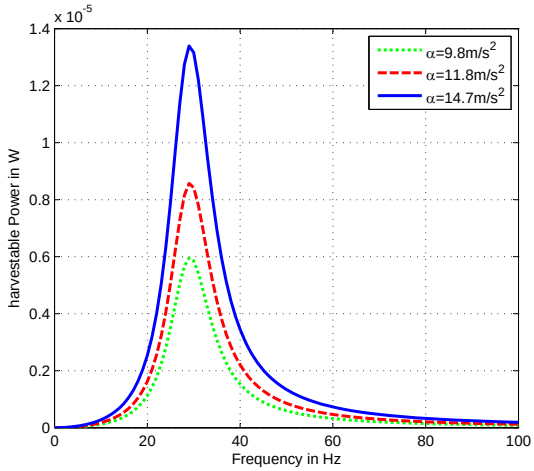

Fig. 4.3: Maximum harvestable power versus frequency

regulator, which can follow the requirement of the load to transfer energy dynamically according to the system load.

So for micro-generator based vibration energy harvester, the voltage boosting should be isolated from the energy harvester instead of influencing the harvester parameters. Consequently, a voltage rectifier built on the commercial available components was simulated as shown in Fig.4.4

Fig.4.4 gives the voltage regulating circuit that not only implements voltage boosting through the charging capacitors, but also can provide power dynamically to the electrical load without changing the working condition of the energy harvester. By monitoring the reference output voltage, the controlled switch can implement the maximum power point tracking (MPPT) function to follow the load requirement. Fig.4.5 gives the simulated result of the maximum power tracking circuit. From which it can be seen that, when the output voltage drops, the duty cycle changes accordingly, which in turn pull up the output voltage back to normal. A detailed description can be found in paper [7].

For the radio frequency electromagnetic wave energy harvester, the voltage boosting is more important, especially for far field radiation at long distance from the energy source. The path loss of the radio wave itself can attenuate the power to a very low level. As it shown in [6], the higher the carrier frequency, the larger the path loss.

This is one reason that, for many years, the radio wave energy harvesting was not given much attention as, most of the time, in wireless mobile communications, the transmitting and receiving antennas are omnidirectional and the transmitter does not

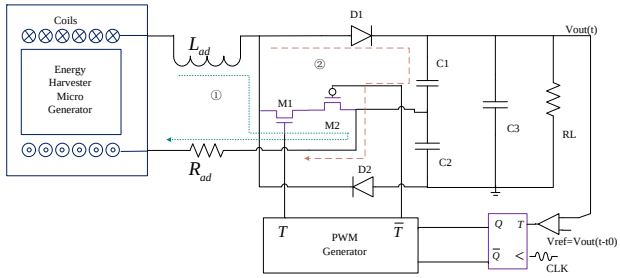

Fig. 4.4: The adaptive Maximum Power Point Tracking circuit .

know the position of the receiver and vice versa.

A wireless sensor network is different from mobile communications in that the sensors are fixed. Thus it is a "wireless" but not "mobile" communication. When the location of the sensor nodes are known to the base station, a directional transmission can be made by using a super directive antenna [5]. This method can be used to compensate the path loss. By using of localization techniques [2] or a predefined location map at the data center, a power beacon can be used to transmit power directly to the sensors. At the same time, the relative locations of the sensor nodes vary from one to another, so directional transmission also needs to be reconfigurable [5]. By using these techniques, the available radio power at the receiver should be increased, although this is not a direct voltage-boosting technique on the voltage regulator after the energy harvester, but it serves to "focus" or "enhance" the harvested voltage.

Another voltage-boosting technique in radio wave energy harvesting is *resonance enhancement*, which is an extra resonance circuit added after the antenna to maximize the output voltage. It is widely known that the common impedance values used in radio frequency engineering are 50Ω, 75Ω or 300Ω. Most of the test and measurement equipment is calibrated with 50Ω built in impedance, so it is a the standard and RF engineering mostly deals with 50Ω. When it comes to energy harvesting, it is however, rarely the case that 50Ω is the best choice for antenna, e.g., the antenna of RFID tags is not necessary to be 50Ω, and in the far field radio wave harvesting, a resonance enhancing stage is used to increase the output impedance in order to have a large output

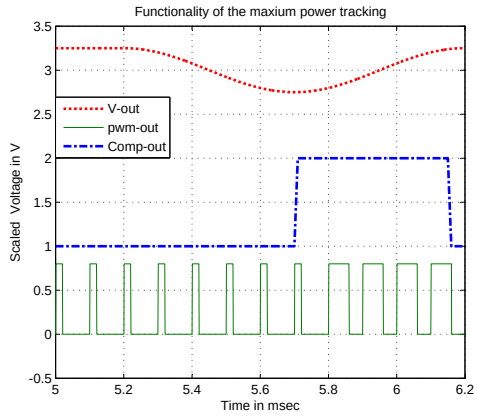

Fig. 4.5: The output voltage can be adjusted by changing the duty cycle of the controlling signal.

voltage.

Another approach to "voltage boosting" is the "threshold voltage reducing" technique, which addresses the problem from a totally different perspective but achieves a similar final effect as "voltage boosting", that is, to power the circuit from a low input voltage.

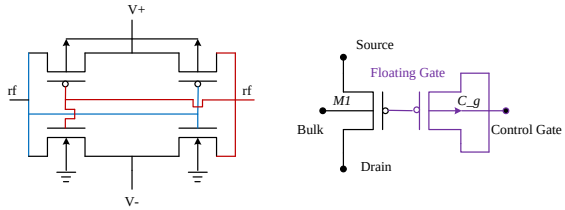

Fig. 4.6: CMOS voltage rectifier and virtual floating gate MOSFET.

Due to semiconductor constraints, a conventional CMOS transistor usually has several hundred milli-volts (400-600mV) threshold voltage to be switched on. However, many energy harvesters, especially the radio wave harvesters, the available output voltage is not sufficient to switch on such a transistor. Even with voltage boosting techniques on the voltage regulator, the energy harvester still needs to be able to power up the boosting stage. Thus the low threshold voltage semiconductors were also investigated.

For the semiconductor fabrication process, the low threshold voltage transistors can

be implemented by adding an "implanted virtual gate" above the virtual tunnel between the source and drain of a transistor. By charging the implanted extra gate and leaving it as a "float" status, the electrons are "trapped" inside the gate and can remain there for more than 10 years. Due to the electrons carriers with negative charge, the transistor can be switched on even if the input is lower than the normal threshold voltage.

However, such "floating gate techniques" require an extra CMOS fabrication stage, since the additional "virtual gate" needs an extra process which will increase the production cost. In order for transistors to have low threshold voltage, an extra procedure is needed to "program" the virtual gates. Thus, the "virtual gate" is proposed using the standard CMOS process to do a similar job, at the cost of an extra MOS transistor configured with floating gate, as shown in Fig. 4.6.

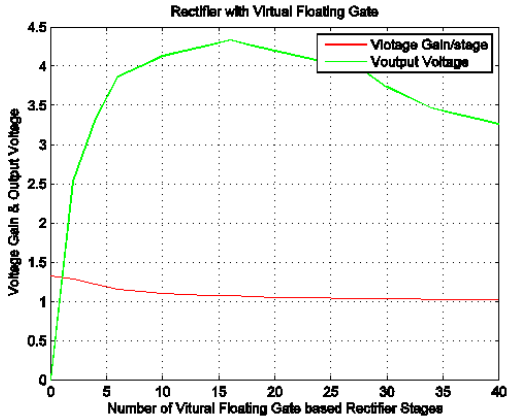

Fig. 4.7: Simulated result on the performance of the voltage rectifier.

With the "floating gate" technique, and assumes input voltage is 200mV, the simulated result is shown in Fig. 4.7. It can be seen that, with 15 stages stack of the "floating gate" rectifier, the output voltage can be higher than 4 V, Thus it is a good way of boost voltage with "floating gate ". The detailed description of such energy harvesting techniques was presented in papers [4], [5], [7], [6].

4 Conclusion of Energy Harvesting

This chapter introduced some basic ways of harvesting energy. Among the various energy harvesting techniques, two of them are chosen. One converts kinetic (vibration) energy to electricity, the other converts electromagnetic energy to electricity.

Based on these two methods, some techniques are investigated and some improvement has been made. The maximum power tracking technique can adjust dynamically

to follow the requirement of the load, while the floating gate voltage boosting technique reduces the threshold voltage of the transistor.

Whilst the discussion on energy harvesting has focused on energy conversion and voltage transformation, energy storage and distribution remain important factors. It has been proposed to use super capacitors to replace batteries in the future for a purely passive sensor node. However, the energy harvesting techniques mentioned in this chapter are primarily considered as a backup power up method and it is assumed that rechargeable batteries or super capacitors are used to store the harvested energy. It would be an interesting topic for purely passive sensor nodes, instead of using rechargeable batteries, to consider using solely super capacitors to power up the circuit.

Combining the harvestable energy assessment in chapter 4 with the energy efficiency calculated in chapter 3, it would be informative to model the wireless link performance budget of the complete wireless sensor network to estimate service life.

References

[1] A. Khaligh, P. Zeng, Z. Cong, "Kinetic energy garvesting using piezoelectric and electromagnetic technologies state of the art," *IEEE Transactions on Industrial Electronics*, vol. 57, pp. 850–860, 2011.

[2] B. Han, A. Kalis, C.B. Papadias, P. Tragas, R.H. Nielsen, R. Prasad, "Low cost localization techniques in structural damage detection," *The IABSE Conference on Assessment Upgrading and Refurbishment of Infrastructures*, vol. 1, pp. 826–831, 2013.

[3] B. Han, A. Kalis, C.B. Papadias, R. Prasad, "Energy efficient MIMO transmission with high order modulation for wireless sensor network," *European Signal Processing Conference (EUSIPCO)*, vol. 1, pp. 1–5, 2013.

[4] B. Han, A. Kalis, C.B. Papadias, R. Soman, M.A. Kyriakides, T. Onoufriou, R.H. Nielsen, R. Prasad, "Energy harvesting for sensors in infrastructure monitoring and maintenance," *The IABSE Conference on Assessment Upgrading and Refurbishment of Infrastructures*, vol. 1, pp. 404–410, 2013.

[5] B. Han, R.H. Nielsen, C.B. Papadias, R. Prasad, "Directional transmission by 3-D beamforming using smart antenna arrays," *International Conference on Wireless Communications, Vehicular Technology, Information Theory and Aerospace Electronic Systems Technology (Wireless ViATE)*, vol. 1, pp. 26–28, 2013.

[6] ——, "Radio frequency energy harvesting for long lifetime wireless sensor networks," *International Symposium on Wireless Personal Multimedia Communications (WPMC)*, vol. 1, pp. 1–5, 2013.

[7] B. Han, S. Vassilaras, C.B. Papadias, R. Soman, M.A. Kyriakides, T. Onoufriou, R.H. Nielsen, R. Prasad, "Harvesting energy from vibration of the structure," *Journal of Vibration and Control*, vol. DOI: 10.1177/1077546313501537, pp. 1–10, 2013.

[8] R.R. Dayal, S. Dwari, L. Parsa, "A new design for vibration-based electromagnetic energy harvesting systems using coil inductance of micro generator," *IEEE Transactions on Industry Applications*, vol. 47, pp. 820–830, 2008.

[9] S. Mandal, R. Sarpeshkar, "Low power CMOS rectifier design for RFID applications," *IEEE Transactions on Circuits and Systems I. Regular papers*, vol. 54, pp. 1177–1188, 2006.

[10] Y.Rao, D.P. Arnold, "An input-powered vibration energy harvesting interface circuit with zero standby power," *IEEE Transactions on Circuits and Systems I. Regular papers*, vol. 26, pp. 1177–1188, 2011.

Chapter 5

Conclusions and Future work

1 Sum up the work

The research on low complexity wireless sensor networks for power efficient communication and energy harvesting had been carried out under different stages/aspects. Started from the radio head on the wireless sensor node, the low complexity wireless MIMO transmitter is introduced, which uses a single active radio head together with active parasitic antenna radiators. Under further investigation, the low complexity MIMO transmitter is supposed to have a better and more stable communication link. With the help of spatial multiplexing, the MIMO symbols can be mapped onto the radiation patterns of the proposed parasitic antennas, which *encode* the MIMO data streams and transmit them into the air. For the receiver, those patterns are considered from a conventional MIMO transmitter. According to simulation, the system performance of a 2×2 single RF MIMO link is almost the same as in the conventional MIMO link. However, due to only half of the RF front end is used, the circuit power consumption reduced to a low level as in a SISO link.

By interpolating higher order modulation, i.e. 16-QAM, the data rate is supposed to be increased and the spectral efficiency can be further increased. The communication protocol of a wireless sensor network is usually at low data rate, but lower data rate means longer transmission time which have to involve certain number of circuit component to be switched on all the time, for a low power consumption or energy efficient concern. The higher data rate at certain distance range can somehow increase the energy efficiency. Based on the analysis of the energy efficiency in terms of joule per bit(J/bit), the circuit power consumption together with the transmission power are considered together for the system analysis. To quantify the energy efficiency, several parameters has to be fixed for a fair comparison. Usually the communication link is a bandlimited system, so the influence of the data rate is controlled by the constellation

size. The parameters that influences the required energy per bit can also be the error probability, which is influenced by the channel model. The MIMO channel is supposed to be different from the SISO channel. The other parameters are also influenced. Taking all those into consideration, the indicative result shows that the single RF over ESPAR with 16-QAM has better energy efficiency for short distance commutations.

Regardless of how energy efficient the circuit is, the batteries supplying energy for the sensor node will die out eventually, and sometimes, the replacement of battery seems impossible. Thus the energy harvesting technique emerges as a back up plan to extend the lifetime of the wireless sensor network. Among all kinds of energy harvesting techniques, the radio frequency based and vibration based energy harvester are introduced. Usually the radio frequency energy are weak, that is due to the radio signal in the air are attenuated by the path loss. However, assuming the transmitter knows the exact location of the receiver, such link can be enhanced by the super directive antenna, then the path loss can be compensated. The critical and similar part for the energy harvester is the voltage regulating/boosting circuit. The floating gate techniques reduces the threshold voltage of a normal CMOS transistor, through cascading the voltage boosting stages, it is possible to have a high output voltage, The vibration based harvester uses a voltage regulator with maximum power tracking techniques, which can deliver the power dynamically according to the load requirement.

Combined with all these techniques, the wireless sensor network performance can be improved in terms of better usage of energy, larger capacity and better radio link reliability. Moreover, the life time of the wireless sensor network can be further improved with adoption of those techniques.

2 Conclusions of the work

During the carrying out this work, several papers have been made at different stages as well as in different aspects. They are described briefly as following:

Paper A gives an insight on low complexity MIMO transmitters, which deal with the load of the parasitic antenna arrays for MIMO transmission.

Paper B describes the matching issues in the parasitic antenna arrays, which also proposed analog tunings for parasitic antenna load.

Paper C introduces several low cost and low complexity wireless sensor network techniques, such as active reflector, multi hop VS single hop.

Paper D is a WWRF submission, which is actually a summary of Paper A and B, but digital tuning for antenna load are considered.

Paper E gives the RSSI based localization in wireless sensor networks, where the RSSI caused errors are analyzed.

Paper F presents the energy harvesting about the piezoelectric micro generator, as well as magnetic based micro generator.

Paper G presents a more detailed analysis of the vibration based micro generator and its voltage conversion circuit with maximum power tracking function that can change the output dynamically according to the load requirement.

Paper H gives the energy harvesting based on radio wave, where the floating gate based threshold voltage suppression technique is introduced and voltage boosting stages are used.

Paper I suggests the super directive antenna is used for directional transmission, which can increase the antenna gain dramatically, especially useful in radio frequency energy harvesting.

Paper J gives energy efficient analysis of the single RF MIMO transmission, the comparison is given with different constellation size including 16-QAM.

Paper K presents the communication performance of the single RF MIMO and comparison with conventional MIMO.

Paper L gives the more detailed description of the single RF MIMO with 16-QAM modulation, from circuit level to system level.

Paper M is an additional work of the main thesis, it gives the application of the energy efficiency in sensor network, which is the optimal sensor position placement.

Paper N is an additional work, which gives the energy efficiency analysis of the one hop sensor network topology, based on the structure of cooperative beamforming of the wireless sensor network.

3 Future work

It will be challenging and interesting in the future work to generate a energy model that take the energy harvesting and energy consumption together into account, which also includes the estimation the dynamic harvestable power in real time and have the energy storage/data storage jointly in the sensor node. The data transfer from the sensor nodes to the data center through advanced communication protocols, e.g, low complexity MIMO techniques or antenna techniques.

Part II

Papers

Paper A

Active Parasitic Arrays for Low Cost Compact MIMO Transmitters

B.Han, V.I. Barousis, A.Kalis, A.G.Kanatas

The paper has been published in the
Proceeding of 5th European Conference on Antenna and Propagation,IEEE Vol. 1, pp. 3663–3667, 2011.

The layout has been revised.

Abstract

recently, electronically steerable passive array radiator antennas have been considered for beam-forming and spatial multiplexing, in order to reduce the size, cost and power consumption of smart antenna systems. However, the re-configurability of such antenna is limited, since parasitic elements were constrained to use only passive loads. If we are to integrate such systems to cost-sensitive devices (as for example in wireless sensor nodes for structural or urban microclimate monitoring), we should be able to fully emulate traditional smart antenna systems, using a single RF feed. This paper presents a method for generating parasitic loads with a negative real part using active circuit blocks. The proposed method could be used for increasing the modulation order of the aforementioned systems, decrease the required number of parasitic elements or even optimize the antenna efficiency in energy-constraint applications. Two alternative designs are presented: a consumer-off-the-shelf JFET based resistance circuit block, which could generate a load real part of up to -15 Ohm with power consumption of 40mW, and a CMOS based negative resistance circuit, which could generate negative resistances of up to -30 Ohm with power consumption around 1mW.

1 Introduction

Recently, a new method has been introduced for implementing multiple-input-multiple-output (MIMO) systems for uplink communications, which mitigates the two major barriers that have been prohibiting such systems to be integrated into mobile terminals over the past decade: antenna size and system cost. The method, initially described in [1], focuses on equipping the MIMO transmitter with a parasitic antenna array known as electronically steerable passive array radiator (ESPAR), which is capable of reconfiguring its radiation pattern on every symbol period, according to a scheme that enables multiple symbol streams to be simultaneously transmitted over the same period. The control of the radiation pattern is performed by changing the reactive loads of the parasitic elements using baseband control signals. The ESPAR antenna meets both the small size and low-cost requirements of modern mobile handsets since it allows for inter-element spacing of $\lambda/20$ or less, and requires only a single active front end path to drive the single active antenna of the array.

The aforementioned concept is modulation dependent, since a different set of pre-compiled patterns must be hard-wired into the implementation of the system. Moreover, the use of reactive loads to control the radiation patterns has its limitations. It has been shown [2] that the ESPAR antenna can be used to support phase-shift-keying (PSK) modulation schemes of any order. However, ESPAR antennas perform quite poorly when quadrate amplitude modulation (QAM) schemes are considered, since the use of

passive loads restricts the re-configurability of ESPAR radiation patterns. Moreover, even for low modulation indexes, it has been shown that the minimum number of parasitic of the ESPAR antenna should be two.

In this work we review our basic design of the feeding network of parasitic elements, in order to support high order modulation schemes using the aforementioned method, and to decrease the number of parasitic for low-modulation indexes (targeting low-rate sensor network communications). The basic idea is related to using negative resistance circuits as loads of the parasitic antennas. Extensive simulation runs have shown that reconfigurable complex loads with a negative real part can significantly extend the capabilities of parasitic arrays to incorporate any modulation scheme. For Negative resistances, whose active circuits do not require the implementation of full radio-frequency/intermediate-frequency (RF/IF) paths, thus preserving the low-cost and low complexity nature of parasitic arrays. In this paper we therefore propose a number of different feeding network implementations using simple low-cost, low-noise transistors, as described in the following.

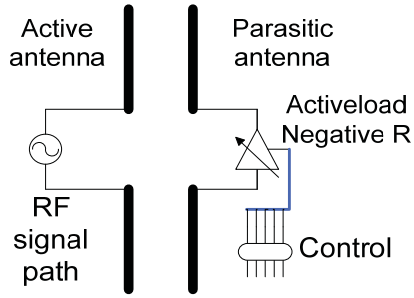

Fig. A.1: The active parasitic antenna with negative Resistance.

2 Application Requirements

In this paper we consider an ESPAR antenna with 2 side by side elements, as shown in Fig.A.1, where the parasitic antenna is connected to an adjustable circuit that provides a complex weight with negative real part and the active antenna is wired to the sole RF chain. The transmit pattern is designed according to [3] and [4], where each symbol is mapped to an orthonormal function, called basis pattern. This concept is known as aerial modulation and was first inspired by the authors in [5]. Thus, given that an ESPAR with two elements supports two basis patterns [3], 2 symbols can be transmitted

simultaneously. Simulating all possible radiated patterns for an inter-element distance $d = \lambda/16$, Table.A.1 reveals that a minimum real part up to almost -22 Ω is required for BPSK symbol vectors. Similar simulations for 16-QAM however show that the real part falls to almost -61 Ω. In Fig.A.2, there is a significant tolerance to the exact resistance values, especially for low modulation factors.

Table A.1: Symbol vector and load requirement

Symbol Vectors	jx	Feeding phase(degrees)
[0 0]	-21.5090 +j23.5047	133.5
[0 1]	-21.5090 +j23.5047	340.2
[1 0]	15.0839 +j23.8743	160.2
[1 1]	-21.5090 +j23.5047	313.5

Increasing the inter-element distance, it has been observed that the minimum real part of the loading becomes more negative. From the circuit point of view this fact leads to a more demanding design that should be avoided. Thinking that an extremely dense antenna placement is not realistic, the inter-element distance has been fixed to $d = \lambda/16$ where λ is the wavelengths. This is a reasonable assumption for ESPAR antennas.

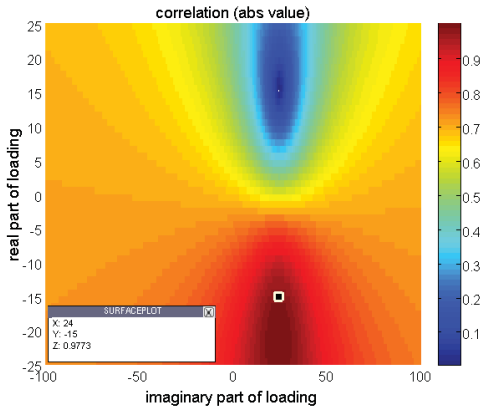

Fig. A.2: Load tolerance for the specified modulation.

Having in mind the proposed application of using negative resistances as loads to parasitic antenna elements, the characteristics of the negative resistance circuit should meet the following requirements:

a). Low Power consumption

By replacing multiple RF-front ends that would otherwise be needed to control the radiation pattern of the antenna with simple active load circuits, the total power consumption

of the multi-element antenna (MEA) transmitter presents higher power efficiency and lower power consumption.
b). Low complexity, compact design
The design significantly reduces the required parts for controlling MEA systems, as well as the need for additional parasitic elements. Therefore, the complexity of the RF front end design is quite lower, which can lead to smaller circuit areas and consequently, lower cost.
c). Low noise and distortion
The design ensures that active loads produce very low noise levels, have weak inter-modulation products and do not distort the characteristics of the transmitted signal.
d). Re-configurability
This is a key feature of the proposed design, which will enable us to extend the approach presented in [1] beyond the limits of PSK modulation formats [2].

3 Circuit Design and Implementation

3.1 Review of Negative Resistor Circuits

Negative resistors have a negative slope on their resistance characteristic curve on the-I plane, and can be either Voltage driven (type-N) or Current driven (type-S). They have been quite popular with oscillation circuit implementations [6] and inductor loss cancellation circuits [5]. In the former, negative resistors commonly imply the presence of a positive feedback, which creates poles on the right half Z-transform plane, but close to the imaginary axis. This is a common rule that ensures the beginning of oscillations. Although the circuit in this case becomes unstable, i.e. the output is increasing; the output practically is restricted due to the non-linearity of a transistor-based control unit. On the other hand, inductor loss cancellation circuits are widely used in filter design [7] [8]. They can enhance the quality factor of the inductors, so that filters perform much better with a sharp stop band dip. In this work we present examples of both approaches, each having its advantages and disadvantages. Namely, we prefer the latter approach for the COTS design and the former for the integrated CMOS design.

3.2 Circuit implementation using COST JFET components

The simplest way to implement negative resistance circuits is by using an operational amplifier as the one shown in Fig.A.3(a). Where the tunable resistance value R_{AB} would be given by [9] [10]

$$R_{AB} = -\frac{R_1 \cdot R_3}{R_2} \tag{A.1}$$

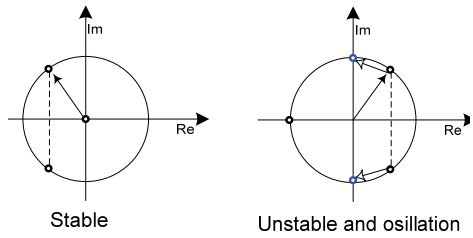

Fig. A.3: Root diagram of the close loop system.

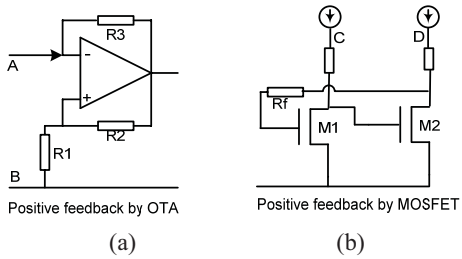

Fig. A.4: Method of generating negative resistance.

However, due to the limited availability of operational amplifiers working at the targeted frequency of 2.5GHz, and in order to minimize the power consumption of the circuit, we preferred to base our design on the NE35M09 low noise JFET transistor, which has a frequency range of 0.4 GHz to 6 GHz. The threshold voltage of NE35M09 has a strong body effect, but for negative resistance implementation, this body effect could be used as an advantage. The influence of this effect on the circuit threshold is given by:

$$V_T = V_{TO} + \gamma[\sqrt{2\,|\varphi_f| + V_{BS}} - 2\sqrt{|\varphi_f|}] \tag{A.2}$$

Where $\varphi_f$is the threshold voltage related voltage factor, and $\gamma$is the body effect factor from 0 to1, here for the JFET $2\,|\varphi_f|$=0.6V,γ=0.7. By reverse biasing the base-drain voltage V_{BS}, when the threshold voltage $V_T$increases, drain source current I_{ds} decreases, giving the effect of a negative resistance. Since only N-channel JFET transistors are available as commercial products [11]. We had to use AC-coupling to realize the positive feedback, as described in Fig.A.5.

In Fig.A.5, the negative resistance is realized using a differential pair with JFET transistors. Transistors J1 and J2 work for the active part of the circuit, degeneration

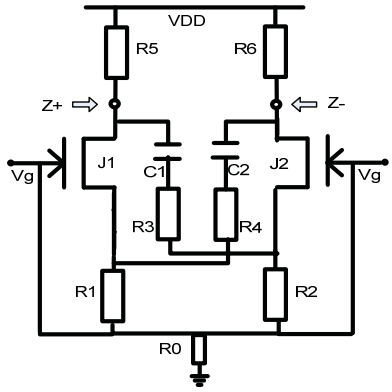

Fig. A.5: Topology of JFET based negative resistance.

resistor R1 and R2 work for the feedback voltage generation, C1,R3 and C2,R4 support the AC coupling, and R3,R4 are used for pole-zeros separation. Resistors R5 and R6 work for the current controlling of the circuit block. Voltage $V_g$works is used to control the impedance value, and consequently it is used to control the negative resistance value. External control of the impedance value is needed so that we can use the same circuit to generate multiple loading values, to support higher modulation indexes in the ESPAR MIMO implementation. Simulated results of the proposed circuit, regarding the impedance load values are presented in Fig.Fig.A.6. Note that the imaginary part of the impedances is not presented, since it can be controlled with external passive components.

Simulation results show that with the proposed COTS design we can easily get negative resistance values from -15Ω to -21Ω, thus satisfying the system requirements shown in figure 3. However, three major caveats remain:

a). Power consumption
The negative resistance circuit block would consume 10mA of current for each transistor, when drain supply voltage is 2.5V. This means that the total negative resistance circuit would consume more than 50mW.

b). Gate-source current
In order to achieve the resistance values given above, the gate should remain connoted. This means that the gate should conduct the current flowing though the antenna, which in reality should be very small for the circuit to operate.

c). Complexity

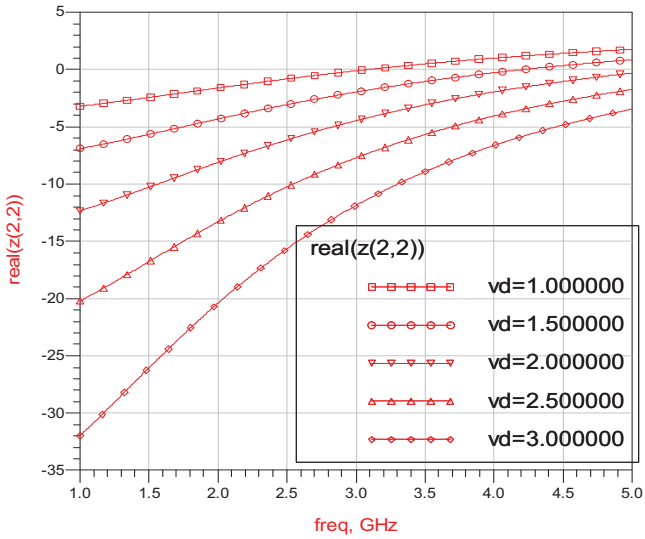

Fig. A.6: Simulation results of the proposed COTS-based circuit.

The impedance value is controlled by changing the supply voltage from 1V to 3V. This requires more external parts to be able to accurately generate the desired control voltage.

3.3 Circuits implemented in CMOS

Using CMOS transistors and a standard CMOS process we can overcome the problems mentioned in the previous paragraph. One of the main advantages here is that we may use both N-type and P-type transistors in the same package, giving to our design more flexibility. The proposed design architecture shown in figure 8 is based on the well known LC-tank voltage controlled oscillator (LC-VCO), whose active part works as the negative resistance. The novelty of the design lies in operating the LC-VCO circuit without the LC-tank, while keeping the VCO negative resistance circuit. One of the main challenges of this approach is that circuit analysis should not be confined to small signal modeling, but be extended to large signal modeling, including analysis of the linear and saturation regions of the circuit. When transistor works on saturation region, the output resistance depends on the small signal cross-conductance gm, given by

$$g_m = \mu C_{ox} \frac{W}{L}(V_{GS} - V_T) = 2\frac{\mu C_{ox}}{2n}\frac{W}{L} I_{ds} = \frac{2I_{ds}}{V_{GS} - V_T} \tag{A.3}$$

Where I_{ds} is the current flowing though transistor, given by

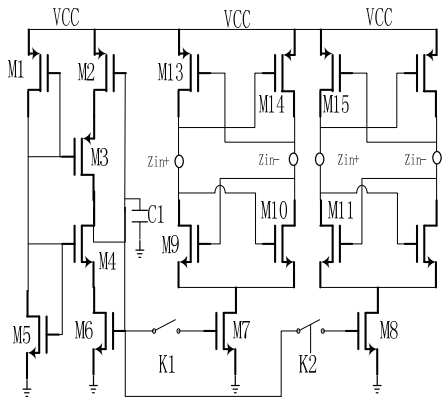

Fig. A.7: schematic of CMOS negative resistance.

$$I_{ds} = \frac{\mu C_{ox}}{2n}\frac{W}{L}(V_{GS} - V_T)2(1 + \lambda V_{DS}) \tag{A.4}$$

Where the V_{GS} is the voltage drops between gate and source of the transistor.

It is evident from the analysis above that as the value of I_{ds} increases, the output resistance decreases. On the other hand, as V_{GS} increases, so does the output resistance.

We take advantage of this effect for controlling the value of the output negative resistance, by introducing a number of control switches (K1 and K2 in the schematic of Fig. A.7). By controlling the states of switches we can control the number of active stages that contribute to the total output admittance, and consequently to the total output impedance. The total admittance of the negative part is therefore,

$$Y_{all\_neg} = K_1 \cdot Y_1 + K_2 \cdot Y_2 + ... + Kn \cdot Yn \tag{A.5}$$

Where K_n take binary values of 0 or 1. If Y_1 is the first stage of the circuit, the total admittance of the active parasitic array is:

$$Y_{total} = Y_{all\_neg} + Y_{antenna} \tag{A.6}$$

Therefore, by using digital control to switch the K_n signals ON and off, we can accurately change he resistance values satisfying the desired modulation requirements. Transistors M1 to M6 work for biasing the circuit, and ensure that switching has minimal influence on the biasing point. Moreover, capacitance C1 is used to reduce the voltage swing on the biasing point. Transistors M7 and M8 work as function of current source. thus providing additional flexibility to the control of the negative resistance value. By changing the basing voltage of M7 and M8, the current flow through the negative block

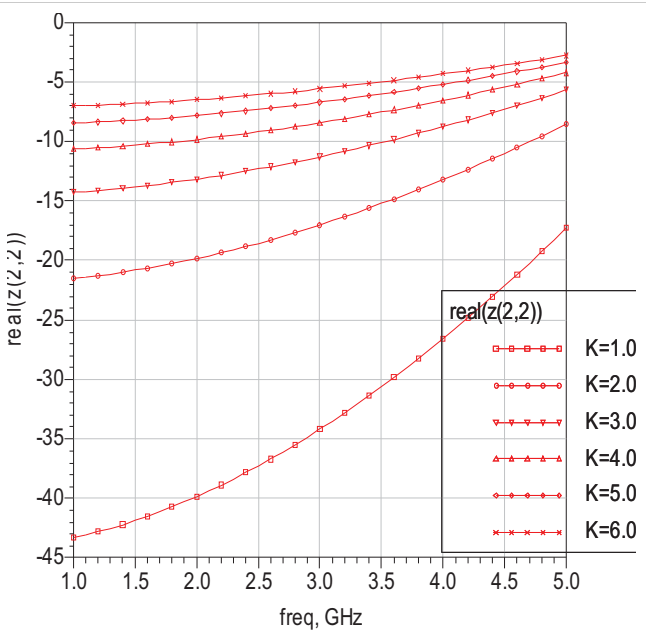

Fig. A.8: simulation result of CMOS negative resistance.

will change thus affecting the output impedance values. However, here we focus on producing discrete values to enable us to implement digital modulation while minimizing the number of parasitic antenna elements.

Finally, M9 to M12 and M13 to M16 work as the key function of negative resistance generation. The NMOS transistors compose cross-coupling pairs, as in typical LC-VCO designs. The proposed circuit architecture ensures low power consumption since we can isolate whole negative resistance blocks through the K_n switches. Fig.A.8 gives the simulated result of the CMOS based negative resistance circuit block, assuming all the stages are under the same configuration. By changing the state of switch K, we can get the desired negative resistance values between -6.09 Ω and -37 Ω. The power dissipation of the proposed CMOS circuit is much lower compared to the COTS JFET-based design.

Comparison of power consumption with JFET based circuit block and CMOS based circuit block, JFET based topology has power consumption of 34mW while CMOS based topology just has power cost of 864uW/stage.

4 Conclusion

Two kinds of negative resistance generation circuits are proposed and simulated, which give an insight that active parasitic arrays for low-cost compact MIMO systems are feasible. Based on the CMOS negative resistance circuit, we have shown that it is quite possible to adopt more complex modulation schemes such as 16- or even 64-QAM, while keeping the same circuit architecture, with little additional complexity. In future work we can focus on implementing more bandwidth-efficient modulation schemes, where challenges include taking into account the parasitic capacitances of CMOS circuits after layout design and fabrication, as well as the setting up time of the negative circuit block, which will influence the symbol rate of the MIMO system

References

[1] A. Kalis, A.G. Kanatas, C.B. Papadias, "A Novel approach to MIMO transmission using a single RF front end," *IEEE Journal on Selected Areas in Communications*, vol. 26, pp. 972–980, 2008.

[2] O.N. Alrabadi, C.B. Papadias, A. Kalis, R. Prasad, "A Universal encoding scheme for MIMO transmission using a single active element for PSK modulation schemes," *IEEE Transactions on Wireless Communications*, vol. 8, pp. 5133–5142, 2009.

[3] O.N. Alrabadi, A. Kalis, C.B. Papadias, A.G. Kanatas, "Spatial multiplexing by decomposing the far-field of a compact ESPAR antenna," *IEEE PIMRC*, vol. 1, pp. 1–4, 2008.

[4] V.I. Barousis, A.G. Kanatas, A. Kalis, "Beamspace domain analysis of Single RF front-end MIMO systems," *IEEE Transactions on Vehicular Technology*, vol. 60, pp. 1195–1199, 2011.

[5] A. Kalis, A.G. Kanatas, M. Carras, A.G. Constantinides, "On the performance of MIMO systems in the wavevector domain," *15th IST Mobile and Wireless Communications Summit*, vol. Myconos, p. Greece, 2006.

[6] L. Chua, J. Yu, Y. Yu, "Biploar-JFET-MOSFET negative resistance device," *IEEE Transactions on Circuits and Systems*, vol. 1, p. 32, 1985.

[7] J. Daniel, J. Glen, P. Jameson, "Maxwell and other great Scottish contributions to world advancement," *IEEE European Conference on Antennas and Propagation (EUCAP)*, vol. 1, pp. 109–111, 2009.

[8] P. Madsen, T. Larsen, J.H. Mikkelsen, J.C. Lindof, "An RF CMOS differential negative resistance for Q-enhancement," *IEEE International Conference on Solid-State and Integrated Circuits Technology*, vol. 2, pp. 1256–1259, 2004.

[9] C. Andriesei, L. Goras, F. Temeamani, "Negative resistance based tuning of an RF bandpass filter," *IEEE European Conference on Circuits and Systems for Communications*, vol. 1, pp. 83–86, 2008.

[10] H. Takagi, G.Kano, "Complementary JFET negative resistance devices," *Journal of Solid State Circuits*, vol. 1, p. 10, 1985.

[11] V. Stornelli, G. Ferri, G. Leuzzi, A. De Marcellis, "0.15-1.3GHz CMOS 2nd order band pass filter with 50 ohm input-output impedance matching," *IEEE International Symposium on Circuits and Systems (ISCAS)*, vol. 1, pp. 21–24, 2006.

Paper B

Matching Parasitic Antenna for Single RF MIMO

B.Han, A.Kalis, R.Prasad

The paper has been published in the
International Conference on Microwave and Millimeter Wave Technology (ICMMT),
IEEE Vol. 1, pp. 1–4, 2012.

Abstract

Single RF MIMO communication emerges a novel low cost communication method which does not consume as much power as the conventional MIMO. The implementation of such single RF MIMO system is done by mapping the weighting factors to the polarizations or the radiation patterns of the antennas. In order to have such performance, an antenna with rich pattern modes is required by the system, thus the ESPAR antenna is investigated. The critical part on such antenna is parasitic element impedance matching. Unlike the conventional smith-chart matching method which assumes the minimal resistance is zero and with goal of 50 Ω or 75 Ω matching, matching on such parasitic antenna will adopt negative value as well. This paper presents a matching network with controllable impedance even to the range of negative values.Here is an abstract.

1 Introduction

Single RF MIMO communication [1] is investigated more and more in the recent research papers, because only one active RF chain is used in the Single RF MIMO transmission, it is a low complexity and low power consumption solution for green communication, which gives a promising future for portable mobile devices on high data rate communication.

With the adopting from the idea of ESPAR antenna, the single RF MIMO is implemented with one active element and one or two parasitic element [2], for compact and portable design, it aims at using just one parasitic element; by switching the radiation patterns driven by the parasitic elements linked to data stream, which was supposed goes to another RF chain in the conventional MIMO communication, the single RF MIMO transmission can reach almost the same performance while keeping the power consumption lower than that of a conventional one.

The implementation of such a system is also under lots of investigation, previous research is most focus on the possibility of generating the special impedance on parasitic element, however, due to the drawback of the direct connection between negative resistance and the parasitic element, only limited impedance value can be driven from such a circuit block, this result in the limited radiation pattern can be driven from the ESPAR antenna, so only simple modulation scheme can be adopted for single RF MIMO transmission. In order to have more complex modulation scheme that can be adopted on this Single RF method, to have better spectrum efficiency, certain circuit block have to be investigated, which should have the capability of turning the impedance with a wide range so that more radiation pattern can be derived for higher modulation scheme.

The organization of this paper is arranged as following: section II introduces the single RF MIMO communication analysis and physical implementation feasibility analysis; section III presents the matching method and technique for parasitic antenna elements; section IV gives the comparison of theoretical analysis and simulation based result.

2 Single RF MIMO Communication

2.1 Single RF MIMO

Assuming the single RF MIMO system is implemented by a single active antenna element and a single parasitic antenna element with inter-element space of $d = \lambda/16$, here λ is the wavelength. One data stream goes into the active RF/IF stage as normal wireless transmission, the other data stream first goes to the mapping circuit, by which the combination of the two data.

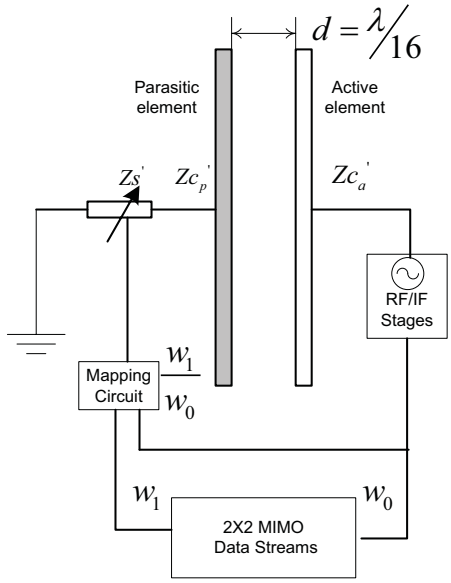

Fig. B.1: Topology of the single RF MIMO with parastic antenna.

The mapping circuit will control the parasitic arrays on the antenna. By switching the parasitic arrays on the antenna, the radiation pattern changes according to the symbols mapped to the parasitic arrays. Thus it works as conventional 2×2 MIMO transmission. The radiation pattern of an ESPAR antenna with 2 elements is expressed

as linear combination of 2 basis patterns $\Phi_n(\varphi)$ as:

$$P(\varphi) = \sum_{n=0}^{2-1} w_n \Phi_n(\varphi) \tag{B.1}$$

It is shown that the shape of the basis patterns depends on the inter-element distance and the coefficients w_n depend on the inter-element distance and the currents. For an ESPAR antenna with $M = 2$ elements the basis patterns are following:

$$\begin{aligned} \Phi_0(\varphi) &= 1/\sqrt{2\pi} \\ \Phi_0(\varphi) &= (e^{jb\cos\varphi} - I_0(jb))/\sqrt{2\pi(1 - I_0^2(jb))} \end{aligned} \tag{B.2}$$

The coefficients in B.1 are given by

$$\begin{aligned} w_0 &= \sqrt{2\pi}(i_0 + i_1 I_0(jb)) \\ w_1 &= i_1 k_1 \end{aligned} \tag{B.3}$$

Based on the aforementioned mathematic analysis, these radiation patterns are mapped by MIMO data streams. The mapping control circuit will change the impedance of the parasitic antenna element.

2.2 Physical Feasibility-Key elements

The parasitic antenna has its self-impedance Z_c of 50Ω,in order to have a better MIMO performance which is not constrained in PSK modulation scheme [3] [4], the active parasitic antenna element is proposed and with a negative resistance [2]. However, the parasitic antenna element itself cannot change the impedance after implementation, thus a controllable matching circuit is needed for this pattern switching based single RF MIMO communication.

According to system analysis based on an ideal dipolar antenna model, a value of -64-j43 Ω is needed for a certain radiation pattern in QAM modulation. With the method from [2] on the active circuit, this paper presents an analysis on the middle-stage matching circuit connected between the active circuit and parasitic antenna.

3 Matching to Parasitic Antenna

3.1 Antenna System Architecture

The topology of the matching circuit and parasitic antenna is shown in Fig. B.2, Z_{neg} is the negative impedance of the active circuit; Z_s is the impedance of the controllable matching circuit; Z_c is the antenna self-impedance, for the parasitic antenna, this impedance is marked Z_{cp} . The main function of the Matching circuit is to combine

the negative resistance Z_{neg} with antenna self-impedance Z_{cp} together and get desired impedance for certain radiation pattern; another important function of the matching circuit is to avoid oscillation: the negative resistance Z_{neg} is actually generated from a positive feedback, so the instability of positive feedback should be overcome by the matching circuit, e.g., when $|\mathrm{Z_{neg}}| > |\mathrm{Z_{cp}}|$ the circuit will become unstable, proper design in the matching block Z_s is required so that the negative resistance circuit will not oscillate with the parasitic antenna.

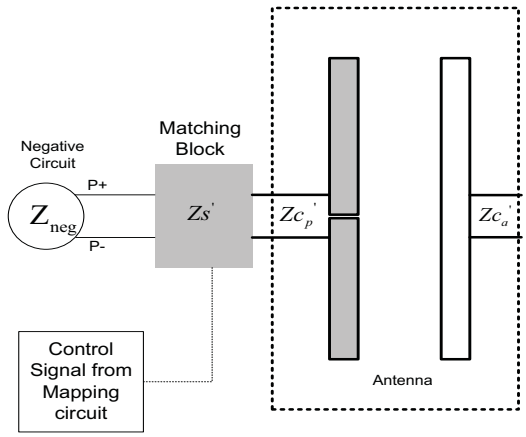

Fig. B.2: Topology of the matching mythology for the parasitic antenna.

The topology (Fig.B.2) shows one active one parasitic antenna element for single RF MIMO communication, which is also supposed to work with high modulation scheme, e.g., QAM. So a variable impedance matching is required, which can be controlled by the signal from mapping circuit. Unlike the conventional RF matching which aims the goal towards 50+j0 Ω or 75+j0 Ω, the matching circuit in this paper aim towards to a certain impedance value, which accounts the negative as well as positive value.

3.2 Matching Topology and Analysis

As the general matching network (Fig.B.2) contains shunt and serials components, the proposed matching network also have impedance and admittance for compensation on real part and imaginary part. Fig.B.2 shows N stages matching according to a specific mathematical calculation, while in this paper we only use one stage for a simplest mathematics experiment. Components $Z_1 - Z_5$ compose a typical L matching circuit. Due to symmetric, only Z_1, Z_2 and Z_3 take effects in the proposed impedance matching. And in this simplest model, terminal C and D are directly connected to Z_2 , Z_5 respectively.

Port 2 is composed of terminal A and B which supposed to connect with negative resistance value; Port 1 is composed of terminal C and D which supposed to connect with the parasitic antenna.

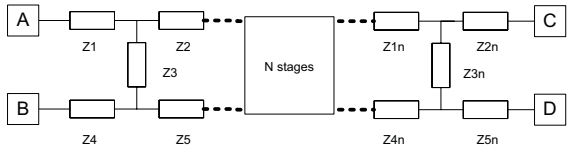

Fig. B.3: Typical matching network consisted of matching unit.

The impedance matching cannot follow the conventional method which based on smith chart calculation, because only positive resistance can be used, all circle on smith chart indicates the impedance ranged from 0 infinite. So the proposed matching is setup by allocating certain resistance or inductance (capacitance) value to the matching network, and simulate the system impedance by setting Port 2 with negative resistance value. The S parameter simulated from the two ports has the following equation B.4 relation with impedance [5] [6]. So by measuring the S parameter, we can get the combined parasitic antenna impedance, which has variable value according to the carrier frequency.

$$\begin{aligned} Z_{11} &= \frac{(1+S_{11})(1-S_{22})+S_{12}S_{21}}{(1-S_{11})(1-S_{22})-S_{12}S_{21}} \\ Z_{22} &= \frac{(1-S_{11})(1+S_{22})+S_{12}S_{21}}{(1-S_{11})(1-S_{22})-S_{12}S_{21}} \end{aligned} \tag{B.4}$$

The calculated Z_{11} in B.4 is the impedance seen from the side of parasitic antenna, which functions for the radiation pattern of the antenna.

By changing the component impedance (inductance) value separately in the matching network, we can have different combinations of antenna impedance on real and imagery part. In simulation, the negative resistance is set to -120-j100 Ω, in order to get antenna impedance with -64-j43 Ω at 2.5GHz, the matching circuit should provide resistance Z_1 with value of 167.5 Ω and the inductance Z_2 with value of 4.82nH, as it shown in Fig.B.4. Fig.B.4 gives one matching value to a specific radiation pattern, e.g., -64-j43 Ω. Two markers m1 and m5 are indicating the real part and imaginary part impedance respectively. The variable R_t and L_t are indicating the resistance and inductance value used in simulation. Due to imperfection of the matching circuit itself and limitation of the available resistance (inductance) values, the practical value plotted from simulation is -63.16-j42.25 Ω, which is slightly different from theoretical analysis.

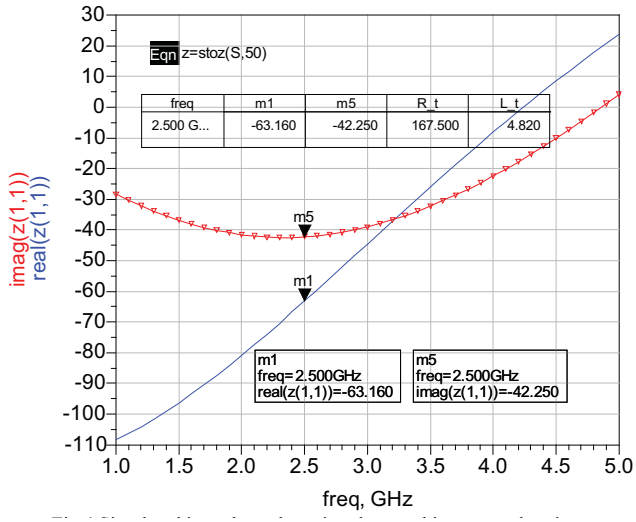

Fig. B.4: Simulated impedance by using the matching network unit.

3.3 Matching Model and Analysis

According to the modulation requirement of the single RF MIMO transmission, the available mapping radiation patterns is determined by the combination of the two data streams, which is w_1/w_0 . In [2], the control of the radiation pattern can be changed directly from the negative generation circuit. By controlling the switches on and off, the negative value can be hanged digitally. But that just work for BPSK modulation, for higher modulation scheme like QAM, certain design method on the controllable matching network is required. With the aforementioned problems, the proposed matching network is a variable matching network with an external control source, as it shown in Fig.5.

The control single for the matching network is generated according to the w_1/w_0 , the control signal should have the random changing ability due to the data stream of w_1 and w_0 are random, so the varying ability of the signal should be high enough to cover all the possible conditions.

Typical design of the control unit is using voltage controlled variable resistor and inductor for the real part and imaginary part separately. The value of Z_1 and Z_2 will be under the function of:

$$Z_1 = f_1(v_1, t); Z_2 = f_2(v_2, t) \tag{B.5}$$

Wheref_1 and f_2 are the relation function of the control signal and the variable impedance values, and v_1, v_2 are the control voltage, which has the relation with w_1/w_0

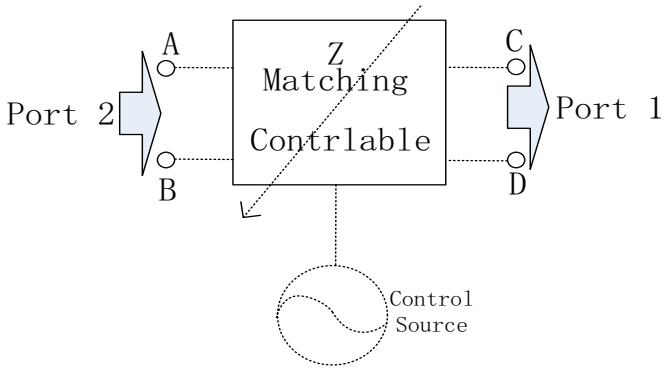

Fig. B.5: Topology of an Analog controlled matching network.

, so finally the relationship between two data stream symbols and the impedance values is:

$$\begin{aligned} Z_1 &= f_1\{u_1\left(w_1/w_0, \sigma\right), t\} \\ Z_2 &= f_2\{u_2\left(w_1/w_0, o\right), t\} \end{aligned} \tag{B.6}$$

Here the coefficient σ and o are the real part influence factor and imaginary influence factor separately, due to the impedance of the inductor is frequency dependent, the time factor t here is for the correction of the influence from control signal, having this relationship between data stream symbols and control circuit will do the desired switching radiation pattern function for the parasitic element on the antenna, another requirement on the control signal is the varying speed, due to speed of the two data stream in single RF MIMO transmission, the control single should change fast enough to catch up with the requirement of switching speed on radiation pattern.

4 Simulated Results

4.1 Setup Environment

The simulation is conducted under the assumption of ideal resistance and inductance matching value is used, which in practice can be considered resistance part and inductance part of the matching component. The pre-calculated resistance(inductance) values are used in the rough simulation; after the plotted curve close to the desired value range, an optimization is used for finding the closeted value. Considered on physical availability, extremely small or extremely large value are also automatically ignored.

4.2 Simulated Result Comparison

The antenna impedance value plotted from simulation is imported back in to the radiation pattern simulation system, in order to see the difference of the radiation patterns between theoretical and practical situation.

The result is shown in Fig.B.6. The dotted curve is the radiation pattern from theoretical values; the solid curve is the radiation pattern from the simulated values. This result shows that the practical values almost follow all the theoretical values.

This means the radiation pattern generated from the practical values have very little variation from theoretical calculation, the proposed method on matching network for single RF MIMO communication is feasible.

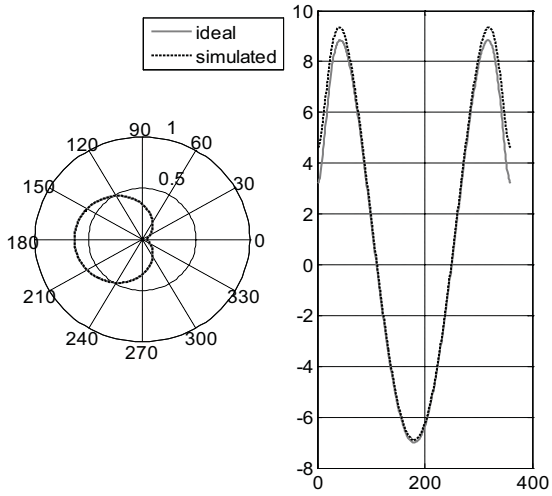

Fig. B.6: Comparsion between practical values and simulated values.

5 Conclusion

A matching technique for negative resistance connection to parasitic element on ESPAR antenna is introduced in this paper, which can be used for single RF MIMO transmission. Combined the negative resistance circuit with parasitic antenna, the matching network also function as radiation pattern switching. Unlike conventional RF matching, the proposed matching is towards certain radiation pattern, with controllable matching component, such network can also support higher order modulation schemes, e.g., QAM. According to comparison between simulation and mathematics calculation, it is feasible

to have such a practical matching network for single RF MIMO communication.

References

[1] A. Mohammadi, F.M. Ghannouchi, "Single RF front End MIMO transceivers," *IEEE Communications Magazine*, vol. 49, pp. 104–109, 2011.

[2] B. Han, V.I. Barousis, A. Kalis, A.G. Kanatas, "Active parasitic arrays for low cost compact MIMO transmitters," *IEEE 5th European Conference on Antennas and Propagation (EUCAP)*, vol. 1, pp. 3663–3667, 2011.

[3] L. Mohammad, M. Abbas, A. Abdolali, "A novel MIMO receiver using antenna selection and time-multiplexed single RF technique," *International Conference on Microwave and Millimeter wave Technology (ICMMT)*, vol. 1, pp. 2051–2054, 2010.

[4] E.K. John, etc, "Achieving MIMO performance with single antenna radios," *The 2010 Military Communications Conference Unclassified Program Waveforms and Signal Processing Track*, vol. 1, pp. 814–819, 2010.

[5] B. Han, M. Liu, N. Ge, "UWB down convert circuit and measurement," *IEEE International Conference on Microwave and Millimeter Wave Technology (ICMMT)*, vol. 1, pp. 1472–1475, 2010.

[6] ——, "A 3-5GHz UWB CMOS receiver with digital control technique," *IEEE 13th International Symposium on Design and Diagnostics of Electronic Circuits and Systems (DDECS)*, vol. 1, pp. 157–160, 2010.

Paper C

Low Cost Wireless Sensor Network for Continuous Bridge monitoring

B.Han, A.Kalis, P.Tragas, R.H.Nielsen, R.Prasad

The paper has been published in the
Proceedings of the Sixth International IABMAS Conference on Bridge Maintenance, Safety, Management, Resilience and Stainability Vol. 1, pp. 96–98, 2012.

The layout has been revised.

Abstract

Continuous monitoring wireless sensor networks (WSN) are considered as one of the most promising means to harvest information from large structures in order to assist in structural health monitoring and management. At the same time, continuous monitoring WSNs suffer from limited network lifetimes, since they need to propagate large amounts of data over regular time intervals towards a single destination in the network. Propagation of information is done through multiple hops, suffering from collisions, retransmissions and therefore high energy consumption. Moreover, since there is a bottleneck effect around the network sink, all routing layer algorithms will always deplete the power of the last tier before the fusion center. Finally, theory shows that in such networks scalability could become an issue since transport capacity per node is severely affected as the number of nodes within the network increases. Therefore, in order for WSNs to be considered as an efficient tool to monitor the health state of large structures, their energy consumption should be reduced to a bare minimum. In this work we consider a couple of novel techniques for increasing the lifetime of the sensor network, related to both node and network architecture. Namely, we consider new node designs that are of low cost, low complexity, and low energy consumption. Moreover, we present a new network architecture for such small nodes, that would enable them to reach a base station at large distances from the network, with minimal energy.

1 Introduction

Smart management of large structures requires the acquisition of large amounts of data from multiple sensors placed on critical points of the structure, which are sampled continuously over very large periods of time. In order to access the sampled data, a network of sensors is formed, responsible for transferring information from the structure to a fusion centre. The use of wireless sensor networks (WSN) has already been proposed for this task, since the use of wireless links overcomes some significant problems [1] related to the cost of network placement and maintenance. However, the use of WSNs does not come without problems. Traditional sensor networks [2], adopting standard wireless schemes to organize the network topology (e.g. Zigbee), are not optimal in terms of energy efficiency [3], Propagation of information is done through multiple hops, suffering from collisions, retransmissions and therefore high energy consumption. Moreover, since there is a bottleneck effect around the network sink, all routing layer algorithms will always deplete the power of the last tier before the fusion center. Finally, theory shows that in such networks scalability could become an issue since transport capacity per node is severely affected as the number of nodes within the network increases. Therefore, in order for WSNs to be considered as an efficient tool to monitor the health state of large structures, their energy consumption should be reduced to a bare minimum. To

overcome the aforementioned problems, low cost, energy efficient wireless sensor network techniques are proposed in this work, which can reduce the power consumption significantly. Namely, we propose the use of an energy efficient RF front end circuit on the sensor node, which is composed of an adaptive antenna scheme and an active reflector node architecture, in order to significantly increase network lifetime. In order to take full advantage of the improved sensor node design, a single hop method [4] is also considered for increasing the energy efficiency of the whole sensor network. This paper is organized as follows: Section 2 focuses on the sensor node design, which includes the proposed adaptive antenna design, and the active reflector architecture; section 3 presents the wireless sensor network single-hop architecture. The conclusion of the paper is given in Section 4.

2 Wireless Sensor Node Design

2.1 Adaptive antenna

One of the key elements of sensor nodes, which is often overlooked, is the device that enables electromagnetic signals to be transmitted and received from the sensor node: the antenna. Traditional wireless sensor network implementations often use wire antennas, while only recently more sophisticated printed antennas were considered for wireless sensor nodes [5]. However, existing antenna designs can be the cause of significant energy waste, regardless of their radiation efficiency characteristics. The reason is that although the antenna itself can be designed to perform in an optimal fashion, when the sensor nodes are deployed in the field, these characteristics are severely affected by the materials and structures in the vicinity of the node. For example, the same antenna that radiates with high efficiency in a wooden structure, it does not radiate next to a concrete structure filled with steel. Therefore, since no one can foresee all the possible environments that a single node will be placed in, the node antenna has to be adaptive in order to adjust its radiation characteristics and achieve optimal radiation efficiency in all possible deployment scenarios.

Recently [6] a novel reconfigurable antenna design was proposed for enhancing the spectral efficiency characteristics of communication.

The proposed antenna is a parasitic antenna array (Figure C.1) known as electronically steerable passive array radiator (ESPAR), which is capable of reconfiguring its radiation pattern. The control of the radiation pattern is performed by changing the reactive loads of the parasitic elements using baseband control signals. The ESPAR antenna meets both the small size and low-cost requirements of sensor nodes since it allows for inter-element spacing of $\lambda/20$ or less, and requires only a single active front end path to drive the single active antenna of the array. In [6] the ESPAR antenna concept was extended to increase the control capabilities of the antenna through the use of negative resistance circuits as loads of the parasitic antennas. Extensive sim-

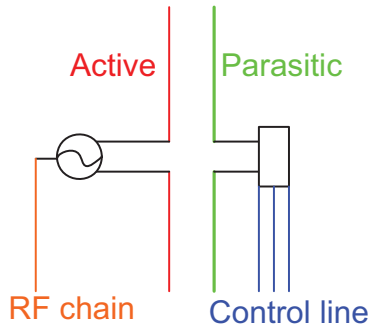

Fig. C.1: Block diagram of ESPAR antenna with a single active element and single parasitic element.

ulation runs showed that reconfigurable complex loads with a negative real part can significantly extend the capabilities of parasitic arrays to incorporate any modulation scheme. Negative resistances, although they are active circuits, they do not require the implementation of full radio-frequency/intermediate-frequency (RF/IF) paths, thus preserving the low-cost, low complexity nature of parasitic arrays.

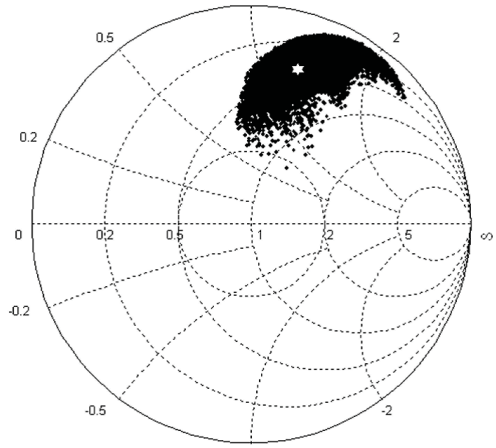

Fig. C.2: ESPAR antenna port impedance for 5000 loading scenarios.

The same concept is proposed here not only for adjusting the radiation pattern of the antenna for efficient communications, but also for matching the port impedance of the ESPAR to the diverse environment characteristics for achieving maximum energy efficiency. An important consideration noted in [7] [8] is that the port impedance of

the ESPAR antenna varies in accordance with the value of reactance employed to load the parasitic elements. Therefore, control of the parasitic results in control of the port impedance. This effect is shown in Fig.C.2, where it is clear that the use of parasitic control can significantly alter the return loss characteristics of the sensor antenna, thus enabling full control of the device and good adaptability to a variety of deployment scenarios.

2.2 Active reflector architecture

In order to further reduce the power consumption of senor nodes, an active reflector node architecture is adopted [9] [10] By shifting the main tasks of information fusion and signal processing to the base station, the transmission circuit on the sensor node can be very simple, as shown Fig.C.3. The main idea in this design is the following: The base station transmits a modulated frequency though its antenna, which serves as a synchronizing and clocking signal for the nodes. When the sensor node receives this signal, it modulates it with sensed data by a voltage controlled amplifier and frequency selection circuit, in order to send information back to base station.

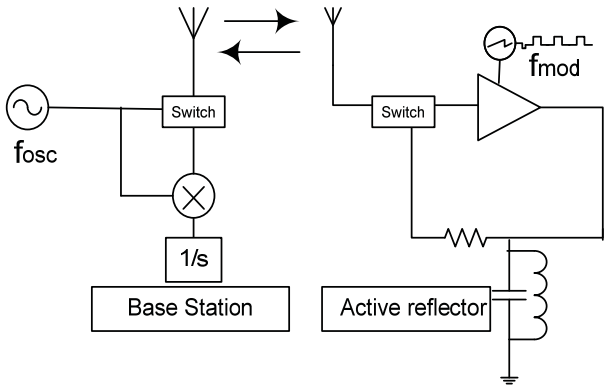

Fig. C.3: Block diagram of an active reflector with FMCW.

The modulated signal on the sensor node can be formed by one or more frequencies using either OOK or the more power efficient FSK modulation. The sensor node can reproduce the carrier frequency directly from the antenna, without using any additional power hungry oscillator. An additional advantage of the proposed active reflector architecture is its inherent localization ability. By processing the phase information of the reflected signal format the base station [11], the distance of the sensor node can be measured. Therefore, when multiple base stations are present, we can retrieve location

information of the sensor nodes without any additional cost.

The main challenge of the active reflector design is the frequency regeneration circuit called injection locked oscillator, which is actually composed of a tunable amplifier. Usually the antenna on the sensor node is single ended, while for the reliability consideration, the symmetric designed amplifier is usually full-differential, calling for a low-return loss balloon design.

Another challenge is the switch design on the active reflector. Usually the switch is controlled by the baseband to determine the transmission period and receiving period. However, for a low cost reflector of a sensor node, the complexity of the baseband circuitry should be minimized. In order to switch the antenna directly on the front end, a high accuracy delay circuit is necessary, which is hard to implement with the traditional shift-register [12] [6] design approach. Instead, the charge capacitor array is a good candidate approach for the delay circuit. Moreover, since the sensor cost is directly related to the silicon area required for the integrated design, and the capacitor array consumes lot of area in CMOS, the in-saturation biased MOSFET switch capacitor [13] will be adopted.

3 Network Architecture

3.1 Energy efficient wireless sensor networks

In addition to the novel sensor node architecture, energy saving techniques are also implemented at the network level, using the appropriate network topology and network coding design. There are many existing schemes for sensor communications, including Zigbee, Bluetooth and Mesh network [14] [15], etc. but none of those techniques meets the requirements of energy efficiency. New techniques that reduce the power consumption of the whole network are therefore investigated. Broadcasting is a good approach to implementing energy efficient communications, because most of the time all the sensor nodes work at a listening mode. When the sensor nodes receive a pre-defined signal from the base station, they switch to active mode and lock their carrier frequency according to the pilot signal. All the sensor data are collected at the fusion center [16]. In a common structural monitoring scenario, such as that of bridge monitoring, base stations can be installed on the bridge pier or the riparian, as shown in Figure 4; a relay station is put in the middle, depending on the topology and the dimensions of the bridge. Although the power consumption of this model is low since the transmission circuit on she sensor is switched off most of the time. There are some problems for this broadcasting method. It needs intelligent techniques for smart utilization of the spectrum and synchronization of the sensor nodes.

Furthermore, many sensor nodes send signals at the same time, making it very difficult for the fusion station to distinguish the received signals. We therefore propose that sensors use a code division multiple access (CDMA) scheme for sharing the link. CDMA

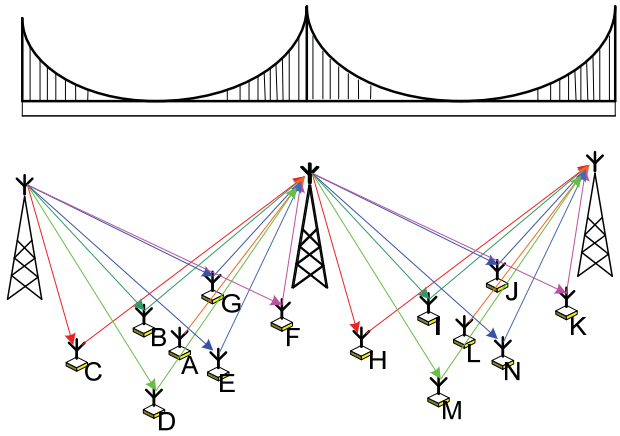

Fig. C.4: Picture of the bridge model (top) and the sensor network topology (bottom).

is implemented using pseudo-random orthogonal sequences for sharing the interference spectrum. This approach has the following advantages: Using synchronized sensors that transmit at the same time a PN-code can be exploited for cooperative beam forming applications as in [17], thus extending the range of sensors and reducing the overall power consumption. Furthermore, for sensors having a direct line of sight to the base station, their position can be obtained by means of time-of-flight measurements.

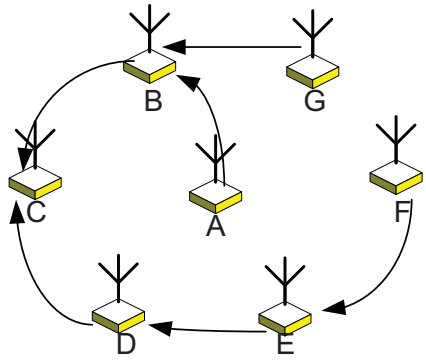

Fig. C.5: Picture of the multi hop communication method.

3.2 Multi hop VS single hop

Another widely used method for propagating data within in wireless sensor networks is the multi-hop communication method [15], where a set of self-organized nodes propagate information by talking with their direct neighbors. This scheme does not require long distance transmissions, which could reduce the energy efficiency per transmission. The multi hop network has its inherent self-organization ability which could increase the reliability of the network dramatically. As shown in Figure 5, assuming that a sensor node A needs to communicate with node C in a bridge monitoring sensor network, when a car passes though and breaks the link between A and C, then node A will send the signal to node C through the nearest node B. With this message forwarding principle, all the sensor nodes can form a realizable ad-hoc network where all the sensor nodes are connected together. The far node F could reach to node C in 3 hops though node E and node D. However, a significant drawback of this transmission scheme is the low energy efficiency of the total network. Each sensor node must have the capacity to work as both a repeater and a client. The data from node F to node C needs four sensor nodes to work together in order to form a link; two of them just consume energy and repeat the message, which is not an energy efficient approach. Assuming a sensor network has the capacity of N sensor nodes, in the worst situation, the farthest sensor node needs (N-2) repeaters to the fusion center, so the maximum message of the whole network is:

$$C_N^1 \times \frac{N \times (N+1)}{2} \tag{C.1}$$

Assuming the average power efficiency of the single hop method described in the previous paragraph, compare to the multi hop method described here, the efficiency ratio for each signal is:

$$\frac{2}{N \times (N+1)} \approx \frac{1}{N^2} \tag{C.2}$$

which is much lower than C.1. This means that at the system level, the multi hop transmission method consumes more power than the single hop, although the communication distance between each node is small, but the whole network needs more nodes to cooperate per single packet transmission. According to this comparison, the geography dimension of the practical sensor network has great influence on the energy efficiency. In the bridge monitoring example, the fusion center is located at the bridge pier or the riparian, therefore the distance between the fusion center and the farthest sensor node is big. Since the energy efficiency per message satisfies formula (C.2), the multi-hop scheme is not the best approach to energy efficient communication. Moreover, in the same example we should also take into account that the sensor node working closer to the fusion centre will act most of the time as a repeater, just forwarding messages from other nodes. As a consequence, this node will die more quickly than others, leading to a quick network partitioning.

3.3 Cooperative beamforming

Recently, a novel sensor network topology for energy efficient communications has been proposed, based on the concept of cooperative beam forming [18]. The main idea behind cooperative beam forming is that the following: assuming N nodes are randomly placed within an area, sharing the same data information, they can be configured to act as a random antenna array and produce a directional beam toward a desired direction [19], as shown in Figure C.6. The beacon station sends a cooperative pilot signal to the sensor nodes, which synchronizes the nodes in such a way that forces the entire sensor array to work as a random antenna array pointing towards the fusion center. The power consumption for each sensor node is low since it exploits the array gain to reach large distances. But the overall transmission power will in this case be N times greater than that of a single node. According to the comparison as it shown in formula (C.2), the energy efficiency ratio in the cooperative beam forming is N, which is higher than 1. Therefore, when nodes cooperate, they can support transmissions over large distances, enabling direct access to a distant fusion center without burdening the network with extra relaying tasks.

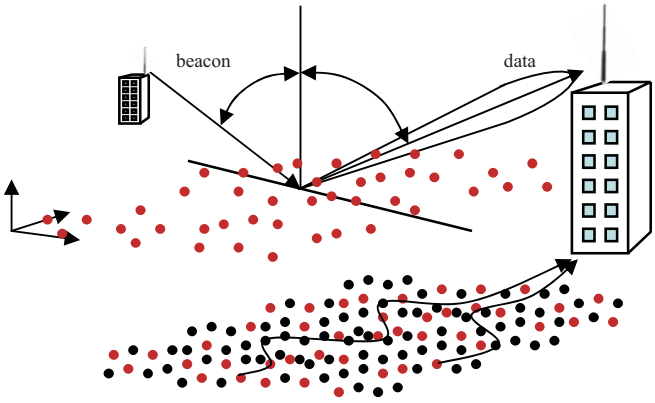

Fig. C.6: Picture of the cooperative beam forming method.

The challenge in cooperative beam forming is the accurate synchronization among sensor nodes. All nodes in the beam forming network have to share information. So careful sensor node design is a critical rule in this method, the adaptive antenna mentioned in section 2.1 and active reflector mentioned in section 2.2 are key elements for the sensor node in this proposed cooperative beam forming network architecture.

4 Conclusion

The challenge in cooperative beam forming is the accurate synchronization among sensor nodes. All nodes in the beam forming network have to share information. So careful sensor node design is a critical rule in this method, the adaptive antenna mentioned in section 2.1 and active reflector mentioned in section 2.2 are key elements for the sensor node in this proposed cooperative beam forming network architecture.

References

[1] M. Bhardwaj, A.P. Chandrakasan, "Bounding the life time of sensor networks via optimal role assignments," *Proceedings of INFOCOM*, vol. 3, pp. 1587–1596, 2010.

[2] T. Harms, S. Sedigh, F. Bastianini, "Structural health monitoring of bridges using wireless sensor networks," *Instrumentation and Measurement Magazine*, vol. 13, pp. 14–18, 2010.

[3] Z. Liu, B. Wang, W. Yang, "Design and deployment of bridge structural health monitoring system based on wireless sensor network," *6th International Conference on Wireless Communications, Networking and Mobile Computing (WiCOM)*, vol. 1, pp. 1–4, 2010.

[4] A. Kalis, A.G. Kanatas, "Cooperative beamforming in smart dust- getting rid of multi-hop communications," *IEEE Pervasive Computing*, vol. 9, pp. 47–53, 2010.

[5] A. Kounoudes, A. Kalis, T. Onoufriou, A. Constantinides, "Smart wireless sensor technology for continuous health monitoring of structures," *IABMAS 2010 International Conference*, vol. 1, pp. 1–4, 2010.

[6] B. Han, V.I. Barousis, A. Kalis, A.G. Kanatas, "Active parasitic arrays for low cost compact MIMO transmitters," *IEEE 5th European Conference on Antennas and Propagation (EUCAP)*, vol. 1, pp. 3663–3667, 2011.

[7] T. Ohira, K. Gyoda, "Electronically steerable passive array radiator antennas for low-cost analog adaptive beamforming," *IEEE Conference on Phased Array System Technology*, vol. 1, pp. 101–104, 2010.

[8] A. Akiyama, K. Gyoda, T. Ohira, M. Ando, "Numerical simulations on beam and or null forming performance of ESPAR antennas," *Electronics and Communications in Japan*, vol. 86, pp. 1–11, 2003.

[9] S. Wehrli, D. Barras, F. Ellinger, H. Jackel, "Inte-grated active pulsed reflector for FMCW radar localization," *IEEE MTT-S International Microwave Symposium Digest*, vol. 1, pp. 81–84, 2009.

[10] S. Krishnan, V.P. Kumar, W. Wang, "UWB-IR active reflector for high precision ranging and positioning applications," *IEEE International Conference on Communication Systems (ICCS)*, vol. 1, pp. 14–18, 2010.

[11] M. Bhardwaj, A.P. Chandrakasan, "Bounding the life time of sensor networks via optimal role assignments," *IEEE Proceedings of INFOCOM*, vol. 3, pp. 1587–1596, 2002.

[12] J. Lan, L.G. Wang, H.K. Zhi, S.Y. Kiat., "A random number generator for low power cryptographic application," *International SoC Design Conference (ISOCC)*, vol. 1, pp. 328–331, 2010.

[13] W.F. Lee, P.K. Chan, "An injectioning switch for switched capacitor circuit applications," *IEEE Transactions on Instrumentation and Measurement*, vol. 54, pp. 2416–2426, 2010.

[14] X. Jiang, Y. Tang, Y. Lei, "Wireless sensor networks in structural health monitoring based on ZigBee technology," *3rd International Conference on Security and Identification in Communication (ASID)*, vol. 1, pp. 449–452, 2009.

[15] F.X. Li, A. Islam, G.C. Perera, P.K. Kolli, "Real time urban bridge health monitoring using a fixed wireless mesh network," *IEEE Radio and Wireless Symposium (RWS)*, vol. 1, pp. 384–387, 2010.

[16] M.J. Whelan, M.V. Gangone, K.D. Janoyan, "High-way bridge assessment using an adaptive real time wireless sensor network," *IEEE Sensors Journal*, vol. 9, pp. 1405–1413, 2009.

[17] H. Ochiai, "Collaborative beamforming for distributed wireless Ad Hoc sensor networks," *IEEE Transactions on Signal Processing*, vol. 53, pp. 4110–4124, 2005.

[18] Y. Kung, "Blind beamforming on a randomly distributed sensor array system," *IEEE Journal on Selected Areas in Communications*, vol. 16, pp. 1555–1567, 1998.

[19] L. Dong, A.P. Petropulu, H.V. Poor, "A cross-layer approach to collaborative beamforming for wireless Ad Hoc networks," *IEEE Transactions on Signal Processing*, vol. 56, pp. 2981–2993, 2008.

Paper D

Explore the Capability of ESPAR Antennas for Low Cost Communication

B.Han, A.Kalis, C.B.Papadias, R.H.Nielsen, R.Prasad

The paper has been presented in the
The 28th Conference on Technologies and Visions for a Sustainable Wireless Internet
Athens,2012.

The layout has been revised.

Abstract

ESPAR antenna systems are composed of one active and several parasitic elements and by changing the characteristic of the parasitic elements on the antenna, the radiation pattern will also change. Such characteristic makes ESPAR antenna useful in many applications, e.g., single RF MIMO transmission. However, for higher modulation schemes like 16-QAM, more radiation patterns are needed which require a wider control range on the parasitic antenna load. In order to explore the capability of ESPAR antennas, negative resistance was proposed, but their values cannot be easily controlled both on the real and imaginary part. So a matching network is required to control the load value. This paper presents an idea of adjusting the parasitic ESPAR antenna loads with controllable passive elements. According to simulation, the control circuit consumes less than 1mW power on 64 patterns selection, which explores the capacity of ESPAR antenna for high order modulation applications

1 Introduction

ESPAR antennas bring a promising future for many low cost communication proposals, such as single RF MIMO communication [1] which is investigated more and more in recent research papers. Because of the low complexity and low power consumption characteristic of the ESPAR antenna, it is an ideal antenna for portable mobile devices. Single RF MIMO transmission can be implemented by using an ESPAR antenna with a single active and one or two parasitic elements [2]. By switching among the radiation patterns driven by the changing characteristic of parasitic elements, such antennas can function as conventional MIMO transmission without additional RF chain, thus the main power consumption is very low. Previous research on such system implementation is limited to simple modulation schemes, e.g. PSK modulation. In order to fully explore the capability of ESPAR antennas for single RF MIMO transmission, higher order modulation schemes have to be investigated. Thus, either more parasitic elements are needed or a wider load range of the single parasitic element. This paper focuses on the latter. As mentioned in [3], only one parasitic and one active element are used for single RF MIMO uplink and the load impedance of the parasitic elements is changed by using a negative resistance circuit. Due to the power constrain on the active circuit, the parasitic element can only use a limited number of load values. This results in limitations in the radiation pattern that can be driven from such an ESPAR antenna, so only simple modulation scheme can be adopted, e.g., QPSK. In order to have more complex modulation while keeping the antenna as simple as it was before, a better load control circuit is needed. The load control circuit should have the capability of turning the impedance within a wider range, so that more radiation patterns can be mapped on. Moreover, the negative resistance generated from a CMOS circuit in [3] can only be controlled on the

real part and each time the real part changes, the imaginary part also changes. However, mapping the circuit to the radiation pattern requires that both the real part and imaginary part of the load impedance can be changed independently and accurately, so an adjusting network from the negative resistance circuit to the parasitic antenna is needed. This paper will present the idea of the implementation of such an adjusting network and with this method we can explore the capacity of ESPAR antennas for low cost single RF MIMO transmission with 16-QAM modulation. The organization of this paper is the following: Section II gives the theoretical analysis, Section III presents the negative resistance and matching and Section IV is the comparison between simulated result and theoretical values. Section V concludes the paper.

2 Requirement of ESPAR Antenna

2.1 System Analysis

Conventional MIMO transmission is implemented by using two or more data streams going into different RF chains, while single RF MIMO transmission uses the same principle but only one active RF chain is used and MIMO is implemented by switching on the different radiation patterns. We are assuming the use of a single active single parasitic ESPAR antenna element for 2x2 MIMO transmission. One data stream goes to the active RF chain; the other data stream first goes to the mapping circuit, where it will be combined with the first data stream. Then their combination is used as a mapping control, to switch among the radiation patterns of the antenna. The mapping circuit actually changes the load impedance of the parasitic element on the antenna, when the antenna load changes, the radiation pattern also changes. In this way, the data stream combination which mapped to the parasitic arrays will switch among the radiation patterns and, thus, a low cost single RF MIMO transmission is implemented.

$$\begin{aligned} &AF = S_1 b_1(\theta,\varphi) + S_2 b_2(\theta,\varphi) \\ &\Rightarrow AF = S_1 \left(b_1(\theta,\varphi) + \tfrac{S_2}{S_1} b_2(\theta,\varphi) \right) \end{aligned} \tag{D.1}$$

The equation above gives the antenna factor with combination of the two data streams used in 2X2 MIMO transmission, S1is from the first data stream, and S2 is from the second data stream, b1 and b2 are the two basis patterns.

2.2 Antenna Implement Requirement

We are assuming that such a single RF MIMO transmission adopting the 16-QAM modulation, and the active element and parasitic element on the ESPAR antenna have an inter-element space of 1/16 wavelength. According to the rough simulation, the minimal load impedance for the 16-QAM pattern is around -65Ω on the real part and

around -80 Ω on the imaginary part. As mentioned in [3], by using active CMOS circuit, we could generate a negative resistance up to -230Ω on the real part and -110Ω on the imaginary part. Assuming the parasitic antenna has the self-impedance of 50 Ω at 2.5GHz, in order to have the combined load value satisfy the radiation requirement, a matching circuit is required between the negative resistance circuit and the parasitic antenna element. For a 16-QAM modulation, the combination of two data streams will generate 256 values. Due to symmetry, only 64 different values are needed. The next section will present this matching circuit, which also does the function of switching among the patterns.

3 Mapping and Switching

3.1 Mapping to the patterns

The topology of the proposed matching antenna system is shown in Fig.D.1. One active element and one parasitic element are coupled on the ESPAR antenna and by changing the load impedance of the parasitic element, the radiation of the whole antenna will change. The negative resistance circuit will generate a constant value, which is considered as large as possible, e.g., -230Ω. The proposed adjusting network is placed between the parasitic antenna and the negative resistance circuit.

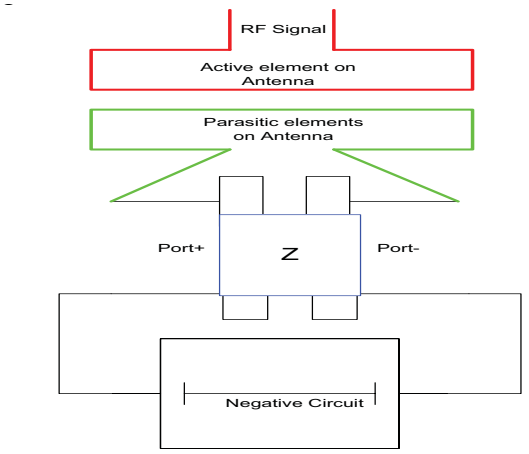

Fig. D.1: Topology of impedance control for the parasitic antenna.

The adjusting network has three main functions: first, it will function as the mapping circuit as mentioned in Section II, which will switch among the 64 load values with

control signal generated from combination of the two data streams; second, the adjusting network will match the negative resistance to the pre-defined load values with the parasitic antenna element; finally a very important function of the matching network is to avoid oscillation as the negative resistance generation block follows the principle of positive feedback, so if phase shift larger than 360 degrees, oscillation will happen. Proper design of the matching block is required for reliability and stability issues.

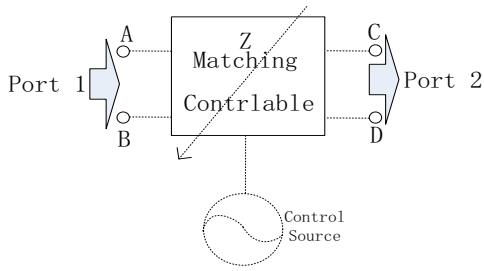

Fig. D.2: Topology of a signal controlled Matching network.

The control single for the matching network is generated according to the data stream S_2/S_1 ; A typical design method of the control unit is using voltage controlled variable resistor and inductor for the real part and imaginary part separately. The impedance on the real part Z_1 and on the imaginary part Z_2 will be under the following relation with mapping signal S_2/S_1:

$$\begin{aligned} Z_1 &= f_1(u_1(\left(\frac{S_2}{S_1}\right), \sigma), t) \\ Z_2 &= f_2(u_2(\left(\frac{S_2}{S_1}\right), o), t) \end{aligned} \tag{D.2}$$

Here the coefficient and are the real part influence factor and imaginary influence factor separately; the time factor t indicates the impedance is frequency dependent. Mapping coefficient u_1 and u_2 indicate the influence of the mapping control. Such a system requires switching among the radiation patterns randomly and the control signal should have the random changing ability due to the data streams of S_1 and S_2 being random. Analog control is not capable of such random switching, so a digital control signal is proposed in the following section.

3.2 Digital switching among the patterns

As mentioned in Section II, a single RF 2×2 MIMO with 16-QAM modulation needs 64 radiation patterns. Therefore the impedance adjusting [4] [5] circuit must be able to switch among 64 different loads values. The proposed idea is shown in Fig. 3, where an

address searching method is used for the complex 64 patterns with just a control signal of 6 bits.

The control network in Fig.D.3 is made using an 8×8 array with two 3-8 converters. RF Port 1 and RF Port 2 are connected to the negative resistance core and parasitic antenna respectively. Each cell inside the array is a digital switch with pre-settled value pairs (see Fig. D.3). In this topology, only 6 bits are required for the 64 loads selection. Each time the transmitted symbols are simply pre-coded and get 6 bits control signal for load selection, and this control signal will be decoded by the `address searching` block (the two 3-8 converters) to get the right value.

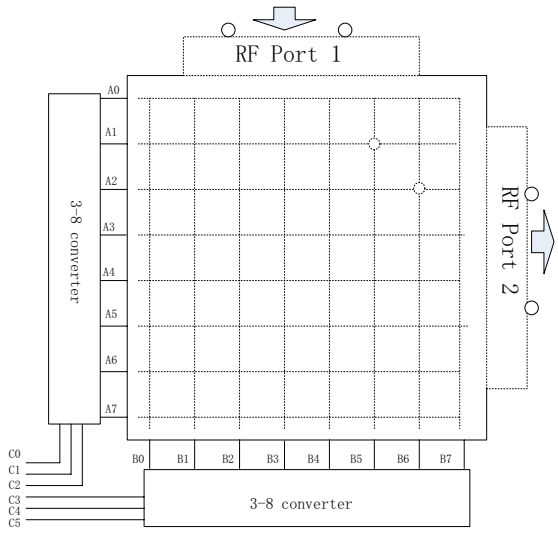

Fig. D.3: Topology of address-searching network for 64 patterns switching.

For example, if the desired load is -63.13 - j42.39 Ω, which is pre-allocated in the matching unit of A1b5; then the control signal 101001 is sent to the control line C5-C0; the control block (3 8 converters) decodes this control signal, then the address searching code 00000010 appears in the A7-A0 branch and 0010000 appears in the B7 B0 branch, the adjusting unit for this load is selected, which is A1B5. Actually this desired radiation pattern located in unit A1b5 can be any other 64 patterns in the pre-allocation, here the load of -63.13 - j42.39 Ω is chosen to have the design of the adjusting network in accordance with the radiation patterns. In the same way, the control signal for A2B6 is 110010. By using this method, selection on 64 radiation patterns can be conducted with just 6 bits signals, which reduces the complexity on the control and selection.

3.3 Matching to the proper value

Inside the matching network, there are 64 smallest matching units (Fig.D.4) which adjust the negative resistance to the antenna load with a pre-defined resistance and inductance values. Through this matching, the antenna load impedance is set to the right value for the radiation pattern. Fig. D.4 gives the architecture of a smallest matching unit inside the matching network. An L matching network is implemented inside each matching unit cell. Each matching circuit is connected between the negative resistance circuit and the parasitic antenna element. [6]

The combined resistance value R_s is composed of a negative resistance Z_N and a tuning resistance R_t, then the combined resistance R_s is considered as the `source` resistance in the matching unit, which is responsible for the real part impedance values; the antenna impedance Z_l is considered as load in the matching unit; the tuning inductance value L_t and capacitance value C_t are considered as tuning variables in the matching unit, which are responsible for the imaginary part of the impedance values.

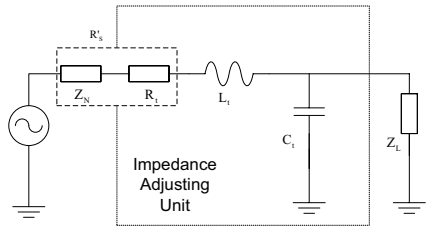

Fig. D.4: A smallest matching unit inside the adjusting network.

Due to the fact that a serialized inductor and a parallelized capacitor can be considered as conjunction components at a specific frequency, only the inductor value L_t is used in the simulation, which is sufficient to change the load impedance on the imagery part.

Fig. D.5 gives the simulated load impedance values on the real part and the imaginary part. By tuning the value of R_t and L_t , we can get the simulated curve in Fig. D.5. Two markers m1 and m5 indicate the real part and imaginary part of the load impedance value at 2.5GHz. From the curve, we know that with the tuning resistance 167.5 Ω and tuning inductance 4.82 nH, the simulated load impedance after matching is -63.16 - j42.25 Ω. The simulation result indicates that the matching between the negative resistance to the antenna load is feasible with physical available passive components; the resistance value and inductance value are practical for implementation. The simulation also indicates that the simulated practical values have slightly differences from the theoretical values. This will be compared in the next section.

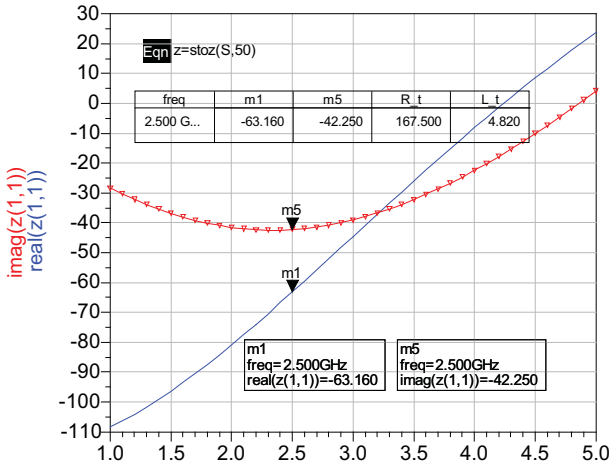

Fig. D.5: Simulated impedance by using the matching network unit.

4 Simulated Results

4.1 Practical Values for 16-QAM

Assuming a 2×2 single RF MIMO transmission with 16-QAM modulation, the first data stream S_1 contains 16-QAM symbols A1 A16; the second data stream S_2 contains 16-QAM symbols B1-B16. So combination of S_2/S_1 has 256 values and due to identical symmetry, 64 load values for radiation patterns are required. For an easy indication, the first 16 values of such combination are shown in Table D.1:

The R_T (in Ω) and L_T (in nH) are the tuning values in each matching unit cell for the first 16 values of the 64 loads. The tuning resistance ranges from 200 to 300 Ω, tuning inductance ranges from 2.14nH to 9.55nH and all these values are feasible for physical circuit implementation. The Re(Z) and Im(Z) are the real part and the imaginary part of simulated load impedance values, which is generated from the tuning values R_T and L_T and all those values are plotted at 2.5GHz.

4.2 Comparsion to the Theoretical Values

The proposed adjusting network is simulated according to the ideal impedance values. Due to the limitation on physical available resistance or inductance values, the simulated values are different from the ideal ones. Taking into account that the practical values have ±0.2-±0.5 mismatching them selves, the simulated impedance value is imported back into the radiation pattern simulation system. The radiation patterns are compared

Table D.1: THE FIRST 16 SYMBOLS FOR 16-QAM SINGLE RF MIMO

Symbols Pairs $[w_0 w_1] = [a_n b_m]$	Symbol $w_0 = a_n$	Symbol $w_1 = b_n$	Load(Ω) Real	Load(Ω) Imaginary
$a_1 b_0$	-1+3j	-3+3j	-39.62	-4.29
$a_1 b_1$	-1+3j	-3+1j	-37.32	-19.13
$a_1 b_2$	-1+3j	-3-1j	-18.13	-25.27
$a_1 b_3$	-1+3j	-3-3j	-7.63	-14.52
$a_1 b_4$	-1+3j	-1+3j	-50.37	6.195
$a_1 b_5$	-1+3j	-1+1j	-81.84	-26.04
$a_1 b_6$	-1+3j	-1-1j	14.11	-56.74
$a_1 b_7$	-1+3j	-1-3j	7.20	12.22
$a_1 b_8$	-1+3j	1+3j	-44.23	25.38
$a_1 b_9$	-1+3j	1+1j	-51.14	69.90
$a_1 b_{10}$	-1+3j	1-1j	44.80	39.21
$a_1 b_{11}$	-1+3j	1-3j	13.34	6.97
$a_1 b_{12}$	-1+3j	3+3j	-29.40	27.69
$a_1 b_{13}$	-1+3j	3+1j	-18.90	38.44
$a_1 b_{14}$	-1+3j	3-1j	0.29	32.29
$a_1 b_{15}$	-1+3j	3-3j	2.60	17.46

in Fig. D.6. The dashed curve is the radiation pattern from theoretical impedance values and the constant curve is the radiation pattern from the simulated impedance values. This result shows that the practical values have perfect coexistence with the theoretical values. This proves that the proposed architecture on weighting coefficient mapping for 16-QAM single RF MIMO communication is feasible. By exploring this more complex modulation scheme, the efficiency of using bandwidth increased dramatically, as well as the spectrum efficiency.

5 Conclusion

An adjusting network for exploring the capability of ESPAR antennas is introduced in this paper. With a given negative resistance, the proposed architecture can control the impedance accurately both on the real and the imaginary part. By adopting an address-searching method, the control circuit can switch among 64 patterns randomly with only a 6 bits signal. The proposed matching unit contains the physical feasible resistance and inductance values, which makes it possible to provide single RF MIMO transmission with 16-QAM modulation through a low cost ESPAR antenna

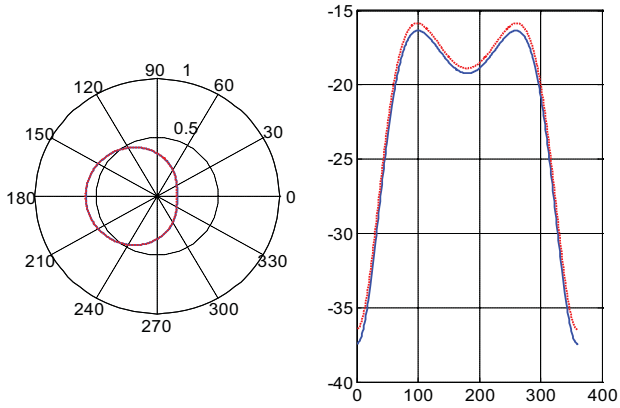

Fig. D.6: Comparison between practical values and simulated values.

References

[1] A. Kalis, A.G. Kanatas, C.B. Papadias, "Novel approach to MIMO transmission using a Single RF front end," *IEEE Journal on Selected Areas in Communications*, vol. 26, pp. 972–980, 2008.

[2] V.I. Barousis, A.G. Kanatas, A. Kalis, "Single RF MIMO systems: exploiting the capabilities of parasitic antennas," *IEEE Vehicular Technology Conference (VTC Fall)*, vol. 1, pp. 1–5, 2011.

[3] B. Han, V.I. Barousis, A. Kalis, A.G. Kanatas, "Active parasitic arrays for low cost compact MIMO transmitters," *IEEE 5th European Conference on Antennas and Propagation (EUCAP)*, vol. 1, pp. 3663–3667, 2011.

[4] I. Ida, J. Takada, T. Toda, Y. Oishi, "An adaptive impedance matching system and considerations for a better performance," *IEEE 5th International Symposium on Multi-Dimensional Mobile Communications*, vol. 1, pp. 563–567, 2009.

[5] E. Kerherve, P. Naud, G. Germain, P. Jarry, "RF antenna matching methods for radar cross section measurements," *IEEE 9th International Conference on Electronics Circuits and Systems*, vol. 1, pp. 85–88, 2009.

[6] B. Han, M. Liu, N. Ge, "A UWB down convert circuit and measurement," *International Conference on Microwave and Millimeter wave Technology (ICMMT)*, vol. 1, pp. 1472–1475, 2010.

Paper E

Localization Techniques in Structural Damage Detection

B.Han, A.Kalis, C.B.Papadias, P.Tragas, R.H. Nielsen, R. Prasad

The paper has been published in the
The IABSE Conference on Assessment Upgrading and Refurbishment of Infrastructures pp. 160–162, 2013.

The layout has been revised.

Abstract

Structural Damage Detection sometimes requires full information of the damage location. If a wireless sensor network is used for damage detection, localization techniques of the wireless sensor network have to be adopted. To locate the sensors in the network, there are mainly two types of methods: range free and range based. The range free method is good at scaling on the network, but such method is not a good solution for low cost design. While the range-based localization methods uses time of arrival (TOA), angle of arrival (AOA), time difference of arrival (TDOA), also received signal strength intensity (RSSI). Among these techniques, the RSSI seems to be an energy efficiency solution for low cost sensor localization. This paper gives the analysis on the RSSI based localization and its accuracy.

1 Introduction

Structural Healthy Monitoring needs to involve a large number of sensors; in some situation such sensors are implemented with wireless transmissions. For structural damage detection, it is necessary that the damage report comes together with its location. The information collected from the sensors should have information of the senor node location. Such issue of the wireless sensor localization has emerged as a topic also in structural damage detection.

Unlike the conventional wireless sensor network, the sensor network used in structural health monitoring has more complicated wireless channel environment. Due to the widely implementation on reinforced concrete in structures, the wireless radio signal can be easily influenced by the surrounding objects, such as shadowing, reflection, scatter and shielding. So the localization method in such environment should be capable of overcoming these barriers; meanwhile, the sensors network should also be designed as simple as possible in terms of energy efficiency concern.

At the same time, if the sensors location is known by the whole network, the routing/planning of signal propagation can be redirected [1], so that the whole system can keep reliable communication. There are two main categories of localization methods, the range free and range based. The range free methods are more easily to be scaled, which is mainly based on the higher layer of the network where the signal is processed digitally [2]. This means a considerable hardware is needed to implement such method. Although the range-based methods are relatively less hardware complexity, the disadvantages is its accuracy. In some case where a large number of the number of beacon is required, this range-based solution can also be complex [3].

The range free localization technique includes the DV-distance, DV-hop and Euclidean methods [4], while the range-based methods has better localization accuracy which includes Received Signal Strength Indicator (RSSI), which measures the atten-

uation of the radio signal; Time of Arrival (ToA), which based on the known speed of the radio propagation speed, and measures the distance by calculating the time delay; Time Difference of Arrival (TDoA), usually it needs two different types of signal and measure their propagation differences between the beacon and the sensor node; Angle of Arrival (AoA), which measure the angle of the arriving signals, and combined with other measured distance, e.g from RSSI it can provide a low cost solution [5].

The paper is organized as following; section1 gives the brief introduction of two main categories localization methods, range-free and range based; section 2 analyses the low cost range-free methods; section 3 presents the low cost range-based methods and its accuracy analysis; a conclusion is given in section 4.

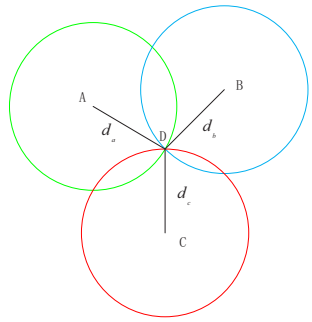

Fig. E.1: Localization a sensor node.

2 Range Free Localization

In the range-free localization methods, there are also algorithms which need a large number of beacon nodes like in range-based, where each sensor will hear several beacon signals at the same time. Also there are algorithm methods based on flooding a network [6].

The DV-distance method is based on adding the distance parameter in each hop during the network flood. The beacons send message with their predefined location information, and the path-length parameter is set to zero. When the signal reaches the receiving node, the path-length will be added with the range, the message will only be forwarded if the current node detects the path length is less than the previous one. Finally each node will have the position information and the minimal path-length to the nearest beacons

The Euclidean method is based on a somehow predefined map of geometry on the node around a beacon. The beacon starts a flood, the nodes around will forward the

information to its neighbours; finally the node will know the distance to the beacon and to other nodes.

The DV-hop methods, The widest technique in this range free localization schemes is DV-Hop algorithm [7], which adopts an updating look- up table based distance vector, it aims at all the nodes being able to get distance information by the hops to the beacon nodes. The look-up table will be updated by the sensor nodes to its neighbours, when the beacon nodes gets the distance between other beacon nodes, the average distance of one hop will be estimated by this beacon, then a correction will be added to the following message, so the entire network will be corrected; when the node receives the correction, the distance between itself and beacon node will be estimated [8].

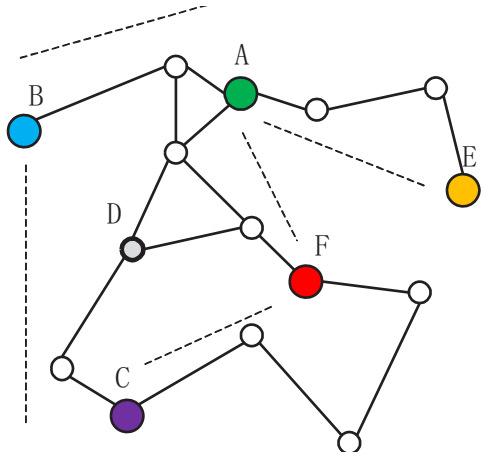

Fig. E.2: Localization the node by DV-Hop.

The broadcasting message from the beacon node will flood throughout the network, the location information of the beacon is contained in the message, in the beginning the hop-counter in the message is set to 1; the sensor node keeps and updates their look-up table, the key information in the look up table is the location coordinate of the beacon (x_i, y_i),and the hop counter to the particular beacon h_{ij} , their value will be updated by the received message. If the received signal message contains lower h_{ij}, the corresponding item in the look up table will be replaced with the information in this message. This message will be flooded outward with h_{ij} +1. Otherwise the received message will be ignored. In this way, all nodes in the network will get the smallest distance in hops to a very beacon nodes.

Once the beacon node obtains location and h_{ij} to other beacon nodes, it estimates

an average size c_i for one hop as in (E.1)

$$\forall j \cap i \neq j, \rightarrow c_i = \frac{\sum \sqrt{(X_i - X_j)^2 + (Y_i - Y_j)^2}}{\sum h_{ij}} \tag{E.1}$$

Where the (x_i, x_j) and (y_i, y_j) are the coordinates of beacon node i and j and h_{ij} is the hop distance from beacon node i to j . Once the average hop size is calculated, the beacon node propagates this information to the whole network; once a unknown node can calculate the distance estimation more than 3 beacons, it uses triangulation to estimate it location.

3 Range based Localization

The range based localization includes RSSI, ToA TDoA and AoA, assuming the sensor node is simply designed for the low cost and energy efficiency constrains, it is necessary that the localization information can be get by just from the RF signal, compared with other methods, the Receiving Signal Strength Indicator gives the simplest way to get the distance information from the sensor to the beacon, because the sensor node need not necessarily to transmit additional signals on the location, just listening to the broadcasting message of the beacon, the node can get its location. so the RSSI is adopted as the low cost localization methods.

At the same time, the RSSI is strongly influenced by the channel characteristic. And for wireless sensors in the structural health monitoring, the wireless channel is much complicated, the multi path, the scatter, and reflection on the structure can heavily influence the accuracy of localization. So the challenge in this localization is the accuracy. Besides, the self-error in the nodes also influence accuracy, such as the battery level of the transmitting and battery level of the receiving, the antenna working environment can also influence the localization accuracy in this methods. In this section the RSSI based localization is analysed and the accuracy due to the influence is also presented.

The Received Signal Strength Indicator (RSSI) uses low complexity hardware for localization, which measures the signal strength of the beacon and converts the signal strength to the distance from the training period in the beginning (to get the channel condition relation with distance.).

Assuming there beacon nodes A,B,C have their know position (x_a, y_a),(x_b, y_b),(x_c, y_c), and assuming there is no interference between each beacon nodes (e.g, they broadcast message at different time slots or using different frequencies.) the node D with unknown position (x, y), The channel path loss is given by E.2 where the signal loss has two main

factor, carrier frequency and distance; usually for a fixed network the carrier frequency is fixed. The path loss is mainly because of distance.E.3

$$L_p = 32.4 + 20\log(f_{(MHz)}) + 20\log(d_{(km)}) \tag{E.2}$$

$$L_p = L_0 + 10\gamma\log(d_{(km)}) \tag{E.3}$$

So the receiving signal strength S has the following E.4 relation with distance, where P_t is the transmission power from the beacon node, G_t is the antenna gain of the transmission beacon node. $G_r$is the antenna gain of the receiving node, and λ is the wave length of the RF carrier.

$$S = PtGrGt\left(\frac{\lambda}{4\pi}\right)^2\frac{1}{d^2} \rightarrow S = K\frac{1}{d_2}; (K = PtGrGt\left(\frac{\lambda}{4\pi}\right)^2) \tag{E.4}$$

Assuming the received signal level from the three beacons are S_a,S_b,S_c, respectively, the measured distance with the signal strength is rewritten byE.6:

$$\begin{aligned} K\Big/\left((x-x_a)^2+(y-y_a)^2\right) &= S_a \\ K\Big/\left((x-x_b)^2+(y-y_b)^2\right) &= S_b (K = PtGrGt\left(\tfrac{\lambda}{4\pi}\right)^2) \\ K\Big/\left((x-x_c)^2+(y-y_c)^2\right) &= S_c \end{aligned} \tag{E.5}$$

Assuming the common coefficient H is given by

$$H = \begin{bmatrix} 2(x_a - x_c) & 2(y_a - y_c) \\ 2(x_b - x_c) & 2(y_b - y_c) \end{bmatrix} \tag{E.6}$$

Then the location of node D is given by

$$\begin{bmatrix} x \\ y \end{bmatrix} = H^{-1}\begin{bmatrix} \left({x_a}^2 + {y_a}^2 - K/S_a\right) - \left({x_c}^2 + {y_c}^2 - K/S_c\right) \\ \left({x_b}^2 + {y_b}^2 - K/S_b\right) - \left({x_c}^2 + {y_c}^2 - K/S_c\right) \end{bmatrix} \tag{E.7}$$

The received RF signal strength can have some variation due to the multi path and scattering as well as shielding, assuming S_{a0}, S_{b0}, S_{c0} are the ideal signal received by single path Line of Sight channel, the actual signal is S_a, S_b, S_c then the error in the signal receiving is given by

$$\Delta S = \frac{(S_a - S_{a0}) + (S_b - S_{b0}) + (S_c - S_{c0})}{{S_{a0}}^2 + {S_{b0}}^2 + {S_{c0}}^2} \tag{E.8}$$

Due to the inaccuracy of the received signal, the distance calculated from the above methods will have error itself, when the error reaches to the distance calculation, this can result in inaccurate determination of the node location, the error caused by such varies can be given from the following equations:

$$\begin{bmatrix} \Delta x \\ \Delta y \end{bmatrix} = H^{-1}\sqrt{K}\begin{bmatrix} 2(S_c - S_{c0})^{-\frac{1}{2}} - 2(S_a - S_{a0})^{-\frac{1}{2}} \\ 2(S_c - S_{c0})^{-\frac{1}{2}} - 2(S_b - S_{b0})^{-\frac{1}{2}} \end{bmatrix} \tag{E.9}$$

The distance absolute error is given by

$$\overrightarrow{r} = x + jy \rightarrow |\Delta\overrightarrow{r}| = \sqrt{\Delta x^2 + \Delta y^2} \tag{E.10}$$

Assuming the signal error from three beacons are the same S_{Er} given by the following:

$$S_{Er} = S_a - S_{a0} = S_b - S_{b0} = S_c - S_{c0} \tag{E.11}$$

The Δr_dis is the distance measurement error, then the distance with error is given in E.12,E.13.

$$\forall i = a, b, c \rightarrow d_i = d_{i0} + Er \times H \tag{E.12}$$

$$Er = |\Delta r\_dis|/H \tag{E.13}$$

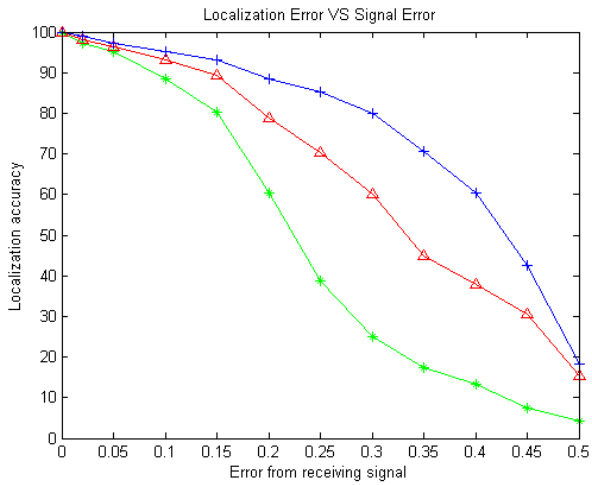

Fig. E.3: Localization Accuracy due to RSSI errors.

The plot indicates the accuracy due to the signal error in Fig.E.3, the higher error from the receiving signals, the worse accuracy of the localization, it becomes 50 percent of the receiving signal is wrong, and then the accuracy rate is almost zero. Which means the RSSI method is highly sensitive to the channel environment, Also from the Fig.E.3 we can see the higher the correction factor, the better accuracy of the localization, which means if a certain correction factor is given to the sensor network, the RSSI based localization is still a good promise for low cost localization

4 Conclusion

Wireless sensors are widely used in structural damage detection. In order to get the health information of the structure accurately, the sensor localization is needed and necessary. At the same time, for the concern on energy efficiency, low cost localization techniques are needed. However, there is always a trade-off between accuracy and complexity, in the range-free based methods, DV-hop is analysed, in the range-based method, the RSSI gives the simplest low cost structure. The accuracy is also analysed. It seems the Receiving Signal Strength Indicator (RSSI) methods gives a good low cost solution, and within the acceptably accuracy.

References

[1] L.S. Mihail, R. Vaidyanathan, "Localization of wireless sensor network with a mobile beacon," in *IEEE International Conference on Mobile Ad-hoc and Sensor Systems*, 2004.

[2] A.K. Usman, K. Soummya, M.F. Jose, L. Smith, "Distributed sensor localization using barycentre coordinates," in *IEEE International Workshop on Computational Advances in Multi-Sensor Adaptive Processing*, 2009.

[3] V. Nat, V. Duc, C. Subhash, S.Y. Lee, "Weighted nonmetric MDS for sensor localization," in *International Conference on Advanced Technologies for Communications*, 2008.

[4] Y.F. Zhou, L. Lamont, "A Map registration localization approach based on mobile beacons for wireless sensor networks," in *IEEE Global Telecommunication Conference*, 2011.

[5] S.A. Khan, B. Daachi B, K. Djouani, "Enhanced sensor localization though compensation of battery level decay," in *IEEE Broadband and Biomedical Communications*, 2010.

[6] S. Chen, R. Shu, S. Zhang, X. Zheng , "Evaluate distance measurement how to influence localization in wireless sensor networks," in *2nd International Conference on Consumer Electronics Communications and Networks, (CECNet)*, 2012.

[7] Z. Xia, C. Chen, "A localization scheme with mobile beacon for wireless sensor netowkrs,," in *6th IEEE International conference on ITS Telecommunications Proceedings*, 2010.

[8] K.Z. Liu, X.P. Yan, F.P. Hu, "A Modified DV-HOP localization algorithm for wireless sensor networks," in *IEEE International Conference on Intelligent Computing and Intelligent Systems*, 2009.

Paper F

Energy Harvesting for Sensors in Infrastructure Monitoring and Maintenance

B.Han, A.Kalis, C.B. Papadias, C, R.Soman, M.Kyriakides, T. Onoufriou, R.H. Nielsen, R. Prasad

The paper has been published in the
The IABSE Conference on Assessment Upgrading and Refurbishment of Infrastructures pp. 288–290, 2013.

The layout has been revised.

Abstract

Infrastructure monitoring and maintenance needs various kinds of sensors; all these sensors are expected to have long lifetime and self- maintenance and not be replaced. For non-destructive infrastructure monitoring, these sensors should be wireless, however, wireless sensors have an inherent problem on energy efficiency and energy consumption. Thus, how to power sensors efficiently or how to design a self-powered sensor is a key issue to this problem. Energy harvesting technique emerges as a new direction on getting power from environment. Piezoelectric and electromagnetic harvesting methods on vibration are analysed in this paper, and a low cost self-powered conversion circuit is modelled and simulated. Other kinds of energy harvesting are also briefly compared with those two methods; the solar-electric, vibration-electric, thermal-electric and electromagnetic-electric energy harvesting methods are briefly compared in this paper.

1 Introduction

Wireless sensors are widely used for structural health monitoring. The advantage of wireless sensors is the easy implementation without affecting the performance of structure, especially in old structures where installing wired sensor is difficult [1]. At the same time, wireless sensors need to be powered during the monitoring period which may last for years. Pure battery powered sensors need some maintenance work and battery replacement. In some cases, such maintenance work is not easy as the sensor location may be remote, or the sensor is embedded inside the structure. So the requirements on the wireless sensor are high power efficiency and long network lifetime.

Typical sensors used for structural monitoring are strain sensors, acceleration meters, temperature sensors, and humidity sensors etc. The sensing unit remains active during the entire monitoring process, while the radio unit on the sensor is active only in the data transmission phase. This offers a good opportunity to harvest energy from the surroundings before transmission. Lots of efforts have been put on the radio part of sensor node/network design [1]. Directional transmission/receiving technique is used in multi-hop sensor network topology, also the active/passive reflector is proposed for the radio part of the sensor node. But these techniques do not offer a perfect solution on one big problem which is the lifetime of the sensor node, which is a very important issue for wireless sensors used on structural health monitoring [2].

Emergence of energy harvesting techniques, has allowed wireless sensors to extend their lifetime greatly. By converting the ambient energy (thermal, kinetic, electromagnetic, solar etc. [3], [4], [5] in the vicinity of the sensor to electrical energy, the sensors can be recharged during the stage of monitoring. Moreover, certain type of low cost sensors (e.g. thermal sensors), can be driven directly using the electrical power from

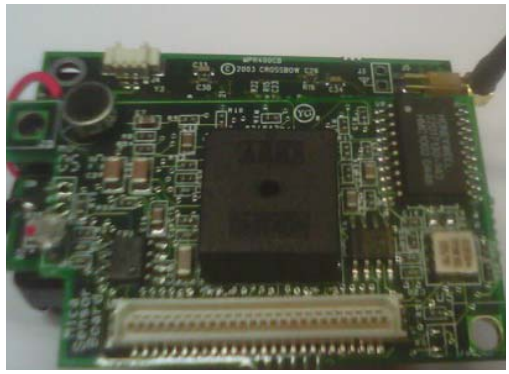

Fig. F.1: A Wireless sensor Node.

the energy harvester (micro generator).

Although, many forms of energy can be converted to electrical energy, the bridge monitoring application restricts the use of some, for instance the large size of structure, limits the energy available from the temperature gradient, also the remote location of the structure restricts the potential to harvest energy from electromagnetic waves. Furthermore, the sensors at times need to be embedded inside the structure, thus making solar energy harvesting and harvesting of wind energy difficult. However, the ambient vibrations of the bridge may be employed for energy harvesting. Thus, this paper presents two methods for harvesting energy from ambient vibrations of the structure.
The paper is organized in 5 sections as follows, section 1 introduces energy harvesting for wireless sensors, section 2 presents the typical vibration function model, section 3 outlines the details of piezoelectric material and magnetic coil electricity generation based on the vibration model, the section also presents a self- powered conversion circuit. Section 4 compares the performance of the two kinetic energy harvesting methods with the performance of other kinds of energy harvesting while section 5 draws conclusions from the obtained analysis and highlights the future expectations from kinetic energy harvesting for structural health monitoring applications.

2 Vibration Model

The natural frequencies of the bridge include axial modes, lateral modes and longitudinal modes. But, the longitudinal bending modes are the most significant modes, as they contribute the most to the harvesting potential. Hence, the vibrations may be assumed as 1-D in the longitudinal direction.

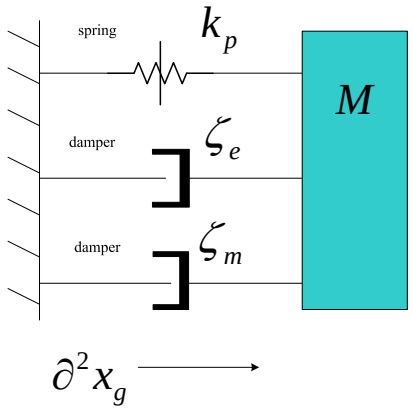

Fig. F.2: The Vibration model.

The energy harvesting unit (it can be Piezoelectric or electromagnetic) is placed on an cantilever which is connected with an additional mass with a stiffness factor k_p , where the k_p has spring effect on the vibration mass [6]. Two equivalent dampers are assumed with mechanical damping factor ξ_m and electrical damping factor ξ_e , the x gives the real-time displacement of the mass and the ∂x give the speed of the movement, and the $\partial^2 x$ gives the acceleration, here is the prescribed ground displacement. The governing equation of such vibration model is given by F.1

$$M\partial^2 x + \zeta_m \partial x + \zeta_e \partial x + k_p x = -M\partial^2 x_g \tag{F.1}$$

$$E = \int_0^t (\zeta_m + \zeta_e)\, \partial x dt \tag{F.2}$$

The ambient vibration with displacement x_g on the ground plane starts the mass vibration x, and such movement has the total energy that can be described by F.2, where ξ_m is the mechanical damping factor and ξ_e is the electrical damping factor. This is a simplest model for converting the kinetic energy to electrical energy, for the different types of harvester; this model is amended slightly according to their specification.

3 Energy Harvesting Technique

3.1 Vibration Based PZT Energy Harvesting

The piezoelectric (PZT) material is put on the cantilever between the bottom and the vibration mass M, where the coefficient Θ stands for the mechanical-electrical coupling, which gives the relation between the mechanical vibration to electrical current or capacitance discharging, as it given by (F.3). Here the ∂x gives the speed of tip displacement of the beam, and the $\partial \upsilon$ is the voltage change according to the time, where υ is the generated voltage between the two plate of piezoelectric (PZT) material. i is the generated piezoelectric (PZT) current which conduct though the load to the two surface of piezoelectric (PZT) material.

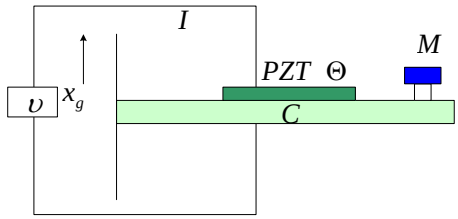

Fig. F.3: The PZT energy harvesting.

$$\Theta \partial x + C \partial \upsilon = i \tag{F.3}$$

As the Θ is the coefficient of mechanical-electrical coupling, the damping factor ξ_e in section 2 also has a relation with the coupling coefficient, the function is given in (F.4), where we assume such coefficient is totally absorbs the energy from the equivalent damping factor ξ_e.

$$\Theta \upsilon + \zeta_e \partial x = 0 \tag{F.4}$$

Substituting the elements in function equation (F.4) to function (F.1), the governing function of the vibration is given by (F.5), where the mechanical factor and electrical factor appears in the same function with the connection by coupling coefficient Θ.

$$M\partial^2 x + \zeta_m \partial x + k_p x - \Theta \upsilon = -M\partial^2 x_g \tag{F.5}$$

Thus the energy in such vibration system is given by

$$E = \int_0^t (\zeta_m \partial x - \Theta \upsilon) dt \Rightarrow E_{electrical} = \int_0^t \upsilon I dt \tag{F.6}$$

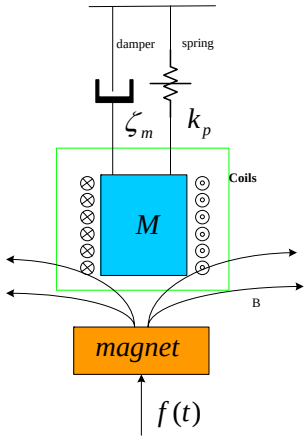

Fig. F.4: The Magnetic harvester.

3.2 Vibration Based Magnetic Energy Harvesting

The magnetic based energy harvester can be employed in many configurations [7], [8], [9]; the simplest model uses a static permanent magnet with one vibration coil which can be modeled as a wire coil attached to a seismic mass. The electricity is generated when the mass vibrates. Then the inducing current flows inside the coil, which can be used to power the load (Fig. F.4). Due to the magnetic flux changes [10], the induced current will flow inside the coil. The current will go through the load in a closed circuit loop. In this way the coil is considered as a micro electrical generator.

Assuming the distance between the oscillating mass and the permanent magnet is , the vibration if driven by an outside force $f(t)$, then the governing function of such a vibration system is given by

$$M\partial^2 x + \zeta_m \partial x + k_p x = f(t) \tag{F.7}$$

The amount of energy harvested by magnetic the harvester depends heavily on the number of the turns of the coils, the vibration frequency, and the amplitude of the displacement.

An improved magnetic energy harvester is shown in Fig.F.5, where the coil is static while the vibrating mass is a two poles magnetic or multi poles magnetic stack. In this configuration each displacement x will cause double or N times magnetic flux change

than in Fig.F.4. The output voltage of such vibration system is given by (8)

$$V_i = n\frac{\partial \Phi}{\partial t} = n\frac{\partial \Phi}{\partial x}\frac{\partial x}{\partial t} = (n)\left(\frac{\partial \Phi}{\partial x}\right)(x') \tag{F.8}$$

Where Θ is the magnetic flux per coil turn, and n is the number of the turns, and x is the displacement of the vibration magnet. For the case of Fig.F.5.

$\partial\Phi/\partial x$ Fig.F.5(a) in (a) is twice that of the one shown in Fig.F.4, and in Fig.F.5(b) is N times bigger than that in Fig.F.4. From the equation (F.1) in section (F.2), the electrical damping factor ξ_e can be derived as

$$F_{ed} \times \partial x = (\zeta_e \partial x)\,\partial x = V_i \times i \tag{F.9}$$

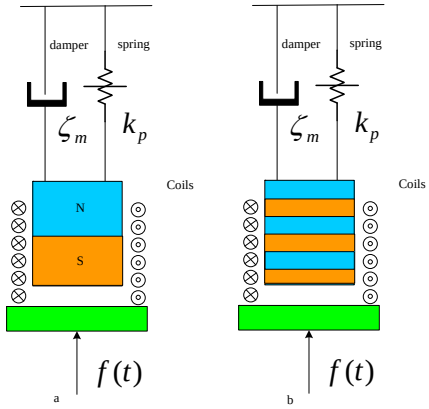

Fig. F.5: Improved Magnetic harvester.

Where F_{ed} is the electrical damping force F.10.

$$F_{ed} = \frac{V_i \times i}{\partial x/\partial t} = n\frac{\partial \Phi}{\partial x} \times i \tag{F.10}$$

Assuming a load R_{load} is connected to the energy harvester, the current in the output, the damping factor is given by F.11

$$\zeta_e = F_{ed}/\partial x = (n\partial\Phi/\partial x)^2 \Big/ R_{load} \tag{F.11}$$

3.3 Vibration to Electrical Energy Converser

The vibration energy converted from PZT or magnetic coil is actually quite weak in terms of voltage and current, in order to be directly used by the sensor node or be used for storage (additional power storage circuit or capacitors are required), the voltage from the energy harvester has to be regulated. All the sensor circuits and the energy storage circuits involve a certain number of transistors or diodes, the typical threshold voltage for a diode is around 500 700mV, for transistor it is required Vgs>400 600mV and $V_{ds} - V_{gs} > V_{dsat}$, (where the V_{gs} is the gate-source voltage and V_{ds} is the drain-source voltage of a transistor. V_{dsat} is the saturation voltage.) It means that at least a 900mV voltage is required to power the circuit. However, the PZT energy harvester and Magnetic harvester cannot provide such high voltage directly, so the conversion circuit is required in order to use the energy from the harvester.

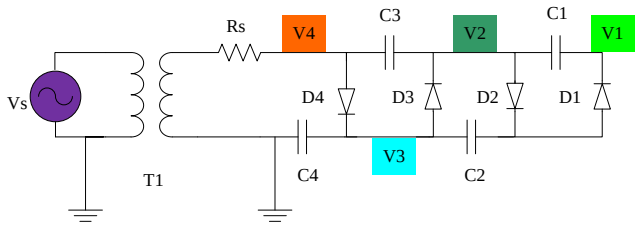

Fig. F.6: Topology of Voltage Multiplier.

Fig.F.6 gives a simple model for a 4 stage voltage multiplier, the power source V_s stands for the energy harvester, the diode D1-D4 and capacitor C1-C4 work as the voltage multiplier core, voltage point V1-V4 are the testing point for the output voltage, and V1 is the final output voltage. The transformer T1 is settled with ratio of 1:1, which is just for verification of the ideal case.

Assuming the voltage from the harvester V_s is 200mV, assuming the vibration frequency is 10Hz, which is assumed as the same frequency of the AC voltage from the energy harvester. A transient simulation is made with step size 10ms and total period 200s. From the Fig.F.7 we can see that after 200 seconds, the output voltage can reach 1,007 V. which is sufficient to power the transistor. The voltage test point V2-V4 are shown in Fig.F.7 according with their different curves. All of these voltages have dynamic value range due to the capacitor C2-C4 are charging and discharging.

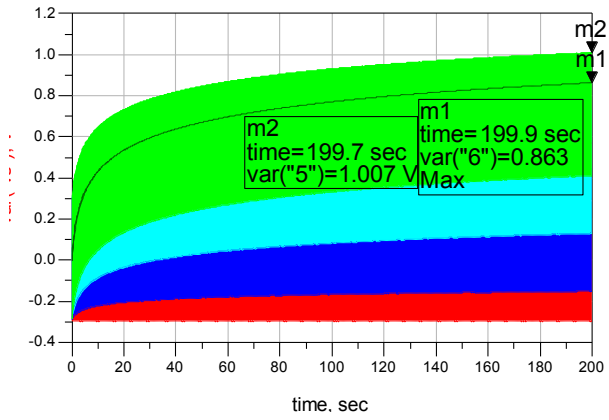

Fig. F.7: Output Voltage of the Converter.

4 Energy Harvesting Comparison

A comparison between all the energy harvesting is given in Table 1. It can be seen that the highest efficiency (power density) is given by the solar cell, however, the solar cell has its limitations during night time, the RF wave and thermal energy harvesting gives the lowest performance. Among the vibration based energy harvesting methods, the magnetic method is much higher than that with piezoelectric method.

So for bridge monitoring or structural health monitoring, the vibration energy harvesting is proposed for continuous energy collection (day and night). Among the vibration energy harvesting method, the magnetic micro generator is recommended for high efficiency energy harvesting.

5 Conclusion

Infrastructure monitoring and maintenance needs various kinds of sensors, all these sensors are expected to have long lifetime and lower needs for battery replacement and maintenance. For non-destructive infrastructure monitoring, these sensors should be wireless, however, wireless sensors have the inherent problem of energy efficiency and

Table F.1: Comparison of Energy Harvesting Techniques

Type	Power Density(W/cm^2)	Limitations
Solar	20μ-200m	Light intensity
Thermal	30μ-30m	Thermal diffeence
RFWave	200p-1m	Distance and RF harmonic
Vibration/PZT	4μ-200μ	Vibration frequency
Vibration/EM	25μ-10m	AC/DC conversion

energy consumption. Thus, how to power for the sensors efficiently or how to design a self-powered sensor is a key issue to this problem. Energy harvesting technique emerges as a new direction on getting powered from the environment, Piezoelectric and electromagnetic harvesting methods on vibration are analyzed in this paper, and a low cost self-powered conversion circuit is modeled and simulated. Other kinds of energy harvesting are also briefly compared with those two methods; the solar-electric, vibration-electric, thermal-electric and electromagnetic-electric energy harvesting methods are briefly compared in this paper. According to the comparison, the electromagnetic harvesting method gives a better performance in the condition of rich vibration but no sunshine environment.

References

[1] B. Han, A. Kalis, P. Tragas, R.H. Nielsen, R. Prasad, "low cost wireless sensor networks for continuous bridge monitoring," in *Bridge Maintenance of Safety Management Resilience and Sustainability*, 2012.

[2] G.E. Niell, L. Niza, A.V. Alex, "Feasibility of structural monitoring with Vibration powered sensors," *Smart Materials and Structures*, vol. 15, pp. 977–986, 2006.

[3] X. Cao, W. Chaiang, Y. King, Y. Lee, "Electromagnetic energy harvesting circuit with feed forward and feedback DC-DC PWM bost converter for vibration power generator system," *IEEE Transactions on Power Electronics*, vol. 22, pp. 679–685, 2010.

[4] L. Guenda L, A. Collado, B. Carvalho, A. Georgiadis, K. Niotaki, "Electromagnetic geo-referenced footprints for energy harvesting systems," in *IEEE Radio and Wireless Symposium, (RWS)*, 2012.

[5] S. Dwari, L. Parsa, "Low voltage energy harvesting systems using coil inductance of electromagnetic micro generators," in *Applied Power Electronics Conference and Exposition*, 2009.

[6] G.E. Niell, L. Niza, A.V. Alex, "Feasibility of structural monitoring with vibration powered sensors," *Smart Materials and Structures*, vol. 15, pp. 977–985, 2006.

[7] R.R. Dayal, S. Dwar, L. Parsa, "A new design for vibration-based electromagnetic energy harvesting systems using coil inductance of micro generator," *IEEE Transactions on Industry Applications*, vol. 47, pp. 820–830, 2009.

[8] A. Khaligh, P. Zeng, Z. Cong, "Kinetic energy garvesting using piezoelectric and electromagnetic technologies state of the art," *IEEE Transactions on Industrial Electronics*, vol. 57, pp. 850–860, 2011.

[9] J. Canarella, J. Selvaggi, S. Salon, J. Tichy, D. Borca, "Coupling factor between the magnetic and mechanical energy domains in electromagnetic power harvesting applications," *IEEE Transactions on Magnetics*, vol. 47, pp. 2076–2080, 2010.

[10] M. Fralick M, B. Dick, H. Jazo, R. Waters, T. Russion, "Characterization and optimization of a novel electromagnetic transduction technique for rotational energy harvesting," *IEEE Sensors Journal*, vol. 1, pp. 1896–1874, 2010.

Paper G

Harvesting Energy from Vibration of the Structure

B.Han, S.Vassilaras,C.B. Papadias,R.Soman, M.Kyriakides, T.Onoufriou,
R.H. Nielsen, R. Prasad

The paper has been published in the
Journal of Vibration and Control Special Issue, 2013.

The layout has been revised.

Abstract

Infrastructure monitoring and maintenance needs various kinds of sensors, all these sensors are expected to have long lifetime and lower needs for battery replacement and maintenance. For non-destructive infrastructure monitoring, these sensors should be wireless, however, wireless sensors have the inherent problem of energy efficiency and energy consumption. Thus, how to power for the sensors efficiently or how to design a self-powered sensor is a key issue to this problem. Energy harvesting technique emerges as a new direction on getting powered from the environment, Piezoelectric and electromagnetic harvesting methods on vibration are analyzed in this paper, and a low cost self-powered conversion circuit is modeled and simulated. Other kinds of energy harvesting are also briefly compared with those two methods; the solar-electric, vibration-electric, thermal-electric and electromagnetic-electric energy harvesting methods are briefly compared in this paper. According to the comparison, the electromagnetic harvesting method gives a better performance in the condition of rich vibration but no sunshine environment, wireless sensors that are monitoring this structural health. This paper presents a new energy harvesting method based on a vibration driven electromagnetic harvester. By using an improved Maximum Power Point Tracking technique (MPPT) on the conversion circuit, the proposed method is shown to maximize the conversion coefficient from kinetic energy to applicable electrical energy.

1 Introduction

Vibrations of man-made structures such as buildings, bridges, railway lines and roads can be very harmful for their structural safety in the long run. For instance, such vibrations can cause inner force imbalance, cracks inside the structures, or instability / unreliability of the riveting point [1]. Vibrations in certain low harmonic frequencies can even cause resonance of the structure that can lead to disastrous consequences such as partial or complete collapse. Structural Health Monitoring (SHM) is adopted as a method that can detect micro-changes inside the structure thus assisting preventive maintenance and issuing alerts for repairs to be conducted ahead of the breakpoint [2]. In order to install such a SHM system, the easiest way is to integrate a grid of wired sensors inside the structure during construction. However, for most of the existing infrastructures it is not a good solution to open holes or run wires to install this type of equipment as this might damage the structure itself or adversely affect its aesthetics and functionality [3]. Furthermore, integrated wired sensors suffer from a number of other limitations such as lack of flexibility to make configuration changes, damaged cabling repairs and hardware upgrades. A solution to the aforementioned concerns is to use a wireless sensor network (WSN) for SHM. A WSN consists of a number of small sensing devices (called sensors or WSN nodes) which send the monitored data to a fusion

center wirelessly and can be easily installed on the surface of the infrastructure without inflicting further damages. For this reason, WSNs are widely used in Structural Health Monitoring [3]. One of the main challenges in WSNs is power consumption. Sensors are commonly powered by batteries which need to be replaced by human personnel when they get depleted. Since this is not always easy to do, the energy lifetime of sensors batteries and thus the frequency of required battery replacements becomes a big concern. There are two ways to extend battery lifetime. One way is by reducing the power consumption of sensors (by designing energy efficient hardware and software) and the other way is by powering the nodes with self-rechargeable batteries capable of harvesting energy from the surrounding environment [4]. See [5] for a detailed discussion on the various types of rechargeable batteries and large capacitors that can be used to store harvested energy.

There are many forms of energy that can be converted to electric energy such as:

a). Solar energy, which can be converter to electric energy by photovoltaic solar cells, but depends on the availability of sunlight at the exact place where the sensor is placed;

b). Electromagnetic energy (RF waves), which can be converter to electric energy by electromagnetic energy converters (used for example in long-range RFIDs), but suffers from signal path loss;

c). Thermal energy, which can be converter to electric energy by thermal energy converters which generate current in the circuit from thermal difference on electro probes, but needs large enough thermal differences; and

d). Kinetic energy, which will be extensively analyzed in this paper.

The most popular methods of energy harvesting and their corresponding power densities and limitations are summarized in Table 1. As shown in Table 1, solar energy harvesting offers the highest power density while thermal energy harvesting comes second. However, in applications where there is not enough sunshine or big thermal differences and the sensors are placed in an environment rich in vibrations, the most convenient way of harvesting energy is to convert the kinetic energy of such vibrations to electric energy. For example in SHM applications where sensors are meant to monitor vibrations and their effects to structures, harvesting the energy of such vibrations comes as a natural choice [6].

From Tab G.1 it is also clear that electromagnetic (EM) based kinetic energy harvesting has much higher power density than piezoelectric (PZT) energy harvesting. Moreover, as pointed out in [5] in civil engineering applications, natural vibration frequencies of structures fall in the range 1-100Hz, which is about an order of magnitude lower than

Table G.1: Comparison of Energy Harvesting Techniques

Type	Power Density(W/cm^2)	Limitations
Solar	20μ-200m	Light intensity
Thermal	30μ-30m	Thermal diffeence
RFWave	200p-1m	Distance and RF harmonic
Vibration/PZT	4μ-200μ	Vibration frequency
Vibration/EM	25μ-10m	AC/DC conversion

what is required for an efficient PZT energy harvester. Therefore an electromagnetic based micro-generator is the preferred method for vibration energy harvesting [7].

In order to maximize the energy output, the energy harvester needs to be placed at the point where the maximum vibration amplitude is attained [7]. The use of an appropriate vibration model for the structure to be monitored can provide an insight on the maximum kinetic energy as well as the energy distribution on the vibrating object. In this paper we are considering vibration models of a bridge and calculate the vibration energy that can be harvested at various points on the bridge. We are also proposing certain optimizations to the micro-generator for energy harvesting, in order to achieve maximum conversion to electrical power. Another issue with EM energy conversion (as shown in Table G.1) is that it generates a very weak AC (Alternating Current) voltage whereas most sensors operate at DC (Direct Current) voltage. A nice overview of power and supply voltage requirements for sensors used for SHM can be found in [8]. To address this issue, we propose a simple rectifier circuit (based on a Maximum Power Point Tracking (MPPT) technique) which can efficiently convert the EM harvester output from a weak AC voltage to a higher DC voltage for the follow-up circuits.

Energy harvesting of micro-vibrations has received considerable attention recently in the scientific literature. A number of different approaches have been proposed for amplifying the very low voltage produced by micro-generators and rectifying the low frequency AC voltage into DC voltage required for follow-up sensor circuitry. [9] provide a nice literature overview of the various approaches and discuss the respective advantages and limitations of each approach.

A broad categorization of approaches is whether they are based on active circuit components (requiring an external power source) or completely passive circuit components. In the first case the circuit output needs to be used to power these active components as well as the follow-up circuit. This creates the need for a boot-strapping phase in which an external power source (e.g., a battery) is typically needed. Passive circuit designs, on the other hand, are usually combined with a transformer (to amplify the input AC

voltage) which has a considerable size and can not be integrated in a compact circuit. In addition such a transformer implies an increased load burden for the harvester.

The same paper [9] goes on to propose an active circuit voltage multiplier based technique that can convert input voltage ranging from 0.35V to 2V and 20-500Hz to a DC output voltage with a gain factor of 8. The proposed circuit design is based on active diodes which can eliminate the threshold voltage problem of traditional passive diodes. However, the circuit topology is based on the conventional voltage stack multiplier which cannot optimally adapt to the power requirements of the follow-up circuit.

A most recent example of a passive circuit approach is [10] which also proposed a parametric frequency increased generator which can convert the low vibration frequency of the bridge to higher frequency mechanical oscillations of the harvester mass, in order to increase harvester performance. As the employed voltage boosting technique is the conventional diode-capacitor stack multiplier, which has the limitation on the threshold voltage of the first stage, the authors introduced a 1:10 transformer connected between the harvester and the voltage rectifier.

A hybrid technique, which uses passive circuit components at the first stage and the output of this first stage to power the active circuit components of the second stage, is introduced in [11]. This second stage circuit also uses actives diodes which can be fabricated using CMOS technology to achieve better integration and compact size. However, a 3-stage amplifier was proposed to be used as a comparator, which increases circuit complexity and reduces reliability. More importantly, the voltage gain achieved by the proposed rectifier circuit is small (about 2×) as it can provide an output voltage of 1.8V at an 1V input voltage.

In this paper, we introduce an electromagnetic energy harvester using a simple, active voltage-rectifier circuit based on the maximum power tracking technique. The proposed circuit can adjust the total load seen at the output of the electromagnetic micro-generator in order to achieve maximum energy conversion efficiency. In addition, rather than considering only the mechanical domain or the electrical domain, we consider the mechanical and electrical damping jointly in order to maximize the harvested energy. Finally, in this paper we present both the mechanical/civil engineering background and an electrical circuit technique for energy harvesting using electromagnetic micro-generators.

The rest of the paper is organized as follows. Section 2 gives the system description and introduces a detailed vibration model for a bridge, including the vibration function of the energy harvester. Section 3 provides an analysis of the electromagnetic micro-generator. The follow-up conversion circuit for voltage regulation and power extraction

is developed in Section 4. Simulation results are presented in Section 5. Finally, the main conclusions of this study are given in Section 6.

2 Vibration Model

2.1 Vibration of the Underlying Structure

The response of a bridge under a moving load P, can be described by Eq.G.1 (Fryba et al., 1999; Stancioiu et al., 2011)

$$m\frac{\partial^2}{\partial t^2}y(x,t) + c\frac{\partial}{\partial t}y(x,t) + EI\frac{\partial^4}{\partial x^4}y(x,t) = \delta(x-\nu t)P \tag{G.1}$$

where $y(x,t)$ is the vertical displacement of the bridge at position x along the bridge and at time t, m is the mass per unit length of the bridge, L is the length of the bridge, c is the damping coefficient, E is the Youngs Modulus of the structure, I is the second moment of area, P is the force applied as a result of the moving load, and v is the magnitude of the velocity of the moving load along the x direction (Ali et al., 2011). The Dirac-delta function on the right side of the equation physically represents the point load that is applied on the bridge while it moves along the bridge. In reality, the bridge is subjected to multiple loads due to several vehicles at a time. The effect of multiple loads can be obtained by superposition of the response to individual loads. This superposition is possible due to the linear response of the bridge structure.

The solution of the partial differential equation Eq. (1) has the general form

$$y(x,t) = \sum_{j=1}^{M} \phi_j(x) q_j(t) \tag{G.2}$$

where $\varphi_j(x)$ is the j^{th} mode shape function of the bridge, $q_j(t)$ is the j^{th} modal displacement, and M is the number of modes of significance, as the contribution of the higher modes is negligible.

The mode shapes $\varphi j(x)$ in the generalized solution of the partial differential equation are independent of time t, and satisfy the boundary conditions, while $q_j(t)$ is independent of the spatial co-ordinate x and satisfy the initial conditions.

Eq. G.2 can be written in the frequency domain as follows

$$Y(x,\omega) = \sum_{j=1}^{M} \varphi_j(x) Q_j(\omega) \tag{G.3}$$

where $Q_j(\omega)$ is the j^{th} modal displacement in the frequency domain.

The natural frequencies and mode shapes of the bridge depend on the sectional properties of the bridge and its boundary conditions. Thus, knowing the modal properties of the structure, end conditions and the excitation due to the moving load, the response of the structure can be simulated.

2.2 Bridge Description

To validate the methodology, a numerical model of the Grand-Mere Bridge, in Quebec, Canada, a typical medium span bridge (Fig. G.1 was used. The aforementioned bridge is a single-cell box-girder type bridge with three continuous spans of 40 m, 181 m, and 40 m, with a wedge shaped cantilever of 12 m at either end. The 40-m spans on either side have a linearly changing cross section. For the central span the depth varies in a parabolic manner. The wedge shaped cantilevers are of solid cross section increasing to a depth of 8.53 m at the external piers. The compressive strength of concrete in mid span is 38 MPa, while compressive strength of the concrete at the end spans is 34 MPa. The bridge has hinged supports at the ends and is simply supported at the internal piers and external piers. More details on this bridge can be found in [12].

2.3 Bridge Modeling

The commercial Finite Element software ABAQUS (version 6.11ed, 2011) was used to simulate the response of the Grand-Mere Bridge under a moving load and extract the significant mode shapes. The girder was modeled using beam elements each of 1 m in length. The section properties for the elements were computed using the data available in [12].

The moving load was assumed to be a 3-axle HS20 truck [13] as this corresponds to 65 percent of the traffic observed on middle span bridges based on Weigh in Motion (WIM) data [14]. Based on statistical analysis, have shown that the average load of a loaded HS20 truck is 600 kN and the load distribution over the three axles can be assumed to be 1:2:2. Thus, the loading scenario for the bridge was simulated as three point loads at fixed distance apart moving at a constant velocity along the bridge.

2.4 Harvester Dynamics

The energy harvester is considered as a single degree of freedom (SDOF) system, which means that the harvester will move at the same direction of the bridge vibration described by $y(x,t)$. The harvester is subjected to a forced vibration as a result of the bridge response to the moving load described in the previous Section [15].

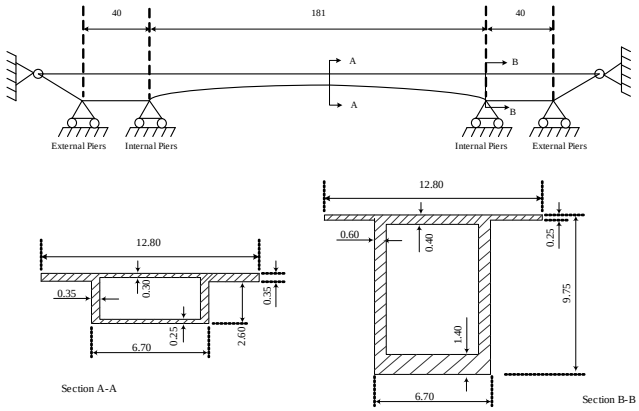

Fig. G.1: Details of Grand-Mere Bridge, all dimensions are in meters.

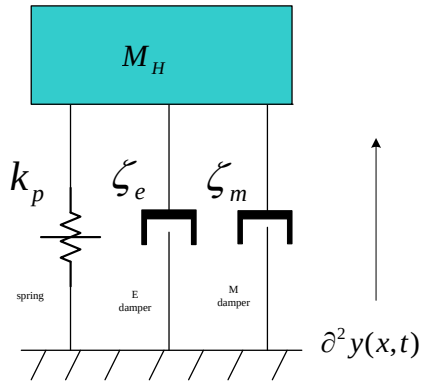

Fig. G.2: Generic vibration harvester conceptual model.

Fig. G.2 gives the conceptual model of the energy harvester, where a moving mass is fixed to the vibration base with a spring and two dampers [16]. The mass of the harvester is given by M_H , the mechanical damping factor is given by ξ_m , the electrical damping factor is given by ξ_e , the stiffness of the spring is denoted by k_p, the acceleration of the vibration base (external excitation) is given by , and the movement of the mass inside the harvester is given by $\partial^2 y(x,t)/\partial t^2$. Thus the vibration function of the energy harvester is given by y_2 [16].

$$M_H \frac{\partial^2 y_2}{\partial t^2} + \xi_m \frac{\partial y_2}{\partial t} + \xi_e \frac{\partial y_2}{\partial t} + k_p y_2 = -M_H \frac{\partial^2 y(x,t)}{\partial t^2} \tag{G.4}$$

This equation is a general equation for all kinds of vibration based energy harvesters; it can be either a piezoelectric energy harvester or an electromagnetic energy harvester. Note that the external excitation of the harvester mass in the right hand side of Eq. G.4 is obtained by solving Eq. G.1. It should also be noted that when calculating the energy harvester vibration equations, we can consider the acceleration of the vibration base $\partial^2 y(x,t)/\partial t^2$ as constant when $\partial^2 y_2/\partial t^2$ is calculated. The total energy that is harvested from the energy harvester is given by [17].

$$E = \int_0^t \xi_{\mathrm{e}} \left(\frac{\partial y_2}{\partial t} \right)^2 dt \tag{G.5}$$

The electrical damping factor ξ_e depends on the electrical circuit driven by the micro-generator. The following equation links the mechanical (velocity of the moving mass) and electrical (output voltage) quantities of the micro-generator

$$\Theta V + \xi_e \frac{\partial y_2}{\partial t} = 0 \tag{G.6}$$

where, Θ is the coefficient of mechanical-electrical coupling, and V is the associated output voltage of the energy harvester. Substituting G.6 into the vibration equation of the energy harvester G.4, we have

$$M_H \frac{\partial^2 y_2}{\partial t^2} + \xi_m \frac{\partial y_2}{\partial t} - \Theta V + k_p y_2 = -M_H \frac{\partial^2 y(x,t)}{\partial t^2} \tag{G.7}$$

For a piezoelectric material based energy harvester, the electrical equation can be expressed as

$$\Theta \frac{\partial y_2}{\partial t} + C \frac{\partial V}{\partial t} = i \tag{G.8}$$

where i is assumed to be the output current, and C is the piezoelectric capacitance.

3 Electromagnetic Energy Harvester

3.1 Electromagnetic Micro Generator

The magnetic-based energy harvester can be implemented in many configurations. The simplest model uses a static permanent magnet with one vibration coil, as shown in Fig. G.3(a).

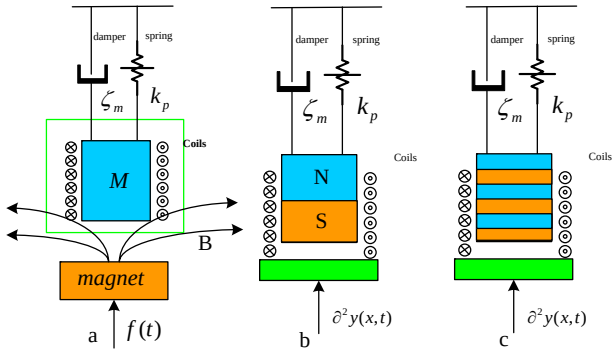

Fig. G.3: Electromagnetic vibration harvester configurations.

The basic depiction of components in the electromagnetic harvester is given in Fig. G.3(a), where the bottom is attached to the bridge. As the vibration $y(x,t)$ induced force, f is applied on the entire harvester the mass M, vibrates inside the coil. Such mechanism can be modeled as a wire coil attached to a seismic mass. An electrical current is generated at the coil when the iron mass oscillates inside the magnetic field created by the magnet. Due to the magnetic flux changes inside the coil, an induced current will flow in the coil, which can be used to power the load. The current will go through the load in a closed circuit loop. In this way the coil is considered as a micro electrical generator.

Let us denote the displacement of the mass inside the coil by y_2 , the oscillating mass by M_H and the force driving the permanent magnet by $f(t)$ Fig. G.3(a). This force is caused by the bridge vibration acceleration $\partial^2 y(x,t)/\partial t^2$. Thus the vibration equation of such an electromagnetic based energy harvesting system is given by Eq. G.4. The total amount of energy harvested by the harvester depends heavily on the configuration parameters of the harvester, such as the number of turns of the coil, N , the topology of the permanent magnetic placement (Fig. G.3 (b)), (Fig. G.3 (c)), the vibration frequency,ω , and the amplitude of the displacement, y_2 , which is influenced by the acceleration, $\partial^2 y(x,t)/\partial t^2$, of the base vibration. Improved magnetic energy harvester

configurations are shown in Fig. G.3, where the coil is static while the vibrating mass consists of two magnetic poles (Fig. G.3 (b)) or a multiple poles magnetic stack (Fig. G.3 (c)). In this kind of configuration, each displacement will cause two or times the magnetic flux change obtained in Fig. G.3 (a). Assuming Φ is the magnetic flux inside each coil turn of the harvester, the output voltage of such an EM energy harvesting system is given by

$$V_i = KN\frac{\partial \Phi}{\partial t} = KN\frac{\partial \Phi}{\partial y_2}\frac{\partial y_2}{\partial t} = KN\frac{\partial \Phi}{\partial y_2}{y_2}' \tag{G.9}$$

where, K , is the number of magnetic stacks, and y_2 is the displacement of the vibrating magnet. Assuming a load with impedance $Z_{Load} = R + jX_{c,l}(\omega)$ is connected to the energy harvester, the current is given by $i = V_i/Z_{Load}$. The total energy harvested in a time interval [0, t] can be expressed as

$$E_{em} = \int_0^t V_i \cdot i \; dt = \int_0^t \left(\frac{KN}{Z_{load}}\frac{\partial \Phi}{\partial y_2}\frac{\partial y_2}{\partial t}\right)^2 Z_{load}\, dt = \int_0^t \left(\frac{KN}{Z_{load}}\frac{\partial \Phi}{\partial y_2}\right)^2 Z_{load}\left(\frac{\partial y_2}{\partial t}\right)^2 dt \tag{G.10}$$

Such energy can be considered as generated by an equivalent (conceptual) electrical force F_{ED}, so that the energy generated from such equivalent force can be written as $W = F_{ed} \cdot y_2$, following the classical physics equation for work. By equating this virtual energy with the actual converted electrical energyE_{em} , we obtain the following expression for the electrical forceF_{ed}

$$F_{ed}\, dy_2 = V \cdot i \, dt \Rightarrow F_{ed} = \frac{V \cdot i}{\partial y_2/\partial t} \text{or} F_{ed} = KN\frac{\partial \Phi}{\partial y_2} \cdot i \tag{G.11}$$

Note that each term in Eq. G.4 represents a force. Thus the electrical force F_{ed} is given in terms of the electrical damping factor as $F_{ed} = \xi_e \frac{\partial y_2}{\partial t}$. Therefore the electrical damping factor depends on the load of the attached electrical circuit and the characteristics of the micro-generator as follows:

$$\xi_e = \frac{F_{ed}}{\partial y_2/\partial t} = \frac{KN}{\partial y_2/\partial t}\frac{\partial \Phi}{\partial y_2} \cdot i = \frac{KN}{\partial y_2/\partial t}\frac{\partial \Phi}{\partial y_2} \cdot KN\frac{\partial \Phi}{\partial y_2}\frac{\partial y_2}{\partial t}\Big/ Z_{load} = \left(KN\frac{\partial \Phi}{\partial y_2}\right)^2 / Z_{load} \tag{G.12}$$

3.2 Equivalent Model in the Electrical Domain

The proposed energy harvester is modeled as shown in Fig. G.4, which gives a schematic illustration of the numerical effective electrical model of the energy harvester that converts energy from mechanical to electrical domain. The small triangles stand for the

different coefficients from various domains and the square rectangle on the main chain stands for the derivation or integration of the main function in the loop. The external source is denoted by the left square rectangle which is assumed to be the external mechanical vibration from the bridge. The entire energy harvester is considered as a limited feedback system with external input

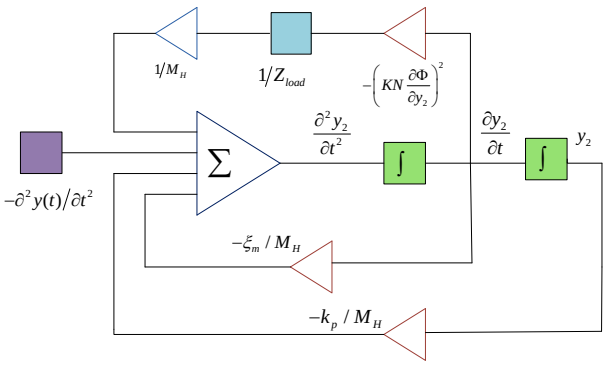

Fig. G.4: Electrical model of the energy harvester.

An alternative representation of the harvested energy in terms of the total available kinetic energy is as follows. Assuming that the number of vibration modes of significance is J, the mechanical energy propagation efficiency from the vibrating bridge to the vibrating mass in the micro-generator is η_j, and the conversion efficiency from mechanical energy of the vibrating mass to the harvested electric energy is λ_j, the total output energy for the energy harvester is given by the following equation

$$E_{eh} = \sum_{j=1}^{J} \eta_j \lambda_j E_m^j \tag{G.13}$$

where E_m^j is the mechanical energy of the j^{th} vibration mode at the point of sensor placement calculated from the vibration model of the bridge. With a fixed total available kinetic energy E_m, the maximum electrical power has an optimal value. Due to the fact that different electric load applied to the energy harvester will affect the electrical

damping factor of the micro-generator, the energy conversion efficiency is dependent on the follow-up circuit to be powered by the harvester. Note that the mechanical energy propagation efficiency η_j depends on the natural frequency of the vibrating mass. For maximum efficiency, this natural frequency should be matched with one of the frequency modes of the bridge at the point where the micro-generator is placed. This is a limitation of the EM micro-generator as a suitable micro-generator should be built according to its point of placement.

Recall that the vibration equation with mechanical damping and electrical damping is Eq. G.4, where the vibration function contains a mechanical damping factor, ξ_m , and also an electrical damping factor, ξ_e . The electrical damping can be physically explained as it is caused by the load connected to the energy harvester, e.g., a big electrical load will exert additional damping for the energy harvester which will make the internal magnetic core more difficult to move. Thus, the load after the energy harvester will influence the effective electrical damping of the harvester which is considered as additional *burden* for the energy converter. In most cases, the load connected to the energy harvester is considered to be a complex number, which means the load is not only a pure resistive load, but also has an energy storage component, which is given by

$$Z_{Load} = R + jX_{c,l}(\omega) \tag{G.14}$$

where R is the pure resistive load and is the imaginary load. For the operation of the energy harvester, since the vibration is dynamic and changing all the time, such changing on the load will change the effective electrical damping factor of the vibration model. The inductor based load model will also change the energy calculation function.

4 Voltage Regulator

4.1 Voltage Regulator Analysis

As mentioned in the previous Section, the electric load of the energy harvester will influence the system conversion efficiency thus an electrical circuit stage after the harvester should be carefully chosen. Besides, the output voltage of the energy harvester is so weak that it cannot be used by the follow-up circuit directly. The most common way of using such harvested energy is to store it in a capacitor and discharge the capacitor to charge the battery or power up the circuit directly. In addition, due to the inherent characteristics of the electromagnetic energy harvester, the amplitude of the output voltage is time varying. Since most low power sensor nodes require a DC voltage, a regulation circuit that can do the conversion from AC to DC is also needed.

This voltage regulator is a circuit stage added between the micro generator and the follow-up circuit. A very common voltage regulator that converts AC to DC is the

`half-bridge-switch` and `full-bridge-switch` voltage regulator which is composed by 4 PN diodes, from which the output current can only flow towards one direction (from VP to VN), as shown in Fig. G.5.

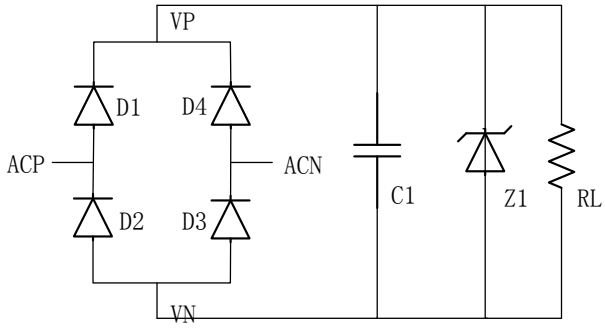

Fig. G.5: Conventional full bridge converter.

The operation of this voltage regulation is very simple. The AC voltage is applied to the points AC_P and AC_N . At the positive cycle of the input AC voltage, the PN diodes D1 and D3 are switched on, thus the current can only flow from AC_P to node V_p and from V_N to AC_N . At the negative cycle, the PN diodes D2 and D4 are switched on, and the current can only flow from V_N to AC_P, and from AC_N to V_p . Therefore, the current can only go out from V_p , and only into V_N and this results into transforming alternating current into current flowing always into the same direction (albeit with varying amplitude). With the further help of the charge storage capacitor C1, the final output voltage will be a close to fixed amplitude DC voltage. However, there are some disadvantages of the `full-bridge-switch` voltage rectifier. First, the threshold voltage of a PN diode which is typically 0.5-0.7V is relatively high, and might not fall in the range of the output voltage of the micro-generator. Second, the `full-bridge-switch` cannot provide any voltage gain to meet the requirements of the following stages.

4.2 Rectifier with Maximum Power Point Tracking(MPPT)

With the aforementioned problem, an improved voltage regulator with Maximum Power Point Tracking (MPPT) technique is proposed in this paper. Unlike to the conventional `full-bridge` voltage regulator, the rectifier shown in Fig. G.6 can boost voltage to a larger value. Moreover, the additional inductor and resistor L_ad , can be selected so that the total load, R_ad , and consequently the electrical damping factor, Z_{load} ξ_e, are optimized for maximum energy efficiency.

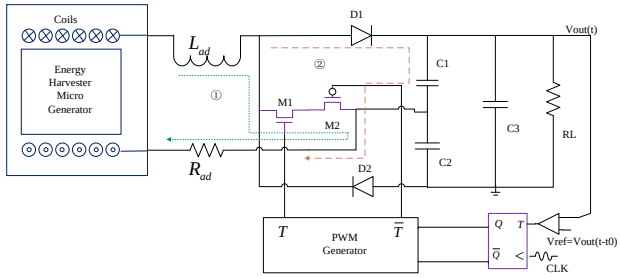

Fig. G.6: The adaptive Maximum Power Point Tracking circuit .

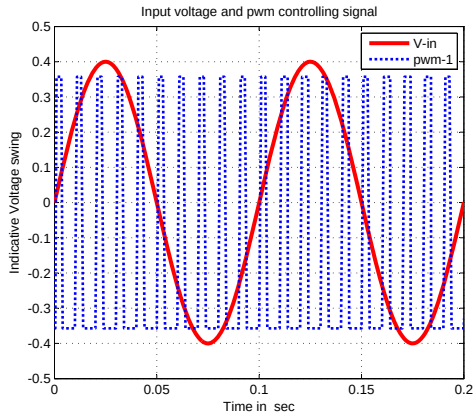

Fig. G.7: The controlling signal (dashed curve) and input voltage (solid curve).

The regulator circuit in Fig. G.6 operates as follows: The two switches M1 and M2 are based on NMOS and PMOS respectively and are turned ON or OFF simultaneously. Using two switches results in a better behavior to bidirectional current flow (current can flow through the switches either from left to right or from right to left). The two switches are turned ON when the controlling signal pwm1 generated by the PWM Generator is positive and turned OFF when it is negative (see Fig. G.7[1]). During the positive cycle of the rectifier input voltage, when the switches M1 and M2 are turned ON by their controlling signal, the current flows as shown in Fig. G.6 - current path 1, through L_ad, M1, M2 and R_ad. After time t_1 (still during the positive cycle of the input voltage Vin as shown in Fig. G.7), switches M1 and M2 are turned OFF, the inductor stored current flows together with the voltage induced current and the aggregate current will go though D1 and charge C1 as shown in Fig. G.6 - current path 2. The switching period is much shorter than the input voltage period, thus the voltage starts accumulating

During the negative cycle of the input voltage, a similar process will take place through the symmetric circuit consisting of D2 and C2. By adjusting the switch-on duty cycle $D = t_1/T_S$ (where t_1 is the ON time and T_s is the controlling signal period) the output voltage can reach a higher value than the input voltage (see Fig. G.8), which is the advantage of such a voltage boosting rectifier compared to the conventional full-bridge AC-DC rectifier. The capacitor C3 is added to further stabilize the output voltage seen by the follow-up circuit RL. Let us now explain the functionality of the D-flip-flop and feedback loop shown in Fig. G.6: When the output of the proposed voltage boosting circuit has reached the required level (typically in the range 3.3V 4.2V for wireless sensors), the feedback mechanism can achieve maximum output when the follow-up electrical load (indicated by RL in Fig. G.6) changes. Such change can be the result of increasing demand at the next stages circuit, e.g., the sensor starts a wireless transmission. The feedback system can then adjust the duty cycle of the controlling signal so that the maximum energy is delivered to the load.

Detecting the demand of the circuit can be done by monitoring the current change or the voltage change; when the power demand is increasing, the current will increase and the output voltage will drop. The mechanism proposed here takes the voltage as a monitoring reference.

The reference voltage (V_{ref}) is a delayed (by t_0) version of the output voltage ($V_{ref}(t) = V_{out}(t-t_0)$). If $V_{ref} < V_{out}$, which means that the system consumes increasing power, the comparator will give an output voltage that triggers the PWM to increase the duty cycle so that the output voltage will be increased to satisfy the follow-up circuit requirements. But when $V_{ref} > V_{out}$, which means that the next stages circuit is not as heavily loaded, the duty cycle will be decreased and the output voltage will be decreased until this feedback is balanced. Thus the maximum power tracking is performed in such

[1]The plots in Fig. 7, 8 and 9 were generated by simulating the circuit in Fig. 6 using the Advanced Design System (ADS) 2008 circuit simulation tool by Agilent Technologies

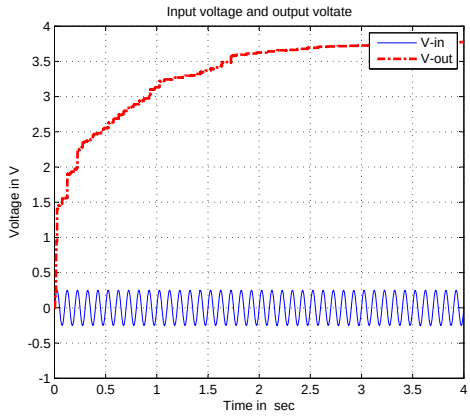

Fig. G.8: The input voltage (solid line) and output voltage (dashed line).

a way that increases the conversion efficiency.

One way (among many other ways) of realizing such feedback is to let the output of the comparator go into a D-flip-flop, which produces two complementary outputs Q and $\overline{Q}$. When $V_{ref} < V_{out}$, the output of the D-flip-flop will drive the PWM generator to increase the pulse duty cycle, which results into increasing the output voltage.

Now let us denote the input voltage to the rectifier by $V_i(t)$ with peak voltage V_{ip} and period T_i, the switching period of the switches M1 and M2 by T_s with associated frequency f_s , and the output voltage of the rectifier by $V_o(t)$. As explained in Section 3, the electrical damping factor of the system is influenced by the changing load $Z_{load} = R + jX_{c,l}(\omega)$. It can be shown that by using the proposed circuit, the total load is given by the following equation

$$Z_{load}(total) = (R\_ad + R_{ef}) + j\omega L\_ad \tag{G.15}$$

where R_{ef} is given by

$$\mathrm{R}_{ef} = 2L\_ad/\beta D^2 T_s \tag{G.16}$$

where D is the duty cycle, T_s is the switching period, and β is given by:

$$\beta = 2\int_0^{2\pi} \sin^2\theta \left[1 - \frac{\sin\theta}{V_0/V_{ip}}\right]^{-1} d\theta \tag{G.17}$$

where θ is given by $\theta = 2\pi t/T_i$. Therefore the total load for the harvester can be derived as

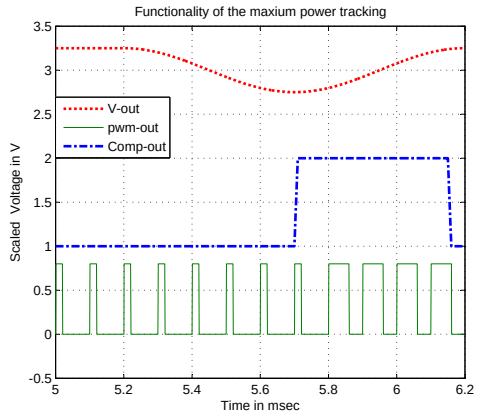

Fig. G.9: The output voltage can be adjusted by changing the duty cycle of the controlling signal.

$$Z_{load}(total) = (R\_ad + \frac{2L\_ad}{\beta D^2 T_s}) + j\omega_i L\_ad = R\_ad + j(\frac{4\pi\omega_s}{\beta D^2} + \omega_i)L\_ad \quad \text{(G.18)}$$

Thus the total load is a complex load, and the switching frequency and input voltage frequency also influence the actual load, which will in turn influence the maximum harvestable power.

Note that the proposed regulator circuit includes active circuit components that need power supply. This implies the need of a bootstrapping phase during which external power is needed (e.g., by a battery). Once the output voltage of the circuit is high enough this can be used to power the active components of it and the external power supply is no longer needed (provided that the micro-vibrations can generate enough energy to keep the power stored at the capacitors above a required level at all times).

5 Simulated Results and Analysis

In this Section we present simulation results based on typical mechanical parameters for the bridge model and vibration model, and suitable electromagnetic parameters for the electromagnetic based micro generator energy harvester, as well as circuit element parameters for the voltage regulator.

The maximum displacement (deflection) at the middle point of the bridge analyzed in Section 2, is obtained assuming a moving load with the characteristics of an HS20 truck presented in Section 2.3.

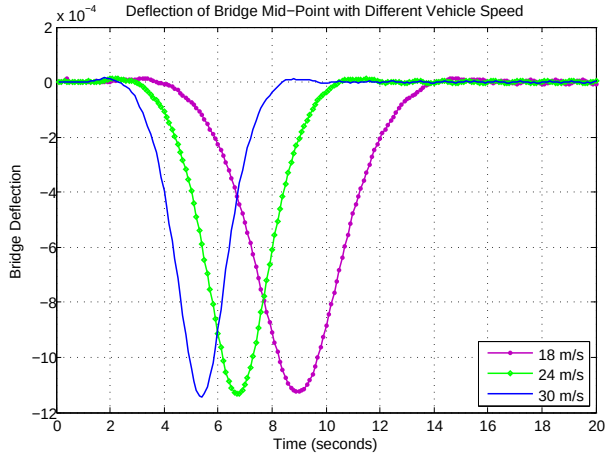

Fig. G.10: Maximum deflection of the mid-point of the bridge at different velocities

From Fig. G.10 we can see the deflection of the mid-point has a maximum of 1.15mm at vehicle speed 30m/s. The figure shows the transient characteristics of the vibration and illustrates that harvestable energy is only available when loads are moving on the bridge. The vibrating mass of the energy harvester is assumed to be $M_H = 9g$ and the mechanical damping $\xi_m = 0.038$. The turn number of the coil is assumed to be $N = 250$, the number of magnetic stacks $K = 6$ and the spring stiffness k_p in the harvester $k_p = 4.186N/mm$. Finally, the flux leakage Φ is assumed as $\partial\Phi/\partial y_2 = 12.5\mu B/mm$, and the load of the harvester has real value $|Z_{load}| = 100\Omega$. Under the assumption of an energy conservation law, the maximum harvestable energy is plotted based on the following formula [17]:

$$P = \frac{\xi_e \omega^2 a^2 M_H^2}{2\left[\omega^2(\xi_e + \xi_m)^2 + (M_H\omega^2 - k_p)^2\right]} \tag{G.19}$$

where α is the maximum value of the acceleration of the energy harvester (given by $\partial^2 y_2/\partial t^2$) and the electrical damping is given by $\xi_e = \left(KN\frac{\partial\Phi}{\partial y_2}\right)^2/Z_{load}$. The harvestable power as a function of the frequency of the oscillating mass in the micro-

generator is shown in Fig. 11. It can be seen that the larger the maximum acceleration value the larger the harvestable power.

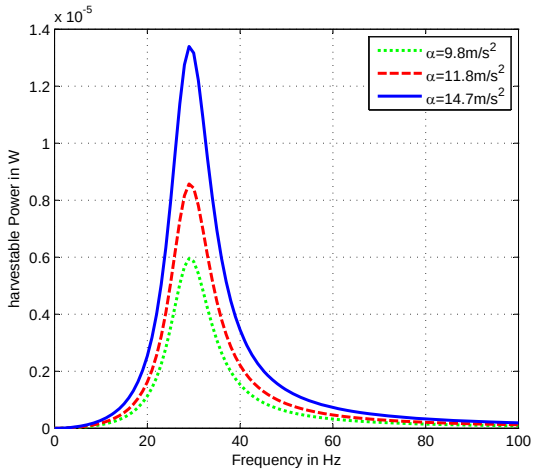

Fig. G.11: Maximum harvestable power versus frequency

As shown in Fig. G.11, given the parameters mentioned above, the peak harvestable power is extracted at a frequency of 30Hz. However this is not a typical natural vibration frequency of a bridge. Usually the maximum acceleration is also a macro parameter that relates to the nature of the vibration and cannot be changed easily. By changing the ratio of the spring stiffness over the harvester mass, we can shift the harvester mass vibration frequency attaining peak power at the natural frequency of the bridge. An example of this technique is shown in Fig. G.12. With a fixed maximum acceleration, by changing the ratio of the spring stiffness / mass, we can shift the power maximizing frequency to a frequency in the 1Hz 4Hz range, which falls into typical bridge natural frequencies.

6 Conclusion

Structural Health Monitoring can benefit immensely from wide use of wireless sensors, due to their inherent characteristics of easy installation with minimal damage to existing structures. However an important concern for wireless sensors is the lifetime of the system, which depends heavily on power supply availability. In order to achieve a long virtually unlimited life-time of the system, the sensor nodes should be able to recharge

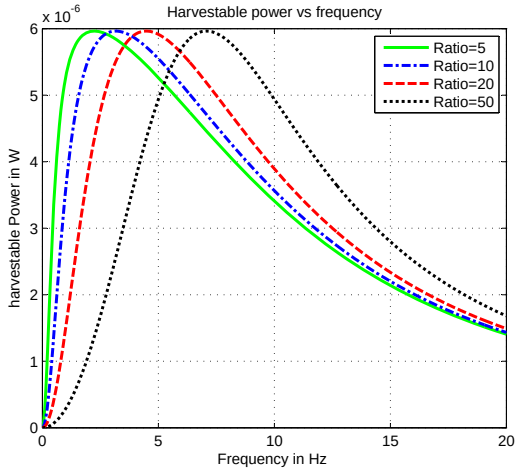

Fig. G.12: Harvestable power changes by changing the spring stiffness / vibrating mass ratio

their batteries through an easy and autonomous way. Energy harvesting emerges as a technique that can harvest energy from the surrounding environment. In this paper kinetic energy harvesting from micro-vibrations of the structures on which sensors are attached in order to monitor their structural health has been investigated. After reviewing mathematical models for bridge micro-vibrations, vibration driven electromagnetic harvester solutions have been analyzed and their limitations have been defined. A Maximum Power Point Tracking based conversion circuit has been introduced that can maximize the conversion coefficient of harvestable kinetic energy to applicable electrical energy. In the future, we plan to implement our circuit design as a real energy harvesting device and conduct real life experiments to evaluate the applicability and efficiency of our solution to micro-vibration energy harvesting for wireless sensors in the field of SHM.

References

[1] S.P. Beeby, M.J. Tudor, N.M. White, "Energy harvesting vibration sources for microsystems applications," *Measurement Science and Technology*, vol. 17, pp. 175–195, 2006.

[2] K. En, M. Nakamura, T. Yanase, et al., "Structural health monitoring system applied to RC buildings with smart sensors and wireless network," *Proceeding of*

World Conference on Structural Control and Monitoring, vol. 16, pp. 12–14, 2010.

[3] J. Lynch, K.J. Loh, "A Summary review of wireless sensors and sensor network for structural health monitoring," *The Shock and Vibration Digest*, vol. 38, pp. 91–128, 2006.

[4] E. Sazonov, H. Li, D. Curry, P. Pillay, "Self-powered sensors for monitoring of highway bridges," *IEEE Sensors Journal*, vol. 9, pp. 1422–1429, 2009.

[5] F. Casciati, R. Rossi, "A power harvester for wireless sensing applications," *Structural Control and Health Monitoring*, vol. 14, pp. 649–659, 2007.

[6] E. Halvorsen, "Energy harvesters driven by broadband random vibrations," *Journal of Microelectronic mechanical Systems*, vol. 17, pp. 1061–1071, 2008.

[7] S. Kulkarni, E. Koukharenko, R. Torah, et al, "Fabrication and test of integrated micro-scale vibration-based electromagnetic generator," *Sensors and Actuators*, vol. 145, pp. 336–342, 2008.

[8] S. Casciat, L. Faravelli, Z. Chen , "Energy harvesting and power management of wireless sensors for structural control applications in civil engineering," *Smart Structures and Systems*, vol. 10, pp. 299–312, 2012.

[9] S. Cheng, R. Sathe, R.D. Natarajan , "A voltage multiplying self-powered AC/DC converter with 0.35V minimum input voltage for energy harvesting applications," *IEEE Transactions on Power Electronics*, vol. 26, pp. 2542–2549, 2011.

[10] J.M. Cullagh, R.L. Peterson, T. Galchev, et al, "Short-term and long-Term testing of a vibration harvesting system for bridge health monitoring." *Proceeding of Power MEMS*, vol. 1, pp. 109–112, 2012.

[11] H. Ulusan, K. Gharehbaghi, O. Zorlu, et al. , "A self-powered rectifier circuit for low-voltage energy harvesting applications." *International Conference on Energy Aware Computing*, vol. 1, pp. 1–5, 2012.

[12] B. Massicotte, A. Picard, C. Ouellet, Y. Gaumond, "Strengthening of a long span post tensioned segmental box girder bridge," *PCI Journal*, vol. 29, pp. 52–65, 1994.

[13] D. Cantero, G. Arturo, E.J. Brien, "Maximum dynamic stress on bridges traversed by moving loads," *ICE-Bridge Engineering*, vol. 162, pp. 75–85, 2009.

[14] B. Jacob, D. Labry, "Evaluation of the effects of heavy vehicles on bridge fatigue," *International Symposium on Heavy Vehicle Weights and Dimensions*, vol. 1, pp. 185–194, 2002.

[15] S.F. Ali, A. Ramaswamy, "Optimal dynamic inversion based semi-active control of benchmark bridge using MR dampers," *Structural Control and Health Monitoring*, vol. 16, pp. 564–585, 2009.

[16] A. Carrella, M.I. Friswell, A. Zotov, D.J. Ewins, A. Tichonov, "Using nonlinear springs to reduce the whirling of a rotating shaft," *Systems and Signal Processing*, vol. 23, pp. 2228–2235, 2009.

[17] N.G. Elvin, N. Lajnef, A. ElviN, "Feasibility of structural monitoring with vibration powered sensors," *Smart Materials and Structures*, vol. 15, pp. 976–986, 2006.

Paper H

Radio Frequency Energy Harvesting for Long Lifetime Wireless Sensor Networks

B.Han, R.H.Nielsen, C.B. Papadias, R. Prasad

The paper has been published in the
International Symposium on Wireless Personal Multimedia Communications (WPMC)
pp. 26–28, 2013.

The layout has been revised.

Abstract

In wireless sensor networks energy scarcity is a major concern on energy consumption, and by properly designing on the node network architecture or selecting efficient protocols of the networks, the maximum energy can be reduced significantly thereby increasing the network lifetime. However, in most of the cases, the sensor nodes are either powered by non-replaceable batteries, or there will be a considerable replacement cost. Thus a self-rechargeable sensor node design is necessary: the sensor node should be able to harvest energy from the environment. Among the existing techniques, harvesting energy from the radio frequency (RF) waves gives the lowest system design. Previous research on RF energy harvesting is based on the model that the radio energy is omnidirectional in the air. In this paper, a directional transmission/receiving model is proposed which can further overcome the path loss of the RF signals. On the node level, a virtual floating gate based CMOS biasing is used for the energy conversion circuit. With the proposed technique, the sensor node is able to harvest the energy from base station up to 30 meters.

1 Introduction

Wireless sensor networks play an important role in the current and future machine-to-machine and Internet of Things use cases, from logistics to environment monitoring where all kinds of sensors are deployed with their respective communication protocols. At the same time, in order to increase the lifetime of the sensor network, energy is a big concern and different kinds of energy efficient protocols and network architectures have been proposed in order to reduce the total energy consumption of the network . However, another approach towards increasing the life time of the sensor network is to let sensor nodes be able to harvest energy from their surroundings [1]. Thus energy harvesting is among one of the most promising ways of extending a wireless sensor network's lifetime by harvesting the energy in another domain such as Chemical, mechanical or Physical and convert it into the electrical domain [2].

There are several ways to harvest energy from the environment, e.g. solar energy harvesting, wind energy harvesting, vibration energy harvesting, tide energy harvesting, thermal energy harvesting and also radiation energy harvesting. also the solar energy, wind energy, as well as tide energy depend heavily on the weather condition and when the weather changes, it cannot guarantee energy to maintain the operation of the sensor node and, in turn, the wireless sensor network. The thermal energy harvesting needs temperature differences between two surfaces high enough to formulate a voltage difference, which is not usually feasible for a sensor node. Vibration energy harvesting is investigated in [3] and is harvested either through a micro-generator which contains a permanent magnet with a moving coil or through piezo electrical material which convert-

ers the energy when there is a mechanical shape change. However, in some cases, where there is no vibration, or the vibration amplitude is not high enough, this method can not provide any energy to be harvested. Based on the above-mentioned shortcoming, this paper proposes harvesting energy from radio frequency signals.

Unlike the method of energy harvesting used in Near Field Communications (NFC), where the RFID tags get energy from the near-field electromagnetic field by mutual coupling of the magnetic coils, and only works for a few centimeters, this paper presents a method for far-field wireless radio signal harvesting, where a new method to overcome the path-loss on the radio frequency signals is adopted.

The remaining paper is organized as the followings: Section II gives the introduction to the proposed system using directional transmission to overcome the path-loss on the wireless signals; Section III introduces the floating gate based energy harvesting circuit for the sensor node design. The proposed system evaluation is given in section IV and conclusions in section V.

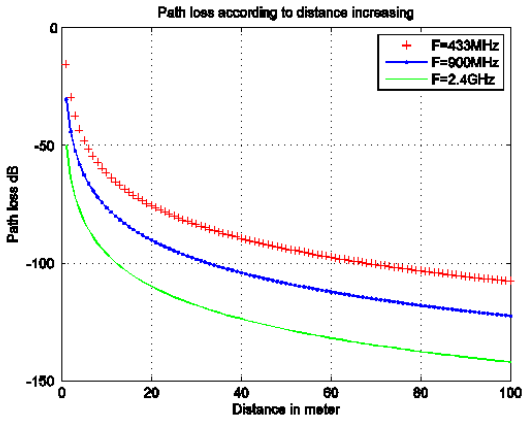

Fig. H.1: Path loss of different carrier frequencies over distance.

2 System Architecture

2.1 Radio Signal over Distance

The proposed architecture enables the sensor nodes to harvest the energy from a power beacon station. However, to harvest energy from the radiation power, one of the biggest issues is the path loss on the wireless signal; there are multiple path-loss models for wireless signals and, without losing of generality, an indicative model of line of sight

(which should be the case for wireless energy harvesting) is adopted as follows:

$$Ls = 32.45 + 20\lg(f(MHz)) + 20\lg(d(km)) \tag{H.1}$$

According to FCC, the most common ISM bands for sensor communication are 433MHz, 915MHz for US and 866MHz for EU respectively along with and 2.4GHz [4], Fig.1 shows the path loss of the signals in those bands over a 100 meter distance. It can be seen that, for short distance range,(0-20m), the path-loss changes dramatically as distance increases, so a lower frequency gives better coverage. However, lower frequency contains less energy at the same time interval. As a compromise, the 900MHz band is considered for RF power transmission and energy harvesting.

As it indicated in (H.1), within a distance of 10 m, the value drops below 51.5 dB. Assuming that the base station uses 2W (which is 33dBm) power for transmission and that an omnidirectional antenna is used (the aperture of the antenna is given in Fig.H.2), which provides 2 to 6 dB antenna gain, based on the aforementioned assumption the available power for the sensor node is around -16.6 dBm, which is equivalent to 20.89 μW.

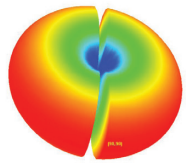

Fig. H.2: Omnidirectional radiation aperture.

Powers in this low range are very weak for the sensor node to harvest, which makes the conversion circuit design very challenging and sometimes impossible. Increasing the transmission power may overcome the path loss problems, but due to the antenna aperture being omnidirectional (Fig.H.2), much power is dissipated in to the air towards unnecessary directions where no sensors are present while this might also cause unwanted interference to other wireless systems.

2.2 Directional Power Transmission

To overcome the aforementioned problems, we propose a directional power transmission for distributed sensor networks. As seen from Fig.H.3, instead of transmitting an omnidirectional radio frequency beam, a high directive RF power beam is transmitted towards the targeted wireless sensor nodes [5] . At the sensor node, the energy in such RF beam will be absorbed by the energy conversion circuit and be converted to electrical energy for the sensor, and then the data can be transmitted back e.g. a data

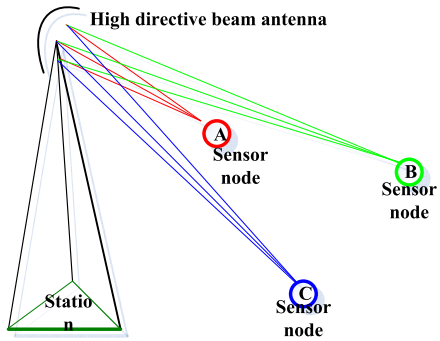

Fig. H.3: Proposed directional Power transmission from base station.

fusion center through the reverse link. In this model, the location of the sensor nodes is assumed to be known by the base station. The transmission antenna can adjust the beam at angle θ, ψ, and composite the path loss according to the distance d .

Meanwhile, in the ideal case, the sensor nodes should also have high directional antennas towards the base station. However, due to the size of the sensor node, this is not feasible and, moreover, adjusting each sensor node towards the base station is also too complicated. Thus in the proposed architecture, the sensor node antenna is kept omnidirectional.

3 Energy Harvesting Circuit in the Sensor Node

3.1 Sensor Node Architecture

In order to reach the goal of long lifetime of the sensor network, the sensor node is also supposed to be battery less and to use the energy from the radiation power only. Therefore the energy conversion circuit that converts RF power to DC power is indispensable in the sensor node. Moreover, in order to have a maximum voltage amplitude of the harvested power, a resonate enhancing stage between the antenna and the energy harvesting circuit in the sensor node is necessary. The proposed node architecture is shown in Fig.H.4, where the resonate enhancing stage is added directly after the antenna. The power harvesting circuit in the Fig.H.4 is responsible for all the circuit block powering.

The RF signal will also be de-modulated by the carrier detection block; the clock signal and the information code will be extracted which will be used by the sensing / control unit. The sensed data will be transferred back to the antenna by the modulation block; all of the circuits are powered by the energy harvesting/storage circuit.

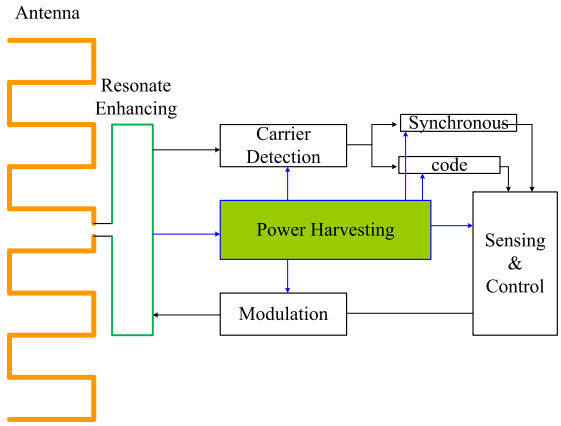

Fig. H.4: Sensor node with energy harvesting circuit block.

3.2 Resonate Enhancing

As mentioned in the previous section, the available power to the sensor node is only 20 μW, but assuming the directional transmission [6] method, the power available to the sensor node at the same distance is around 30 μW, which is still weak. If a conventional 50 Ω RF circuit is directly used for energy conversion, the available voltage is around only 70 to 100 mV, which is not high enough for a MOS transistor to work. With the

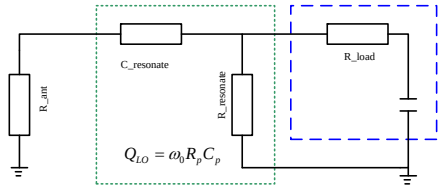

Fig. H.5: Resonate enhancing circuit model.

aforementioned concern, a high Q resonate-enhancing circuit is added between the sensor antennas to the energy harvest circuit to have a high peak-to-peak output voltage. The main function of the high Q resonate-enhancing is to increase the output impedance of the antenna, which will finally increase the output voltage.

Assuming the RF power transmitted from the base station reaches to the sensor

node with strength of P_{rad} [7] , then the available power for the sensor is given by:

$$P_A = G_r \mathrm{P}_{rad} \lambda^2 / 4\pi \tag{H.2}$$

where G_r is the receiving antenna gain, and λ is the wavelength, the voltage converted from such power will be given by:

$$V_{in} = \sqrt{(1 - |\Gamma|^2) G_r \mathrm{P}_{rad} Q_L \lambda^2 / 2\pi Y_p} \tag{H.3}$$

where Y_p is the admittance of the enhancing circuit, Q_L is the quality factor of the enhancing circuit, Γ is the reflection coefficient,which are constrained by the following equation:

$$\left| \int_0^\infty Ln(|\Gamma(\omega)|) d\omega \right| \leq \frac{\pi}{R_p C_p} = \frac{\pi \omega_0}{Q_{LO}} = \frac{B\pi}{2} \tag{H.4}$$

where ω_0 is the centering frequency, B is the signal bandwidth, R_p and C_p are the effective resistance and capacitance as it mentioned in Fig.H.5, $R_{resonace}$ and $C_{resonance}$ respectively. The next stage is a voltage rectifier, where the threshold voltage of the MOSFET and the minimal RF power P_{min} as it is given by:

$$P_{\min} = {V_{th}}^2 C_p \omega_0 / 2Q_{L0}(1 - e^{-j\frac{2\pi\omega_0}{BQ_{L0}}}) \tag{H.5}$$

3.3 Voltage Rectifier Design

The voltage that goes out of the resonate enhancing circuit is an Amplitude Changing (AC) signal; in order to be properly used by the following circuits, a voltage rectifier is added to convert the AC power to DC power. A widely used architecture for converting AC voltage to DC voltage is the full bridge rectifier, which keeps the first half clock period as forward biasing PN diode while reverse the phase of the other half clock period and finally a folded sin wave is generated at the output [8]. However, the PN diode has high threshold voltage, which is not a good candidate for energy harvesting circuit. An improved voltage rectifier is designed by CMOS transistor as it shown in Fig.H.6, where the PMOS transistor M1, M2 and NMOS transistor M3, M4 are switched on/off alternatively as the peak-peak RF voltage (V_{rf}) changes, thus the voltage difference at node $V+$and $V-$ is given by:

$$(V_+ - V_-)_{\max} = 2(V_{rf} - V_{drop\_n} - V_{drop\_p}) \tag{H.6}$$

Where the maximum available output voltage is determined by V_{rf}, $V_{drop_n}$and V_{drop_p}, which are the voltage drops of the MOS transistor and output voltage of the resonate circuit respectively.

However, the voltage rectifier should convert the voltage for the following circuits, so a voltage-boosting technique design is required. Meanwhile, the conventional voltage-boosting techniques work well with 1.2 V or higher supply voltage and adopt a switching capacitor technique, which is not the case for the energy harvesting circuit because of the low voltage constrain and relatively high threshold voltage of the MOS transistor. Furthermore, the switching capacitor technique requires additional clock, which again requires complex circuits and such clock circuits cannot be self-powered. The proposed solution is to reduce the threshold voltage of the MOS transistor and adopting a voltage-boosting technique to increase the output voltage

3.4 Floating Gate

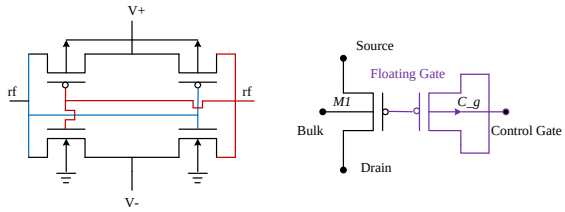

Fig. H.6: CMOS voltage rectifier and virtual floating gate MOSFET.

Towards such direction, many kinds of low threshold voltage techniques have been investigated [4] [9]. e.g. the sub-threshold region biasing, which biases the transistor at the weak inversion, so that a weak input signal can influence the output significantly; also substrate biasing, which biases the transistor by using the voltage difference between the substrate base and the transistor gate; last but not the least, is the floating gate technique: by adding a high programming voltage on a floating gate, the charges are injected into the floating gate; even when the programming voltage is removed, the electrons are still trapped in the floating gate due to the high impedance of the gate oxide layer and such electrons can remain in the floating gate up to 10 years. Due to the existing of the electrons in the floating gate, the threshold voltage of the transistor can be reduced dramatically.

However, adding a floating gate in the MOS transistor will increase the fabrication cost in the CMOS process as, the substitution method is to design a virtual floating gate using the standard CMOS process. As shown in Fig.H.6, the gate of the PMOS transistor M5 is connected to a MOS capacitor C_g, where a high impedance node is formed to trap the electrons in M5, when a high voltage control gate is added on the control gate of the C_g, electrons from the channel of M5 will be trapped at the floating gate, which will act as a virtual gate-source biasing of transistor M5, thus the threshold

voltage will be reduced.

3.5 Voltage Boosting/Increasing

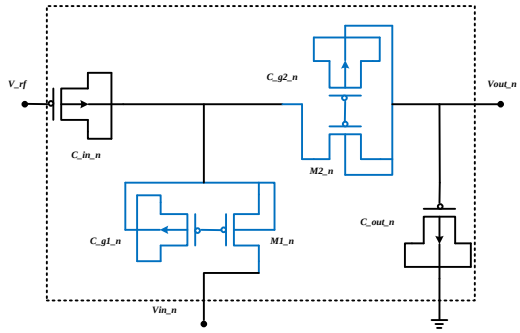

Fig. H.7: Floating gate based voltage boosting unit.

Based on the virtual-floating gate transistor which has low threshold voltage, voltage boosting is designed using a voltage doubling technique. As shown in Fig.H.7, two virtual floating gate transistors M_{1-n} and M_{2-n} are used as the circuit direction controller where the current can only flow from V_{in-n} to V_A and from V_A to V_{out-n}, M_{1-n} also works as a voltage holder, which will *remember* the previous voltage with the help of two MOS capacitors C_{in-n} and C_{out-n}, the circuit equation of such three port network is given by the follows: the charges in capacitors C_{in-n} is given by:

$$(V_{rf} - V_A)C_{in\_n} = Q_{1\_n} \tag{H.7}$$

for the C_{out-n}, it is given by:

$$(V_{out\_n} - 0)C_{out\_n} = Q_{2\_n} \tag{H.8}$$

while the current function is given by:

$$i_{1\_n} = dQ_{1\_n}/dt = C_{in\_n}(dV_{rf}/dt - dV_A/dt) \tag{H.9}$$

assuming the transistor M_{1-n} has a conducting-on resistance of R_{in-1},then it is written by:

$$(V_{in\_n} - V_A)/R_{in\_1} = i_{in\_n} \tag{H.10}$$

similarly applying for M_{1-n} and C_{out-n} ,

$$i_{out\_n} = dQ_{2\_n}/dt = C_{out\_n}dV_{out\_n}/dt \tag{H.11}$$

$$(V_A - V_{out\_n})/R_{in\_2} = i_{out\_n} = i_{1\_n} + i_{in\_n} \tag{H.12}$$

When V_{rf} is at its negative phase, the V_A is given by $V_{in-n} - V_{th-1}$, where V_{th-1} is the threshold voltage of the virtual floating gate transistor M_{1-n}, and the the voltage drop cross capacitor C_{in-n} is $V_{rf} + V_{in-n} - V_{th-1}$. During the positive phase of V_{rf}, the output voltage is given by:

$$V_{out\_n}(n) = 2V_{rf} + V_{out\_n}(n-1) - V_{th\_1} - V_{th\_2} \tag{H.13}$$

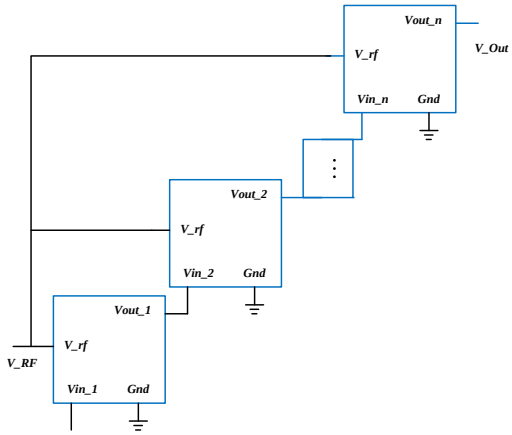

Fig. H.8: Proposed voltage rectifier with voltage booting unit.

To have a high output voltage, a N-stage such voltage boosting unit is cascaded as shown in Fig.H.8 and the output voltage is given by:

$$V_{out\_n}(N) = N(2V_{rf} - V_{th\_1} - V_{th\_2}) \tag{H.14}$$

4 PROPOSED SYSTEM SIMULATION

4.1 Simulated Results of the Voltage Rectifier

The proposed virtual-floating gate based rectifier is simulated with the assumption that the input voltage is 100 mV to 250 mV, given the assumption that the CMOS circuit is simulated in UMC0.18 μm process and the voltage gain/stage as well as the maximum output voltage are simulated according to the Fig.H.7 and Fig.H.8 where the maximum number of stages is chosen at 40. It can be seen from the Fig.H.9 that, with the number of stages at 20, the proposed system can reach 3V output voltage.

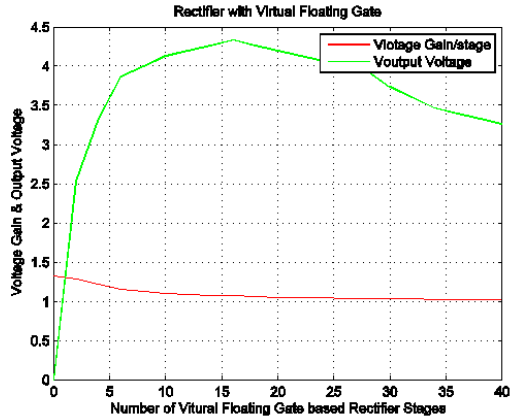

Fig. H.9: Simulated result on the performance of the voltage rectifier.

4.2 Simulated Results of the Proposed Directional Power transmission System

The proposed system is using resonate enhancing circuit on the senor node and a directional transmission at the system level. Assuming the directional transmission system with the Line of Sight (LOS) model is used, the maximum available harvestable RF voltage at the sensor node is plotted in Fig.H.10, from which can be seen that, with

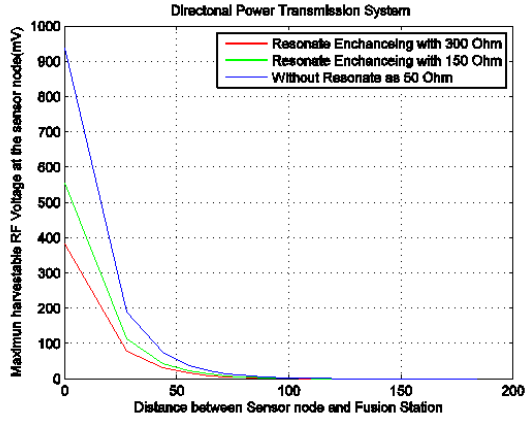

Fig. H.10: Available output voltage with different resonance enhancing.

a resonate enhancing circuit which provides an output impedance at 300 Ω, the maxi-

mum available voltage is above 100 mV within the range of 30 meters, however without resonate enhancing circuit, such range with the same output voltage is limited in 10 meters.

Another system level simulation is given by comparing the directional RF power transmission with the conventional omnidirectional transmission, as shown in Fig.H.11:

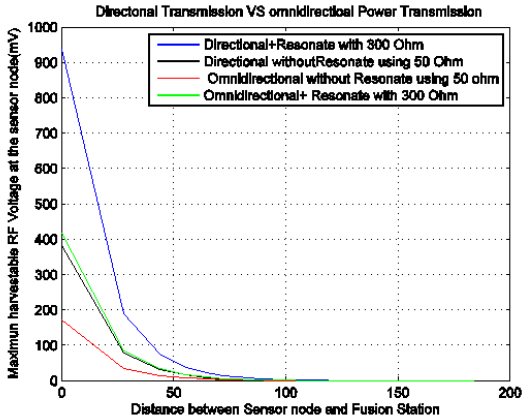

Fig. H.11: Output voltage with different power transmission methods .

From the figure it can be concluded that, without directional power transmission and without the resonate enhancing circuit, the system can only work at a short distance, while with resonate enhancing, even an omnidirectional power transmission can support a system up to 10 to 15 meters, and, when using the directional RF power transmission and resonate enhancing circuit, the system can work up to 30 meters.

5 Conclusion

Wireless sensor networks are becoming still more widely used in modern life and a consequence the life time of the wireless sensor network is becoming of still more importance and reason for concern. In order to guarantee a sufficiently long lifetime of the sensor network, the sensor node should be self-rechargeable or be self-powered by harvesting energy from its environment. Compared with other energy harvesting techniques, this paper proposed a method based on RF energy harvesting: on the system level a directional power transmission method is used to overcome the path loss and reduce interference with other systems. On the sensor node level, a voltage boosting technique is adopted in order to increase the output voltage; meanwhile the floating gate is adopted in the sensor node to provide a better conversion range. According to

simulation, the proposed system is able to work without battery on the sensor node while reaching a distance of up to 30 meters from sensor node to the base station.

References

[1] G.E. Niell, L. Niza, A.V. Alex, "Feasibility of structural monitoring with vibration powered sensors," *Smart Materials and Structures*, vol. 15, pp. 977–985, 2006.

[2] Y.Rao, D.P. Arnold, "An input-powered vibration energy harvesting interface circuit with zero standby power," *IEEE Transactions on Circuits and Systems I. Regular papers*, vol. 26, pp. 1177–1188, 2011.

[3] R.R. Dayal, S. Dwari, L. Parsa, "A new design for vibration-based electromagnetic energy harvesting systems using coil inductance of micro generator," *IEEE Transactions on Industry Applications*, vol. 47, pp. 820–830, 2008.

[4] T. Le, T. Fiez, "Efficient far-field radio frequency energy harvesting for passively powered sensor networks," *IEEE Journal of Solid State Circuits*, vol. 43, pp. 1287–1302, 2008.

[5] T.M. Kim, F. Sun, A. Paulraj, "Low-complexity MMSE precoding for coordinated multipoint with per-antenna power constraint," *IEEE Signal Processing Letters*, vol. 20, pp. 395–398, 2013.

[6] F. Sun, E.D. Carvalho, C. Thai, P. Popovski, "Beamforming design for coordinated direct and relay systems," in *46th Annual Conference on Information Sciences and Systems (CISS)*, 2012.

[7] S. Mandal, R. Sarpeshkar, "Low power CMOS rectifier design for RFID applications," *IEEE Transactions on Circuits and Systems I. Regular papers*, vol. 54, pp. 1177–1188, 2006.

[8] Y. Rao, D.P. Arnold, "An input-powered active AC/DC converter with zero standby power for energy harvesting applications," *IEEE Energy Conversion Congress and Exposition (ECCE)*, vol. 1, pp. 4441–4446, 2010.

[9] B. Han, M. Liu, N. Ge, "A 3-5GHz UWB CMOS receiver with digital control technique," *IEEE 13th International Symposium on Design and Diagnostics of Electronic Circuits and Systems (DDECS)*, vol. 1, pp. 157–160, 2010.

Paper I

Directional Transmission by 3-D Beam-forming using Smart Antenna Arrays

B.Han, R.H.Nielsen, C.B. Papadias, R. Prasad

The paper has been published in the
International Conference on Wireless Communications, Vehicular Technology, Information Theory and Aerospace Electronic Systems Technology(Wireless ViATE)
pp. 1–5, 2013.

The layout has been revised.

Abstract

Beam forming is a widely used antenna technique to adjust the radiation beam towards one direction, which is quite useful for interference alignment, and overcome multiple access interference, common channel interference as well as multi path fading, thus increases the capacity of mobile networks. Thus fixed antenna array can be configured to be smart antenna with the help of digital signal processing technique. However, all the conventional 2-D beam forming is implemented by a fixed vertical angle of in the Spherical coordinates, while only consider the beam pattern on cylindrical coordinates. As the trend of modern communication, where the femto cell is proposed for the future base station, directional transmission is reconsidered in terms of better coverage and better frequency reuse. In order to have maximum transmission efficiency as well as minimal interference, a 3-D beam is necessary. This paper presents a 3-D beam forming technique that can be used for high directional transmission.

1 Introduction

Smart antenna is made of several antenna units, with each of them combined with a *complex* weighting coefficient, that can deal with signal processing in spatial domain. By adding a delay based weighing coefficient, the antenna can also be able to deal with signal in both spatial and time domain. Smart antenna makes the Spatial Division Multiple Access possible, which is able to distinguish multiple access by different signal path while even with same time division, same frequency and address code. With the help of adaptive antenna theory and high resolution array signal processing, smart antenna gives a good promise for future wireless communications.

Beam forming is one of the most dominant and widely used techniques in smart antennas, it is a technique that combines the radiation pattern of each antenna elements on the the antenna arrays to form a directional and energy concentrated beam [1]. The active antenna array system is merging the RF part in communication system with the antenna, and control every steering vector to the antenna array, to form a directive beam. By adding weight on the amplitudes and phases of the signals from multiple antennas, the beam can have the ability of space selectivity. At the direction of interest, the antenna array can get the constructive interference gain, while for the rest directions, the array can generate destructive interference [2]. It is determined by the antenna array geometry along with relative per antenna element magnitude/phase weighting.

Compared with omnidirectional or broadcast transmission, the gain from beam forming increases significantly. It can increase the capacity on the edge of the cellular network and increase the coverage at the edge; also the spatial electivity can be increase significantly by using reinforming, which can reduce the interference between the cellular as well as between the users, further, the spectrum efficiency can also be increased [3].

However, the conventional 2-D beam forming can only control the horizontal angle ϕ , where by steering weighting coefficient on the antenna arrays, the beam can be selected among the range of $[0,\ 2\pi]$. However, in the conventional 2-D beam forming, the vertical angle θ is neglected or is fixed at one value, e.g.$(\pi/2$ or $\pi/4)$. So the flexibility of the antenna array is constrained, which can only control one plane and in some cases, the vertical angle of the wave can also influence the phase from the antenna array, so a 3-D beam control is necessary [4]. This paper presents an idea on 3-D beam forming and control technique with a 4×4 antenna array. A 3-D Spherical coordinates is presented in Figure (I.1).

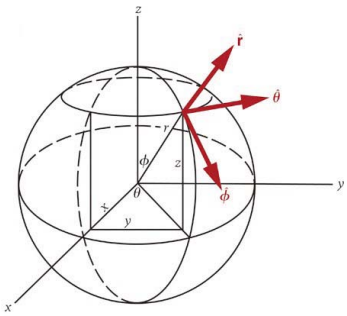

Fig. I.1: A 3-D view of the antenna space.

The remaining of the paper is organized as the followings: Section II gives the System analysis of the beamforming and the conventional beam forming techniques; Section III introduces the proposed 3-D beam forming and its analysis. The proposed evaluation and conclusions are given in section IV.

2 Beamforming System Analysis

2.1 Smart Antenna Advances

Antenna Diversity in wireless communications has two main catalogs: the transmission diversity, which uses the multiple transmitter to a single receiver(MISO) can increase the robustness of the signal at low SNR, and can not increase the date rate; while the receiving diversity, which uses single transmitter and multiple revivers (SIMO), that can combine the same signal and increase the SNR, increase the coverage. while MIMO can increase the data rate and spectrum efficiency by taking the advantage of spatial multiplexing [5]. in LTE release8/9, the down link MIMO can increase the data rate of

a single user significantly, while the multiple user terminal cooperate to form a MIMO can increase the coverage of the cellular sector [6] [7].

In LTE-Advanced, the MIMO link requires $(4 \times 4)/(2 \times 2)$ for down-link/uplink, with $(8 \times 8)/(4 \times 4)$ reaches the maximum speed for the single user. However the challenge of the MIMO techniques is the size of the device is going to be bigger, the power consumption is bigger, and the cost is higher, also the design is more difficult. By combing spatial multiplexing with beam forming. The converge can be increased significantly [4] [8].

The advantage of 3-D beam is obvious, it has been nominated in the standard that 3-D beam forming and pre-coding can increase the SNR of the target user. the antenna array system can trace the location of the user, and supply a dynamic coverage to reduce the interference among users so that the total capacity of the system can be increased. Besides, the 3-D beam forming can also be combined with 3-D MIMO technique, according to the channel information, the super-narrow beam can be formed towards a single user, which is more accurate than the conventional beam forming that can provide the beam at range of a sector [9].

2.2 Beamforming Theory

Beam forming can be used for compensating the path loss or fading/distoration generated by multiple path, also reduce the interference among users in the same channel. Smart antenna uses digital signal processing methods to form the beam, which can be updated by the adaptive algorithm *softly* without changing the hardware configuration. By weighting and sum up the signals on antenna elements, the main beam can be directed to the targeted user while the zero-beam can be pointed at the interference [10].

There are two main catalog of beam forming by using smart antennas, phase array spatial signal processing and beam spatial signal processing. Phase array spatial signal processing sum up all the received signals by weighting them separately with their corresponding coefficient, then forms the pattern with the main lobe towards the target user. Due to all the array unit are adjusted by the weighting coefficient, this can be considered as full-adaptive array signal processing [11].

The beam spatial signal processing is actually made by two steps: first sum up all the elements in the array with their corresponding weighting coefficient, form multiple beam with different directional speed; then weighting the beam with another weighting coefficient to form the array pattern. In this way, not all the array elements get the optimal weighting coefficient, just part of them [9].

2.3 Adaptive Algorithm in Smart Antennas

The main method of smart antenna signal processing is adaptive antenna processing algorithm, which can be cataloged into two major sectors: the non-blind and blind methods.

The non-blind based methods need reference signals, e.g., the pilot frequency channel or pilot PN sequence. The receiver knows what the transmitter sends, thus adjust the weighting according to certain algorithm criterion, to make the maximum correlation between antenna output and input. Such criterion includes Minimum Mean Square Error (MMSE),Least Mean Square (LMS) and LS. while in the blind based methods, pilot signal is not mandatory, the weighting coefficient is adjusted by using the characteristic of the carrier signals, e.g., subspace, finite set of symbols, etc [6].

The non-blind algorithm gives better accuracy and better converge speed, while needs more system cost. A comprise way is to combine the non-blind with blind methods, first get the raw weighting factor by non-blind algorithm, then do adjusting and tracing by the blind algorithm [12].

3 The 3-D beam forming

3.1 Limitation of the 2-D Beamforming

The conventional beam forming using a fixed switchable beam arrays, where the ideal direction(beam) is either selected by the feedback from the user terminal with the maximum SNR, or selected by Direction of Arrival(DoA)from the receiver. By using the adaptive beam beam forming and antenna arrays, the beam is adjusted by the feedback of the channel quality, so that the maximum SNR can be reached, the channel estimation will change the antenna weighting and beam pattern. By using zero-cancellation technique, the interference from other cellular can be cancelled [11].

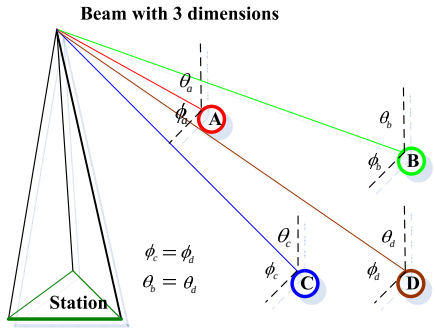

Fig. I.2: The 3-D beam for multiple user access .

However, despite the advantage of the conventional beam forming, there are still unsolved problems with the current system: When the users are close to the base station,

or where the beamforming at the user level is required, the conventional beam forming loses the resolution capability when the users are at the same horizontal angle. e.g. Figure I.2 indicates that when user (node) C and D are at the same horizontal angle $\phi_c = \phi_d$, then the convectional 2-D beam forming can not distinguish these two users (nodes)since they are on the same direction of horizontal angle. User/node C and D can only be distinguished each other by using a 3-D beam that can have both horizontal and vertical resolution. As shown in Figure I.2, user A and the rest CAN easily be distinguished by ϕ_a or θ_a; user B and D have the same vertical angle $\theta_d = \theta_b$, but still can be distinguished by the horizontal angle which fall in the range of convectional beamforming, but also be distinguishable by 3-D beam, since in 3-D beam forming, all the conventional 2-D beam forming still works at their respective plane.

It is obvious that the conventional 2-D beam forming can work on a 2 dimension, while in applications where the 3-D geometry of the real network is considered, It requires the beam should be able to control both on horizontal and vertical direction. Thus a 3-D beam forming antenna is analyzed simulated in the following section.

3.2 3-D Beamforming Analysis

The conventional antenna arrays that is used for beam forming only have the phase array on one axis, thus the conventional phase is described by ϕ, the travelling distance of two wave is given by $d_r \times cos(\phi)$. However in a 3-D beam, such value is given by $d_r \times cos(\phi) \times cos(\theta)$, without losing of generality,$|d_r| = |d_x, d_y|$, the corresponding distance is given by $d_y \times cos(\phi)$ and $d_x \times cos(\theta)$,where d_y and d_x are interlacement distance of the antenna array along horizontal and vertical direction respectively. Figure. I.3 gives the geometry of the antenna used for simulation in this paper. each element has its own feeding port which will be weighted by the corresponding coefficient.

Assuming the received signal S can be expressed as the following :

$$S = \begin{bmatrix} S(t)e^{j3\psi} & S(t)e^{jv}e^{j3\psi} & S(t)e^{j2v}e^{j3\psi} & S(t)e^{j3v}e^{j3\psi} \\ S(t)e^{j2\psi} & S(t)e^{jv}e^{j2\psi} & S(t)e^{j2v}e^{j2\psi} & S(t)e^{j3v}e^{j2\psi} \\ S(t)e^{j\psi} & S(t)e^{jv}e^{j\psi} & S(t)e^{j2v}e^{j\psi} & S(t)e^{j3v}e^{j\psi} \\ S(t) & S(t)e^{jv} & S(t)e^{j2v} & S(t)e^{j3v} \end{bmatrix} \tag{I.1}$$

where e^{jnv} stands for vertical weighting and e^{jmv} stands for horizontal weighting, the $m, n \in [1,\ 4]$ are vertical elements number and horizontal elements number respectively. The total output beam can be summed up as it expressed in the following:

$$Y = \sum \sum W. \times S \tag{I.2}$$

where the W is the weighting coefficients matrix and the optimal weighting is given by:

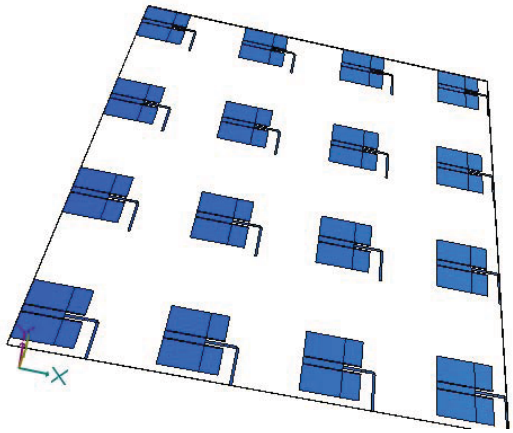

Fig. I.3: An antenna array for 3-D beam forming with 4×4 elements.

$$W^* = \frac{1}{4}\begin{bmatrix} e^{-j3\psi} & e^{-jv}e^{-j3\psi} & e^{-j2v}e^{-j3\psi} & e^{-j3v}e^{-j3\psi} \\ e^{-j2\psi} & e^{-jv}e^{-j2\psi} & e^{-j2v}e^{-j2\psi} & e^{-j3v}e^{-j2\psi} \\ e^{-j\psi} & e^{-jv}e^{-j\psi} & e^{-j2v}e^{-j\psi} & e^{-j3v}e^{-j\psi} \\ 1 & e^{-jv} & e^{-j2v} & e^{-j3v} \end{bmatrix} \tag{I.3}$$

the solution for 3-D beam forming as mentioned in [1] is based on the assumption that: apply a 2-D beam forming at the vertical beam on first last column of the antenna array and get the optimal weighting vector W_V (I.4); while apply a 2-D beam forming at the horizontal beam on the last row of the antenna array and get the weighting vector W_H (I.5) [1].

$$W_H = \frac{1}{2}[1 \quad e^{-jv} \quad e^{-j2v} \quad e^{-j3v}] \tag{I.4}$$

$$W_V = \frac{1}{2}[e^{-j3\psi} \quad e^{-j2\psi} \quad e^{-j\psi} \quad 1] \tag{I.5}$$

then the vertical and horizontal weighting vectors are extended to be a weighting array W, which is given by:

$$W^* = [W_H W_H W_H W_H]. \times [{W_V}^T {W_V}^T {W_V}^T {W_V}^T] \tag{I.6}$$

Assuming the Angle of Arrival (AoA) for the user is given by (ϕ, θ), then the optimal beam forming weighing on horizontal and vertical axis is given by (I.7) and (I.8) respectively:

$$\frac{1}{\sqrt{N_t}}[1 \quad e^{-j2\pi 1 d_y \cos\phi} \ldots e^{-j2\pi(N_t-1)d_y \cos\phi}]^T \tag{I.7}$$

$$\frac{1}{\sqrt{N_t}}[1 \quad e^{-j2\pi 1 d_z \cos\theta} \ldots e^{-j2\pi(N_t-1)d_z \cos\theta}]^T \tag{I.8}$$

when the horizontal angle ϕ fits normal distribution among $[0,\ 2\pi]$, and vertical angle θ fits normal distribution among $[0,\ \pi/2]$, then ϕ, θ fits independent two-dimensional normal distribution. Thus $d_y cos\phi \in [-d_y,\ d_y]$, and $d_x cos\theta \in [0,\ d_x]$, while $e^{-jkx2\pi} = e^{-jk(x+1)2\pi}$, so $mod(d_y cos\phi,\ 1) \in [0,\ 1)$; $mod(d_x cos\theta,\ 1) \in [0,\ 1)$ [1].

Based on the aforementioned analysis,the optimal recoding for the 4×4 array is given by (I.9):

$$\begin{bmatrix} 1 & 1 & 1 & ... & 1 \\ 1 & e^{-j2\pi 1\frac{1}{N}} & e^{-j2\pi 1\frac{2}{N}} & .... & e^{-j2\pi 1\frac{N-1}{N}} \\ 1 & e^{-j2\pi 2\frac{1}{N}} & e^{-j2\pi 2\frac{2}{N}} & .... & e^{-j2\pi 2\frac{N-1}{N}} \\ \vdots & \vdots & \vdots & \ddots & \vdots \\ 1 & e^{-j2\pi(N_t-1)\frac{1}{N}} & e^{-j2\pi(N_t-1)\frac{2}{N}} & .... & e^{-j2\pi(N_t-1)\frac{N-1}{N}} \end{bmatrix} \tag{I.9}$$

3.3 Simulation and Analysis

The directivity of the 3-D beamforming using 4×4 antenna arrays is plotted in Figure I.4, where the working frequency is assumed to be around 900MHz, which falls into the typical ISM band for wireless sensors, also in the lower band of HSPA/HSPA+. The peak direcitvity is found at 21.1dBi towards "$z+$" direction on z axis, while the side lobe is -10dBi towards other direction and no radiation towards "$z-$" direction.

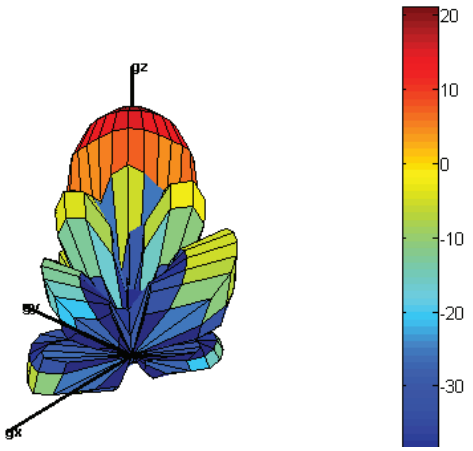

Fig. I.4: Directivity plot of the 3-D beam forming.

A comparison is made by using the aforementioned methods,as shown in Figure I.5,

the directivity of the antenna is simulated with the relative Power and the directivity. It is obvious that, by the 2-D beam forming is better than the omnidirectional, while

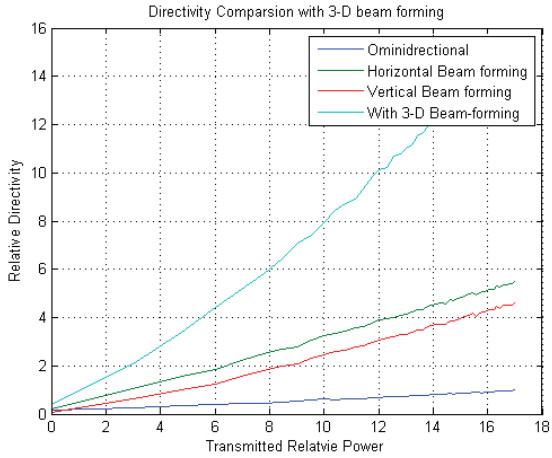

Fig. I.5: Comparison on directive ability of 3-D beam forming.

the horizontal beam forming is better than pure vertical beam forming is also true for the practical situation since most of the conventional beam forming are only considering the horizontal beam forming. The significant increase of the infectivity of the 3-D beam forming indicates that by using the 3-D beam forming, more beam forming gain can be gained, and the network can be designed more flexible.

4 Conclusion

The conventional beamforming mostly considers the beam pattern on cylindrical coordinates, which can select the beam in 2 dimension. By using adaptive algorithm, which can form a spatial directive beam that make the main lobe of the pattern towards the target user while let the side lobe towards the interference,that can make full use of the signal and reduce the effect of the interference. However, as the trend of modern communication, where the femto cell is proposed for base station, the Directional Transmission is necessary in terms of coverage and frequency reuse. The 3-D beamfroming with high directicivy can make the feasible a 3-D beam is necessary, this paper presents a 3-D beam forming technique and the preliminary simulated result shows that the 4×4 antenna array can provide 21dBi directicvity gain and rougphly N^2 times better than conventional 2-D beamforming.

References

[1] Y. Hei, X. Li, H.Yang, "A beamforming detector for variable-rate group space-time coded systems," *4th International Conference on Wireless Communications, Networking and Mobile Computing (WiCOM)*, vol. 1, pp. 1–3, 2008.

[2] R.A. Speciale, "Advance design of phased-array beamforming networks," *IEEE Antennas and Propagation Magazine*, vol. 38, pp. 22–34, 1996.

[3] N.A. Salmon, J. Beale, J. Parkinson, S. Hayward, P. Hall, "Digital beamforming for passivle millimeter wave security imanging," *The Second European Conference on Antennas and Propagation*, vol. 1, pp. 1–11, 2007.

[4] H. Christoph, S.Christoph, "Digital beamforming technology for phased array antennas," *2nd International Conference on Space Technology (ICST)*, vol. 1, pp. 1–4, 2011.

[5] F. Sun, E.D. Carvalho, "A leakage-based MMSE beamforming design for a mimo interference channe," *IEEE Signal Processing Letters*, vol. 19, pp. 368–371, 2012.

[6] F. Zhang, L. Xu, M. Chen, "The design of beam-forming for broadband beam-steerable parametric array," *International Conference on Mechatronics and Automation (ICMA)*, vol. 1, pp. 1580–1585, 2012.

[7] F. Sun, L. Lu, T. Sorensen, "Designs of precoding for lte tdd using cell specific reference signals ," in *IEEE Globecom Workshops*, 2010.

[8] T. M. Kim, F. Sun, and A. Paulraj, "Low-complexity MMSE precoding for coordinated multipoint with per-antenna power constraint," *IEEE Signal Processing Letters*, vol. 20, pp. 395–398, 2013.

[9] C. Sun, A. Hirata, T. Ohira, N.C. Karmarkar, "Fast beamforming of electronically steerable parasitic array radiator antennas: theory and experiment," *IEEE Transactions on Antennas and Propagation*, vol. 52, pp. 1819–1832, 2004.

[10] L. Li, J.Zhang, "New leakage-based Iterative coordinated beam-forming for multi-user MIMO in LTE-Advanced," *IEEE International Conference on Communications (ICC)*, vol. 1, pp. 2308–2312, 2012.

[11] Y. Hei, K. Yi, X. Li, "Iteration interference cancellation decoding for multi-user MIMO uplink transmission system," *9th International Conference on Signal Processing*, vol. 1, pp. 2037–2040, 2008.

[12] Y. Qun, Y. Yi, X. Cao, X. Yao , "Analysis of DOA and adaptive beam forming including mutual coupling," *IEEE International Conference on Signal Processing Communications and Computing (ICSPCC)*, vol. 1, pp. 1–4, 2011.

Paper J

Energy Efficient MIMO Transmission with High Order Modulation for Wireless Sensor Network

B.Han, A.Kalis,C.B. Papadias, R. Prasad

The paper has been published in the
European Signal Processing Conference(EUSIPCO), pp. 1–5, 2013.

The layout has been revised.

Abstract

Energy efficiency emerges as a big concern in wireless sensor networks, where the lifetime of the system depends heavily on energy consumption. In a sensor network, the energy is consumed both by the circuit and the radio link. The radio link performance can be improved by using spatial multiplexing, but the conventional way of spatial multiplexing requires large antenna space and consumes more energy. Thus single RF MIMO transmission is proposed, which maps MIMO symbols on the radiation patterns to reduce power consumption. This paper presents the energy efficiency analysis over different schemes, which extends single RF MIMO capability with 16-QAM constellation though compact ESPAR antenna with only 2 elements. A detailed analysis on the minimal required energy is given, which shows that the proposed single RF MIMO with 16-QAM signaling has similar bit error rate performance with better energy efficiency.

1 Introduction

The life time of wireless sensor network draws a lot of attentions both from industry and academia. Since most of sensor nodes are powered by batteries which are not easily replaceable, the energy must be used efficiently in order to maximize the lifetime of the network. The energy consumption can be cataloged into two main parts [1]: the energy consumed by the circuit on the sensor node, and the energy consumed by the transmission in the radio link. In order to have a long life time of the network, those two parts have to be reduced. The transmission energy cost relies on the distance of the radio link, the topology of the network, the channel condition, etc. The circuit energy consumption depends on the amount of circuit blocks that are switched on during a certain period, such period can be reduced by having a higher data rate in transmission.

The spatial multiplexing technique can help the wireless sensor network with a better performance on the radio link [2], such as larger capacity, higher data rate, etc. When the radio link is enhanced, the number of routing/hoping nodes can be reduced [3], which increases energy efficiency of the network. However, the conventional spatial multiplexing needs more RF chains, which increases circuit power consumption. Moreover, the antennas are spaced far away from each other, which makes having multiple antennas on a single sensor node very difficult. Thus the single RF MIMO transmission is introduced, which maps MIMO symbols onto the radiation patterns. By using Electronic Steerable Parasitic Arrays Radiators (ESPAR) antenna [3], the radiation patterns can be modulated by changing the load of the parasitic elements on the antenna, which is equivalent as conventional MIMO symbols faded though independent channel. At the same time, ESPAR antenna has compact size, which can be installed on a sensor node.

The energy efficiency on the radio link depends on the channel diversity, the baseband signaling, etc. Higher modulation schemes has better data rate which can lead to better

circuit efficiency, but the total system energy efficiency needs to be reconsidered since the error probability has been changed. This paper proposes a way of improving the radio link in the wireless sensor network as following: Using single RF transmission with 16-QAM modulation over ESPAR antenna with only 2 elements spaced by $d = \lambda/16$. By numerical simulations in terms of system performance, the proposed method has the bit error rate similar as conventional MIMO transmission; while in terms of required energy per bit analysis, it gives better energy efficiency.

The remaining part of this paper is organized as following: section 2 gives the concept and simulation of single RF transmission over ESPAR antenna with 16-QAM signaling; section 3 analysis the energy efficiency over different configuration/constellation in wireless sensor network, also gives a comparison of the energy efficiency over those configurations; a conclusion is given in section 4.

2 MIMO Over ESPAR Antenna

2.1 System Model

A proposed architecture of Single RF transmission over ESPAR antenna contains 2 closing by elements spaced by $d = \lambda/8$. Two MIMO data streams are mapped to two orthogonal radiation patterns, which gives the total pattern as:

$$P(\theta, \varphi) = \sum_{n=0}^{2-1} w_n \Phi_n(\theta, \varphi) \tag{J.1}$$

where $\Phi_n(\theta, \phi)$ $(n \in \{0, 1\})$ is the basis pattern, and w_n $(n \in \{0, 1\})$ is the weighting coefficient (which is also corresponding to the transmitted symbol) [4], Mapping of the MIMO symbols onto the radiation pattern is done by changing the parasitic load, given a 2-elements ESPAR antenna parameter Z_{21}, Z_{22}, the load value and the transmitted symbols are linked by [4]:

$$x_1 = -\left(\left[\frac{w_0}{w_1} - \frac{2\pi I_0(jb)}{k_0 k_1}\right]\frac{k_1}{k_0} Z_{21} + Z_{22}\right) \tag{J.2}$$

where $b = 2\pi d$ and d is the inter-element distance normalized to wavelength, and $I_0(jb)$ is the zero-th order modified Bessel function of the first kind. Assuming an ESPAR antenna is designed as Figure J.1, where port 1 is connected to active RF chain and port 2 is connected to adjustable loads. FR4 with E_r=4.3 is used as substrate and metal thickness is 0.0254mm. The self-impedance of the antenna is given by: $Z_{11} = Z_{22} = 48 + j15\Omega$ and $Z_{21} = Z_{22} = 35 + j10\Omega$.

Two data streams w_0 and w_1 with 16-QAM signaling are mapped to basis patterns $\Phi_1(\varphi), \Phi_0(\varphi)$. w_0 goes to the conventional RF chain and w_1/w_0 goes to a mapping block

Fig. J.1: ESPAR antenna and a sensor node.

that controls the loadings. Combination of two data streams with 16-QAM constellation has 256 numbers, due to symmetric, (e.g. $(1+j)/(1-j) = (3+3j)/(3-3j)$), w_0/w_1 only requires 64 values. Varying all the symbol combinations, the required load in (J.2) is found to be in the range of $\{-81 \sim +76\} + j\{-56 \sim +69\}\Omega$.

2.2 Circuit for parasitic Load

Complex load is proposed to satisfy system's requirement, and such load should also ranged with both positive and negative values. As mentioned in [5], where CMOS technique was used for load design, the proposed design in this paper uses the similar technique while extending the controllable range on both real part and imaginary part. UMC-0.18μmRF process is used for the load design with the topology shown in Figure J.2. Negative load is simulated by inserting a probe though the differential port ({Port+, Port-} in the figure). Transistors M6-M11 work as biasing circuit; M1-M4 work as cross-coupling core which generates negative resistance; M5 works as the main current source of the core circuit. Transistor M12 works as a capacitor to stabilize the biasing.

The generated load is given by (J.3) , such load is valid under DC biasing, at high frequency the value will change.

$$R_{neg} = -\frac{L}{uC_{ox}W(V_{gs} - V_{th})} = -\frac{1}{2}\sqrt{\frac{2n}{uC_{ox}}\frac{L}{W}\frac{1}{I_{ds}}} \tag{J.3}$$

uC_{ox} is CMOS process related coefficient; W/L is the ratio of width and length of the transistor; I_{ds} is the *biasing* current controlled by M5. V_{gs} is the *gate-source* voltage, V_{th} is the threshold voltage, g_m is the *trans-conductance* of (M1-M4). n is the ratio of *drain-source* voltage V_{ds} and *gate-source* voltage V_{gs}. According to the simulation, the load of such circuit block is -113+j76 Ω at 2.5GHz.

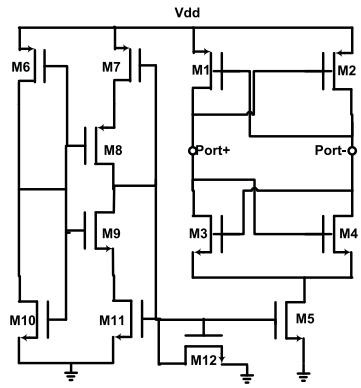

Fig. J.2: Active circuit for negative resistance generation.

2.3 Load Switching Circuit

The CMOS load can be changed by changing the currentI_{ds}, but the side effects on the imaginary part is nonpredictable. In order to have a stable design, the proposed system uses a fixed CMOS load and adds a switching stage for generating the 64 variable loads.

The switching stage is composed of passive element, and connects between the CMOS load and parasitic antenna element, which is shown in Figure J.3. It is an 8×8 array that contains 8 vertical beams and 8 horizontal beams. 64 cells are formed between the cross point of the beams, each cell contains a resistor and inductor with fixed values. By selecting the appropriate combination of array beams (the vertical and horizontal), one of the cells can be chosen, which gives the compensated loading value for parasitic antenna.

One indicative example is given by selecting the first horizontal and 5th vertical beams, where $a_1b_5$is selected, thus the CMOS Load combines with the compensation load inside unit a_1b_5 to form a load with -83.24-26.92jΩ for parasitic antenna, the corresponding resistor and inductor value are 4.85Ω and 5.82 nH respectively. It can also be concluded from Figure J.4, The load value varies little over 90MHz frequency band.

2.4 System Performance

The performance of Single RF MIMO is evaluated by comparing bit error rate with conventional MIMO, the result is shown in Figure J.5. It can be seen that, in the ideal case, there's no big difference between single RF MIMO and conventional MIMO.

The aforementioned system performance is simulated only with consideration of baseband signal power, which is noted by Eb/No. In order to transmit such amount of

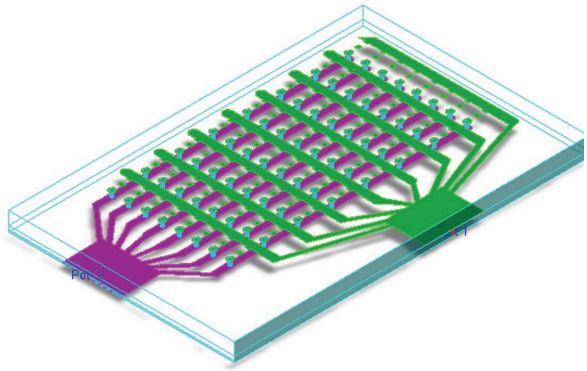

Fig. J.3: Loading array for 16-QAM MIMO mapping.

signal bits into the air, radio frequency circuits are required, which involve mixers, power amplifiers, frequency synthesizers,etc. Conventional MIMO system needs M_t number of such RF Chain for transmission, while Single RF MIMO transmission just uses one. Thus it is expected with less power requirement, a detailed energy efficiency is analysed in the next section.

3 Energy Efficiency Analysis

3.1 Energy for the Transmission Link

The total energy consumption in a wireless sensor network depends both on the radio link and circuit consumption on the sensor nodes. Without losing of generality, we assume G_t is the antenna gain of a transmitter, and G_r is the antenna gain of the receiver for a single link; for a MIMO radio link, we assume there are M_t number of transmit antennas and M_r number of receiving antennas. The power consumed by the radio transmission is noted as P_T, while the power consumed by the circuit is noted as P_C. Assuming the data rate of such a link is given by R_b, Thus the energy efficiency (required energy for one bit) is defined as [1]:

$$E_{bt} = (P_T + P_C)/R_b \tag{J.4}$$

Which is defined by joule per bit (J/bit). (J.4) indicates that, for a given data rate, system energy efficiency linearly follows the total power consumption.

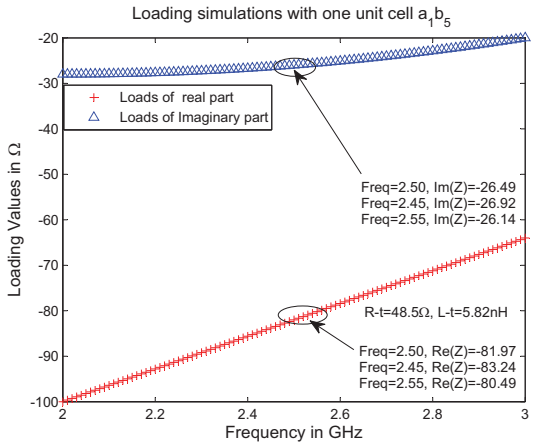

Fig. J.4: Simulated loading with variations.

A typical circuit power consumption of a radio link includes mixers (P_{mix}), frequency synthesizers (P_{sys}) and power amplifier (P_A) (transmission), low noise amplifier P_{lna}(receiving), as well as analog to digital converter (P_{adc}) and digital to analog converter (P_{dac}). The power amplifier is the last stage on the transmission chain, and its efficiency and linearity influence the output power, which are considered in the power for transmission P_T. Assuming P_T relates to the actual power amplifier consumption P_A by $P_T = (1+\alpha)P_A$, where α is given by $\alpha = \xi/\eta - 1$, and ξ, η are linearity factor and drain efficiency respectively. For a M-arry signaling, ξ is related to the Peak to Average Power Ratio (PAPR) given by $\xi = 3(M - 2\sqrt{M} + 1)/(M - 1)$.
The circuit power consumption P_C is modeled with minimal circuit blocks required in sensor communication, as shown in (J.5), where for a SISO link, M_t, M_r is assumed to be 1.

$$P_C = M_t(P_{adc} + P_{mix} + P_{sys}) + M_r(P_{mix} + P_{sys} + P_{lna} + P_{dac}) \tag{J.5}$$

The required transmission power from the power amplifier P_A can be calculated though the radio link budget. The channel $\boldsymbol{H}$ among the transmitters and receivers is modeled as following: the distance d_{ij} among the i^{th}transmitter and j^{th}receiver is assumed to be d; the attenuation coefficient κ is assumed to represent the fading (with κ ranged from 2 to 4 according to the fading condition). according to [1], The energy budget is shown as following:

$$P_A = \overline{E}_b \times R_b \times \left(\frac{4\pi}{\lambda}\right)^2 \times \frac{U_{link} N_F}{G_t G_r} \times d^{\kappa} \tag{J.6}$$

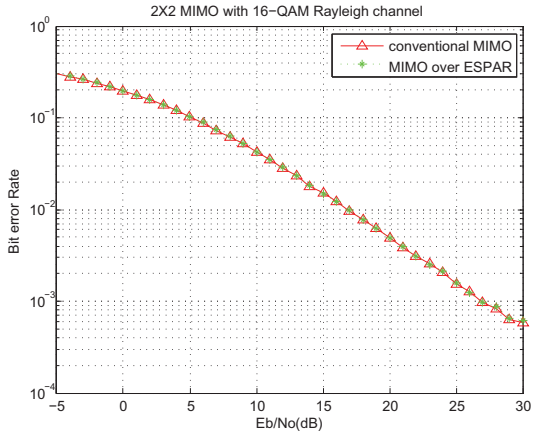

Fig. J.5: Simulated bit error rate performance.

where $\overline{E}_b$ is the required energy per bit for a given error probability $\overline{P}_b$, and R_b is the data rate noted by bit/s, U_{link} is the link compensation due to the hardware variation and system interferences. N_F is the noise figure given by $N_F = N_r/N_o$. Thus the energy required for a single radio link with data rate R_b is given by [6]:

$$P_T = (1+\alpha) \times \overline{E}_b \times R_b \times \left(\frac{4\pi}{\lambda}\right)^2 \times \frac{U_{link} N_F}{G_t G_r} \times d^{\kappa} \tag{J.7}$$

3.2 Energy and Error Probability

The theoretical error probability for a BPSK signaling is given by:

$$\overline{P}_b = Q(\sqrt{2\gamma_b}) \tag{J.8}$$

where γ_b is given by $\gamma_b = \overline{E}_b/N_o$ in a SISO link, for MIMO system, $\gamma_b = (|\mathrm{H}|_F^2 \cdot \overline{E}_b)/(M_t \cdot N_o)$, where $|\mathrm{H}|$ is the channel matrix. According to chernoff bound, the error probability is approximately given by:

$$\overline{P}_b = \varepsilon_{\mathrm{H}}(Q(\sqrt{2\gamma_b})) \leq (\frac{|\mathrm{H}|_F^2 \cdot \overline{E}_b}{M_t \cdot N_o})^{-M_t} \tag{J.9}$$

Where M_t is the number of transmission antennas, the required energy per bit $\overline{E}_b$ (J/bit) can be derived as :

$$\overline{E}_b \geq \frac{M_t \cdot N_o}{|\mathrm{H}|_F^2 \, \overline{P}_b^{\frac{1}{M_t}}} \tag{J.10}$$

Thus, the required power for transmission (J.7) can be derived as:

$$P_T = (1+\alpha)\frac{M_t \cdot N_o}{|\mathrm{H}|_F^2 \, \overline{P}_b^{\frac{1}{M_t}}} R_b \left(\frac{4\pi}{\lambda}\right)^2 \frac{U_{link} N_F}{G_t G_r} d^{\kappa} \tag{J.11}$$

It is noticed that in (J.11), the power for transmission is related to data rate, when considering the energy efficiency, such data rate should be divided as in (J.4). Thus the energy per bit for transmission is independent of data rate, while the energy per bit for circuit consumption depends on the data rate, which can be expressed as:

$$E_{bt} = \frac{(1+\alpha) M_t \cdot N_o}{|\mathrm{H}|_F^2 \, \overline{P}_b^{\,1/M_t}} \left(\frac{4\pi}{\lambda}\right)^2 \frac{U_{link} N_F d^{\kappa}}{G_t G_r} + \frac{Pc}{Rb} \tag{J.12}$$

For higher order signaling, e.g., M-arry signaling (16-QAM is used in this paper), the error probability [2] is given by:

$$\overline{P}_b \approx \varepsilon_H \left(\frac{4}{b}(1 - 1/2^{b/2}) Q\left(\sqrt{\frac{3b}{M-1}\gamma_b}\right)\right) \tag{J.13}$$

Where $M = 2^b$ and b is the constellation size. M-arry signaling has better data rate than BPSK within a same bandwidth, and such ratio is represented by the constellation size b. Error probability (J.13) can be approximated as following under chernoff bound.

$$\overline{P}_b \leq \frac{4}{b}(1 - 1/2^{b/2}) \left(\frac{3\overline{E}_b b \, |\mathrm{H}|_F^2}{2M_t \cdot N_o (2^b - 1)}\right)^{-M_t} \tag{J.14}$$

And the required energy per bit for M-arry signaling with constellation size b is given by:

$$\overline{E}_b \geq \frac{2}{3}\left(\frac{4\left(1 - 1/2^{b/2}\right)}{b\overline{P}_b}\right)^{1/M_t} \frac{M_t \cdot N_o}{|\mathrm{H}|_F^2} \frac{(2^b - 1)}{b} \tag{J.15}$$

Thus the energy per bit of the M-arry signaling system within same bandwidth as BPSK can be derived as:

$$E_{bt} = \frac{2M_t N_o (1+\alpha) U_{link} N_F d^{\kappa} 4^2 \pi^2}{3 \, |\mathrm{H}|_F^2 \, (2^b - 1)^{-1} b^{1/M_t} G_t G_r \lambda^2} \left(\frac{4}{\overline{P}_b}\right)^{\frac{1}{M_t}} + \frac{Pc}{b \cdot Rb} \tag{J.16}$$

Where an assumption is made as $\left(1 - 1/2^{b/2}\right) \simeq 1$. From (J.4),(J.12),(J.16) It can be concluded that, for a fixed amount of data, the circuit power consumption can be reduced by a scheme with better data rate; the transmission power consumption per bit is independent of data rate but depends on the error probability; for higher signaling,

the error probability is different from that of a lower constellation. The energy efficiency of the single RF MIMO is modeled as following: Only one RF amplifier is used while the channel matrix H is considered as the same as that in conventional MIMO. The Circuit power consumption P_C only considers one mixer, one frequency synthesizer is used at transmitter.

3.3 Energy efficiency Comparison

An energy efficiency comparison between conventional SISO transmission and single RF MIMO is given with the aforementioned assumptions. The system parameters are defined as following: The channel fading factor κ is assumed to be 2, the carrier frequency of the sensor network is 2.5GHz (which is also the ESPAR antenna center frequency), the antenna gain on the SISO radio link with conventional architecture is given by G_t=3dBi and G_r=3dBi, for ESPAR antenna G_t=2.5dBi, for conventional MOMO, the channel matrix H is considered as 2×2 with diversity order of 4. M_t is considered to be 2 and M_r is considered as 2, $U_{link} = 40dB$, $NF = 10dB$, $N_0 = -174dBm/Hz$, the system bandwidth is considered as 10KHz, where for BPSK signaling, the data rate is R_b=10Kb/s, for 16-QAM, the data rate is considered as $4\times R_b$.

The circuit power consumption model is based on the parameters mentioned in [1], where the mixer power is assumed to be 30mW, the frequency synthesizer is considered as 50mW, the low noise amplifier is considered as 20mW. the drain efficiency η of power amplifier is conspired as 0.35, the analog to digital converter and digital to analog converter is considered 10mw and 12mw respectively.

An indicative comparison is given in Figure J.6, where the minimal required energy per bit to reach error probability of $P_b = 10^{-3}$ is plotted over the transmission distance. It indicates that, by using QAM modulation with MIMO, the power efficiency is better than the conventional BPSK in SISO with distance less than 20 meters (which is a reasonable distance for inter-sensor communication), while using sinlge RF MIMO transmission with higher order constellation, e.g., 16-QAM as mentioned in this paper, the required energy per bit is further reduced.

4 Conclusion

Energy efficiency influences the lifetime of the wireless sensor network, while most of the energy in WSN is consumed by the radio link as well as circuit cost. With the help of spatial multiplexing, a better efficiency can be achieved. However, it is not easy to implement conventional MIMO on a sensor node, thus single RF MIMO transmission with 16-QAM signaling is proposed in this paper, which uses an ESPAR antenna with 2 elements spaced by $\lambda/16$ on the sensor node. A detailed energy analysis and indicative system performance evaluation is given. It shows that the proposed architecture has a

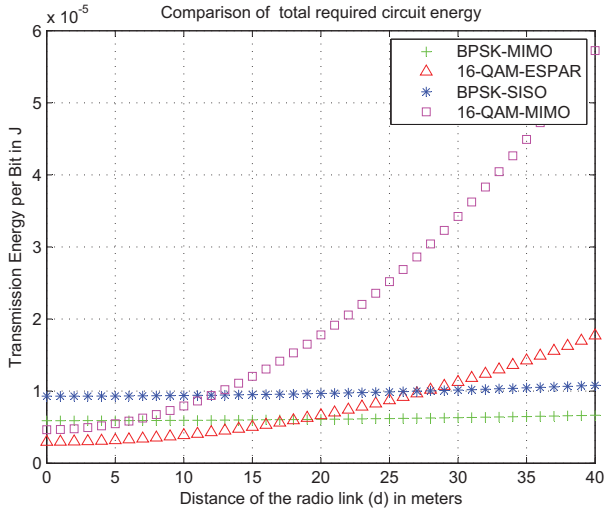

Fig. J.6: Comparison of minimal required energy.

better energy efficiency than the conventional MIMO; for the inter-sensor distance less than 20 meters, it requires less energy than other signaling.

References

[1] S. Cui, A.J. Goldsmith, A. Bahai, "Energy efficiency of MIMO and cooperative MIMO techniques in sensor networks," *IEEE Journal on Selected Areas in Communications*, vol. 22, pp. 1089–1098, 2004.

[2] S.K. Jayaweera, "Virtual MIMO based cooperative communication for energy-constrained wireless sensor networks," *IEEE Transactions on Wireless Communications*, vol. 5, pp. 984–989, 2006.

[3] O.N. Alrabadi, C.B. Papadias, A. Kalis, R. Prasad, "A universal encoding scheme for MIMO transmission using a single active element for PSK modulation schemes," *IEEE Transactions on Wireless Communications*, vol. 8, pp. 5133–5143, 2009.

[4] V.I. Barousis, A.G. Kanatas, A. Kalis, "Beamspace domain analysis of single RF front-end MIMO systems," *IEEE Transactions on Vehicular Technology*, vol. 60, pp. 1195–1199, 2011.

[5] B. Han, V.I. Barousis, A. Kalis, A.G. Kanatas, "Active parasitic arrays for low cost compact MIMO transmitters," *IEEE 5th European Conference on Antennas and Propagation (EUCAP)*, vol. 1, pp. 3663–3667, 2011.

[6] E.P. Tsakalaki, O.N. Alrabadi, A. Kalis, C.B. Papadias, R. Prasad, "Non cooperative space-time communication for energy efficiency in sensor networks," *IEEE Transactions on Communications*, vol. 60, pp. 48–54, 2012.

Paper K

MIMO over ESPAR with 16-QAM Modulation

B. Han, V.I. Barousis, C.B. Papadias, A. Kalis, R. Prasad

The paper has been published in the
IEEE Wireless Communication Letters, DOI 10.1109/WCL.2013.13.130433, 2013.

The layout has been revised.

Abstract

MIMO systems have become an indispensable part of modern wireless standards, e.g. LTE advanced. However, in applications with strict energy and size constraints, an alternative MIMO scheme with reduced hardware complexity would be attractive. Towards this direction, parasitic antennas with a single feeding port have been proposed to emulate MIMO transmission with PSK signaling. In order to support higher order constellations, this letter presents a smart loading scheme that enables the multiplexing of two 16-QAM signals over the air. Accompanying simulations show that this can be achieved by using a single feeding port and parasitic antennas.

1 Introduction

MIMO systems have been widely known as a promising technology that offers significant spectral efficiency gains. When the capacity of modern communications is concerned, the sum rate scaling of down-link in the broadcast channel can be attained by having M antenna elements at the base station, even with a single antenna at the mobile terminals [1] [2]. But even in the case of a base station, e.g. an access point in an indoor environment, its compact size and hardware complexity should be seriously considered. For these reasons, there has been some recent interest on using Electronically Steerable Parasitic Array Radiators (ESPAR), as they provide high beamforming capabilities [3] as well as compact size [4] [5]. Meanwhile, by switching parasitic loads [6] [7], the ESPAR is also considered for spatial multiplexing and MIMO emulation [8], [9] with significantly reduced hardware complexity [10]. Indeed, a proof-of-concept experiment in an indoor environment [11] shows that spatial multiplexing over the air is possible with a single RF chain and parasitic antennas. But there are some limitations on previous solutions for MIMO transmission, e.g. still there's still no universal solution that is able to encode signals of an arbitrary constellation. This stems from the fact that commonly imaginary parasitic loads have been assumed, which limit the beam-shaping capabilities of ESPAR antennas and eventually an arbitrary beam-shaping is not possible.

With the aforementioned problems, we suggest in this paper to waive the constraint of imaginary parasitic loadings and propose an advanced *complex* loading architecture that enables the aerial multiplexing of two 16-QAM signals with a single RF chain and parasitic antennas. Recent progress in [12] shows that a fixed negative real, i.e. ohmic, part could aid towards this direction. Without loss of generality, the proposed architecture is built on a planar and linear ESPAR antenna with 2 elements, i.e. one active and one parasitic, and with inter-element spacing of $\lambda/8$ (where λ is the wavelength). It is understood that the proposed design approach can be scaled-up to more complex ESPAR geometries and more complex signaling formats.

The rest of the paper is organized as follows: Section II gives a theoretical framework

of the pattern-shaping mechanism of ESPAR for MIMO transmission. Sections III and IV propose an appropriate novel design that implements the *complex* parasitic loading. Section V verifies the proposed analysis and provides indicative performance results.

2 Theoretical Framework

Single RF MIMO is implemented with one active antenna element and several closely placed parasitic elements that are connected to variable loadings [10]. By appropriately adjusting the value of parasitic loads, the current distribution across the elements changes and therefore the radiation pattern can be controlled. Based on this fundamental principle, single RF MIMO with ESPARs obey the following rule; *Instead of driving data streams to different active antenna elements as in the conventional case, the signals modulate orthogonal aerial modes of the ESPAR's pattern.* This can be viewed as encoding different symbols to a single transmit pattern [8] and results in an effective spatial multiplexing emulated at the beamspace domain. The azimuthal pattern of an arbitrary ESPAR with M-1 parasitic elements can be decomposed as [8]:

$$P(\varphi) = \sum_{n=0}^{M-1} w_n \Phi_n(\varphi) \tag{K.1}$$

where in this case M=2 and $\{w_n\}_{n=0}^{M-1}$ represent the complex symbols for transmission that modulate a set of orthonormal modes $\{\Phi_n(\varphi)\}_{n=0}^{M-1}$ given by [8]

$$\begin{aligned} \Phi_0(\varphi) &= 1/k_0 \\ \Phi_1(\varphi) &= \left[e^{jb\cos\varphi} - 2\pi I_0(jb)/k_0^2\right]/k_1 \end{aligned} \tag{K.2}$$

where $b = 2\pi d$ and d is the inter-element distance normalized to wavelength, while $I_0(jb)$ is the zero-th order modified Bessel function of the first kind. It holds that $\int_0^{2\pi} \Phi_0(\varphi)\,\Phi_1^*(\varphi)\,d\varphi = 0$ and the modes remain orthogonal as long as there exists a reasonable amount of scattering, i.e. an adequate number of different propagation paths. As it has been validated in a proof-of-concept experiment of single RF MIMO [11], such conditions are met in a typical indoor environment. Therefore, the ESPAR modes in (K.2) will likely fall into independent fading. The single RF MIMO paradigm is illustrated in Figure K.1, where the ESPAR elements are separated by $\lambda/8$, the active port is connected to the sole RF chain and the parasitic element is connected to the tunable load [13]. The transmitting signals are mapped onto the basis patterns $\Phi_0(\phi)$ and $\Phi_1(\phi)$. By using a conventional MIMO receiver the baseband signals can be retrieved successfully. Based on [8], the weighting coefficients in (K.1) are expressed as:

$$\begin{aligned} w_0 &= i_0 k_0 + 2\pi i_1 I_0(jb)/k_0 \\ w_1 &= i_1 k_1 \end{aligned} \tag{K.3}$$

where k_0 and k_1 are given by:

$$\begin{aligned} k_0 &= \sqrt{2\pi} \\ k_1 &= \sqrt{2\pi + \left(\pi/k_0^2 - 1\right) 8\pi^2 I_0^2\left(jb\right)/k_0^2} \end{aligned} \tag{K.4}$$

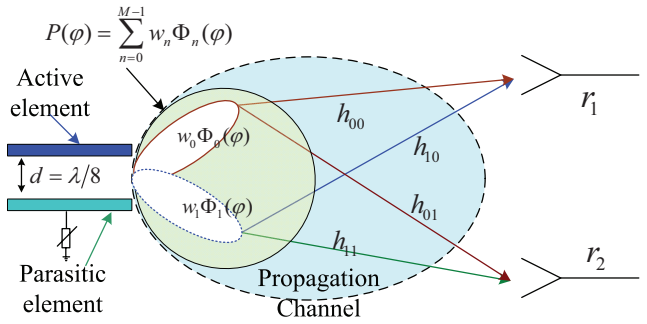

Fig. K.1: The proposed concept of MIMO over ESPAR antenna.

The currents as seen from the antenna ports are given by:

$$\mathbf{i} = (\mathbf{Z} + \mathbf{X})^{-1}\mathbf{v} \tag{K.5}$$

where $\mathbf{Z}$ is the antenna coupling matrix [10], $\mathbf{X}$ is a diagonal matrix with the loading values at the main diagonal, and $\mathbf{v} = \left[\begin{array}{cccc} v_s & 0 & \ldots & 0 \end{array}\right]^T$. For $M = 2$, (K.2) can be expanded as

$$\left(\left[\begin{array}{cc} Z_{11} & Z_{12} \\ Z_{21} & Z_{22} \end{array}\right] + \left[\begin{array}{cc} 50 & 0 \\ 0 & x_1 \end{array}\right]\right)\left[i_0 \;\; i_1\right]^T = \left[v_s \;\; 0\right]^T \tag{K.6}$$

where 50 Ω is assumed to be the load on the active port (Port 1) and x_1 is the parasitic load. Due to the reciprocity theorem $Z_{21} = Z_{12}$. The load value x_1 is obtained by (K.6) as:

$$x_1 = -\left(\frac{i_0}{i_1}\mathrm{Z}_{21} + \mathrm{Z}_{22}\right) \tag{K.7}$$

Combining (K.7) and (K.3) the loading value becomes:

$$x_1 = -\left(\left[\frac{w_0}{w_1} - \frac{2\pi I_0(jb)}{k_0 k_1}\right]\frac{k_1}{k_0}Z_{21} + Z_{22}\right) \tag{K.8}$$

3 16-QAM Multiplexing with ESPAR antennas

The proposed loading architecture of the ESPAR antenna is illustrated in Figure K.2. As it will be shown, this architecture provides the appropriate complex loading that enables the ESPAR antenna to multiplex successfully over the air a signal vector $[w_0\ w_1]^T$ emerging from a 16-QAM constellation. According to Figure K.2 the signal w_0

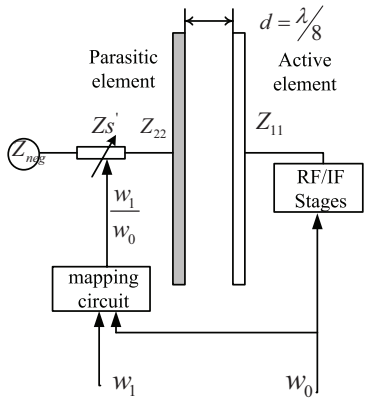

Fig. K.2: Architecture of the ESPAR antenna with 2 elements.

is driven directly to the sole RF chain, while as indicated in (K.8) the loading values are determined by the ratio of the transmitted symbols, i.e. w_1/w_0. Assuming a 16-QAM constellation with Gray mapping, there are totally 256 possible symbol vectors $[w_0\ w_1]^T$, but due to symmetry only 64 loading values are required. Indicatively, 16 out of 64 loads are shown in Table K.1, as computed by (K.8) for an ESPAR antenna simulated in IE3D design software. The coupling matrix as obtained by IE3D is given by:

$$\begin{bmatrix} Z_{11} & Z_{12} \\ Z_{21} & Z_{22} \end{bmatrix} = \begin{bmatrix} 52.81 - j11.09 & 40.27 - j20.75 \\ 40.27 - j20.75 & 52.81 - j11.09 \end{bmatrix} \tag{K.9}$$

As shown in Table I, the values of both the real and imaginary part could be positive or negative. The required imaginary values can be implemented by a passive circuit with lumped elements, while the negative values on the real part by an active circuit, e.g. with a cross-coupling technique and CMOS transistors [12]. In this paper, the proposed design is composed by an active circuit similar as in [12] with a fixed negative impedance value, cascaded by a controllable passive impedance array. Thus the loading circuit can be controlled both on real part and imaginary part.

Table K.1: THE FIRST 16 SYMBOLS FOR 16-QAM SINGLE RF MIMO

Symbols Pairs $[w_0 w_1] = [a_n b_m]$	Symbol $w_0 = a_n$	Symbol $w_1 = b_n$	Load(Ω) Real	Load(Ω) Imaginary
$a_1 b_0$	-1+3j	-3+3j	-39.62	-4.29
$a_1 b_1$	-1+3j	-3+1j	-37.32	-19.13
$a_1 b_2$	-1+3j	-3-1j	-18.13	-25.27
$a_1 b_3$	-1+3j	-3-3j	-7.63	-14.52
$a_1 b_4$	-1+3j	-1+3j	-50.37	6.195
$a_1 b_5$	-1+3j	-1+1j	-81.84	-26.04
$a_1 b_6$	-1+3j	-1-1j	14.11	-56.74
$a_1 b_7$	-1+3j	-1-3j	7.20	12.22
$a_1 b_8$	-1+3j	1+3j	-44.23	25.38
$a_1 b_9$	-1+3j	1+1j	-51.14	69.90
$a_1 b_{10}$	-1+3j	1-1j	44.80	39.21
$a_1 b_{11}$	-1+3j	1-3j	13.34	6.97
$a_1 b_{12}$	-1+3j	3+3j	-29.40	27.69
$a_1 b_{13}$	-1+3j	3+1j	-18.90	38.44
$a_1 b_{14}$	-1+3j	3-1j	0.29	32.29
$a_1 b_{15}$	-1+3j	3-3j	2.60	17.46

4 Switching Among The Loading Values

4.1 Loading Switching

The negative impedance circuit as given in [12] produces a fixed load value with -133.7-j97.6 Ω. The required load in Table K.1 ranges around (-81∼+45)+j(-56∼+69)Ω. Therefore, a load switching stage is necessary to transfer the fixed impedance of the active CMOS circuit to the desired parasitic loading (e.g. those in Table K.1). A proposed solution for this purpose is the switching stage shown in Figure K.3 that is shown to be connected between the negative resistance circuit and the parasitic antenna element (see Figure K.2). Instead of using one analog tunable load, 64 loading pairs with discrete values are used, each of them corresponding to a specific load (i.e. pattern). Thus an 8×8 array contains 64 complex loading cells, where each cell contains a resistor and an inductor. The array in Figure K.3 is controlled by the vertical and horizontal vectors, which are made by two 3-to-8 converters. In this design, only 4 control bits are required to select one out of the 64 values. C_0 is used for selection of the vertical and horizontal converter, while $C_1 \dots C_3$ is used for address-searching of the desired load position in the array. For example, when $C_0 = 0$ the vertical converter $A_0 \dots A_7$ is selected and if $C_1 \dots C_3 = 010$ the value a_1 is returned. Similarly, when $C_0 = 1$, the horizontal

converter $B_0 \dots B_7$ is selected and for $C_1 \dots C_3 = 101$ the value of b_5 is returned. Thus, the symbol vector $\begin{bmatrix} w_0 & w_1 \end{bmatrix}^T = \begin{bmatrix} a_1 & b_5 \end{bmatrix}^T$ is selected that corresponds to a loading of -81.84-j26.04 Ω (see Table K.1). According to the calculation with pure load

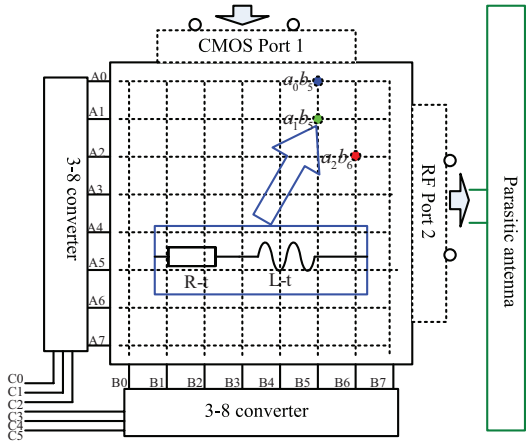

Fig. K.3: The digital controllable impedance switching circuit block.

concern and tuning simulation with high frequency concern, the corresponding resistor and inductor values inside the tuning cell in Figure K.3 are 48.5 Ω and 5.82 nH respectively. These values correspond to the impedance that adjusts the fixed impedance of the CMOS circuit to the required parasitic loading. However, due to non-idealities risen up at high frequencies, the lumped elements suffer from additional parasitic effects that typically cause a small shift at the ideal, i.e. desired, impedance value [14] on the order of ±2 Ohms. This has been validated also in ADS microwave design software. However, it should be emphasized that a de-embedding technique (e.g. [15]) can deal with such effects by taking their impact into account a priori. Hence, it is understood that the treatment of the parasitic effects, at least to some extent, is a matter of implementation.

4.2 Return loss of the ESPAR Antenna

As has been illustrated in Figure K.2, at each signaling period the loading value at the parasitic element is determined by the symbol vector for transmission (see also (K.8)). Since the ESPAR's input impedance depends on the parasitic loading [16], it means that it is a function of the symbol vector and therefore it will change over time resulting in mismatch effects. Those effects are captured by the return loss that represents the reflection coefficient of the antenna array [16]. For all the required 64 loading states the

return loss is found to be always below -12dB at 2.5 GHz, which is acceptable. Figure K.4 gives the return loss as a function of the frequency for the first 16 loading values, as obtained by the IE3D software.

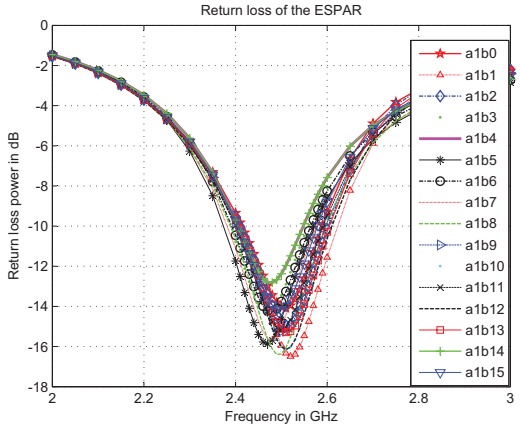

Fig. K.4: Indicative return loss curves of the designed ESPAR antenna.

5 Performance Evaluation

A system evaluation of the proposed architecture is given by comparing its bit error rate performance against the one of a conventional MIMO transmitter. In both cases a Rayleigh fading channel is considered and conventional zero-forcing MIMO receiver with two uncorrelated omnidirectional antennas is assumed. Following a similar approach as in [10] and [8], it can be verified that a MIMO system with an ESPAR transmitter and a conventional receiver can be described by the convenient system equation $\mathbf{y} = \mathbf{H}\mathbf{w} + \mathbf{n}$, where $\mathbf{y}$ is the received signal vector, $\mathbf{w}$ is a vector that holds the coefficients in (K.1), i.e. the signals for transmission and $\mathbf{n}$ is the Gaussian noise. The h_{mn}-th entry of the channel matrix $\mathbf{H}$ represents the complex gain between the n-th transmitted orthonormal mode $\Phi_n(\varphi)$ and the m-th received antenna element.

Knowledge of $\mathbf{H}$ can be obtained by a two-slot training period, where at the n-th slot the ESPAR applies its n-th mode and the receiver estimates the n-th row of $\mathbf{H}$. In transmission mode, given the symbol vector $\mathbf{w}$, (K.8) gives the corresponding loading value that in turn generates the required radiation pattern $P(\varphi)$ in (K.1). It is noted that a loading deviation would reflect to a radiation pattern $P_e(\varphi) = P(\varphi) + E(\varphi)$,

where $E(\varphi)$ models the error due to the load deviation. In this case

$$\begin{aligned}\hat{w}_m = \int_0^{2\pi} P_e(\varphi)\,\Phi_m^*(\varphi)\,d\varphi = \int_0^{2\pi} P(\varphi)\,\Phi_m^*(\varphi)\,d\varphi \\ + \int_0^{2\pi} E(\varphi)\,\Phi_m^*(\varphi)\,d\varphi = w_m + \varepsilon\end{aligned} \tag{K.10}$$

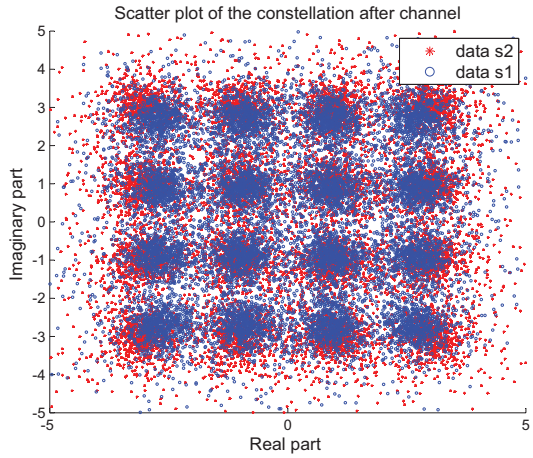

Fig. K.5: Scattering plot of the 16-QAM symbols after channel.

Therefore, a loading deviation can be seen as an extra source of random noise. Figure K.5 shows a scatter plot of the transmitted and the recovered 16-QAM signals, after influenced by a Rayleigh channel with E_b/N_o=10dB. Figure K.6 indicates that the performance of the single RF MIMO, using the exact loading values, is equivalent to the one obtained by conventional MIMO transmission. A non-ideal case would experience additional non-idealities that have been modeled as a random loading perturbation of $\pm 2\Omega$ in both the real and imaginary part of the loading values. As it is shown, the performance of the proposed architecture remains robust within a reasonable SNR range where the majority of the cellular networks [2] are used to operate in. Reasonably, at high SNR regime, the effect described in (K.10) dominates and this justifies a high SNR plateau. Again, it is mentioned that load shifts due to possible imperfections can be absorbed by proper calibration. Based on the results, instead of a conventional and power-hungry MIMO transmitter that requires two separate RF chains, a comparable performance is achieved with reduced hardware complexity, i.e. with a sole RF chain and compact ESPAR antennas. Instead of assigning different signals to the diverse

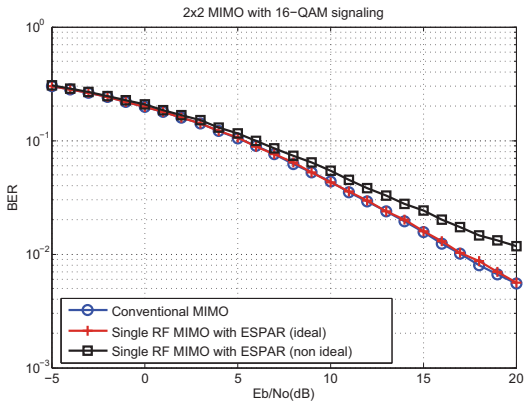

Fig. K.6: Bit error performance of the proposed system.

transmit elements, this is achieved by forming a single pattern as explained in detail in [8]- [13] and also illustrated in Figure K.1.

6 Conclusion

Motivated by the continuously increasing demand for high spectral efficiency and compactness, this letter proposes a novel loading scheme that enables ESPAR antennas to multiplex QAM signals over the air by encoding them to a single beam pattern. Unlike its conventional counterparts with increased hardware complexity, the proposed approach requires only a sole RF chain and it takes advantage of the parasitic elements that are placed in close vicinity with the active one. The evaluation results are very promising, as they draw a satisfactory performance of the proposed single RF MIMO scheme, as compared against the well-known traditional architecture.

References

[1] G. Caire, S. Shamai, "On the achievable throughput of a multiantenna gaussian broadcast channel," *IEEE Transactions on Information Theory*, vol. 49, pp. 1691–1706, 2003.

[2] H. Huang, C. B. Papadias, S. Venkatesan, *MIMO Communication for Cellular Networks*, Springer Science, Ed. Springer, 2012.

[3] C. Sun, A. Hirata, T. Ohira, N.C. Karmarkar, "Fast beamforming of electronically steerable parasitic array radiator antennas: theory and experiment," *IEEE Transactions on Antennas and Propagation*, vol. 52, pp. 1819–1832, 2004.

[4] S. Ebadi, G. Xun, "A microstrip patch electronically steerable parasitic array radiator (ESPAR) antenna with reactance-tuned coupling and maintained resonance," *IEEE Transactions on Antennas and Propagation*, vol. 60, pp. 1803–1813, 2012.

[5] D. Ireland, R. Schlub, "Dielectric embedded ESPAR (DE-ESPAR) antenna array for wireless communications," *IEEE Transactions on Antennas and Propagation*, vol. 53, pp. 2437–2443, 2005.

[6] A. Kalis, A. G. Kanatas, C. B. Papadias, Ed., *Parasitic Antenna Arrays for Wireless MIMO Systems*. Springer, 2013.

[7] Md.R.Islam, M. Ali, "Switched parasitic body-worn array for high data rate wireless applications," *IEEE Antenna and Wireless Propagation Letters*, vol. 11, pp. 693–696, 2012.

[8] V.I. Barousis, A.G. Kanatas, A. Kalis, "Beamspace domain analysis of single RF front-end MIMO systems," *IEEE Transactions on Vehicular Technology*, vol. 60, pp. 1195–1199, 2011.

[9] O.N. Alrabadi, J. Perruisseau-Carrier, A. Kalis, "MIMO transmission using a single RF source: theory and antenna design," *IEEE Transactions on Antennas and Propagation*, vol. 60, pp. 654–664, 2012.

[10] A. Kalis, A.G. Kanatas, C.B. Papadias, "A Novel approach to MIMO transmission using a single RF front end," *IEEE Journal on Selected Areas in Communications*, vol. 26, pp. 972–980, 2008.

[11] O.N. Alrabadi, C.Divarathne, P. Tragas, A. Kalis, N.Marchetti, C.B. Papadias, R. Prasad, "Spatial multiplexing with a single radio: proof of concept experiments in and Indoor enviroment with a 2.6GHz prototype," *IEEE Communications Letters*, vol. 15, pp. 178–180, 2011.

[12] B. Han, V.I. Barousis, A. Kalis, A.G. Kanatas, "Active parasitic arrays for low cost compact MIMO transmitters," *IEEE 5th European Conference on Antennas and Propagation (EUCAP)*, vol. 1, pp. 3663–3667, 2011.

[13] O.N. Alrabadi, C.B. Papadias, A. Kalis, R. Prasad, "A universal encoding scheme for MIMO transmission using a single active element for PSK modulation schemes," *IEEE Transactions on Wireless Communications*, vol. 8, pp. 5133–5143, 2009.

[14] C. Bowick, J. Blyer, C. Ajluni, *RF Circuit Design.* Newnes Elsevier, 2008.

[15] T. Hirano, J. Hirokawa, M. Ando, H. Nakano, Y. Hirachi, "Demembeding of lumped -element chractersitcs with the aid of EM analysis," *IEEE Antenna and Propagation Society Internation Symposium*, vol. 1, pp. 1–4, 2008.

[16] C. Balanis, *Antenna Theory, Analysis and Design.* Wiley, 2005.

Paper L

A single RF MIMO Loading Network for High Order Modulation Schemes

B.Han, V.I.Barousis, A.Kalis, C.B. Papadias, A.G.Kanatas, R. Prasad

The paper is to appear in the
International Journal of Antenna and Propagation, Hindawi , 2013.

The layout has been revised.

Abstract

MIMO systems have been established as a promising technology for achieving high data rates and reliable communications over the wireless channel. However, the hardware complexity and size requirements of such systems have become the main limiting factors that hinder their wide integration in portable terminals. To deal with this problem, a novel MIMO transmitter architecture with just a single radio frequency (RF) chain has recently been introduced that is built on parasitic antenna arrays. Under this perspective, MIMO transmission is achieved by shaping directly the radiation pattern with the aid of analog tunable loads. Recently, it has been shown that a such single RF MIMO architecture is able to support all PSK modulation formats. Motivated by the remarkable benefits of MIMO technology and the low cost and implementation complexity of this alternative architecture, this paper extends its capabilities and proposes a novel loading circuit architecture for parasitic antennas that will permit them to support MIMO transmission with more complex signaling, i.e. QAM and a single RF chain

1 Introduction

The continuously increasing demand for high data rates and reliable communications usually requires a large bandwidth, which has become more and more precious, thus spatial multiplexing has drawn attentions for the reason of better spectrum efficiency, and Multiple input and Multiple Output Techniques can also benefit with larger capacity and better fading mitigation. However, it is composed of considerable hardware complexity, as well as the large antenna spaces in the conventional MIMO architectures, Thus it is not an ideal solution for mobile devices.

A variety of techniques have already dealt with the afore-mentioned problems. The antenna selection techniques have the beamforming ability which select a subset [1] [2] of appropriate antenna elements to be connected to the radio frequency (RF) chains [3] [4], actually forms certain beam towards the desired direction [5]. Although these techniques lead to some complexity savings , they often cause significant performance degradation as compared to the conventional MIMO systems. Alternatively, antenna sub-array formation techniques are applied mainly to the receiver side and are based on the fundamental idea that every RF chain is fed with a linear combination of an appropriate subset of the available antenna elements [6] [7] . Commonly, these approaches cope with the problem of implementation complexity algorithmically, by activating appropriate antenna elements based on their responses. Another popular approach lies on the investigation of novel multi-element antenna con-figurations with strict size constraints [8].

An alternative perspective on MIMO technology, on which this paper focuses, was recently introduced [9] [10]. This architecture is able to provide compact MIMO transceivers

with a single RF port and is known as single RF MIMO [11]. Instead of the conventional trend of using arrays with multiple active elements, the proposed scheme is built on parasitic antenna arrays with a single active, i.e. single feeding port. Such antennas consist of an active element surrounded with multiple parasitic in close proximity and are known as Electronically Steerable Parasitic Antenna Radiators (ESPARs) [12] [13]. Due to the strong mutual electromagnetic coupling among all elements, the active elements feeding induces strong currents to all parasitic. In this way, all parasitic participate to the radiation mechanism affecting the shape of the radiation pattern. Further current control, which in turn means beam-shape control, is possible with low cost tunable load circuits attached to all parasitic. Tuning those circuits, henceforth called loads, the effective coupling among all neighbor elements changes, causing a corresponding change at all currents and consequently at the radiation pattern:

$$P(\theta,\varphi) = \mathbf{i}^T \mathbf{a}(\theta,\varphi) = \sum_{n=0}^{M-1} i_n a_n(\theta,\varphi) \tag{L.1}$$

In (L.1), M is the number of ESPAR elements and $\mathbf{a}(\theta,\varphi)$ is the steering vector of the array. The $(1 \times M)$ current vector $\mathbf{i}$ is given by:

$$\mathbf{i} = u_s(\mathbf{Z} + \mathbf{X})^{-1}\mathbf{v} \tag{L.2}$$

where $\mathbf{Z}$ is the $(M \times M)$ electromagnetic coupling matrix of the ESPAR antenna, $\mathbf{X} = diag\begin{bmatrix} R_s & jx_1 & \cdots & jx_{M-1} \end{bmatrix}$ is the load diagonal matrix that adjusts the radiation pattern, R_s is the antenna termination impedance, while $v = \begin{bmatrix} 1 & 0 & 0 & \cdots \end{bmatrix}^T$ is a $(M \times 1)$ vector and is the feeding signal to the active port.

It should be strongly noted that in applications with quite strict size constraints, e.g. mobile devices, single RF MIMO often achieve even higher capacity performance as compared to their conventional counterparts [14] [15]. Therefore it is evident that single RF MIMO is a novel and promising technology, able to bring the MIMO benefits to mobile devices without significant hardware burden [16]. A proof-of-concept experiment of this architecture can be found in [17] [18]. According to all references on this topic listed above, the breakthrough of this approach is that multiplexing with a single RF port is achieved by encoding multiple symbols to a single radiation pattern $P(\theta,\varphi)$ as described in Section II.

Although it has been shown (both theoretically and experimentally) that MIMO is possible with a single RF port, a challenging and persisting problem concerns the design of novel and low cost load circuits for the appropriate tuning of the parasitic elements. This affects the beam shaping abilities of ESPAR antennas and by large dictates their capability to sup-port demanding modulation schemes. Moving towards that direction, the authors in [19] investigate an efficient methodology to enable 16-PSK transmission using loading circuits built on varactor diodes. Those components, commonly used in ESPAR antenna designs, constitute a kind of electronic diodes whose bias voltage

controls their capacitance. Therefore, they provide a tunable pure imaginary load to the parasitic. Clearly, due to the advent of 3G and 4G communications, the extension to higher modulation schemes is of great interest and requires a sophisticated design of the loading circuit, since intuitively the required radiation patterns that *carry* the symbols for transmission become more demanding.

This is the main objective of this paper. The challenging problem of enabling ESPAR antennas to multiplex high order modulated signals (e.g. QAM) over the air, imposes the design of more sophisticated circuits that provide complex loading with positive or negative real part. This in turn extends the capabilities of parasitic antennas, and enables them to produce the required patterns, according to the single RF MIMO concept. We demonstrate the advanced capabilities of our approach using a simple 2-element ESPAR antenna with one active and one parasitic element connected to the novel loading circuit in order to multiplex multiple symbols emerging from a 16-QAM constellation on a single set of indicative radiation patterns.

This paper is organized as follows: Section 1 provides a brief description of the radiation characteristics of ESPAR antennas at the beamspace domain. This modeling approach is crucial in mapping the different symbol vectors for transmission onto a single radiation pattern and finally to the appropriate loading values. Section 2 describes the design of an active circuit that provides a voltage controlled negative resistance. As shown, the dynamic range of this resistance is indicated by the possible symbol combinations and the modulation format. Section 3 presents the load-switching and control concept and simulated results on the achievable bit-error probability of a communication link utilizing the proposed architecture. Due to the imperfection of the practical components, the comparison between theoretical values and practical values is given in Section 4.

2 Beam Space Domain Representation of ESPAR Antennas

2.1 A Brief Review

It is understood that in contrast to conventional multiport antenna arrays, ESPAR antennas do not offer spatial degrees of freedom (DoFs) due to the existence of a single active element. Thus, the conventional way of assigning multiple transmit symbols to different active elements is not applicable and at first glance MIMO communication is not possible. However, thanks to the tunable parasitic and the consequent beamforming abilities of ESPAR antennas, the symbols for transmission can be encoded directly on a single radiation pattern. This functionality can be viewed clearly through the beamspace representation of ESPAR antennas, as explained in detail in [14] [15]. In particular, the beamspace domain of an antenna array can be seen as a signal space where any

radiation pattern of the antenna can be represented by a point, or equivalently a vector, within that space. This space is defined by the number of orthonormal functions that constitute the aerial degrees of freedom (ADoFs). To reflect their physical meaning, these orthonormal functions are known as basis patterns. Following [16] and, without loss of generality, considering propagation over the azimuth plane, i.e. $\theta = \pi/2$, the radiation pattern of an ESPAR antenna with M elements, including the active one, is expressed as a linear combination of M basis patterns as:

$$P(\varphi) = \sum_{n=0}^{M-1} w_n \Phi_n(\varphi) \tag{L.3}$$

It has been shown that the shape of all basis patterns depends on the inter-element distance, while the coefficients w_n depend on the inter-element distance and the currents[1].

2.2 Application to an ESPAR with 2 Elements

For an ESPAR antenna with 2 elements the basis patterns are given by [16]:

$$\begin{aligned} \Phi_0(\varphi) &= 1/k_0 \\ \Phi_1(\varphi) &= \left(e^{jb\cos\varphi} - 2\pi I_0(jb)/k_0^2\right)/k_1 \end{aligned} \tag{L.4}$$

where

$$\begin{aligned} k_0 &= \sqrt{2\pi} \\ k_1 &= \sqrt{2\pi + \left(\pi/k_0^2 - 1\right) 8\pi^2 I_0^2(jb)/k_0^2} \end{aligned} \tag{L.5}$$

and the coefficients in (L.1) are given by

$$\begin{aligned} w_0 &= i_0 k_0 + 2\pi i_1 I_0(jb)/k_0 \\ w_1 &= i_1 k_1 \end{aligned} \tag{L.6}$$

where $b = 2\pi d$, d is the inter-element distance normalized to wavelength and $I_0(x)$ is the zero-th order modified Bessel function of the first kind. Equation (L.3) reveals the functionality of the single RF MIMO transmitter: Indeed, letting the coefficients w_n be the complex symbols for transmission of any signal constellation, (L.3) shows that two symbols have been attached, i.e. mapped, to different basis patterns. Thus, symbols are not driven to diverse active antenna elements as in the conventional case, but they modulate orthogonal radiation patterns. In this way, at every symbol period the shape of the transmit pattern changes according to the symbols for transmission. Although this functionality looks very similar to beamforming, indeed it is a multiplexing operation defined at the beamspace domain, since the transmit symbols are encoded to

[1] Due to electromagnetic coupling the currents are also distance-dependent

the pattern. The ESPAR receiver in turn assesses the impinging signals by switching among orthogonal patterns within a symbol period [14]. A similar single RF receiver is proposed in [11]. In this way, MIMO transmission is emulated at the beamspace domain with single RF transceivers. It is noted however, that this paper focuses on the design of the single RF transmitter and therefore the bit error probability in Section VI has been derived assuming a conventional MIMO receiver. It should be strongly noted that the number of ADoFs theo-retically is equal to the number of all elements. As mentioned in [14] and [15] however, the inter-element distance affects the effective number of ADoFs, i.e. those with significant contri-bution to the total radiated power that can practically be ex-ploited for transmission. In this paper, an ESPAR antenna with 2 elements is considered, where the inter-element distance is fixed to $d = \lambda/16$. For such an inter-element distance two ADoFs are present and beam-shaping is possible [16], which in turn means that according to (L.3) multiplexing over the air can be achieved with a single RF port.

2.3 Loads Values for All Possible Symbol Vectors

A common assumption in the literature is that usually the loads of the parasitic elements are implemented by a special kind of diode, called varactor, where its bias voltage controls the capacitance of the element. Although this is a low cost implementation approach, able to provide a large range of capacitive values, often the pure imaginary load restricts the beam-shape abilities of the ESPAR antenna, and thus the ca-pability of the antenna to produce all the necessary radiation patterns dictated by (L.3). This fact becomes particularly evident as the symbol constellation becomes more complex.

Although the use of pure imaginary loads has enabled the authors in [19] to en-code any PSK modulated symbols onto the radiation patterns of a 3-element ESPAR, imposing a higher constellation commonly used in modern wireless communica-tions, e.g. QAM, imaginary loads can no longer cope with producing the whole set of desired radiation patterns. This Section shows how the beamspace domain representation of ESPAR antennas can be used to solve this problem, and define the loading values for all possible transmit symbol vectors, emerging from a 16-QAM modulation, using complex loads. Recalling (L.3), the pattern becomes:

$$P(\varphi) = w_0 \left(\Phi_0(\varphi) + \sum_{n=1}^{M-1} \frac{w_n}{w_0} \Phi_n(\varphi) \right) \tag{L.7}$$

Equation (L.7) indeed describes the triggering operation of the transmit ESPAR antenna. The first symbol w_0 is driven to the sole RF port, while the ratio w_n/w_0 $(n = 1, ...M - 1)$ determines the shape of the pattern. Next, without loss of generality, an ESPAR antenna with $M = 2$ elements is considered. The schematic of the single RF MIMO transmitter is depicted in Fig. 1 that includes the ESPAR antenna and the

triggering unit. At each symbol period the tuning procedure maps the symbol ratio w_1/w_0 to a complex load x_1 that should be applied to the parasitic element. In this way the ESPAR is configured to the desired pattern, indicated by w_1/w_0 , and MIMO transmission is achieved as explained in Section II. According to the constellation of the 16-QAM, the combination of w_1/w_0 would result to 256 possible radiation patterns. However, due to the symmetry of the w_1/w_0 ratio, this number finally reduces to 64. The transformation of the symbols to the load values are found by expanding (2) as:

$$\left(\begin{bmatrix} Z_{11} & Z_{12} \\ Z_{21} & Z_{22} \end{bmatrix} + \begin{bmatrix} 50 & 0 \\ 0 & jx_1 \end{bmatrix} \right) \begin{bmatrix} i_0 & i_1 \end{bmatrix}^T = \begin{bmatrix} u_s & 0 \end{bmatrix}^T \tag{L.8}$$

From (L.8), and assuming $Z_{21} = Z_{12}$, we can get the required load value x_1 by

$$x_1 = -\left(\frac{i_0}{i_1} Z_{21} + Z_{22} \right) \tag{L.9}$$

According to (L.6), the above value can be rewritten as:

$$x_1 = -\left(\left[\frac{w_0}{w_1} - \frac{2\pi I_0 (jb)}{k_0 k_1} \right] \frac{k_1}{k_0} Z_{21} + Z_{22} \right) \tag{L.10}$$

where Z_{21} is mutual coupling of the two antenna elements . Applying (L.10), Table I shows indicative loading values for different transmit symbol vectors. It can be shown that the real part of the antenna load might be positive or negative. In other words, if we were to take full advantage of the parasitic array capabilities, the loading circuit controlling the parasitic antenna loads should be able to provide a complex loading, which can be realized with a novel active circuit design. In this paper we describe such a design approach, which is the subject of Section 3 and 4.

3 Complex Loads Circuit

3.1 Negative Resistance Circuit

System Level Requirement

From the aforementioned requirements, it is evident that an ESPAR antenna with 2 elements could multiplex two 16-QAM symbols given that the loading values are allowed to be complex with the real, i.e. the resistive, part ranging from negative to positive values. Apparently, this can be achieved by replacing the passive varactor-based loading unit that has been used widely so far, by a novel active circuit design. To emphasize on this novel approach, hereafter the parasitic elements will be denoted as active-loaded parasitic.

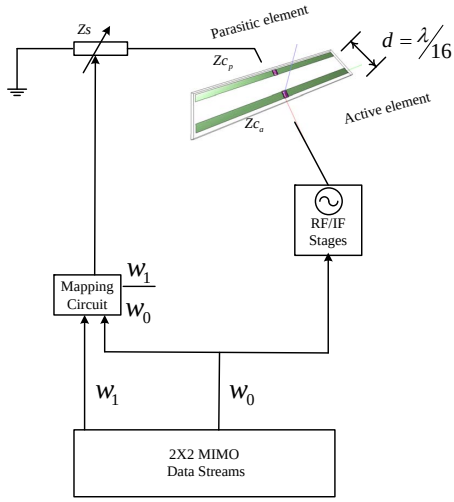

Fig. L.1: Topology of the proposed single RF MIMO Transmission system.

To the authors best knowledge, the idea of active-loaded parasitic has been first introduced in [20]. In particular, the main idea therein was to design a unit able to generate 4 negative values that are found to be appropriate for multiplexing two QPSK signals. Although in [20] along with the desired real part the proposed unit inevitably generates an imaginary component too, it has been found that this does not influence the performance, as long as the imaginary component has been designed in such a way so as to support the desired functionality in low-order constellation formats. Indeed, the imaginary component can be seen as creating a different QPSK constellation, which can be mapped to the typical one. On the contrary, as the modulation format becomes more complex the number of the required loading states increases and a similar equivalent constellation cannot be found. In particular, according to (L.3) the multiplexing of two 16-QAM symbols is translated to a set of demanding patterns that can be produced only with active-loaded parasitic. Furthermore, an equivalent constellation in this case cannot be verified easily, implying that one should be dealt with the inevitable imaginary component that comes with the desired resistive part. This paper therefore, proposes a universal transmitter architecture with ESPAR antennas, comprised of active-loaded parasitic elements and a single RF chain. It will be shown that the proposed alternative is able to multiplex high-order modulation symbol formats over the air.

To achieve that goal, we propose the architecture shown in Fig. 2. The active circuit in this figure is responsible to generate a constant negative resistance, which corresponds to the minimum value required for the given modulation scheme. To compensate the

Table L.1: Mapping of 16 symbol vectors and load values

Symbols Pairs $[w_0 w_1] = [a_n b_m]$	Symbol $w_0 = a_n$	Symbol $w_1 = b_n$	$Re(x_1)$ Ω	$Im(x_1)$ Ω
$a_1 b_0$	-1+3j	-3+3j	-23.91	-8.12
$a_1 b_1$	-1+3j	-3+1j	-27.47	-2.92
$a_1 b_2$	-1+3j	-3-1j	-23.36	4.47
$a_1 b_3$	-1+3j	-3-3j	-17.07	4.19
$a_1 b_4$	-1+3j	-1+3j	-24.18	-14.43
$a_1 b_5$	-1+3j	-1+1j	-43.07	-13.59
$a_1 b_6$	-1+3j	-1-1j	-22.54	23.35
$a_1 b_7$	-1+3j	-1-3j	-11.87	7.75
$a_1 b_8$	-1+3j	1+3j	-16.80	-18.52
$a_1 b_9$	-1+3j	1+1j	-6.12	-34.12
$a_1 b_{10}$	-1+3j	1-1j	14.40	2.82
$a_1 b_{11}$	-1+3j	1-3j	-4.48	3.65
$a_1 b_{12}$	-1+3j	3+3j	-11.60	-14.96
$a_1 b_{13}$	-1+3j	3+1j	-5.30	-15.23
$a_1 b_{14}$	-1+3j	3-1j	-1.19	-7.85
$a_1 b_{15}$	-1+3j	3-3j	-4.75	-2.64

imaginary component of the active circuit and adjust the loading to the desired complex value, a passive impedance adjusting circuit is also interpolated. In this way, the parasitic element is finally loaded with the desired complex loading value.

In our design approach we initially estimate the lower bound of the loading. It is reminded that (L.10) gives the complex load as a function of the symbol ratio w_1/w_0 and the inter-element distance d . Evaluating (L.10) for different inter-element distances and assuming 16-QAM signaling one obtains Fig. 3. In particular, for each inter-element distance all possible loading values are computed and the minimum one is plotted. As observed, for inter-element distance of $d = \lambda/16$, the minimum value of $Re(x_1)$ is found no smaller than -63.13 Ω. To provide a sense of the impact of the modulation order to the loading, Fig. 3 includes also a curve that corresponds to the 64-QAM modulation scheme. Clearly, as the modulation scheme becomes more complex, the beam-shape requirements of the ESPAR become more demanding and this is reflected to larger range of the required loading. It is noted that in this figure the mutual coupling between the two antenna elements is computed for each inter-element distance using the theoretical formula presented in chapter 8 of [21]. Although this theoretical treatment assumes ideal dipoles in free space, it still provides a representative example of the dependence of the beam-shaping requirements with the modulation order. In Section V, a realistic antenna design is assumed.

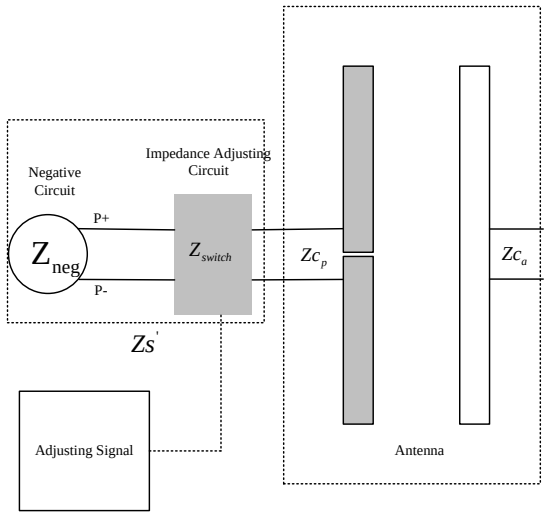

Fig. L.2: Topology of impedance control for the parasitic antenna.

The simplest way to create an active circuit with tunable impedance is by using an operational amplifier (Op-Amp), which has a large open loop gain. However, commercial op-amps or Low Noise Amplifiers (LNAs) usually provide a small open loop gain at high operating frequencies, e.g. 1.9 GHz or 2.4 GHz. Taking also into account that usually such components are power hungry; they do not meet the low-power requirements of mobile terminals. To satisfy the aforementioned constraints, subsection IV.B describes a novel circuit that is designed based on the Complementary Metal Oxide Semiconductor (CMOS) technology.

An Active Circuit Design for Generating Tunable Nega-tive Resistance

Fig.L.4 shows the schematic of the proposed active circuit. The design is based on two cross-coupled transistor pairs and a feedback loop that is established by the four capacitors. The necessity of the feedback will be explained later on. The PMOS transistors M1, M2 and the NMOS transistors M3, M4 are biased independently by voltages V_{b1}, V_{b2} respectively. The individual biasing provides not only extra design flexibility, but also improved tuning capability. The NMOS transistor M5 works as a current source and it is designed with enlarged width W and length L to reduce the flicker noise. The DC-biasing components $R_1 - R_4$ are resistors with high value to provide isolation from the circuit that set the biased voltages. The circuit is powered by V_{dd}=1.2V, which is a trend in portable applications. The tunable resistance is measured between the ports

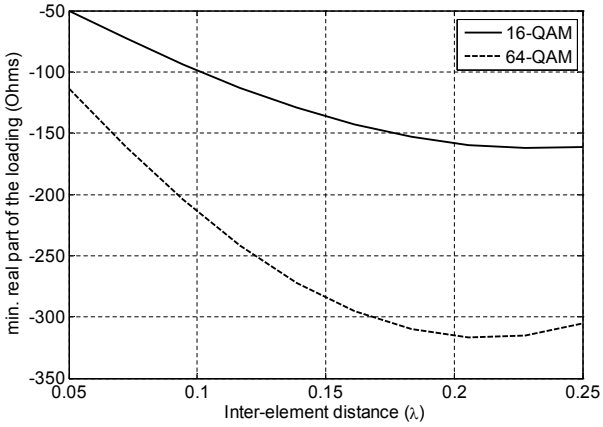

Fig. L.3: Minimum negative resistance value according to theory simulation.

$P_{ort}+$ and $P_{ort}-$ in Fig. L.4 and is given by the following equation [22]:

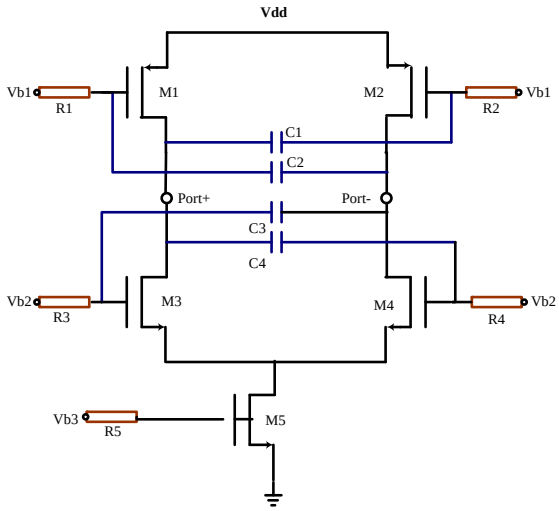

Fig. L.4: Negative resistance block using cross coupling architecture.

$$\begin{aligned} R_{neg} &= -\frac{1}{(g_{mn}+g_{mp})} = -\frac{1}{2}\frac{V_{gs}-V_{th}}{I_{ds}} \\ &= -\frac{(u_n+u_p)L}{u_n u_p C_{ox} W(V_{gs}-V_{th})} = -\frac{1}{2}\sqrt{\frac{(u_n+u_p)2n}{u_n u_p C_{ox}}\frac{L}{W}\frac{1}{I_{ds}}} \end{aligned} \tag{L.11}$$

where g_{mn}, g_{mp} are the trans-conductances of NMOS transistor and PMOS transistor respectively, expressed as

$$g_{m(n,p)} = u_{(n,p)} C_{ox} \frac{W}{L}(V_{gs} - V_{th}) = 2\frac{I_{ds}}{V_{gs} - V_{th}} \tag{L.12}$$

Moreover, $\mu_{(n,p)}C_{ox}$ is a process related coefficient, W/L is the ratio of channel width and channel length of the transistor, I_{ds} is the current flowing though the transistor, V_{gs} is the voltage between gate and source and V_{th} is the threshold voltage of the transistor. The smaller the current I_{ds}, the smaller negative resistance we get. In sub micrometer processes, the effect of the channel length should be taken into consideration and therefore [22]:

$$\begin{aligned} I_{ds} &= \frac{u_n u_p C_{ox}}{2(u_n+u_p)}\frac{W}{L}(V_{gs} - V_{th})^2(1 + \lambda_{tr} V_{ds}) \\ R_{neg} &= -\frac{(u_n+u_p)L}{u_n u_p C_{ox} W(V_{gs}-V_{th})(1+\lambda_{tr}V_{ds})} \end{aligned} \tag{L.13}$$

where the λ_{tr} is coefficient related to the effect of the channel length, and V_{ds} is the voltage between the source and drain of the transistor.

Simulated Negative Resistance Values

Based on the aforementioned theoretical analysis, we set the size of the transistors M1 and M2 to $W/L = 10/0.18$. Regarding the transistors M3 and M4 this value is set to $W/L = 45/0.18$, while the current source M5 operates with a bias current of 1mA. The capacitors C1-C4 are set to 1pF and the resistors R_1-R_4 are 1 $M\Omega$. The active circuit in Fig.L.4 has been characterized by the S parameters obtained in Advanced Design System (ADS) software, which is electronic design automation software for RF, microwave, and high speed digital applications. Based on this design setup, a fixed negative resistance value is selected by setting appropriately the bias voltages.

This value is shown in Fig.L.5 as a function of frequency. The horizontal axis is the frequency in GHz and vertical axis is the impedance value in Ω. Two markers indicate the real and imaginary parts of the impedance respectively. According to the simulation, the real part of the impedance at 2.5GHz is found around -230.6 Ω and the imaginary part around -117.9 Ω. It is noted that this impedance is finally adjusted to the desired loading by the impedance matching network presented in Section V. Bearing in mind the minimum resistance value requirement shown in Fig. L.3, which is -63.13 Ω for a 16-QAM modulation, the result of the proposed negative resistance unit is more than sufficient.

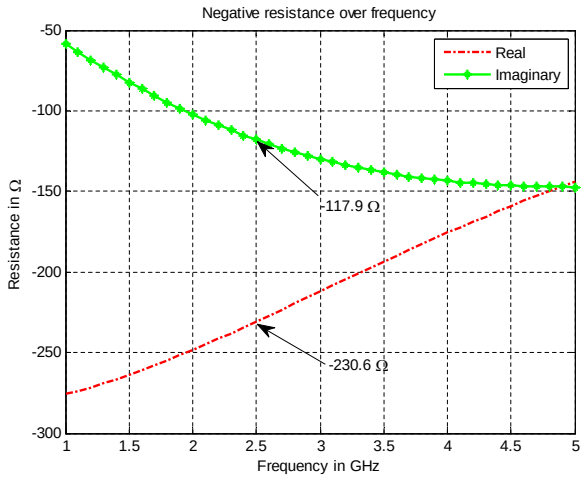

Fig. L.5: Simulated negative resistance values.

3.2 Loads Switching

Adjusting Stages

According to the proposed circuit architecture shown in Fig.2, in order to compensate the imaginary component of the active circuit and adjust the load to the desired value, an adjustable passive impedance matching network should be included. According to that figure, a circuit unit with impedance between its ports equal to Z_s is attached to a parasitic element

with a characteristic impedance of Z_{C_p} . Designing the ESPAR antenna with metal thickness of 0.0254mm and substrate with FR4 material with thickness 0.813mm and ε_r=4.3 , the self-impedance of the passive element on ESPAR antenna is measured in IE3D as Z_{C_p}=Z_{C_a}=48+j15 Ω, while the mutual coupling is found equal to Z_{12}=35+j10Ω.

As shown in Fig.L.6, the proposed adjusting unit is composed of 64 discrete values, where each one contains a resistive component R_{adj} and an inductive component L_{adj}. The load network can be implemented by an 8x8 array with two 3-to-8 converters. CMOS Port 1 is connected to a negative resistance core as the one described in Fig. 4, and the RF Port 2 is connected to the parasitic antenna. Each cell inside the array is a digital switch with pre- set value pairs. In this topology, only 6 control bits are required to determine one out of 64 loads. Based on this implementation approach, each symbol vector is mapped to a 6-bit code-word and at each signaling period the appropriate one

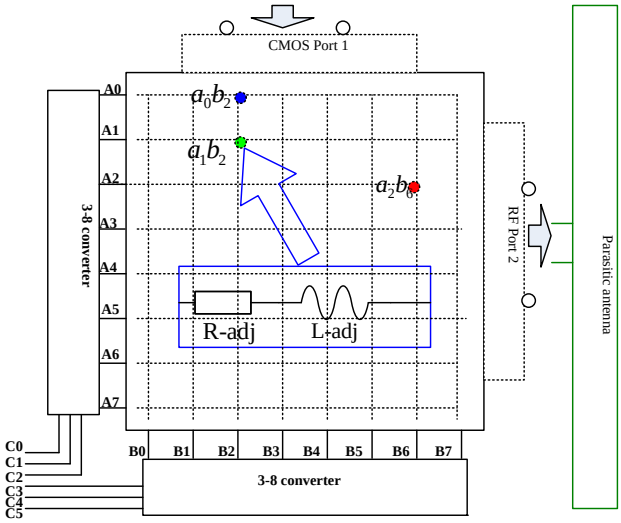

Fig. L.6: Topology of the proposed digitally controlled adjusting network.

applies to retrieve the correct value of the load matrix. An example of such encoding is shown in Fig.L.6.

Letting the desired practical load be -27.915-j-2.228 Ohms, then the code-word 011001 is applied to the bus line. After decoding, the address searching code 00000010 appears the $A_7 - A_0$ branch and 00000100 appears in the $B_7 - B_0$ branch to select the correct impedance, which in this example corresponds to the grid position a_1b_2 . Therefore, by applying this method, the selection among 64 possible radiation patterns can be conducted with just 6-bit code-word, which reduces the implementation complexity and printed circuit board space.

Performance and Tolerance Simulation

At high frequencies, the non idealities due to parasitic effects have to be also considered, as indicated in Fig.L.7 [23]. According to that figure, the impedance of the resistor and the inductor including the parasitic effects is given by

$$\begin{aligned} Z_{res} &= j\omega L_{2\_P} + \frac{1}{j\omega C_{2\_P} + 1/R_2} \\ Z_{ind} &= \frac{j\omega L_1 + R_{1\_P}}{1 + j\omega C_{1\_p}(R_{1\_P} + j\omega L_1)} \end{aligned} \tag{L.14}$$

The practical non-idealities that count not only for the parasitic effects but also for the mounting pad influence have been simulated in ADS. Taking into account this model, we observed a variation from the desired values in the order of around 2.5 Ω

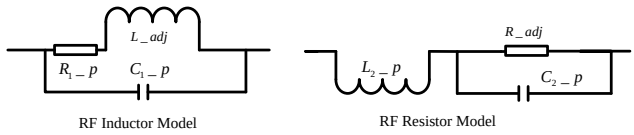

Fig. L.7: Small circuit model of resistor and inductor at high frequency.

It is noted that this deviation is representative for all loading states, as shown indicatively for 16 loading states in Table II.

Table L.2: Comparison between ideal loads and Practical Simulated loads with parasitic effects(Simulated by ADS)

Symbols Pairs $[w_0 w_1] = [a_n b_m]$	Practical $Re(x_1)$	Practical $Im(x_1)$	$Re(x_1)$ Ω	$Im(x_1)$ Ω
$a_1 b_0$	-20.16	-9.23	-23.91	-8.12
$a_1 b_1$	-23.04	-4.48	-27.47	-2.92
$a_1 b_2$	-19.56	1.27	-23.36	4.47
$a_1 b_3$	-20.05	2.68	-17.07	4.19
$a_1 b_4$	-20.14	-16.42	-24.18	-14.43
$a_1 b_5$	-48.75	-10.47	-43.07	-13.59
$a_1 b_6$	-25.17	20.12	-22.54	23.35
$a_1 b_7$	-13.41	10.17	-11.87	7.75
$a_1 b_8$	-14.21	-15.01	-16.80	-18.52
$a_1 b_9$	-7.31	-29.05	-6.12	-34.12
$a_1 b_{10}$	16.21	4.16	14.40	2.82
$a_1 b_{11}$	-6.02	1.86	-4.48	3.65
$a_1 b_{12}$	-10.7	-18.4	-11.60	-14.96
$a_1 b_{13}$	-7.8	-17.24	-5.30	-15.23
$a_1 b_{14}$	-2.82	-6.48	-1.19	-7.85
$a_1 b_{15}$	-6.37	-4.01	-4.75	-2.64

It should be worthy noted, that the adjusting matching network in Fig.L.7 has been proposed as an easy-to-implement solution, with a fixed and predefined impedance values. Applying a de-embedding technique (e.g. [24] [25]), one could be easily compensate possible parasitic effects during the design procedure by taking them into account and optimizing the final impedance values on the grid. Therefore, it is understood that the treatment of the parasitic effects, at least to some extent, is a matter of implementation. In Section VI however, we illustrate the impact of possible loading perturbations that

might be present, on the performance in terms of bit error probability.

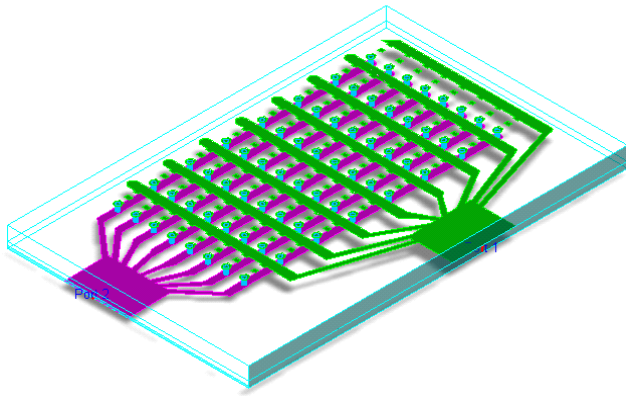

Fig. L.8: 3D view of the proposed load switching array produced in ADS design software.

4 Performance Evaluation

The presence of small perturbations on the loading states might change the shape of the desired pattern given in (L.3). Indicatively, Fig. 9 shows a comparison between a desired pattern and the corresponding one with the simulated loadings without including other non-idealities. As observed, the loading found with the proposed architecture gives an almost exact picture of the desired pattern. As it will be demonstrated, this high accuracy is achieved in all cases. For a complete com-parison, a third version of the pattern is also depicted in Fig. L.9

that is produced including a perturbation of 1.5 Ohm at both the real and imaginary part of the loading. Figure 11 offers valuable comparison of the bit error probability when a conventional zero-forcing receiver with two antenna elements is utilized and the ESPAR antenna at the transmitter (as described in Fig. L.3) multiplexes two 16-QAM signals. As observed, the performance using the theoretical loading values is identical to the one obtained with the simulated ones, implying the capability of the proposed loading design to produce very accurate impedance values. However, to illustrate the dependence of the performance due to possible and inevitable non-idealities, Fig. L.10 includes the effect of small perturbations on the desired loadings. It follows that random perturbations ranging Ohms around the desired loadings cause a reasonable performance degradation of 2 dB in high Eb/No regime. However, since it is expected that in future wireless systems mobile devices will operate in the low Eb/No regime, the possible

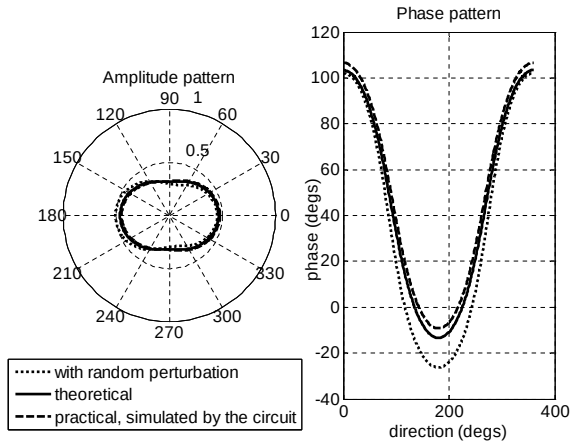

Fig. L.9: Theoretical and practical radiation patterns gains and phase.

loading perturbations cause negligible performance degradation, and those non-idealities can be ignored.

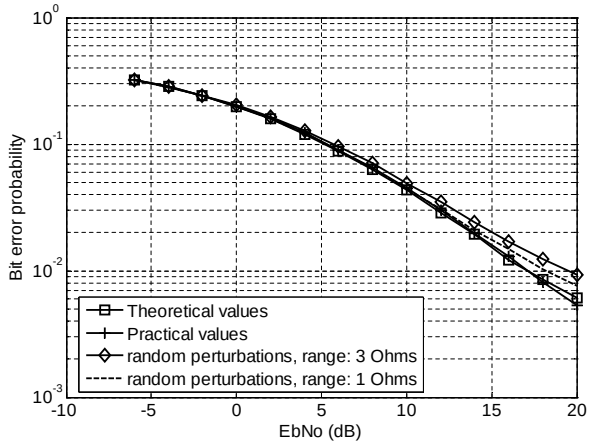

Fig. L.10: Bit error probability performance, under various loading conditions.

Eventually, the end-to-end performance could be further improved by using more robust receiving techniques such as ordered successive cancellation (OSUC) zero-forcing,

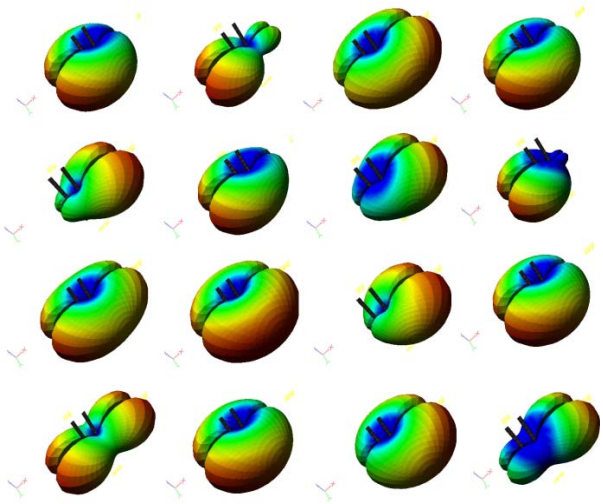

Fig. L.11: Simulated first 16 radiation patterns with the simulated load values.

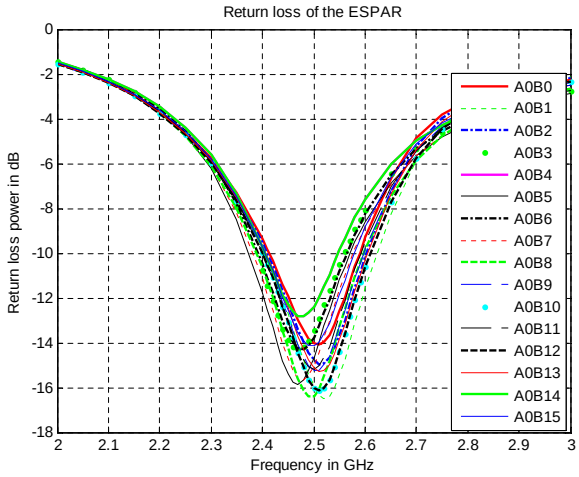

Fig. L.12: Simulated indicative return loss of the first 16 load values.

or even more complex ones [26]. For completeness, Fig. 11 illustrates 3D examples of radiation patterns; Fig. L.12 shows the indicative return loss over the first 16 load values, all of them are obtained in IE3D software, where each of them corresponds to a different 16-QAM symbol vector for transmission.

5 Conclusion

This paper presents a novel loading architecture that enables a reliable MIMO transmission using a single RF chain and a parasitic antenna array with closely spaced elements. Instead of the conventional trend of using purely imaginary loads, complex loading values are generated via an active circuit design. The consequent additional flexibility is found to improve significantly the beam-shaping abilities of parasitic antennas. This in turn enables such antennas to multiplex 16- QAM signals over the air and therefore, to emulate MIMO transmission with a single RF chain. The remarkable hardware savings and the reduced antenna dimensions, constitute the proposed architec-ture a strong candidate for battery-charged and lightweight devices. Although this architecture is demonstrated for 16-QAM signals, clearly the same design procedure can be followed for an arbitrary signaling format.

References

[1] A. Gorokhov, D. Gore, A. Paulraj, "Receive antenna selection for MIMO spatial multiplexing: theory and algorithms," *IEEE Transactions on Signal Processing*, vol. 51, pp. 2796–2087, 2003.

[2] ——, "Receive antenna selection for MIMO spatial multiplexing: theory and algorthims," *IEEE Transactions on Information Theory*, vol. 49, pp. 2687–2696, 2003.

[3] P.Karamails, N.Skentos, A.G. Kanatas, "Slecting array configruations for MIMO systems: an evolutionary computation approach," *IEEE Transactions on Wireless Communications*, vol. 3, pp. 1994–1998, 2004.

[4] D.A. Gore, A.J. Paulraj, "MIMO antenna subset selection with spacetime coding," *IEEE Transactions on Signal Processing*, vol. 50, pp. 2580–2588, 2002.

[5] P.J. Voltz, "Characterization of the optimum transmitter correlation matrix for MIMO with antenna subset selection," *IEEE Transactions on Communications*, vol. 51, pp. 1779–1782, 2003.

[6] P.Theofilakos, A.G. Kanatas, "Capacity performance of adaptive receiver antenna subarray formation for MIMO systems," *EURASIP Journal on Wireless Communications and Networking*, vol. 2007, pp. 56 741.1–12, 2007.

[7] ——, "Maximising capacity of MIMO systems with receive antenna subarray formation," *Electronics Letters*, vol. 44, pp. 1204–1206, 2008.

[8] J.Villanen, P.Suvikunnas, C.Icheln, J.Ollikainen, P. Vainikainen, "Performance analysis and design aspects of mobile-terminal multiantenna configurations," *IEEE Transactions on Vehicular Technology*, vol. 57, pp. 1664–1674, 2008.

[9] A. Kalis, A.G. Kanatas, C.B. Papadias, "A Novel approach to MIMO transmission using single RF front end," *IEEE Journal on Selected Areas in Communications*, vol. 26, pp. 972–980, 2008.

[10] ——, "An ESPAR antenna for beamspace MIMO system using PSK modulation schemes," *IEEE International Conference on Communications (ICC)*, vol. 1, pp. 5348–5353, 2007.

[11] R. Bains, R. Muller, "Using parasitc elements for simpementing the rotating antenna for MIMO receivers," *IEEE Transactions on Wireless Communications*, vol. 7, pp. 4522–4533, 2008.

[12] R. Harrington, "Reactively controlled directive arrays," *IEEE Transactions on Antennas and Propagation*, vol. 26, pp. 390–395, 1978.

[13] C. Sun, A. Hirata, T. Ohira, "Fast beamforming of electronically steeralbe parastic array radiator antennas: the theory and experiment," *IEEE Transactions on Antennas and Propagation*, vol. 52, pp. 1819–1832, 2004.

[14] V.I. Barousis, A.G. Kanatas, A. Kalis, "Beamspace domain analysis of single RF front-end MIMO systems," *IEEE Transactions on Vehicular Technology*, vol. 60, pp. 1195–1199, 2011.

[15] V.I. Barousis, A.G. Kanatas, "Aerial degrees of freedom of parasitic arrays for single RF front end MIMO receivers," *Progress In Electromagnetics Research B*, vol. 35, pp. 287–306, 2011.

[16] V.I. Barousis, A.G. Kanatas, A. Kalis, "Single RF MIMO systems: exploiting the capabilities of parasitic antennas," *IEEE 74th Vechicular Technology Conference*, vol. Sep, pp. 5–8, 2011.

[17] O.N. Alrabadi, J. Perruisseau-Carrier, A. Kalis, "MIMO transmission using a single RF source: theory and antenna design," *IEEE Transactions on Antennas and Propagation*, vol. 60, pp. 654–664, 2012.

[18] O.N. Alrabadi, C.Divarathne, P. Tragas, A. Kalis, N.Marchetti, C.B. Papadias, R. Prasad, "Spatial multiplexing with a single radio: proof -of- concept experiments in and Indoor enviroment with a 2.6GHz prototype," *IEEE Communications Letters*, vol. 15, pp. 178–180, 2011.

[19] O.N. Alrabadi, C.B. Papadias, A. Kalis, R. Prasad, "A universal encoding scheme for MIMO transmission using a single active element for PSK modulation schemes," *IEEE Transactions on Wireless Communications*, vol. 8, pp. 5133–5142, 2009.

[20] B. Han, V.I. Barousis, A. Kalis, A.G. Kanatas, "Active parasitic arrays for low cost compact MIMO transmitters," *IEEE 5th European Conference on Antennas and Propagation (EUCAP)*, vol. 1, pp. 3663–3667, 2011.

[21] C. Balanis, *Antenna Theory, Analysis and Design.* Wiely, 2005.

[22] B. Razavi, *RF Microelectronics.* Prentice Hall, 1998.

[23] C. Bowick, J. Blyer, C. Ajluni, *RF Circuit Design.* Newnes Elsevier, 2008.

[24] T. Hirano, J. Hirokawa, M. Ando, H. Nakano, Y. Hirachi, "Demembeding of lumped -element chractersitcs with the aid of EM analysis," *IEEE Antenna and Propagation Society Internation Symposium*, vol. 1, pp. 1–4, 2008.

[25] B. Han, M. Liu, N. Ge, "A UWB down converter ciruit and measurement," *IEEE International Conference on Microwave and Milimeter Wave Technology*, vol. 1, pp. 1472–1475, 2010.

[26] A. Paulraj, R.Nabar, D.Gore, *Introduction to Space-Time Wireless Communications.* Combridge University Press, 2003.

Paper M

Wireless Sensor Placement based on SHM Requirements and net Energy Consumption

R. Soman, T. Onoufriou, R.A. Votsis, C.Z. Chrysostomou, M.A. Kyriakides, B.Han

The paper has been published in the
The 2nd International Conference on Civil Engineering and Building Materials Vol. 1, pp. 271–275, 2012.

This paper is an extra work of the thesis main body, more details of this paper can be found from the publisher.

The layout has been revised.

Abstract

Structural Health Monitoring (SHM) techniques have undergone a paradigm shift due to new emerging technologies and developments in the field of remote communications. The use of Wireless Sensor Networks (WSN) has been on an increase in the last decade due to its low cost deployment, easy of maintenance and increasing efficiency. However, the battery life of the sensors in such networks is limited which puts severe restrictions on the using of such technology. Thus there is a need to enhance the life time of the network through optimizing the energy usage of sensors, which can be achieved through energy harvesting using ambient vibrations. However, if the sensor placement is for achieving network longevity alone, it might lose vital information, thus sensor placement is important for the SHM. This paper focuses on optimizing the location of the sensors to cater to the specific requirements of structural engineering while adhering to the energy limitations imposed due to the use of WSN. In this paper an Optimal Sensor Placement problem taking into consideration the application demands and the net energy usage of the sensor is formulated and solved making use of Genetic Algorithm for a near optimal solution.

1 Introduction

The increased demands of load carrying and the ageing of the structure have put a high demand on the tools for performance monitoring of the structure in the last two decades. Thus, Structural Health Monitoring (SHM) has become a necessity than a luxury. In fact, the bridge owners demand that, the bids for design and construction of new infrastructure to include a design of a SHM system to be deployed right in construction phase. SHM systems can trigger alarms of any deterioration early enough so as to schedule maintenance in advance thus offering an opportunity to reduce the cost of maintenance, and prevent severe structural deterioration.

The traditional SHM system makes use of sensors, data loggers, computers and large lengths of wires, which are expensive and offset the savings in the maintenance cost. Over the years, it has become apparent that the large lengths of the wires also lead to other problems like increased time for deployment, inflexibility of the system and susceptibility to damage [1]. As a result, the use of wireless sensor networks (WSN) is becoming more popular. WSNs allow similar level of performance as the wired system at a lower cost and also offer greater robustness and flexibility [2]. However, the WSN have limited battery life, and hence a low network lifetime which is orders of magnitudes less than the design life of the structure.

Energy harvesting is an upcoming area to counter this disparity in the lifetimes. Energy Harvesting can be done through the use of solar, wind, or vibration of the structure itself. The energy potential of solar energy and wind energy are quite high

and it has been shown feasible by some experiments [3]. However, the solar energy and wind energy restrict the location of the sensors as they need to be in the open and cannot be embedded in the structure, which at times is a functional requirement of the sensors. Hence, use of vibration energy for harvesting is being investigated. The problem with vibration energy is that the energy potential is quite low and at times the energy is not sufficient for the independent use. So, an external battery source in addition to the harvester is required. Although harvesting of vibration energy is not a permanent solution due to its low energy density, it might be able to increase the network lifetime significantly. In addition, by managing the energy consumption of the sensor nodes through optimal sensor placement, the network longevity can be further improved.

This research work investigates the problem of optimal sensor placement considering the information content, the energy consumption of sensor nodes and the energy harvesting potential using PZT harvesters making use of cantilever type harvester. The paper not only tries to highlight the savings and the improvement in performance that can be achieved through a multi-objective optimization. Genetic Algorithm (GA) is employed to optimize the sensor locations for higher network lifetime and information quality for the sensor placement problem on a medium-span bridge. For the case study, it is assumed that accelerometer are deployed to measure the response of the system allowing us to extract the mode shapes and the natural frequencies of vibration. The accelerometer are incorporated on an Imote2 [4] sensor platform which is popularly used for SHM applications in bridges and is equipped with state-of-the-art hardware for wireless communication.

2 Relevant Work

2.1 Structural Health Monitoring

The optimal sensor placement problem has been tackled by researchers in various fields. Over the years many researchers have employed diverse optimizing principles [5] [6]. The selection of the principle depends on the application at hand, for modal identification the Effective Independence Method (EFI) [7] has been widely accepted. Once the optimizing principle is chosen there are variety of optimizing methodologies which can be used, like the Genetic Algorithm (GA), [8] [9] [10], Simulated Annealing [8], the L-search Algorithm [11](. The selection of the tool is highly objective to the application and the sample space. Each of the methods has its own set of advantages and shortcomings which should be carefully considered before employing a specific tool.

2.2 Wireless Sensor Networks

WSNs have found wide scale application in many areas. Each of these areas poses a different set of challenges to this technology and a lot of work has been application-specific in this regard. A summary of the various optimization principles in the field of WSN is given by [12]. The field of Energy Harvesting has been identified as a possible solution to the problem of limited network lifetime of WSNs. Much work has been done in this field, using solar energy [13], wind energy and vibration energy [14] to show the feasibility of the principle. There are advantages and disadvantages associated with each type of energy. For instance, solar energy and wind energy have a high energy density and can be used for energy intensive applications but the required equipment needs more space. Also, there are cases (e.g. corrosion sensors) where sensors may have to be embedded in concrete making the solar energy harvesters not feasible. The vibration energy harvesters are useful in such circumstances even though they have lower energy potential. As the vibration harvesters are more universal in nature, the effect of vibration energy harvesting on the OSP is investigated in this work.

3 Framework of Methodology

3.1 Outline

In the current work, a methodology is proposed for OSP with respect to SHM requirements and Energy constraints in WSN. The method allows a better network lifetime through the use of Energy Harvesting. The method also demonstrates the level of influence of incorporating the energy harvesting potential of a sensor location in the optimization principle, and how the system performance is improved. The proposed methodology optimizes the location of the sensors based on the information quality indicated by the determinant of the FIM and the least energy usage, taking into consideration the energy harvesting potential of each point. The optimization is carried out through the use of GA.

3.2 Bridge sturcture

To validate the methodology a numerical model of a long span segmental box-girder bridge (Figure M.1) was used for extracting the mode shapes. (Grand-Mere Bridge, Quebec, Canada) The aforementioned bridge is a single-cell box-girder type bridge with three continuous spans of 40 m, 181 m and 40 m, with a wedge shaped cantilever of 12 m. at either end. The 40 m spans on either side have a linearly changing cross section (Figure M.1). For the central span the depth varies parabolically. The wedge shaped cantilevers are of solid cross section increasing to a depth of 8.53 m at the external piers. The compressive strength of concrete in mid-span is assumed to be 38 MPa,

while compressive strength of the concrete at the end-spans is assumed to be 34 MPa. The bridge has hinged support at the ends and is simply supported at the internal piers and external piers [15].

3.3 Structural Health Monitoring

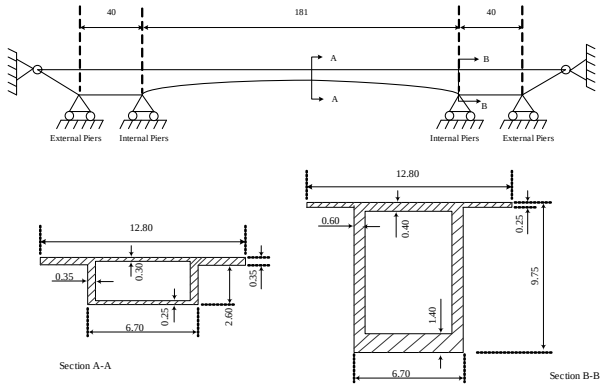

Fig. M.1: Details of Grand-Mere Bridge, all dimensions are in meters.

As discussed in Section 2, there are many principles on which the OSP can be based upon. The most popular method for OSP with respect to SHM requirements is the Effective Independence Method (EFI) which is based on the Fisher Information Matrix (FIM) determinant [7] The FIM is given by

$$A_0 = \sum_{i=1}^{s} {\phi_s}^{iT} \phi_s = A^i \tag{M.1}$$

where A_0= Fisher Information Matrix and $\phi_s^i = i_{th}$ row of the modal partition ϕ_s corresponding to the i_{th} degree of freedom The FIM is essentially the inverse of the covariance matrix, as the covariance matrix is the entropy of the information content of the system, the norm chosen (determinant) needs to be minimized and hence the FIM determinant needs to be maximized.

3.4 Energy Model

As stated in Section 2, energy is one of the parameters which has restricted the extensive use of WSN in SHM. Thus, increasing network lifetime through minimum usage of energy is one of the optimizing principles.

There are many energy models for estimating the energy usage of the wireless sensors during operation; the simplest model is the exponential model. The relation for the energy transmission is given by [16].

$$E_d = d^{\alpha} + c \tag{M.2}$$

where, E_d= Energy spent for transmission, d is the distance between communicating nodes, α is the path loss exponent 3.51 for open spaces with no multipath communication possible, [17] and is dependent on the environment in which the sensors are placed and c is the technology based path loss coefficient [18]. The locations of the sensors are taken to be linear and the routing is assumed to be such that each node is in communication with 2 nodes exactly, one from which it receives the signals of all preceding nodes and one to which it transmits the data. This routing algorithm was chosen for its simplicity. Two sink nodes at the internal piers at either ends of the bridge are assumed, and both the sink nodes are wired. The measurement of the vibrations is assumed to be carried out every hour for a period 15 sec at a sampling frequency of 200 Hz. The values are in accordance with the values used in actual monitoring applications [19]. Furthermore, each sample of data consists of 6 bits of information including the sensor identity as given by the IEEE standards 802.15.4. The algorithm identifies the node with the maximum difference in the energy requirement and the harvested energy and marks it as the weakest link. Due to the simple routing adopted, no redundancy is observed and failure of any node will lead to the failure of the system.

3.5 Energy Harvester

The two primary vibration-based energy harvesting devices are electro-magnetic or piezoelectric. Both methods of harvesting have their merits, but the piezoelectric harvesters are considered to be more robust and therefore are considered in the simulations. The piezoelectric harvesters use the strain induced due to the external loading for the generating electricity. The mathematical formulation of the energy potential is given by [14].

$$E_h = \int_0^{\infty} \frac{V(t)^2}{R_1} dt \tag{M.3}$$

The potential depends, on the bridge structure, the location along

its length and the physical properties of the harvester itself. The harvested energy is given by where, E_h is the harvested energy $V(t)$ is the voltage across the resistor

Table M.1: Parameter Values for Harvester [1] [3] [22] [23]

Parameter	Value	Unit
Mass	0.1	kg
Damping Ratio	0.038	
Stiffness	5	N/m
Frequency	1.0523	Hz
Electromechanical Coupling	3.69e-5	μC/m
Capacitance	2.866	nF
Coupling Coefficient	0.214	
Time Constant of Harvester	0.9	
Load on Bridge	600	kN
Types of Truck	HS20	
Numbers of Alex	3	
Speed of Truck	27	m/s
Traffic Density	8183	trucks

in the time domain R_1 is the load resistance The mathematical formulation of $V(t)$ is given by [14] The harvester parameters can be found in [3] but the length and the stiffness values were modified to match the natural resonant frequency of the bridge. The values used for simulation of loads and the harvester are given in Table M.1. The loading parameters for simulation were taken from the AASHTO codes [20] and the Weigh in Motion (WIM) data [21]. The simulations for the harvesting were carried out in ABAQUS 6.8-2 on numerical model shown in section 3.2 The net Energy for optimization is the difference between the Energy required for transmission and Energy Harvested by the harvester.

4 Results and Evaluations

The effect of a moving load on a bridge was modeled in ABAQUS. Analyses were performed to compute the energy potential at the nodes of the FE model, using the present day hardware for piezoelectric energy harvesting. Once the energy potential was computed, the GA [10] was used as the optimizing tool. In order to make the system efficient, extensive sensitivity analysis was carried and the parameters for the GA were selected. The cost function was defined as the ratio of Q and E where Q is the determinant value of FIM and E is the maximum difference between the energy consumption and the energy harvesting of a particular node for the given sensor placement. The goal was to maximize the cost, while keeping the values of Q and E both within limits. Population size was taken as 512. A higher number increases the computational load

without improving the solution by a great margin. The mutation rate of 0.15 gives the best solution for the chosen parameters, and hence has been chosen. The number of generations was selected to be 5000 generations which gives a near optimal solution.

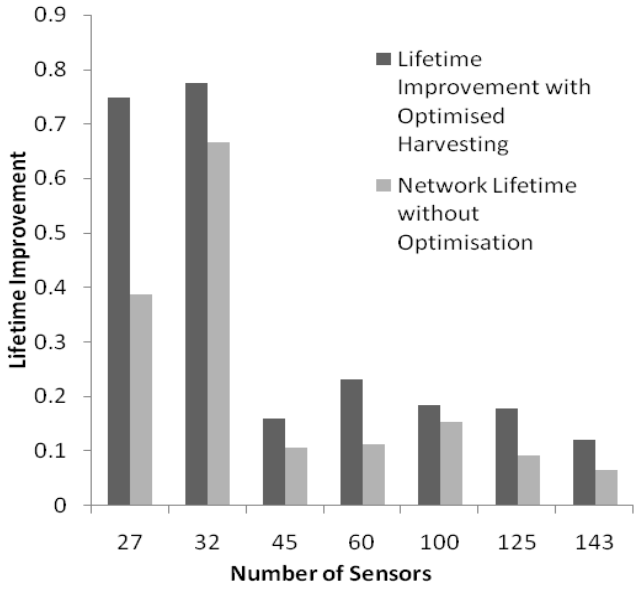

Fig. M.2: Bar Chart showing Improvement in Network Lifetime.

Figure 3 shows the effect of energy harvesting on the network lifetime. It can be clearly seen that the network lifetime is improved by over 30 percentage for less number of sensors. In addition, while the number of sensors increases, the rate of increase in network lifetime is reduced. Simulations were run with and without taking harvesting into consideration in the optimization. Table 2 gives the values for the simulations with and without the harvesting placement normalized with the placement without energy harvesting. As shown, there is improvement in the Q/E_{har} ratio for each number of sensors, thus showing that there is considerable improvement in the performance on the sensor placement when the harvesting is considered during optimization. As can be seen from column Q, by incorporating harvesting, there is greater freedom in the placement of sensor and hence we get a better Q value. Also, the Column Q/E_{nor} shows that without considering the harvesting in the optimization problem there is an improvement in the overall fitness and hence indicates the need to include the harvesting parameter for better results.

Table M.2: Performance Evaluation with Energy Harvesting

Number of Sensors	Q	E_{har}	E_{nor}	Q/E_{har}	Q/E_{nor}
27	1.02	0.64	0.72	1.58	1.40
32	1.43	1.19	1.25	1.24	1.14
45	2.23	2.19	1.99	1.22	1.12
60	1.10	0.93	1.00	1.18	1.10
100	1.03	0.90	0.96	1.14	1.07
125	1.01	0.91	0.99	1.10	1.02
143	1.03	0.97	1.01	1.06	1.02

5 Conclusion

The limited amount of work in the overlapping area of WSN and SHM of structures is evident through the literature review. The proposed methodology aims at addressing such lacking of work in this area and proposing a method to optimize the sensor location, for maximum information quality and minimum energy usage. The methodology formulates a minimization problem, and employs the GA for reaching a near optimum solution. The GA was chosen due to the simplicity it brings to the problem and also it is ideally suited for Multi-Objective Optimization. The fitness function is defined as the ratio of the information quality and energy consumption of the sensor node. The net energy consumption is given by the differences between e energy requirement and the energy harvesting potential of that node under ambient vibrations. The comparison of the performances of the wireless network with and without energy harvesting shows that there is considerable improvement in the network lifetime. This improvement is seen even when the harvesting is not considered as an optimization principle and hence harvesting may be used even for the existing deployed sensor networks for higher network lifetime. In addition, by incorporating the harvesting potential of the nodes, we can improve the network lifetime by 70 percent which shows the suitability of the methodology proposed to new deployment projects. Also the improvement in the information quality is a positive of this method and hence will be gladly accepted by the structural engineers. From the promising results obtained in the simulations, experimental validation of the methodology is recommended. Also, the significant improvement in network lifetime along with the developments in the sensor technology, advances in communication and hardware technology make the possibility that the network and the structure lifetime may be comparable in the future. Thus in nutshell, this paper presents very promising methodology using GA for multi disciplinary problem of sensor placement optimization for SHM using WSN and points at a wide area of research.

References

[1] B. Jacob, D. Labry, "Evaluation of the effects of heavy vehicles on bridges fatigue," *7th International Symposium in Heavy Vehicle Weights and Dimensions*, 2002.

[2] C.B. Yun, H. Sohn, H.J. Jung, B.F. Spencer, T. Nagayama, "Wireless sensing technologies for bridge monitoring and assessment," *Bridge Maintenance, Safety, Management and Life Cycle Optimization*, pp. 113–132, 2010.

[3] N.G. Elvin, N. Lajnef, A. Elvin, "Feasibility of structural monitoring with vibration powered sensors," *Smart Materialsand Structures*, vol. 15, pp. 977–986, 2006.

[4] *Crossbow, Inc, 2007, Imote2 Hardware Reference Manual, PN: 7430-0409-01.*

[5] G. Heo, M.L. Wang, D. Satpathi , "Optimal transducer placement for health monitoring of long span bridge," *Soil Dynamics and Earthquake Engineering*, vol. 16, pp. 495–502, 1997.

[6] V.Fedorov, P. Hackl, "Optimal experimental design: spatial sampling," *Calcutta Statistical Association Bulletin*, vol. 44, pp. 173–174, 1994.

[7] D. Kammer, "Sensor placement for on-orbit modal identification and correlation of large space structures," *Journal of Guidance, Control and Dynamics*, vol. 14, pp. 251–259, 1991.

[8] K. Worden, A.P. Burrows, "Optimal sensor placement for fault detection," *Engineering Structures*, vol. 23, pp. 885–901, 2001.

[9] C. Papadimitriou, "Optimal sensor placement methodology for parametric identification of structural systems," *Journal of Sound and Vibration*, vol. 278, pp. 923–947, 2004.

[10] L.R. Haupt, S.E. Haupt, Ed., *Practical Genetic Algorithms, Second Edition.* John Wiley & Sons Inc, 204.

[11] B. Li, D. Wand, F. Wang, Q. Yi, "High quality sensor placement for shm systems: refocussing on application demands," *IEEE INFOCOM*, 2010.

[12] M. Younis, K. Akkaya, "Strategies and techniques for node placement in wireless sensor networks: a survey," *Ad Hoc Networks*, vol. 6, pp. 621–655, 2008.

[13] S. Jang, H. Jo, K. Mechitov, S. Sim, B.F. Spencer, G. Agha, S. Cho, H. Jung, C. Yun, J.A Rice, "Autonomous structural health monitoring using wireless smart sensors on a cable stayed bridge," *Bridge Maintenance, Safety, Management and Life Cycle Optimization*, pp. 113–132, 2010.

[14] S.F. Ali, M.I. Friswell, S. Adhikari, "Analysisof energy harvesters for highway bridges," *Journal of Intelligent Material Systems and Structures*, vol. 22, 1929.

[15] B. Massicotte, A. Picard, C. Ouellet, Y. Gaumond, "Strengthening of a long span post tensioned segmental box girder bridge," *PCI Journal*, vol. 29, pp. 52–65, 1994.

[16] S. Olariu, I. Stojmenovic, "Design guidelines for maximizing lifetime and avoiding energy holes in sensor networks with uniform distribution and uniform reporting," *IEEE INFOCOM*, 2006.

[17] E. Tanghe, W. Joseph, L. Verloock, L. Martens, H. Capoen, K.V. Herwegen, W. Vantomme, "The industrial indoor channel: large scale and temporal fading at 900, 2400, 5200 mhz," *IEEE Transactions on Wireless Communication*, vol. 7, pp. 2740–2742, 2009.

[18] W.R. Heinzelman, A. Chandrakasan, H. Balakrishnan, "Energy efficient communication protocol for wireless microsensor networks," in *Proc of 33rd Hawaii International Cinference on System Sciences*, 2000.

[19] S. Kim, S. Pakzad, D. Culler, J. Demmel, G. Fenves, S. Glaser, S. Turon, "Wireless sensor networks for structural health monitoring," *In Proceedings of the 4th international conference on Embedded networked sensor systems*, pp. 427–428, 2006.

[20] *Standard Specifications for Highway bridges, American Association of State Highway and Transportation Officials.* AASHTO, 1989.

[21] A. Getachew, E.J. OBrien, "Simplified site-specific traffic load models for bridge assessment," *Structure and Infrastructure Engineering*, vol. 4, pp. 303–311, 2007.

[22] D. Cantero, G. Arturo, E.J. OBrien, "Maximum dynamic stress on bridges traversed by moving loads," *Proc. of the ICE-Bridge Engineering*, vol. 162, pp. 75–85, 2009.

[23] A.S. Nowak, "Live load model for highway bridges," *Structural Safety*, vol. 13, pp. 53–66, 1993.

Paper N

Energy efficiency of cooperative beamforming in wireless sensor networks

M.B. Rajashekara, B.Han, S.Vassilaras, A.Kalis

The paper has been submitted to
International Journal of Antenna and Propagation Special Issue, 2013.

This paper is an extra work of the thesis main body, more details of this paper can be found from the publisher.

The layout has been revised.

Abstract

Cooperative beamforming has been proposed as a technique that can be used to allow sensors in a Wireless Sensor Network to transmit their data to a distant fusion center in one hop by combining low power individual transmissions. This technique replaces traditional multi-hop communication and inter sensor communication thus leading to considerably energy savings and simpler node designs. It is based on spread spectrum techniques and a binary frequency shift keying modulation scheme. In this paper, we present an energy efficiency analysis of this cooperative beam forming scheme in terms of minimal required energy per bit for a desired Bit Error Rate (BER) at different network sizes (in terms of number of nodes and covered area). We derive the average BER expressions for the direct sequence spread spectrum synchronous system with binary frequency shift keying modulation scheme, over AWGN channel and a realistic propagation channel with a Line-of- Sight and multipath components, taking multi-user interference into account. In order to obtain a detailed formulation of the overall energy requirements, we have proposed a battery operated sensor node architecture with low power consumption and analyzed the power requirements of each circuit element. The energy model analysis considers both transmission energy and circuit energy consumption. Through analytical expressions and simulation results we have also illustrated the transmission energy and total energy savings that can be achieved with cooperative beamforming. Our analysis can be used to estimate the expected energy consumption and resulting lifetime of a WSN using the one-hop communication technique prior to its deployment in the field

1 Introduction

In recent years there has been increasing interest in Wireless Sensor Networks (WSN) and their applications. Wireless sensor networks are becoming important in a number of areas, including environmental monitoring, structural health monitoring, precision agriculture, military and security surveillance. Wireless sensors are usually small in physical dimensions and operated by battery power. After the deployment of sensors over a large area their batteries replacement or recharging is a tedious and costly task. Hence extending the energy lifetime of WSN is extremely important. Optimal WSN design should

consume the minimum amount of energy required in the transmission and circuit part to provide reliable communication [1]. Information transmission in WSN is commonly accomplished through the use of multi-hop communication. But this kind of communication scheme suffers from inter-node information collisions and may require retransmissions which result in added complexity and high energy consumption. A novel network architecture has been recently proposed and studied in the literature based on collaborative beamforming to bypass multi-hop transmissions, so that nodes can access

the fusion center directly.

In [2], the performance of collaborative beamforming is analyzed using the theory of random arrays. The authors assume that each sensor node has a single isotropic antenna and all the nodes within each cluster collaboratively transmit the same signal such that the signals in the desired direction are coherently added. It is shown that with K collaborative sensor nodes, a diversity of order K can be achieved asymptotically. But the disadvantage with this approach is that the information has to be shared among nodes in the cluster, burdening the network with additional short-range communications.

In [3] Kalis et al. proposed a novel scheme using cooperative beamforming and spread spectrum techniques to overcome the above limitation and allow each node to transmit its own data. A base station placed at a large distance from the WSN deployment area sends a synchronization beacon to the sensors at regular time intervals. The beacon signal is a pure sinusoid, which is received at each node with a slight phase difference due to different propagation delays. Once the nodes are triggered, they can modulate their own sensed data with the carrier frequency (internally generated) to produce the required output carrier. The modulation scheme and multiple access technique used is binary frequency shift keying (BFSK) with direct sequence spread spectrum (DSSS/BFSK). The authors extended this work in investigating directive beamforming gains for different sensor network densities [4]. Performance analysis has also been carried out under fading conditions. More specifically the average loss in directivity gain has been studied when the received signal from each sensor node follows a Rician distribution. Another notable improvement in the same paper is that the multiple access capability of the sensor network is achieved by employing an DSSS with on-off keying orthogonal signalling scheme instead of DSSS/BFSK.

In this paper, we analyze the energy consumption characteristics of the above cooperative beamforming scheme. Energy efficiency analysis in WSN and wireless communications in general has received considerable attention in the literature. In [1], the authors examined the use of error control codes in

WSNs from an energy efficiency point of view. The authors derived an expression for the critical distance at which the decoder's energy consumption per bit equals the transmit energy savings per bit due to coding gain. For distances above this critical distance the use of coding achieves energy savings compared to an uncoded system. Within the scope of minimizing energy consumption, the parameters under consideration are throughput and delay requirements [5], [6], [7]. In this context, the best modulation scheme to minimize the total energy required to send a given number of bits is studied. As energy optimization is a critical issue in the design of low power WSNs, an energy efficient virtual multiple input multiple output (MIMO) based communication architecture is proposed for distributed and cooperative WSNs [7]. In the same paper the parameters of interest are energy and delay efficiencies which are derived using semi-analytic techniques. Energy consumption comparison of MIMO and single input single output (SISO) systems is carried out considering the extra training overhead required

in MIMO systems.

By optimizing the transmission time and the modulation parameters [6] shows energy savings over coded and uncoded systems. For coded systems, the authors show that the benefit of coding varies with the transmission distance and employed modulation scheme. However, in most of the proposed schemes the nodes are densely distributed and the average distance between inter sensor nodes is usually below 10 m. In such kind of scenarios, when circuit energy consumption is considered along the signal path then it might so happen that it becomes comparable to the transmission energy in the total energy consumption.

Although energy analysis of various WSN architectures has been extensively studied, to the best of our knowledge, no such analysis has been published for the case of cooperative beamforming schemes studied in [3], [4]. This energy consumption study is the main subject of this paper. We start our analysis by characterizing the BER performance of DSSS/BFSK with and without beamforming gain over AWGN and Line-of-Sight (LoS) with multipath components by deriving analytical expressions and through computer simulations. In order to analyze the circuit energy consumption (in addition to the transmit energy requirements) we also propose a sensor node circuit architecture with low power consumption of each module and derive the total circuit energy requirements. Finally, we derive the total energy consumption per bit at each node by taking the beamforming gain and circuit power consumption into account.

The remaining of the paper is organized as follows. In Section 2, the system model and the wireless sensor node architecture are described in detail. In Section 3, a brief description is given about cooperative beamforming. In Section 4, analytical derivation of DSSS/BFSK for average bit error rate over AWGN and LoS with multipath components is discussed. In section 5, we introduce the energy consumption model analysis. In Section 6, we summarize our conclusions based on the results.

2 System Model

WSNs are characterized by the dense deployment of sensor nodes that continuously observe physical phenomena with applications in a wide range of fields including industrial process control, security and surveillance, environmental sensing, and structural health monitoring. In this paper, we assume that a number of sensors need to be deployed in an open field in order to collect real time data. The field is assumed to be close to planar, i.e., elevation differences are very small. We further assume that the sensors nodes are uniformly distributed in circular area with radius Rmax. The common receiver which collects data from all nodes (fusion center) is located far away from the sensor area as indicated in Fig.N.1. Each node is equipped with a single isotropic antenna.

The location of the receiver in spherical coordinates is assumed to be (d, θ_0, ϕ_0), where $\theta \in [0, \pi]$ is the elevation angle and $\phi \in [0, \pi]$ is the azimuth angle. The location of each sensor can be represented by (r_k, φ_k) where $r_k \in (0, R_{\max})$. Since the receiver

is far away from the sensor area, $d \geq R_{\max} \geq r_k$. Without loss of generality, the total number of senor nodes inside the area is assumed to be K, thus $1 \leq k \leq K$. Also, the density of the sensor nodes inside the area of $\pi {R^2}_{\max}$ max is low so that the inter sensor distance is large enough so that unwanted mutual coupling among the senor nodes antennas is avoided.

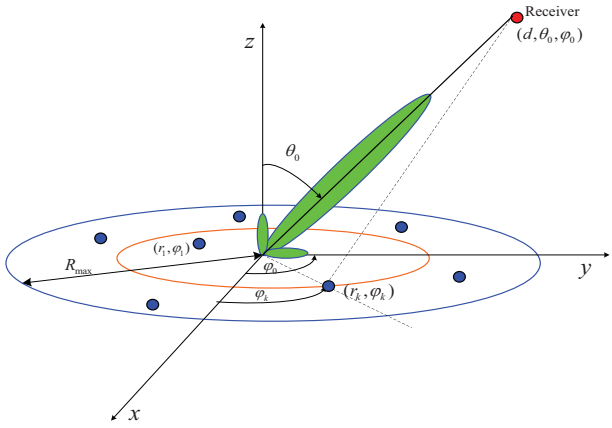

Fig. N.1: Wireless sensor network topology.

The beacon station is placed at a large distance from the sensor area which at a position symmetric to the receiver in Fig.N.1. The beacon station sends a sinusoidal synchronization signal to all the sensor nodes inside the area at regular time intervals. All sensor nodes use this beacon signal to synchronize their transmissions in a way that has been shown to produce a strong beam in the direction of the receiver. By using an external beacon signal for synchronization the need of accurately synchronized internal clocks is alleviated. By using a DSSS with BFSK modulation scheme first proposed in [3] all nodes can modulate the transmitted signal so that each node transmits its own sensed data to the fusion center. In order to analyze the energy efficiency of such one-hop communication scheme in a practical way, we assume that the sensor nodes draw transmission and circuit power from their batteries and not from the beacon signal. Although a sensor node architecture that act as active reflector which can reflect the beacon signal to the receiver is conceivable, using batteries to power up sensor nodes is more realistic and avoids distance and regulatory limitations as well as node design complexities which increase the cost of a sensor node.

The node design is shown in Fig.N.2. As it can be seen in this Figure, the incoming sinusoidal signal from the antenna is passed through a SAW filter. This type of filter exhibits excellent frequency response characteristics, controlled impedance and power handling all at a low cost and small size. SAW filters are passive and consume low power.

Thus they provide sharp frequency selectivity at the 2.45GHz Industrial, Scientific and Medical (ISM) band [8]. A high frequency amplifier is used whose function is to amplify the carrier signal. The carrier signal is further enhanced by the injection-lock in LC oscillator, which will follow the carrier frequency sent by the beacon station. A fractional PLL [9] is used to modulate the sensed data. The advantage of fractional PLL is that the output frequency can be at any desired value within a given reference frequency range. A low power digital type Analog to Digital Converter (ADC) [10] is used for converting the sensor measurements of environmental parameter into digital values. These digital data will be processed and spread by the spreading code. Meanwhile, due to the phase changing disadvantage of BPSK modulation which cannot form co-phased array, the BFSK modulation is used. Thus, the two frequency tones f_1 and f_2 will be modulated by the signal 0 and 1 respectively. With the help of fractional PLL, an inverter based selector can accommodate two different frequency division ratios into the phase locked loop. The fractional PLL itself can accommodate two different frequencies by changing the input ratio of $\Sigma\Delta$ integrator, i.e., $(a_n) = 1/2$ and M/N=245000/249999, but it needs certain setting up time for each symbol period. In order to have a better data rate, the proposed architecture uses two separate dividers that one of them will be selected by the data 0 or 1. The phase frequency detector (PFD) detects the frequency differences between the reference frequency (from the Active LC oscillator) and the divider output frequency. Then it gives the compared output to the voltage controlled oscillator (VCO), and adjusts it until the phase difference is zero. Thus the output of the PLL will have the output frequency defined by the divider.

Multiple channel access is achieved by using a direct sequence spread spectrum scheme where the information sequence from each node is multiplied by using orthogonal spreading codes. The orthogonal code is independent of the data and in our analysis we adopt Walsh-Hadamard sequences where each node spreads its data with an orthogonal spreading code of length K, and modulates it by a BFSK modulation scheme. Also the nodes are time synchronized by the beacon which implies that there is no time offset at the receiver. Walsh-Hadamard codes have good orthogonal properties when they align in time. The analytical expression for BFSK modulated signal is given by:

$$s_i(t) = \sqrt{\frac{2E_b}{T_b}} \cos(2\pi f_i t + \phi), 0 \leq t \leq T_b, i = 1, 2 \tag{N.1}$$

where, $f_i = f_c + \Delta f$is the frequency tone in Hz corresponding to the transmitted symbol, and is therefore a function of the carrier frequency f_c and the transmitted bits. The term ϕ modeled as a random variable, is the phase associated with the frequency f_i. Eb is the bit energy and Tb is the bit duration. To ensure orthogonality for a coherent BFSK system, the minimum separation between the frequency tones of a given node should be equal to $R_b/2$, where R_b is the information (data) rate.

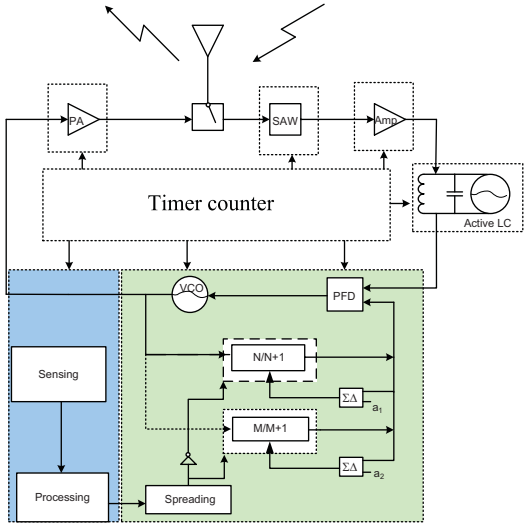

Fig. N.2: Sensor node architecture.

3 Cooperative Beamforming

The close form expression of the beamforming gain can be expressed as [2]

$$D_{AV} = \frac{2\pi}{\int_0^{\pi}\int_{-\pi}^{\pi} P_{AV}(\theta,\varphi)d\theta d\varphi} \tag{N.2}$$

where $P_{AV}(\theta,\varphi)$ is given by

$$P_{AV}(\theta,\varphi) = \frac{1}{K} + \left(1-\frac{1}{K}\right)^2 \left|2\cdot\frac{J_1\alpha(\theta,\varphi)}{\alpha(\theta,\varphi)}\right|^2 \tag{N.3}$$

here K is the total number of sensor nodes and $J_n(x)$ is the n_{th} order Bessel function of the first kind. The parameter is linked with the parameters in Fig.N.1 by the following equation:

$$\alpha(\theta,\varphi) = 4\pi\frac{R_{\max}}{\lambda}\sin\frac{\varphi}{2}\sin\theta \tag{N.4}$$

where λ is the carrier wavelength. In this paper, we consider a carrier frequency of 2.45G Hz which results in a wavelength around 12cm. The quantity R_{max}/λ is referred

to as the area radius normalized to wavelength. In Fig.N.3, the beamforming gain in dBi is plotted as a function of the sensors deployment area normalized by λ^2 and the number of sensor nodes K, according to Eq. (N.3). It

can be observed that, when the normalized area is at fixed, as the number of sensor nodes increases the gain gets saturated. This is because as more nodes are condensed in a fixed area, the inter sensor distance becomes smaller which finally can cause mutual coupling among the sensor node antennas, thus degrading the beamforming gain. For more details on cooperative beamforming we refer the reader to [2] and [3]

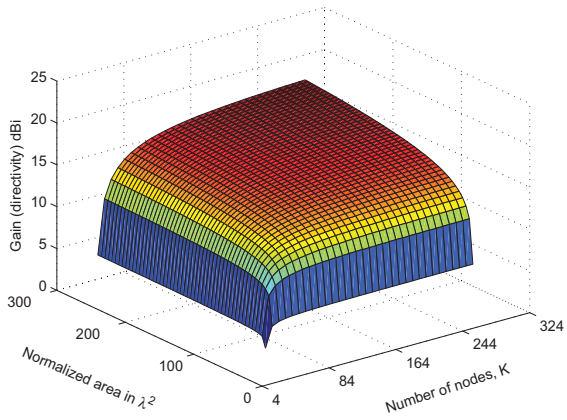

Fig. N.3: Beamforming gain over normalized area and sensor nodes.

In this paper, in order to analyze the energy efficiency of this cooperative beamforming technique, we assume that the sensors are deployed in an area of $20\lambda^2$. Meanwhile, in order to avoid mutual coupling among the sensor nodes, we assume that the maximum number of sensors within this area is 64, and analyze the energy efficiency for 4, 8, 16, 32 and 64 nodes respectively as discussed in Section V.

4 Bit Error Rate Analysis

In this section, we analyze the performance of the DSSS / BFSK scheme in synchronous systems. The performance metric considered here is Bit Error Rate (BER). If the transmit power required to achieve a given BER is known, then for a desired data transmission rate and maximum tolerable BER the transmit power budget can be calculated (as it will be discussed in the next Section). To the best of our knowledge, the analysis presented in this Section is missing from the related literature possibly due to the low

popularity of the DSSS / BFSK modulation scheme. The most obvious modulation scheme employed in CDMA system is phase shift keying (PSK) and is well studied for single- and multi-user scenarios [11]. This modulation scheme is ruled out in our specific beamforming application because due to its random phase changes it cannot achieve co-operative beamforming. The assumptions under which the model is presented are listed below:

- BFSK modulation is used for the information signal with P being the average power of the signal and G the beamforming gain.
- The length of the spreading code used is the same as the number of nodes in the network.
- Each data bit has a period of Tb and each chip has a period of Tc. The pulse shape is rectangular having an amplitude of 1 for both the information signal and the spreading code respectively.

4.1 AWGN Channel

The received bandpass signal is a sum of the transmitted signals from all the K nodes and it is perturbed by Gaussian noise, given by

$$y(t) = G\sum_{k=1}^{K}\sqrt{2P}x_k(t) + n(t) \tag{N.5}$$

where, $n(t)$ is the additive white gaussian noise with mean = 0 and variance = 1. In the above expression the equivalent bandpass signal is given by

$$x_k(t) = \cos\{2\pi[f_c + d_k(t+\tau_k^{Rx})s_k(t+\tau_k^{Rx})\Delta f]t + \phi_m\} \tag{N.6}$$

where, ϕ_m is the phase introduced by the BFSK modulator at each node, τ_k^{Rx} is the delay from the synchronization station to the k_{th} sensor node, $d_k(t)$ is the information signal and $s_k(t)$ is the spreading code. At any time instant, approximately half of the nodes will be transmitting at frequency f_1 and the remaining half at frequency f_2. Thus Eq. (N.5) can be split into two components as shown below

$$\begin{aligned} y(t) = {} & G\sum_{k=1}^{K/2}\sqrt{2P}d_k(t+\tau_k^{Rx})s_k(t+\tau_k^{Rx})\cos(2\pi f_1 t + \phi_1) \\ & + G\sum_{k=1}^{K/2}\sqrt{2P}d_k(t+\tau_k^{Rx})s_k(t+\tau_k^{Rx})\cos(2\pi f_2 t + \phi_2) + n(t) \end{aligned} \tag{N.7}$$

A correlation based receiver is used to obtain the associated decision statistic, Z from which a decision is made concerning the bit transmitted. In the following derivation we

have assumed desired user is node 1 and all the other $(K-1)$ nodes are interference. This holds the same while decoding for the other nodes as well. Therefore, it can be written as

$$Z = \int_0^{T_b} y(t) s_1(t + \tau_1^{Rx}) \cos[2\pi(f_c + m\Delta f)t] dt \tag{N.8}$$

where, m =±1. Substituting Eq. (N.5) into Eq. (N.8), it can be written as

$$\begin{aligned} Z = & \int_0^{T_b} \sqrt{2P} d_1(t + \tau_1^{Rx}) s_1(t + \tau_1^{Rx}) \cos(2\pi f_1 t + \phi_1) \cos[2\pi(f_c + m\Delta f)t] dt \\ & + \int_0^{T_b} \sum_{k=2}^{K} \sqrt{2P} d_k(t + \tau_k^{Rx}) s_k(t + \tau_k^{Rx}) s_1(t + \tau_1^{Rx}) \cos[2\pi(f_c + m\Delta f)t + \phi_m] \cos[2\pi(f_c + m\Delta f)t] dt \end{aligned} \tag{N.9}$$

Eq. (N.9) can be decomposed into three components as $Z = D + I + N$, where D is the desired signal in the channel, I is the interference term due to the presence of multiple nodes information and N is a Gaussian random variable. After mathematical manipulation we get

$$D = \pm\sqrt{\frac{PG}{2}} T_b \delta(i,j) \cos\phi_{i,j} \tag{N.10}$$

$$Var[N] = \frac{N_0 T_b}{4} \tag{N.11}$$

$$I = \frac{PG{T_b}^2}{4} \sum_{k=2}^{K} {R^2}_{k,1} \tag{N.12}$$

with $d_1(t + \tau_1^{Rx}) = \pm 1$, $\delta(i,j) = 1$ for i = j, otherwise $\delta(i,j) = 0$, $\delta(i,j)$ is the phase of the reference signal (receiver local oscillator), N_0 is the noise power spectral density and $R_{k,1} = \int_0^{Tb} s_k(t) s_1(t) dt$ is the normalized periodic cross-correlation between the spreading codes of node 1 and node k. The signal-to-noise-interference ratio (SNIR) is written as

$$SNIR = \frac{E\left[D^2\right]}{Var[N] + I} \tag{N.13}$$

Approximating the multi-node interference as Gaussian [12], the probability of bit error is given by

$$Pe = Q(\sqrt{SNIR}) = Q\left[\sqrt{\frac{1}{\frac{1}{GE_b/No} + \sum_{k=2}^{K} {R^2}_{k,1}}}\right] \tag{N.14}$$

where $E_b = P \times T_b$ and $Q(\cdot)$ is the Q function.

Simulation results of average BER for the DSSS / BFSK modulation scheme with and without beamforming gain over AWGN channel are shown in Fig.N.4. First, the conventional BFSK is implemented for a multi-user scenario. It can be observed from the Figure that as the number of nodes increases, the BER follows the AWGN theoretical curve and it is the same as in the single user case (the curves for 1, 4, 16 and 32 nodes without gain coincide). This is because, we have used perfectly orthogonalWalsh-Hadamard spreading codes. Through simulation we have also noticed that the error performance degrades when other types of spreading codes like Gold sequence or M-sequence is used. Our aim here is to study the comparative performance with and without beamforming gain as the number of nodes increases and the required signal-to-noise ratio (SNR) at the receiver in order to achieve a specific error rate. It is evident from Fig.N.4 that as the number of nodes increases, the BER improves because of beamforming gain, since the gain increases with an increasing number of nodes. When the beamforming gain saturates as the density of the nodes increases, there is no further improvement in the BER. Note that these results were obtained by Monte-Carlo simulation and that the BER was averaged over the decoded data of all nodes. In order to achieve a specific BER, the required SNR (E_b/N_0) at the transmitter can be low due to the beamforming gain which will improve the SNR at the receiver. For example, for 32 nodes, the required E_b/N_0 is 0dB for 10^{-4} error rate.

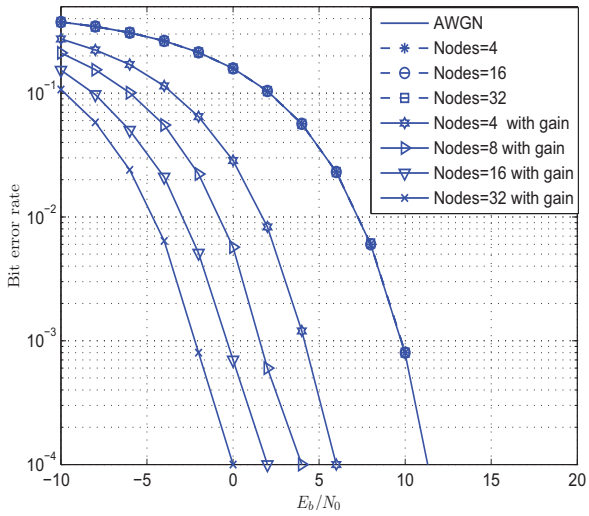

Fig. N.4: Average bit error rate over AWGN channel.

4.2 Propagation channel with LoS and multipath components

In a more realistic setting, the received signal power is composed of a LoS component from all the nodes which are co-phased, many multipath components and is corrupted by Gaussian noise. The LoS component has a deterministic value whereas the multipath signal is stochastic in nature. The received signal power at a distance d from the transmitting source can be expressed in free space using the Friis transmission formula [12] assuming that there are no objects present to affect propagation,

$$P_{Rx,LoS} = P_{Tx}\left(\frac{\lambda}{4\pi d}\right)^2 G_{tr} \tag{N.15}$$

where, λ is the carrier wavelength, P_{Tx} is the transmitted power and G_{tr} is the gain of the antenna. For an isotropic antenna, $G_{tr} = 1$. When the modulated data at the nodes are transmitted using the concept of random array (cooperative beamforming), then all the nodes transmitted signals are cophased and have at least one LoS component with beamforming gain. Further Eq. (N.15) becomes

$$P_{Rx,LoS} = P_{Tx}\left(\frac{\lambda}{4\pi d}\right)^2 G G_{tr} \tag{N.16}$$

where, G is the beamforming gain. In our analysis, the multipath component is modeled as a random variable where the received amplitude is Rayleigh distributed and the associated phase is uniformly distributed. The probability density function of the Rayleigh distribution is given by [13]

$$f_{ak}(a) = ae^{-a^2/2}, a \geq 0 \tag{N.17}$$

where, the fading Random Variables (RVs) are independent Rayleigh distributed and account for the fading channel atten6 uation of all signals. Each RVa_k represents the envelope of a complex Gaussian process with unit variance 1. Applying RV transformation, Eq. (N.17) can be expressed in terms of received

$$f_\gamma(\gamma) = \frac{1}{\gamma}e^{-\gamma/\overline{\gamma}} \tag{N.18}$$

where $\gamma = {a_k}^2 \frac{E_b}{N_o}$ is the instantaneous SNR and $\overline{\gamma} = E\left[{a_k}^2\right] \frac{E_b}{N_o} = \Omega \frac{E_b}{N_o}$ is the average SNR at the receiver with Ω being the mean power. The probability of bit error rate for BFSK modulated system over AWGN can be written as

$$P_e = Q(\sqrt{\gamma}) \tag{N.19}$$

The expression for the BER over Rayleigh distribution can be obtained by averaging Eq. (N.19) over the distribution of the fading channel Eq. (N.18) as

$$P_e = \int_0^{\infty} Q(\sqrt{\gamma}) f_\gamma(\gamma) d\gamma$$
$$Pe = \frac{1}{2}\left[1 - \sqrt{\frac{\overline{\gamma}}{\overline{\gamma}+2}}\right] \tag{N.20}$$

For the multi-node case, we model the interference from the other nodes as Gaussian [11] which can be expressed as

$$P_e = \frac{1}{2}\left[1 - \sqrt{\frac{\overline{\gamma}_{mu}}{\overline{\gamma}_{mu}+2}}\right] \tag{N.21}$$

where,where, γ_{mu} is the average signal-to-noise plus interference ratio, defined as $\overline{\gamma}_{mu} = \Omega SNIR$

The SNIR can be obtained from Eq. (N.13). Note that the beamforming gain is not considered for the multipath:

$$SNIR = \frac{1}{\frac{1}{E_b/N_o} + \sum_{k=2}^{K} R^2{}_{k,1}} \tag{N.22}$$

Thus,

$$P_e = \frac{1}{2}\left[1 - \sqrt{\frac{\Omega SNIR}{\Omega SNIR + 2}}\right] \tag{N.23}$$

where, $\Omega = E[a_k^2]$. Without loss of generality, we have assumed $a_1 = a_2 = ...a_k = a$ in our simulation. Fig.N.5 shows the BER vs E_b/N_0 plot over a propagation channel with LoS and multipath components at a distance d = 500m. It can be observed from the Figure that the BER is high when there is no LoS communication.When there is LoS component along with the multipath components added up at the receiver, the error performance improves gradually as a function of the SNR. Further more, an increase in the number of nodes results into increasing beamforming gain and hence the performance improves. Here, Monte-Carlo simulation is used for multipath fading channel and the BER is averaged over all nodes.

5 Energy Efficiency

In this Section, we evaluate the energy efficiency of the considered cooperative beamforming technique. In order to have a complete analysis of energy requirements we have proposed a sensor node architecture in Fig.N.2 and consider the total energy consumption at all signal processing blocks at the transmitter. However, base-band signal processing blocks at the transmitter and the energy consumption at the receiver are intentionally omitted. Also, we only consider uncoded data transmission in our analysis.

The energy requirements of Error Correction Codes (ECC) and will be studied in our future research work.

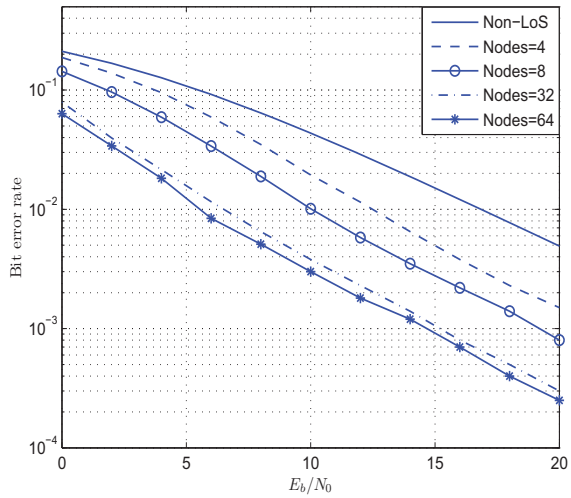

Fig. N.5: Bit error rate over LoS and Multipath components at d=500m.

The total average power consumption is divided into two components: (a) Power consumption of the power amplifier P_{PA}, which is dependent on the transmit power P_{Tx}, and (b) Power consumption of all other circuit modules, Pc. The total circuit power consumption is given by

$$P_C = P_{SAW} + P_{AMP} + P_{LC} + P_{PLL} + P_{ADC} \tag{N.24}$$

where, $PSAW$, $Pamp$, PLC, P_{PLL} and P_{ADC} are the power consumption values for the SAW filter, the amplifier, the active LC oscillator, the fractional-N PLL and the ADC respectively. The transmit power P_{Tx}can be calculated according to the equation given by [12]

$$P_{Tx} = \frac{E_b R_b (4\pi)^2 d^\beta}{G_t G_r \lambda^2} M_l N_f I_l \tag{N.25}$$

where, for a given BER requirement E_b is the required energy per bit at the receiver, R_b is the system information rate, d is the long-haul transmission distance, G_t and G_r are the transmitter and receiver antenna gain respectively, $\lambda$is the wavelength, β is the path loss exponent (typically $2 \leq \beta \leq 5$,with β= 2 representing free-space propagation), M_l is the link margin, N_f is the receiver noise figure, and I_l is the insertion loss of the SAW

filter. The power consumption of the power amplifier can be given by [14]

$$P_{PA} = \alpha P_{Tx} \tag{N.26}$$

where, $\alpha = \frac{\xi}{\eta} - 1$, with ξ the Peak-to-Average-Power Ratio (PAPR) and η the drain efficiency of the power amplifier. For constant modulus modulations like BFSK, [14]. Depending on the specific application and on the modulation scheme, there are situations in which amplitude linearity, can be traded for efficiency and RF output power. Such applications include constant amplitude schemes like BFSK which can tolerate high levels of amplitude distortion. Hence, we are able to use class E power amplifiers especially for WSN applications [15]. Finally, the total power consumption is given by

$$P_T = P_{Tx} + P_{PA} + P_C = (1+\alpha)P_{Tx} + P_C \tag{N.27}$$

The total energy consumption per bit for a fixed data rate can be obtained as

$$E_{b,t} = \frac{P_T}{R_b} = \frac{(1+\alpha)P_{Tx} + P_C}{R_b} \tag{N.28}$$

Substituting Eq. (25) in Eq. (28), we arrive at

$$E_{b,t} = \frac{(1+\alpha)E_b(4\pi)^2 d^\beta M_l N_f I_l}{G_t G_r \lambda^2} + \frac{P_C}{R_b} \tag{N.29}$$

5.1 AWGN Channel

In order to model the energy efficiency of the system under consideration, the power consumption of the proposed node architecture and related system parameters are defined in Table I. The low power consumption values are taken from the references [9], [10], [8], [15]. The BER over AWGN for DSSS / BFSK system has been obtained in Eq. (N.14). By making use of the Chernoff bound in the high SNR regime, it can be written as

$$P_e \leq \frac{1}{2}\exp\left[-\frac{1}{2}\left(\frac{1}{\frac{1}{GE_b/N_o} + \sum_{k=1,k\neq i}^{K} R^2{}_{k,i}}\right)\right] \tag{N.30}$$

where we made use of the Chernoff bound for the Q-function: $Q(x) = \frac{1}{2}e^{-x^2/2}$. After simplification, the required energy per bit at the receiver for a given BER requirement can be obtained as

$$E_b \leq \frac{No}{G\left[\frac{1}{|2\log(2P_e)|} - \sum_{k=1}^{K} R^2{}_{k,i}\right]} \tag{N.31}$$

Table N.1: System parameters and power consumption of the circuit block

Parameters	Symbols	Values
Carrier Frequency	f_c	2.45GHz
Frequency separation	Δf	10KHz
Frequency tone for bit 0	$f_1 = f_c + \Delta f$	2.45001GHz
Frequency tone for bit 1	$f_1 = f_c - \Delta f$	2.44999GHz
Data rate	R_b	20KHz
PAPR	ξ	1
PA efficiency	η	0.485
SAW Insertion loss	I_l	-1.5dB
Frequency recovery	P_{LC}	5.4mW
Fractional-N PLL	P_{PLL}	14.5mW
Sensing interface	P_{ADC}	0.28mW
Link margin	M_l	40dB
Noise figure	N_f	10dB
Noise PSD	$N_0/2$	3.98×10^{-21}
Required BER	P_e	10^{-3}
Path loss exponent	β	2
Tx and Rx antenna gain	$G_t G_r$	5dBi

By approximating the bound as an equality, the total energy consumption per bit over an AWGN channel according to Eq. (N.29) and Eq. (N.31) can be obtained as

$$E_{b,t} = \frac{(1+\alpha)E_b(4\pi)^2 d^\beta N_0 M_l N_f I_l}{G_t G_r \lambda^2 G \left[\frac{1}{|2\log(2P_e)|} - \sum_{k=1,k\neq i}^{K} R^2{}_{k,i}\right]} + \frac{P_C}{R_b} \tag{N.32}$$

From Eq. (N.32), it is clear that the required transmission energy is reduced by a factor equal to the beamforming gain G. Fig.N.6 depicts the total energy required per bit in a AWGN channel as a function of the communication distance, d. As the distance increases, the required total energy per bit also increases. With only one node the energy requirement increases nearly exponentially. By making use of cooperative beamforming, it is evident from Fig.N.6 that the total required energy per node reduces significantly. As the number of cooperating nodes increases, the energy requirement decreases. The signals from all the nodes are co-phased resulting in the formation of a high gain radiation pattern. This allows for communication over long-haul distances with a minimum energy requirement. Consequently, the sensor node battery energy is saved and the node life time can be extended. We now shift our analysis to shed some light into the relative contributions of transmission and circuit energy consumption to

the overall energy consumption as a function of beamforming gain and communication distance. Let us observe that the beamforming gain only affects the transmit energy consumption; the per node circuit energy consumption is fixed. Fig.N.7 depicts the transmit energy and then total energy consumption as a function of distance for 4, 8, and 32 nodes. It can be observed that up to a distance of, d 250m, there is always a significant difference between the transmit and total energy consumption even with a large gain factor (large number of nodes). The reason is that for small distances the required transmit energy is small and the circuit energy is a big part of the total energy consumption. Thus, increasing the beamforming gain has no significant effect in the overall energy saving. A second important remark is that the required transmit energy per bit does not depend on the data rate whereas the circuit energy is reduced with increasing data rate. At $d = 368m$, the transmit energy of 4 nodes intersects with the

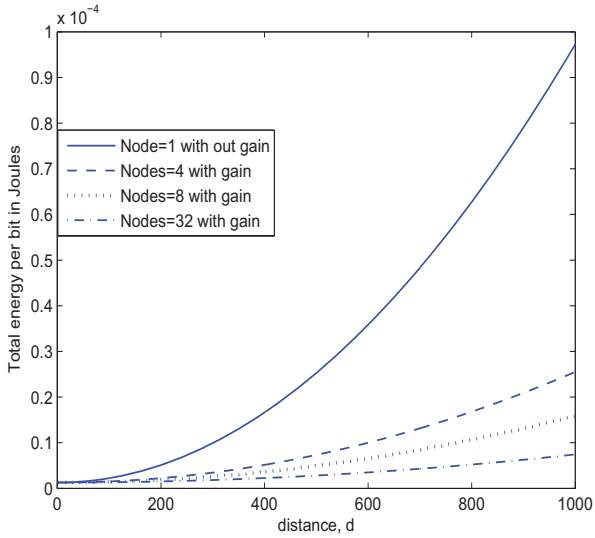

Fig. N.6: Total energy required per bit over AWGN channel.

total energy of 8 nodes. This implies that for distances over $d > 368m$, the total energy consumption of 8 nodes with the circuit energy consumption considered in this paper would by lower than the total energy consumption of 4 nodes with an extremely high data rate (extremely low circuit energy consumption). Similarly the transmit energy of 8 nodes becomes equal to the total energy of 32 nodes at a distance $d = 387m$.

5.2 Propagation channel with LoS and multipath components

The transmit power can be calculated given the required received power using Eq. (N.16) as

$$P_{Tx} = P_{Rx,LoS}\frac{(4\pi d)^2}{\lambda^2}\frac{1}{GG_tG_r} \tag{N.33}$$

where, $G_{tr} = G_tG_r$ is the antenna gain and $P_{Rx,LoS}$ can be expressed in terms of the

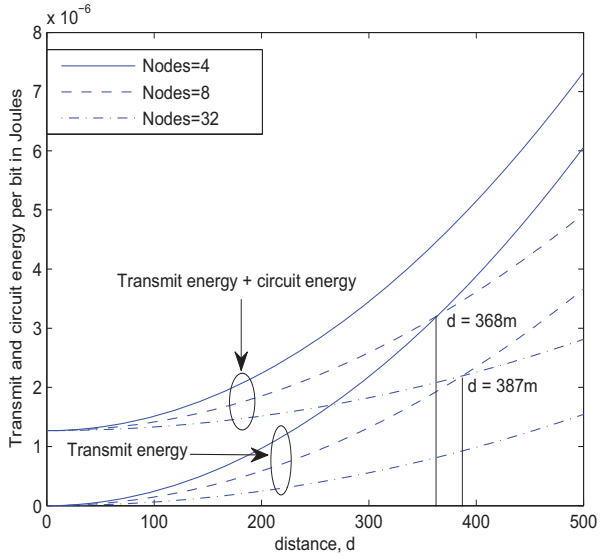

Fig. N.7: Comparison of transmit and circuit energy over distance.

required energy per bit as $E_b \times R_b$. After mathematical manipulation, the parameter $\overline{\gamma}_{mu}$ in (N.21) can be expressed in terms of P_e as

$$\overline{\gamma}_{mu} = \frac{(1-2P_e)^2}{2P_e(1-P_e)} \tag{N.34}$$

Using $\overline{\gamma}_{mu} = \Omega SNIR$, and Eq. (34), we obtain the energy per bit E_b as

$$E_b = \frac{(1-2P_e)^2 N_0}{\left[\Omega 2P_e(1-P_e) - (1-2P_e)^2 \sum_{k=1,k\neq i}^{K} R^2{}_{k,i}\right]} \tag{N.35}$$

Hence considering the power consumption of the power amplifier, other hardware process variations along with the noise and using Eq. (N.33) and Eq.(N.35), the total transmission energy per bit, E_t can be obtained as

$$E_t = \frac{(1+\alpha)(4\pi)^2 d^\beta M_l N_f I_l (1-2P_e)^2 N_0}{GG_tG_r\lambda^2 \left[\Omega 2P_e(1-P_e) - (1-2P_e)^2 \sum_{k=1,k\neq i}^{K} R^2{}_{k,i}\right]} \tag{N.36}$$

Now, considering the circuit energy consumption, the total energy per bit can be obtained as:

$$E_{b,t} = \frac{(1+\alpha)(4\pi)^2 d^\beta M_l N_f I_l (1-2P_e)^2 N_0}{GG_tG_r\lambda^2 \left[\Omega 2P_e(1-P_e) - (1-2P_e)^2 \sum_{k=1,k\neq i}^{K} R^2{}_{k,i}\right]} + \frac{P_C}{R_b} \tag{N.37}$$

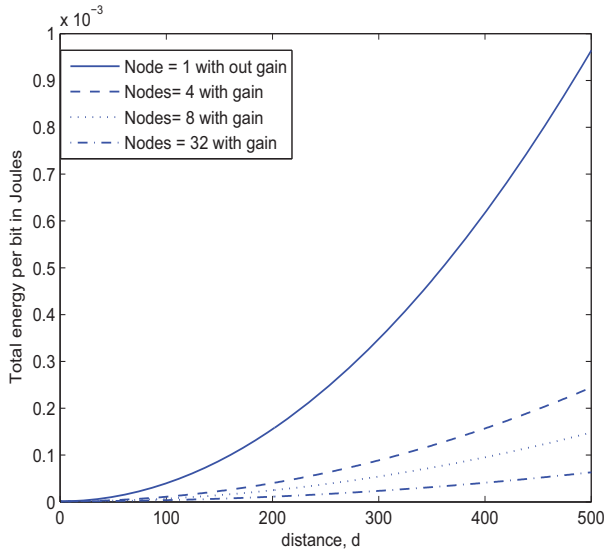

Fig. N.8: Total energy required per bit over a channel with LoS and multipath components.

Fig.N.8 shows the total energy required per bit over a channel with a LoS and multipath components as a function of distance. It is intuitive that if the multipath components add up destructively, then the received signal power decreases and hence the required energy per bit is supposed to be higher in order to mitigate the effect of fading. This can be clearly observed from Fig.N.6 and Fig.N.8: not only as the distance increases, the total energy consumption per bit also increases, but in the latter Figure the energy requirement is higher than in the former.

6 Conclusion

In this paper, we have investigated the energy consumption requirements of a cooperative beamforming scheme which eliminates multi-hop communication in WSN. In order to obtain a detailed formulation of the overall energy requirements, we have proposed a battery operated sensor node architecture with low power consumption and analyzed the power requirements of each circuit element. We then derived

the mathematical expressions for average BER over AWGN channel and a channel with LoS and multi-path components considering multi-node interference for the employed DSSS / BFSK modulation scheme. Monte-Carlo simulations were conducted in order to obtain BER curves with and without beamforming gain over the assumed channel models. The energy model analysis considered both transmission energy and circuit energy consumption. Through analytical expressions and simulation results we have also illustrated the transmission energy and total energy savings that can be achieved with cooperative beamforming. Our analysis can be used to estimate the expected energy consumption and resulting lifetime of a WSN using the one-hop communication technique prior to its deployment in the field.

References

[1] S.L. Howard, C. Schlegel, K. Iniewski, "Error control coding in low power wireless sensor networks when is ecc energy efficient," *EURASIP Journal on Wireless Commun. and Networking*, pp. 1–14, 2006.

[2] H. Ochiai, P. Mitran, H.V. Poor, V. Tarokh, "Collaborative beamforming for distributed wireless ad hoc sensor networks," *IEEE Trans. on Signal Processing*, vol. 53, pp. 4410–4124, 2005.

[3] A. Kalis, A.G. Kanatas, G.P. Efthymoglou, "A co-operative beamforming solution for eliminating multi-hopop communications in wireless sensor networks," *IEEE Journal on Selected Areas in Commun.*, vol. 28, pp. 1055–1062, 2010.

[4] A.G. Kanatas, A. Kalis, G.P. Efthymoglou, "A single hop architecture exploiting cooperative beamforming for wireless sensor networks," *Physical Commn Elsevier*, vol. 4, pp. 237–243, 2011.

[5] S. Cui, A.J. Goldsmith, A. Bahai, "Energy efficiency of mimo and cooperative mimo techniques in sensor networks," *IEEE Journal on Selected areas in Commun*, vol. 22, pp. 1089–1098, 2004.

[6] ——, "Energy constrained modulation optimization," *IEEE Trans on Wireless Commun*, vol. 4, pp. 2349–2360, 2005.

[7] K.J. Sudharman, "Virtual mimo-based cooperative communication for energy-constrained eireless sensor networks," *IEEE Trans. on Wireless Commun*, vol. 5, pp. 984–989, 2006.

[8] V. Novgorodov, S. Freisleben, J. Hornsteiner, M. Schmachtl, B. Vorotnikov, P. Heide and M. Vossiek, "Compact low loss 2.4ghz ism band saw bandpass filter on the ltcc substrate," *Asia Pacific Microwave Conference (APMC)*, vol. 1, pp. 2072–2075, 2009.

[9] A.F. mark, P.F. Michael, "14mw fractional-n pll modulator with a digital phase detector and frequency switching scheme," *IEEE Journal of Solid-State Circuits*, vol. 43, pp. 2464–2471, 2008.

[10] Richard Wee Tar Ng and Liter Siek, "Low power digital type adc," *International Symposium on Integrated Circuits (ISIC),*, pp. 289–292, 2011.

[11] L. Hanzo, L. L. Yang, E. L. Kuan and K. Yen, Ed., *Single-and multi-carrier DS-CDMA: multi-user detection, space-time spreading, synchronisation, standards and networking.* John Wiley & Sons, 2003.

[12] B. Sklar, Ed., *Digital Communications: Fundamentals and Applications, 2nd ed.* Prentice Hall P T R, 2001.

[13] M. K. Simon and M. S. Alouini, Ed., *Digital Communication over Fading Channels, 2nd ed.* New York: Wiley, 2005.

[14] Q. Tang, L. Yang, G.B. Giannakis, T. Qin, "Battery power efficiency of ppm and fsk in wireless sensor networks," *IEEE Trans. on Wireless Commun*, vol. 6, pp. 1308–1319, 2007.

[15] H.s. Oh, T. Song, S.H. Baek, E. Yoon, C.K. Kim, "A fully integrated 1 V, +9.5 dBm power amplifier for wireless sensor network," *Radio and Wireless Symposium*, vol. 1, pp. 235–238, 2006.